UNIVERSIDADE D
COIMBRA

Maria Margarida Lopes Correia Gomes Porto Gouveia

ELECTRON SPIN RESONANCE DATING OF MARINE AND FLUVIAL TERRACES OF CENTRAL PORTUGAL

DATAÇÃO DE TERRAÇOS MARINHOS E FLUVIAIS DE PORTUGAL CENTRAL POR RESSONÂNCIA PARAMAGNÉTICA ELECTRÓNICA

Tese no âmbito do Doutoramento em Geologia, área de especialização em Processos Geológicos, orientada pelo Prof. Doutor Pedro Manuel R. Roque Proença Cunha, Prof. Doutor António Antunes Martins e Prof. Doutor Christophe Falguères e apresentada ao Departamento de Ciências da Terra da Faculdade de Ciências e Tecnologia da Universidade de Coimbra

Dezembro de 2020

Faculdade de Ciências e Tecnologia
da Universidade de Coimbra

ELECTRON SPIN RESONANCE DATING OF MARINE AND FLUVIAL TERRACES OF CENTRAL PORTUGAL

Datação de terraços marinhos e fluviais de Portugal Central por Ressonância paramagnética electrónica

Maria Margarida Lopes Correia Gomes Porto Gouveia

Tese no âmbito do Doutoramento em Geologia, área de especialização em Processos Geológicos, orientada pelo Prof. Doutor Pedro Manuel R. Roque Proença Cunha, Prof. Doutor António Antunes Martins e Prof. Doutor Christophe Falguères e apresentada ao Departamento de Ciências da Terra da Faculdade de Ciências e Tecnologia da Universidade de Coimbra.

Dezembro de 2020

UNIVERSIDADE D
COIMBRA

This work was supported by the Fundação para a Ciência e Tecnologia through the grant SFRH/BD/116038/2016 and MARE - Marine and Environmental Sciences Centre. This work also had the contribution of a project (research grant) under the Programa de Acções Integradas Luso Francesas -2017 and the Programa Pessoa 2018 – Cooperation Portugal/France.

A autora é a única responsável por qualquer erro, inexatidão ou omissão de conteúdo.

Agradecimentos /Acknowledgements

Estas primeiras palavras só poderiam ser de agradecimento a todos os que me acompanharam ao longo destes quatro anos.

Em primeiro lugar, devo um especial agradecimento ao Prof. Doutor Pedro R. Roque Proença Cunha, orientador, amigo e o grande responsável por esta caminhada. Agradeço a confiança que sempre depositou em mim, o encorajamento, a dedicação e acompanhamento rigoroso, orientação perspicaz, as conversas enriquecedoras e os valiosos ensinamentos que me transmitiu.

Ao Prof. Doutor António Antunes Martins, orientador e amigo, que sempre me deu o maior apoio em todas as questões relacionadas com geomorfologia, mesmo longe esteve sempre presente e quando necessário fazia questão de acompanhar todos os trabalhos.

To Prof. Dr Christophe Falguères supervisor and friend, by the support, knowledge and opportunity of work with the ESR dating methodology. Thank you for giving all the attention and for the welcome during my stay in Paris. Thank you for allowing me to work with your scientific team in MNHN.

À Fundação para a Ciência e Tecnologia (FCT), pelo apoio financeiro através de uma bolsa e pelo financiamento ao abrigo do Acordo Bilateral Programa Pessoa.

Ao ex-Director do Departamento de Ciências da Terra da Universidade de Coimbra, Prof. Dr. Alexandre Tavares agradeço o apoio na instalação do Laboratório OSL/ESR, bem como aos respetivos técnicos e colaboradores (em especial à Ana Barbara Costa, Sr. D. Carminda Neves e ao Sr. Carlos Maia) pelo apoio necessário para o desenvolvimento dos trabalhos desta tese.

Ao MARE - Centro de Ciências do Mar e do Ambiente, e a todos os colaboradores, em especial à Vânia Pereira, pela sua ajuda e atenção na gestão dos fundos necessários para as estadias em França.

Às Câmaras Municipais de Coimbra, Figueira da Foz e Peniche por terem disponibilizado a cartografia às escalas 1/10,000 e 1 /2,000 e ao LNEG pela disponibilização de cartografia geológica 1/25.000 da área de Coimbra (com um especial agradecimento aos Doutores Ruben Dias e Catarina Moniz).

To the C.E.N.I.E.H. (Centro Nacional de Investigación de La Evolución Humana, Spain) and its staff (namely, Davinia Moreno) for the irradiation and bleaching of the E.S.R. quartz samples.

To the whole MNHN team, for their support in obtaining the results of this thesis. I must especially thank Prof. Dr Pierre Voinchet, Prof. Dr Jean-Jacques Bahain, for their patience, indispensable lessons for my dating work, and dear Eslem to make me feel more accompanied during my stay in Paris. Thank you for your friendship and affection, your hospitality and your kindness.

Ao Prof. Dr. Alberto Gomes, pela amizade, ajuda nas interpretações geomorfológicas, participação nas campanhas de campo e pelo conhecimento que me foi dando ao longo destes anos de trabalho.

Ao Prof. Dr. Alcides Pereira, pela ajuda dada ao longo da tese, nomeadamente respeitante à interpretação dos dados e medições feitas no Laboratório de Radioatividade da Universidade de Coimbra.

To Prof. Dr David Bridgland and Prof. Dr Martin Stokes to some advice in the thesis grammatical correction.

Ao Prof. Dr. Silvério Figueiredo, Dr. Telmo Pereira e Dr. José André, participantes nas campanhas de campo para amostragem de sedimentos para datação, agradeço todas as discussões como contributo também para esta tese.

Aos meus colegas e amigos, Rui Mota e Pu Yang pelo companheirismo e ajuda na aprendizagem da Geologia. Agradeço-vos toda a cooperação durante estes anos;

À Marta Reis e à Claúdia Caro pela amizade, pelas palavras de motivação, pela paciência e apoio sem fim. Sempre atentas em todas as etapas do doutoramento.

Aos meus companheiros de gabinete, Sérgio Sêco, Bruno Rodrigues e João Duarte. Obrigada pelo vosso apoio incondicional, conselhos e demonstração de amizade durante este percurso.

Às minhas irmãs, sobrinhas, sobrinhos, a todos os meus familiares e amigos, pelo interesse demonstrado e pelas palavras de incentivo.

Ao meu marido, Manel, por ser o meu companheiro, o meu porto-seguro, pelo grande apoio e suporte que me tem dado ao longo da vida e por aceitar comigo todos os desafios, por vezes mais exigentes para os dois, mas sempre atento aos passos do caminho.

Aos meus queridos filhos, Margarida, Vasco e Constança, pela paciência e cuidado com a mãe. A minha força veio sempre de vocês, o sentir que, de alguma forma, vos transmito o exemplo de nunca deixarem de lutar pelo que se propõem, sempre.

À minha Mãe, pelo apoio incondicional, pelo olhar atento, cuidado e ajuda, por ser o meu exemplo de Mulher e de Mãe.

Ao meu Pai que confio estar hoje também a festejar no Céu, onde não há limite de tempo nem de espaço, mas somente Amor.

Bem hajam todos!

Abstract

The interface between land and sea has varied over a long period of time, and it continues to the present. Despite the marine incursion at about 3.7 Ma, which covered extensive areas of the Atlantic coast of continental Portugal, glacial and interglacial periods occurred during the Pleistocene. As sea-level changes, the base level of erosion also changes, affecting fluvial processes and consequently, the shape of the coastline in detail. The marine and fluvial terraces located in the lower river valleys are terrestrial archives that have been the subject of detailed study. They make it possible to document the environmental changes during periods of high sea level and climate oscillations during the Pleistocene (2.58 Ma - 11 ka).

The neotectonic activity, whose time span includes the final Pliocene to the present day, can be known by studying stratigraphic and geomorphological references, particularly in the coastal zone and river valleys. Thus, the culminating sedimentary unit (UBS13) of sedimentary basins and the marine and fluvial terraces present in the study area are crucial elements for the characterisation of active tectonics. For this purpose, due to the interval of application of the Electron Spin Resonance (ESR) absolute dating method (300 ka - 3 Ma), the present study used this method to date the UBS13 unit, the terraces of the vestibular areas of the Mondego and Tejo rivers, as well as the accessible and better preserved coastal terraces between the Mondego and Espichel Capes. The absolute dating study was crucial given the lack of absolute ages on the central Portuguese coast, particularly in the Lower and Middle Pleistocene marine terraces and the Lower Mondego River valley (LMV). Moreover, this work had an enhanced challenge, to test the possibility of using the ESR method in quartz samples with ages up to 3.7 Ma.

This thesis's main objective was the detailed interdisciplinary study (geomorphology, lithostratigraphy, sedimentology, tectonics and ESR dating) to characterise terraced staircases and their correlation. The tectonic geomorphology of the LMV reach was studied. The differential tectonics and active faults present in the studied sectors were interpreted. The long- and short-term tectonic uplift rates of the area under study (distinguishing the most and least elevated sectors) were calculated, and the results were compared between the several studied sectors (marine and fluvial).

The study of differential tectonics in the study area confirmed a continuous crustal uplift, with some periods of greater acceleration along the Pleistocene related to intraplaque compression caused by the convergence between African and Eurasian plates.

Keywords: culminant unit, marine and fluvial terraces, ESR dating, sea-level variations, active tectonics.

Resumo

A interface entre terra e mar tem sofrido variações ao longo do tempo até aos dias de hoje. Para além da incursão marinha ocorrida à cerca de 3.7 Ma que cobriu extensas áreas da orla atlântica de Portugal continental ocorreram durante o Plistocénico, períodos glaciários e interglaciários cujo máximo nível marinho foi superior ao actual. Os terraços costeiros e os terraços fluviais situados nos troços inferiores de rios, são arquivos terrestres que foram objecto de estudos detalhados, pois permitem documentar as mudanças ambientais ocorridas durante períodos de alto nível do mar e as oscilações climáticas durante o Plistocénico (2.58 Ma - 11ka).

A actividade neotectónica, cujo intervalo de tempo compreende o Pliocénico final até ao presente, pode ser conhecida pelas referências estratigráficas e geomorfológicas nomeadamente na zona costeira e nos vales fluviais. Assim, a unidade sedimentar (UBS13) das bacias sedimentares e os terraços marinhos e fluviais presentes na área de estudo são elementos cruciais para a caracterização da tectónica activa. Para isso, devido ao intervalo de aplicação do método Electron Spin Resonance (ESR) (300 ka - 3 Ma), o presente estudo utilizou este método de datação absoluta para datar a unidade UBS13, os terraços das áreas vestibulares dos rios Mondego e Tejo, bem como os terraços marinhos acessíveis e mais bem preservados entre o Cabo Mondego e o Cabo Espichel. O estudo de datação absoluta foi crucial face à inexistência de idades absolutas ao longo da costa central portuguesa, nomeadamente em terraços do Plistocénico Inferior e Médio e ainda no troço vestibular do Baixo Mondego. Teve a importância acrescida de avaliar a possibilidade de utilização deste método em sedimentos com idades superiores aos 3 Ma.

O principal objectivo desta tese foi o estudo pormenorizado interdisciplinar (geomorfologia, litostratigrafia, sedimentologia, tectónica e de datação por ESR) para a caracterização das escadarias de terraços, fluviais e marinhos, e sua correlação. Foi feito um estudo geomorfológico detalhado no vale do Rio Mondego, entre Coimbra e a Figueira da Foz. Interpretou-se a tectónica diferencial e as falhas activas presentes nos sectores estudados. As taxas de soerguimentos tectónico de longo e de curto termo da área em estudo foram calculadas (distinguindo-se os sectores mais e menos soerguidos) e os resultados foram comparados entre os vários sectores estudados (marinhos e fluviais).

O estudo da tectónica diferencial ao longo da margem costeira Centro-Ibérica permitiu confirmar um contínuo soerguimento crustal existente, com aceleração de taxa de soerguimento ao longo do Plistocénico relacionado com a compressão intraplaca causada pela convergência entre a placas Africana e Euroasiática.

Palavras-chave: Unidade culminante, terraços marinhos e fluviais, datação ESR, variações do nível do mar, tectónica activa.

List of Contents

List of Figures

List of Tables

List of Equations

CHAPTER I. GENERAL INTRODUCTION AND THESIS OUTLINE

I.1 Introduction

Sea level has fluctuated cyclically over geological time, with eustatic variations driven by climatic oscillations with impact on the coastline position worldwide. Indeed, the Quaternary period (comprising the Pleistocene and Holocene Epochs) was characterised by the occurrence of repeated, intense glacial phases interposed by warm phases (interglacial) globally widespread. As a result, the sea level had fluctuated almost continuously between interglacial levels, and during times with maximum glaciation, when sea level was more than 100 m lower than today (e.g., Siddal et al., 2007). The interaction between fluctuations of sea level during the Pleistocene and regional tectonic uplift is evidenced at the Atlantic coast, as along the Western Iberia coastline and expressed by marine terraces, caves and groundwater speleothems developed in coastal caves (e.g., Haws et al., 2011; Figueiredo et al., 2015; Gelder et al., 2018; Normand et al., 2018; Pedoja et al., 2014, 2018; Ressurreição, 2019), and generally are represented as marine terrace sequences.

The study of the Pleistocene sedimentary deposits along the coast makes possible to recognise the periods of erosion and deposition recorded on the marine platforms by sea-level variations and the evolution of the coastline related to those variations and by the neotectonics. Besides understanding the climatic cycles during the past (in the Pleistocene-Holocene Epochs), the active tectonic behaviour, allows understanding the topographic development in the future, based on the calculated uplift rate tendencies. Furthermore, stratigraphic records are precious records to understand the behaviour of natural systems (e.g., Cattaneo and Steel, 2003; Mauz et al., 2013), in particular non-stationary responses where the statistical mean change with time (e.g., seismic cycles, climate trends, sea-level rise).

In the inland, the Plio-Pleistocene culminant unit and the fluvial terraces preserved in river valleys, are also the most relevant geomorphic records about climate change and vertical crustal movements (regional or differential), contributing to infer rates of the fluvial incision (e.g., Burbank and Anderson, 2012) and providing important insights to understand the long-term landscape evolution (e.g., Bridgland and Westaway, 2014). The external controls on fluvial terrace formation (alternation of fluvial incision and aggradation) has been widely debated in the literature (e.g., Kukla, 1975, 1977, Bull, 1990; Antoine, 1990; Li, 1991; Bridgland, 1994, Tyràcek, 1995; Matter et al., 1995; Van den Berg, 1996, Saucier, 1996; Maddy, 1997; Bridgland, 2000; Bridgland and Westaway, 2008).

Moreover, main changes of fluvial downcutting rates broadly match with relevant orbital-forced climatic changes occurred during the Pleistocene and especially with the Middle-Pleistocene transition (MPT;~ 0.781 Ma), coupling the substitution of the Early Pleistocene "41 ka world" by the younger Middle-Late Pleistocene "100 ka world"(e.g., Siddal et al., 2007; Spratt and Lisiecki, 2016).

The marine terraces of mainland Portugal have been the subject of studies since the 40s, (e.g., Martins, 1949; Teixeira, 1979; Almeida, 1997), but without taking into account the influence of local and regional tectonics (e.g., Pereira, 1990; Araújo, 1991). More recently, several geomorphological markers have been used to characterise the Quaternary vertical movements. In coastal regions, a regional Pliocene wave-cut platform dated as ca. 3.7-3.61 Ma (Diniz et al., 2016) and some dated Pleistocene marine terraces (e.g. Soares, 2007; Bennedetti et al., 2009; Ramos et al., 2012; Figueiredo et al., 2013; Carvalhido et al., 2014, Ressurreição, 2018) has been used for this purpose. Considering these issues associated with marine terrace research along the Iberian Atlantic passive margin we describe, and date impressive marine terrace staircases developed onto the rocky headlands of central Portugal: the Mondego Cape, Peniche Peninsula, Abano beach - Raso Cape and Espichel Cape. The staircases span the Early, Middle and Late Pleistocene stages, thus providing key reference sites of coastal landscape development, with differential uplift rate.

The UBS13 sedimentary unit is thought to record the re-establishment of Atlantic drainage in the Lower Tejo and Mondego Cenozoic basins following a period of endorheism during the late Tortonian–Zanclean (~9.6 to 3.7 Ma) (e.g. Cunha, 2019). In an attempt to address the dearth of geochronological data at the beginning of the fluvial incision stage, the unit UBS13 in the Mondego and Lower Tejo Cenozoic basins was dated by using the ESR method.

The terraces of the Lower Mondego Valley (LMV) and Mondego Cape were previously studied, mainly by geomorphology and lithostratigraphy (Soares, 1993, 1999; Soares et al., 2007; Ramos, 2000; Cunha, 2002; Santos, 2009; Ramos et al., 2012), but the present work focused on detailed geomorphology and ESR dating.

In the Lower Tejo River (LTR), the fluvial terraces have already been characterised in previous studies (e.g., Mozzi et al., 2000; Cunha et al., 2000; 2008; 2012; 2016; Martins et al., 2009; 2010b, Rosina et al., 2014), although still with rare absolute ages in the uppermost terrace levels.

The previous knowledge of the marine terrace staircases of Peniche, Raso Cape and Espichel Cape was quite limited (e.g., Cunha et al., 2015).

The contribution of ESR methodology to date the sedimentary units and to calculate the uplift rate in several sectors was crucial. Notwithstanding, the present study tested the ESR potential to date quartz sediments up to 3.7 Ma.

This multidisciplinary investigation aims to increase the knowledge concerning the sea-level and tectonic controls in the sedimentary and landscape evolution of central-western Portugal during the Pleistocene.

I.2 Objectives

Human society is at its most (?) interglacial period but very conditioned by a progressive "Global Warming", with associated climate changes and rising sea level in the last century. Besides the marine incursion that 3.7 Ma ago had a sea-level ca. 25 m a.s.l. (Miller et al., 2005), and covered extensive areas of the Atlantic coast of Portugal, reaching 13 km from the current coast, in the predominantly cold interval of the Pleistocene several interglacials have occurred whose maximum sea level was higher than the present (e.g., MIS 5, MIS 7 and MIS 11).

The purpose of this study is to characterise sea-level changes, climatic variations, sedimentary environment evolution and active tectonics in a coastal area with a human occupation, in a time interval (Pleistocene) comprising interglacial and glacial periods.

Therefore, the study of the geological record documenting the latest marine incursions (the marine deposits associated with the culminating sedimentary unit and the coastal terraces) is crucial as allows the characterisation of relative sea-level and environmental changes. Coastal terraces record the maximum of each interglacial marine incursion, generally with overlapping lagoon, aeolian and colluvial levels; the fluvial terraces record longer intervals as the accommodation space of these sectors is determined by the eustatic variations, tectonics and the climate-controlled river discharge (water /sediment supply). In this research, the coastal area between Mondego and Espichel capes and the Tejo and Mondego lower sectors were studied.

A new dating methodology of international relevance, Electro-spin resonance (ESR), has been used to date the older Pleistocene units to achieve the proposed objectives. It allowed to obtain the long-term (last ~1.8 Ma) and short-term incision/uplift rates for the study area sectors; it has enabled the identification of active faults.

A regional survey focused on the study of sedimentary units in selected sections with marine and fluvial deposits were conducted at western central Portugal at Mondego Cape, Abano – Raso Cape, Espichel Cape, S. Vitória, Peniche and Rio Maior, but also along the lower Mondego and the lower Tejo valley. The research was supported by up-to-date methods, such as ESR dating and detailed geomorphological cartography.

I.3 Thesis structure

This thesis contains four main chapters (Fig. I.1) that were prepared to be submitted as scientific papers. The research resulted in several scientific publications, from presentations at international and national meetings to papers published in international peer-reviewed journals. The scientific papers are presented in their original form, except for some layout changes. Consequently, some repetitions in the text concerning methods and materials are inevitable.

Chapter II presents the methodologies used in the study, emphasising the absolute dating method used in the present work.

In addition to the presentation of the thesis structure, several important subjects are described to allow a better comprehension of the studied theme, such as the main objectives and the motivation that led us to initiate this doctoral project.

Chapter III corresponds to a published paper and deals with the culminant sedimentary unit of the sedimentary basins (UBS13). For the first time with ESR, this chapter aims to study the chronology of this unit of the Mondego and Lower Tejo Cenozoic basins. This chapter was published in the International Journal of Global and Planetary Change.

Chapter IV focuses on the geomorphological, tectonic and geochronologic study of the marine terraces sequence, comprising sedimentary deposits from different interglacial high stands (MIS 21 to MIS 5) in the Peniche peninsula (to be submitted).

Chapter V refers to the identification and interpretation of active faults during the Quaternary and estimation of incision/uplift rates by using geomorphic markers as dated references. It is based on a detailed geomorphological mapping of the terrace staircases of LMV (between Coimbra and Figueira da Foz) and at the Mondego Cape (paper to be submitted).

Chapter VI focuses on the geomorphological, sedimentary, and geochronological study of the marine terraces of the Espichel Cape, Abano beach - Raso Cape and the upper fluvial terraces of the Lower Tejo reach IV. The ESR allowed to correlate the terrace staircases and estimate uplift rates in an area with a high population and significant historical seismic activity records. This chapter corresponds to a paper for submission to a scientific journal.

Chapter VII comprises the final discussion and the main conclusions of this research. A comparison between all the studied marine staircases of Mondego Cape, Peniche, Abano beach - Raso Cape and Espichel Cape, but also fluvial sectors, is made. The uplifting trend during the Quaternary using the results obtained with the crucial chronological data of each terrace staircase is summarised and interpreted. Further considerations regarding future studies are presented.

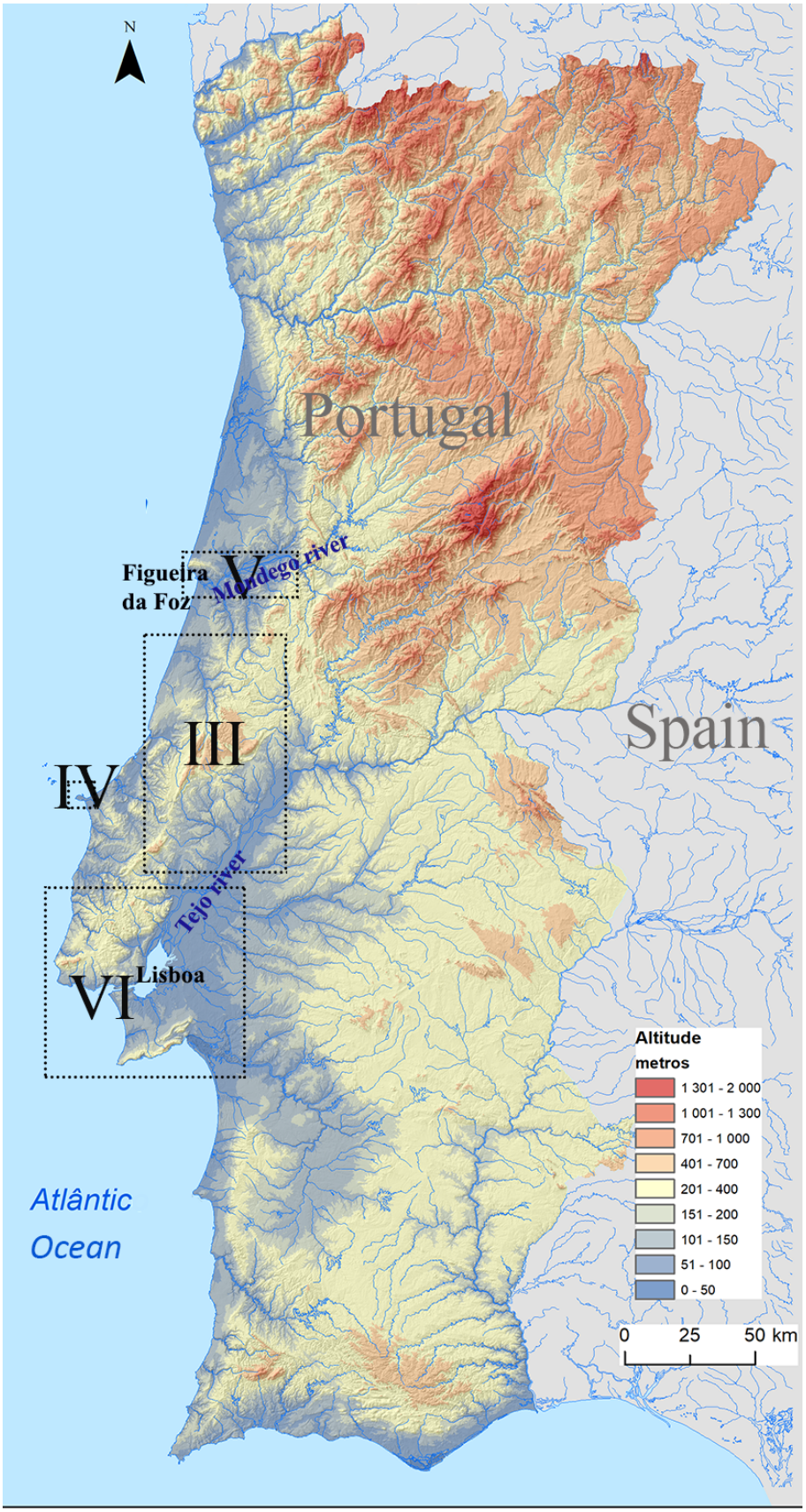

Figure I. 1 The geographical position of the study areas in each chapter (III, IV, V and VI), in western central Portugal.

CHAPTER II. METHODOLOGIES

The methodologies used in this study aimed to analyse fundamental aspects for the geological study of the coastal platform between Mondego and Espichel capes, including the terraces at the lower river reaches. The scientific areas are geomorphology, lithostratigraphy, sedimentology, tectonics and ESR dating.

The methodologies are grouped according to the type of work: office, field and laboratory.

The ESR dating method is firstly analysed in detail as it is yet a less used technique, namely in Portugal and as it is one of the bases of this work.

II.1. Geochronological dating methods

Environment changes, climate and tectonism, have been investigating using ESR. An important facet of the development of a geochronological technique is the potential of the age range. Methodological developments in the last few years had allowed the successful application of ESR dating method to date geological samples covering the whole period of Quaternary (e.g. Schwarcz et al., 1994; Falguères et al., 1999; Curnoe et al., 2001; Bahain et al., 2007; Rink et al., 2008). This is one of the very few numerical dating methods that can cover the entire Pleistocene, even if the large majority of the applications are between c. 20 ka and 800 ka (Duval et al., 2018).

There are other methods available to determine the ages of geological events with different time range applicability (Fig.II.1). These techniques are based on the rate of growth of specific radioactive isotopes (e.g., $^{40}K/^{39}Ar$, $^{40}Ar/^{39}Ar$, $^{230}Th/^{234}Ur$, $^{26}Al/^{10}Be$), the rate of decay of cosmogenic-produced radionuclides (e.g., ^{14}C) the rate of chemical alteration of organic and inorganic materials (e.g., Amino acid racemisation, cation-ratio), by global time markers (e.g. palaeomagnetism, stable oxygen isotopes) and by the rate of accumulation of radiation damage in crystals (e.g., thermoluminescence, optically stimulated luminescence, ESR, fission tracks).

However, only a few can be utilised for the types of materials found in Quaternary deposits and with different precision achieve (e.g., Preusser et al., 2009; Tarling, 2012).

Luminescence methods are mainly applied to quartz or feldspars. When stimulated by heat, the resulting signal is called thermoluminescence (TL), and when stimulated by light (photons), the resulting signal is called either optically stimulated luminescence (OSL) and or infrared stimulated luminescence (IRSL) when is stimulated by infrared light.

ESR dating has a larger time range than any other Quaternary dating methods, extending from a few thousand to more than 3 Ma (Fig. II.1), depending on the radiation dose rates that the materials experience during their depositional history.

The most important dating applications lie in the time range beyond the applicability of ^{14}Carbon dating of marine carbonates as by U-series and amino acid racemisation techniques, but younger than the lower limit of ^{40}Ar/^{39}Ar dating for most volcanogenic samples (although some as young as 10 ka have been successfully dated). The scarcity of volcanic samples and U-series datable calcium carbonates in most depositional contexts render the ESR and luminescence methods even more important chronometric tools in this time range. Alternatively, both TL and OSL methods use quartz grains to estimate the age of sediment deposition. With ESR also it is possible to date both carbonates and quartz grains. By this potential, the ESR can date Pleistocene marine and fluvial quartz sediments and extend the applicability range up to Pliocene sediments.

The chronometric dating methods cannot be all used to date geological samples on a given site, since it depends on the presence (or absence) of suitable materials for this purpose, which is closely related to the geological context and the presumed age of the site.

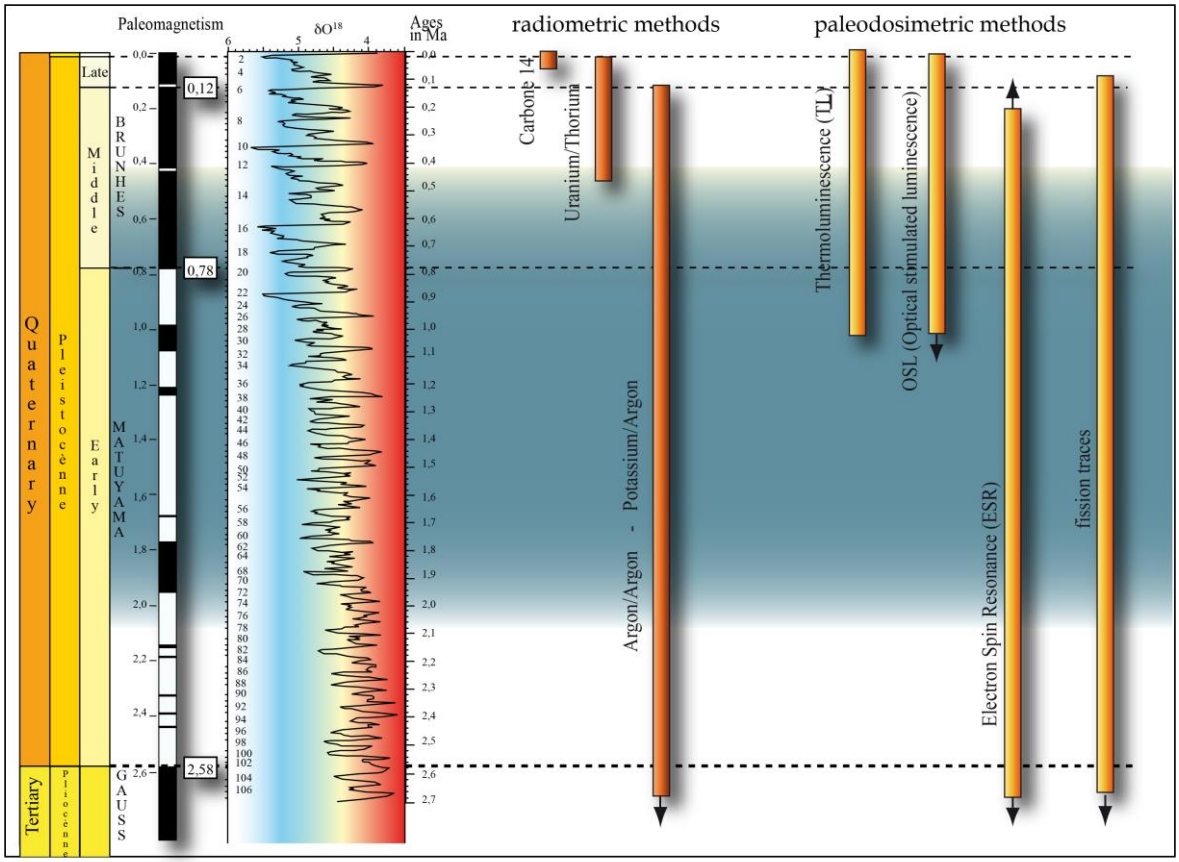

Figure II. 1. Examples of chronometric dating methods with an approximated time range application. Time scale is logarithmic (modified from Voinchet, personal com).

The ESR dating method ESR (Electron Spin Resonance), also called EPR (Electron Paramagnetic Resonance) has been widely applied to dating in researches of the Quaternary. This method was first developed by Zavoisky (1945) and then since the advances in microwave and solid-state electronics, (Ikea, 1993). ESR is a non-destructive analytical method that has been applied in a wide range of studies and application areas such as solid-state physics and molecular chemistry, and more recently in radiation dosimetry, biochemistry, geological and archaeological sciences. The first geochronological study using ESR were made on apatite crystal (Zeller et al., 1967). Some dating attempts were also performed on quartz at the beginning of '70s (McMorris, 1971) but just in 1975, with the dating of a stalactite from Akiyoshi cave in Japan, carried out by Ikeya that the ESR becomes a dating method (Ikeya, 1975). Since then, this new dating method has increasingly been applied in geology, geography and archaeology fields. It has been developed to apply it to different types of materials such as hydroxyapatite (e.g., Schwarcz, 1985; Grün et al.,1988; Grün and McDermott 1994; Falguères et al., 1997, 2010), fossil bones (e.g., Ikeya, 1978, Yokoyama et al., 1981, 1982), continental and marine carbonates (Ikeya, 1978; Bahain et al., 1994, 1989; Pirouelle et al., 2007), corals, fossil teeth, quartz (e.g., Yokoyama et al., 1985; Grün et al., 1988, Voinchet et al., 2003, 2004, 2007), evaporites (e.g., Ikeda and Ikeya, 1992; Aydas et al., 2011), and sediments baked by lava flow (e.g., Yokoyama et al., 1985a). Its application to quartz has been attempted to estimate the age of a wide range of sedimentary contexts (intra-faults, fluvial incision, interbedded volcanic rocks) and the age of formation of heated ceramics.

This methodology has often been used for the dating older fluvial terraces and archaeological sites, covering a time range <1 Ma (Grün et al., 2006; Falguères et al., 2006), namely in the Iberian Peninsula (Table II. 1) in recent years (e.g., Rosina et al., 2014; Moreno et al., 2012, 2017; Mendez Quintas, 2018). This study focuses on the ESR method in quartz-rich sediments, from marine and fluvial Pleistocene sediments and to date the Pliocene sedimentary culminant unit (UBS13) deposited before the beginning of the fluvial incision of the current rivers.

Table II. 1. Some relevant published ERS works in the world undertaken in the last two decades.

References	Methodology	Country
Toyoda et al., 2000;	ESR	
Rink et al., 2001	ESR/ US	Amud Cave, Israel
Falguères et al., 2001; 2006; 2015	ESR; ESR/US	Asia Indonesian
Voinchet 2002	ESR	France (Loir, Creuse,)
Schellmann et al., 2004	ESR/US/ C14	Barbados,Ciprus; Patagonian At.Coast
Voinchet et al., 2003; 10; 13; 15; 20	ESR/ US	France; China; Morocco
Cordier et al., 2006; 2012	OSL/ ESR	France;Germany,Sarre V.
Duval et al., 2009;2012;2013; 2020	ESR	France
Tissoux, 2007	ESR	France
Bahain et al.,2007; 2020	ESR/ US	N France
Martinez et al., 2010	ESR/US	Spain, Barcelona
Antoine, 2015	ESR-ESR-US	France,Seine,Yonne, Somme
Liu e al., 2015	ESR	China
O'Connor et al., 2010	ESR /OSL/TL/c14	East Timor
Viveen et al., 2012	OSL/ ESR	NW Iberia, Minho River
Moreno et al., 2012;2015; 2017; 2019	ESR	Spain
Jull, 2013	ESR	South Africa; Barbados
Odriozola et al., 2014	ESR	La Fuente, Spain
Rosina et al., 2014	ESR	**Portugal, Tejo river**
Abakumov et al., 2015	ESR	Siberian arctic islands
Duval and Guillarte, 2015	ESR	Spain, France, Algerian, Italy
Sharma and Chand, 2016	ESR/OSL/radiocarbon; Be TCN	India (Himalaya; Nepal)
He et al., 2015	ESR, OSL	China, Tibet
Bailiff et al., 2016	OSL/ ESR	Canada
Sancho et al., 2016	ESR	Ebro basin
Tsakalos et al., 2018	ESR /US	Cyprus
Yurnald, 2018	ESR/US	Indonesia
Delmas et al., 2018	ESR /Be	Pyrenees
Mendez-Quintas et al., 2018	ESR/OSL	Spain
Qiu et al., 2018	ESR	SW China
Jia et al., 2019	ESR	China
Bartz, 2019	ESR /TT OSL	NE Morocco
Del Val et al., 2019	ESR	Bay Biscay, Spain
Demuro et al., 2020	ESR	Galicia, Spain
Gutierrèz et al., 2020	ESR	NE, Spain
Gouveia et al., 2020	ESR	**Portugal**

There have been variations in the types of materials most used in Quaternary dating studies, using ESR dating method over the last 40 years. In the last decade, the quartz and fossil tooth enamel and bones were the most used (Fig. II.2).

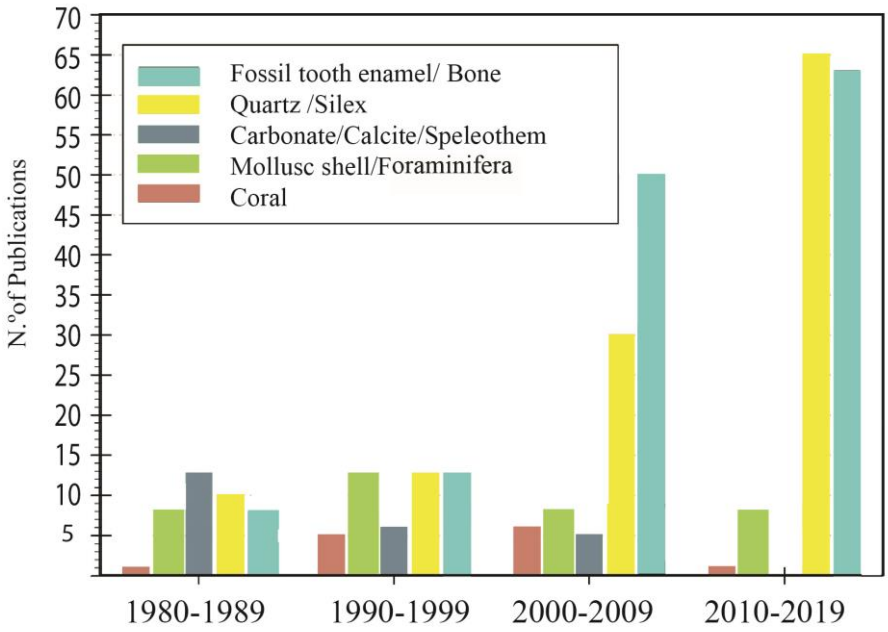

Figure II. 2. Evolution with the time of the most popular ESR dating applications since 1980, expressed by n.º of publications (adapted from Duval et al., 2020).

II.2. Physical Principe of ESR

ESR dating is based on passage effects of radiations in the mineral lattice. The radiogenic isotopes contained in the sample emit energy, which passes through and interacts with the point defects in the crystalline lattice of the mineral.

An electron may be considered as a negatively charged particle that turns on itself. This movement is called "spin" and induces, a magnetic field "μe" in the vicinity of the electron. Therefore, the electron spin orientation will be reversed simultaneously. The radioactive nuclides (U, Th, and K) present in nature emit a variety of rays. Natural radiations (α, β, γ) ionises atoms or molecules and break the paired electrons that will be trapped by some other atoms. At this instant, they stay with a magnetic moment, μe, due to the unpaired electron spins. Atoms, ions, and molecules whose opposite spin electrons associated in pairs have zero overall magnetic moments and are "diamagnetic". However, if the element has unpaired electrons, their global magnetic moment is non-zero and it is called "paramagnetic".

When a mineral is formed or reset, all electrons are in the ground state.

Negatively charged electrons are knocked off atoms in the ground state (valence band) and transferred to a higher energy state (conduction band); positively charged holes remain near the

valence band. After a short time of diffusion, most electrons recombine with holes, thus returning the mineral to its original state, forming again magnetically neutral electronic pairs. However, all-natural minerals contain defect sites (e.g., lattice defects, interstitial atoms) at which electrons and holes can be trapped. The trapped electrons and holes form paramagnetic centres which can be detected with an ESR spectrometer, giving rise to a characteristic ESR signal (e.g., Grün, 1989).

The intensity of this signal is directly proportional to the number of electrons trapped in the crystal structure. This number of electrons depends on the intensity of the radioactivity to which the sample has been subjected, the number of traps available in the structure (radiosensitivity) and the duration of radiation exposure (age) (e.g., Grün, 1997).

II.3. Zeeman Effect

Because an electron has a magnetic moment, it acts like a compass or a bar magnet when it is placed in a magnetic field, B_0. According to the direction of its magnetic moment, it will be orientated in the same or opposite direction than the magnetic field, leading to the split of the unpaired electronic populations in two different energy levels. The energy-yielding different spin states under the external magnetic field are known as the Zeeman Effect. It will have a state of lowest energy when the moment of the electron, μ, is aligned with the magnetic field and a state of highest energy when μ is aligned against the magnetic field. The two states are labelled by the projection of the electron spin, Ms, on the direction of the magnetic field (H). Because the electron is a spin 1/2 particle, the parallel state is designated Ms = -1/2 and the antiparallel state is Ms = +1/2 (Weil et al., 1994).

These energy differences, ΔE, can be measured because of an important relationship between ΔE and the absorption of electromagnetic radiation. According to Boltzmann law, electromagnetic radiation will be absorbed if:

$$\triangle \mathrm{E} = h\upsilon (1)$$

where h is Planck's constant (6.625×10^{-34} J) and ν is the frequency of the radiation (Hz).

From quantum mechanics, the basic equations of ESR are obtained:

$$\mathrm{E} = \mathrm{g}\ \mu\mathrm{B}\ \mathrm{H}\ \mathrm{Ms} = \pm\ \mathrm{g}\ \mu\mathrm{B}\ \mathrm{H}\ (2)$$

g-factor, (g) is a proportionality constant that determines the position of the peaks of the ESR spectrum. In the case of a free electron, g = 2.0023, but the value of "g" also depends on the orbital moment created by the motion of the unpaired electron around the nucleus and its interaction with the magnetic spin moment.

Bohr magneton, (μB) is the natural unit of the electronic magnetic moment,

$$\Delta \mathrm{E} = \mathrm{E2} - \mathrm{E1} = \mathrm{h}\nu = \mathrm{g}\ \mu\mathrm{BH}\ (3)$$

Two facts are well-defined from Equation 2 and Equation 3 and shown in Figure II. 3: (1) the two spin states have the same energy in the absence of a magnetic field; (2) the energies of the spin states diverge linearly as the magnetic field increases.

Because we can change the energy differences between the two spin states by varying the magnetic field strength, we have an alternative means to obtain spectra. We could apply a constant magnetic field and scan the frequency of the electromagnetic radiation as in conventional spectroscopy. Otherwise, we could keep the electromagnetic radiation frequency constant and scan the magnetic field (Fig. II.3). A peak in the absorption will occur when the magnetic field "tunes" the two spin states so that their energy difference matches the energy of the radiation. This field is called the "*field for resonance*" and is used in ESR spectrometers because it offers superior performance (Weil et al., 1994).

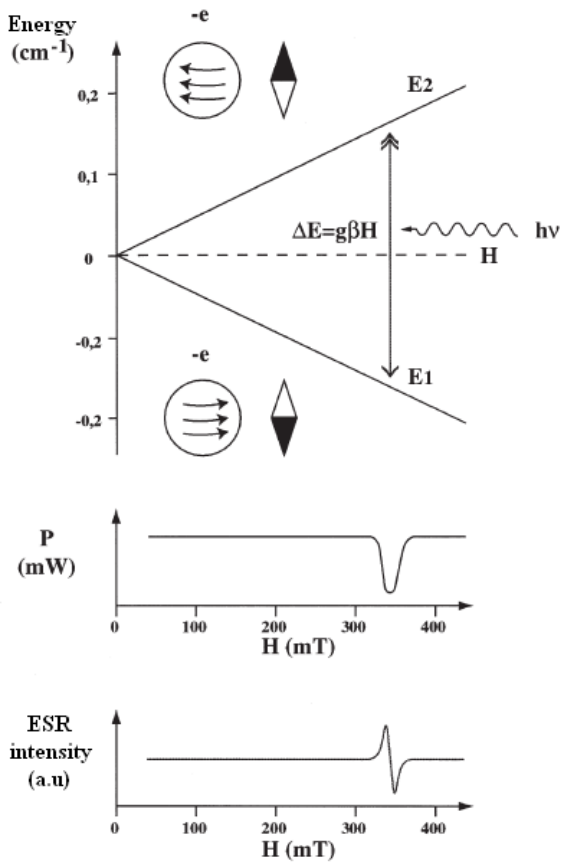

Figure II. 3. Variation of the spin state energies as a function of the applied magnetic field (Ikeya, 1993).

The absorption of energy causes a transition from the lower energy state to the higher energy state. In conventional spectroscopy, ν is varied or swept and the frequencies at which absorption occurs correspond to the energy differences of the states. Radiation in the gigahertz range is used for ESR experiments.

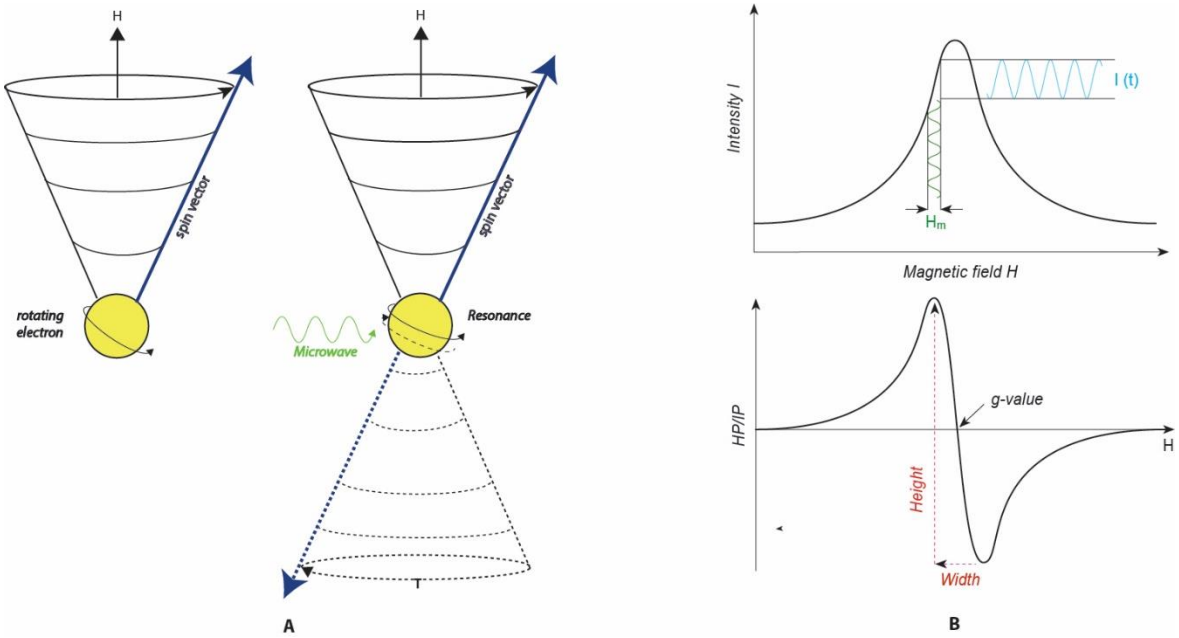

Figure II. 4. Diagrammatic representation of ESR and the application of g-values in geochronology. A - A free electron in a negative ion vacancy is subjected to a strong magnetic field, and the spin axis of the electron defines a precession encircling the direction of the applied magnetic field defined by vector H. The contemporaneous application of a microwave at right angles to the magnetic field induces resonance behaviour of the electron, resulting in a change in its direction of spin. B –The ESR spectrum and defined g-value are derived from a comparison of the microwave absorption signal compared with magnetic field intensity (H), applied in the form of an oscillating magnetic field (Hm).

II.4. Anisotropy of g factor

Another important mark for identifying a compound for resonance behind the field is the frequency, as spectra can be acquired at several different frequencies. The g-factor, being independent of the microwave frequency, is much better for that purpose. Notice that high values of g occur at low magnetic fields and vice versa.

The g-value is dependent on the orientation of the crystal field concerning the external field. For the powder samples (where the g-values are averaged) a cubic crystal shows one symmetric line, axial two ($g_{\parallel}$ and $g_{\perp}$) and rhombic three (gx, gy and gz) (Grün, 1989) (Fig. II.5)

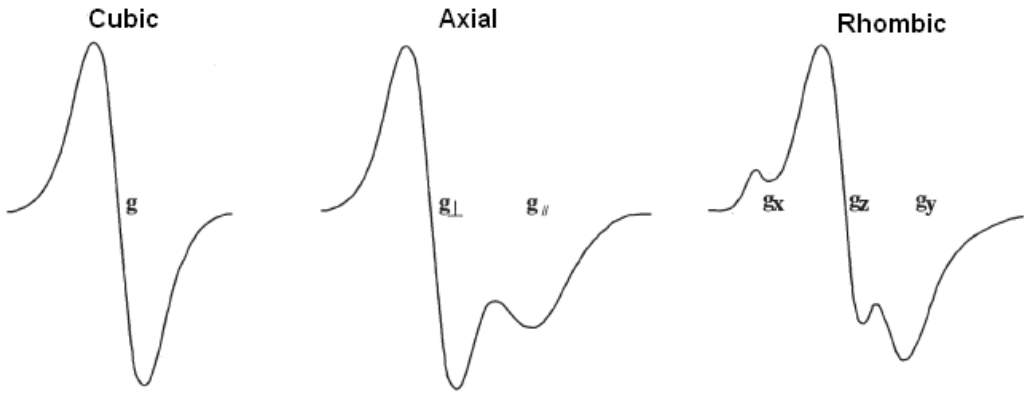

Figure II. 5. Effect of anisotropy on the ESR line from a single centre (after Grün, 1989)

II.5. ESR Spectrometry

ESR spectrometry is used to detect the attenuation of the microwave resulting from the absorption and thus to record the ESR signal of the studied sample corresponding to the first derivative of the absorption signal (Fig. II.4B). For its observation, it is necessary to obtain the resonance condition either by varying the frequency of the microwave or by varying the intensity of the magnetic field. As it is technically simpler to change the field, one operates with a fixed frequency and a variable field. The value of the magnetic field used depends on the selected frequency band. In ESR spectrometry, there are several possible frequency bands. In this work, we use the X band at a frequency of 9.75 GHz and a mean magnetic field of 0.348 T.

II.5.1 ESR Spectrometer

An ESR spectrometer (Fig. II.6) is composed of three main elements: A fixed frequency microwave generator (klystron), an electromagnet that delivers a stabilised magnetic field and a detection system capable of recording variations in the intensity of the microwave. Finally, a cooling device of the cavity formed of a liquid nitrogen circuit contained in a dewar is used during low-temperature measurements (Fig. II. 6D).

An ESR spectrum is generally defined by six parameters (Assenheim, 1966) (Fig. II. 5A, B):

1. The intensity of the signal;
2. g value of the resonance;
3. the line shape;
4. the stability of the paramagnetic centres observed;
5. the electronic splitting – fine structure;
6. the hyperfine structure.

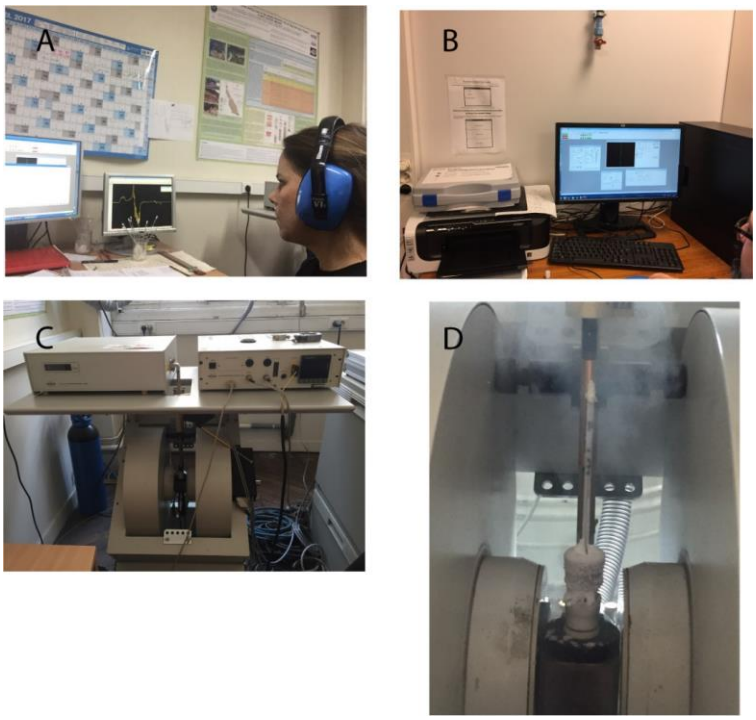

Figure II. 6. MNHN's ESR spectrometry area: A, B - ESR intensity measurement, C- EMX Bruker X-band spectrometer connected to a digital temperature control system; D - resonance cavity detail where the liquid nitrogen converted into gas go through.

During a measurement, the microwave emitted by the generator passes through the sample which is placed in a resonance cavity between the two coils of the electromagnet. During resonance phenomenon, part of the microwave energy passing through the cavity is absorbed by the sample and recorded by the detector. To amplify this signal and to eliminate disturbances, a low intensity oscillating magnetic field (Hm) generated by the Helmholtz coils is superimposed on the external magnetic field (H). This field induces a modulation of the absorption signal, and it is this modulated signal that is recorded as an ESR signal.

II.6. Paramagnetic centres

As mentioned above, the increase of paramagnetic defects in natural non-conducting minerals is the basis of ESR dating. Constant exposure to ionising radiation will cause a number of trapped electrons to increase linearly with time, provided that there is a sufficient number of defects to collect electrons, (Henning and Grün, 1983).

Various centres can usually be observed by ESR spectroscopy in quartz for geochronological purposes, (Fig. II.7), as Titanium (Ti), Aluminum (Al), Germanium (Ge) (Falguères et al., 1991, Weil, 1984).

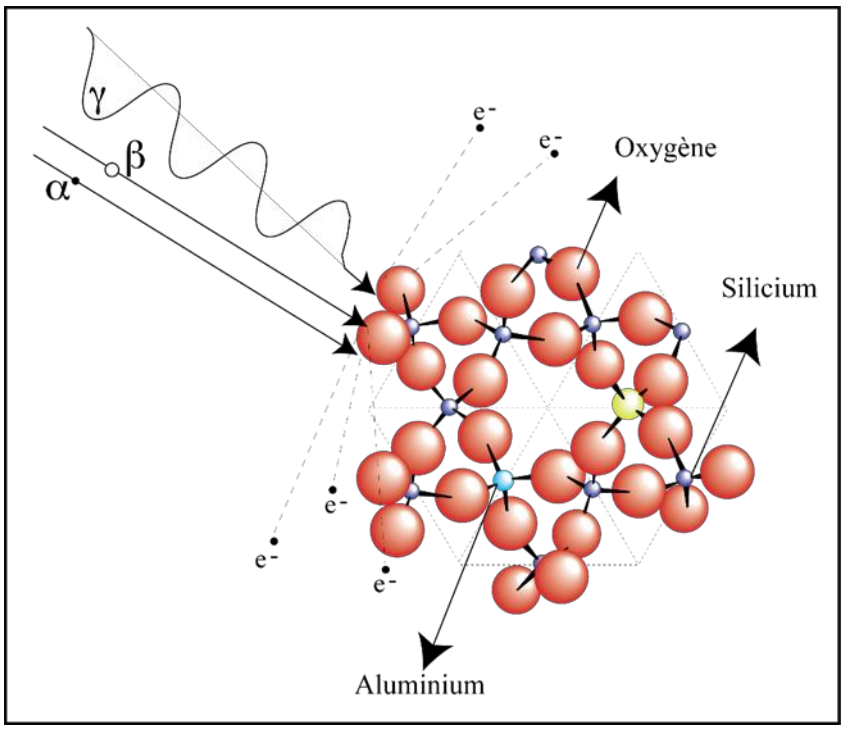

Figure II. 7. Representation of Al (blue circle) and Ti (yellow circle) atoms replacing a silicon atom in the crystalline lattice of quartz (modified from Voinchet, 2002).

However, two types of paramagnetic centres exhibit good stability over time in a crystal lattice: those resulting from an atom vacancy and those resulting from atom replacement.

Each of them has specificities in terms of radiosensitivity, thermal stability or resetting kinetics, which makes them more or less interesting depending on the geological context and the period studied (Ikeya, 1993). For example, Germanium (Ge) centre can be measured at room temperature but is hardly present in natural samples.

The Al and Ti centres are usually present in most of the Quaternary quartz grains, nevertheless, may only be observed at low temperature (<110 K) (Yokoyama et al., 1985; Duttine et al., 2002; Duval et al., 2015). The Al centre is the most studied paramagnetic centre (Voinchet el al., 2003;

Duval et al., 2012, 2015) and its behaviour is generally well known, like its radiation-sensitive (Lin et al., 2006), it is bleaching kinetic (Voinchet et al., 2015), and its main specificity lies in the presence of an unbleachable residual ESR intensity that has to be accurately considered in the evaluation of the past radiation dose absorbed by the sample (e.g. Tissoux et al., 2007, 2012)

Moreover, the Al centre (Fig. II.8,9) can be used for dating quartz grains deposited during the last million years thanks to its thermostability (Laurent et al., 1998). In this work, the dating of the samples was done from the use of the Al centre and Ti – Li centre (option D from Duval, 2015).

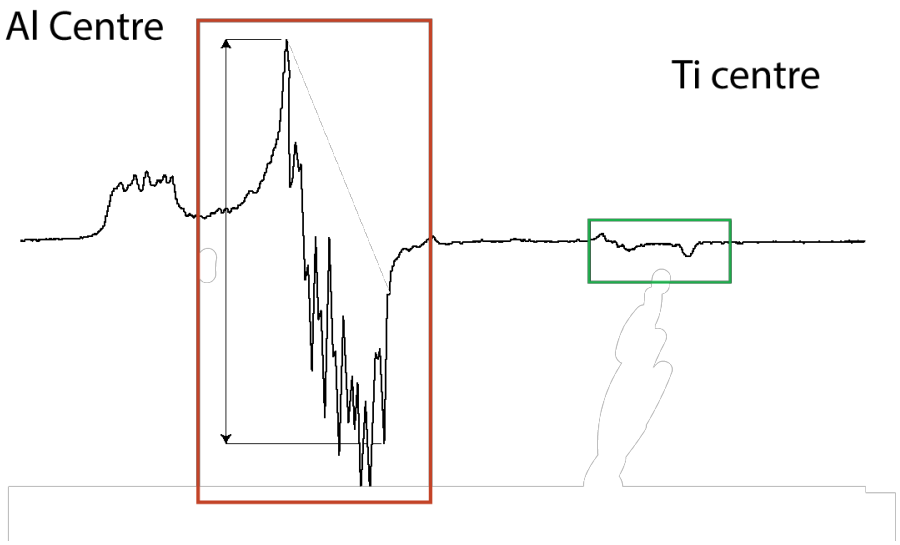

Figure II. 8. Example of ESR signals obtained at low temperature from natural quartz, showing both Al and Ti centres signal (modified from Tissoux et al., 2007).

II.6.1. Aluminium Centre

In natural quartz, an aluminium atom (Al^{3+}) replacing a silicon atom (Si^{4+}), having an extra electron, accompanies an alkali ion for charge compensation (M^{+}) such as H^{+}, Li^{+} or Na^{+} (Weil, 1984, Halliburton 1989). The defect thus formed is diamagnetic. If this diamagnetic defect undergoes ionising radiation, an electron will be displaced, and the *paramagnetic centre* will be formed.

$SiO^{4-}_{4} + Al^{3+} + M^{+} \rightarrow AlOMSi^{4+}$

Formation of a paramagnetic centre: $AlO_4(M) \rightarrow AlO^{3-}_{4} M^{+} e -$

ESR Signal of the Al centre

The Al centre has a complex ESR spectrum which is observed at low temperature (T <110 K). This hyperfine structure is the result of numerous interactions (Voinchet, 2002) between the unpaired electron and the nuclear spins of $_{27}$Al ($I = \frac{5}{2}$) and $_{29}$Si ($I = \frac{1}{2}$). The interaction between the electron and the nucleus of $_{17}$O ($I = \frac{1}{2}$) produces a hyperfine structure.

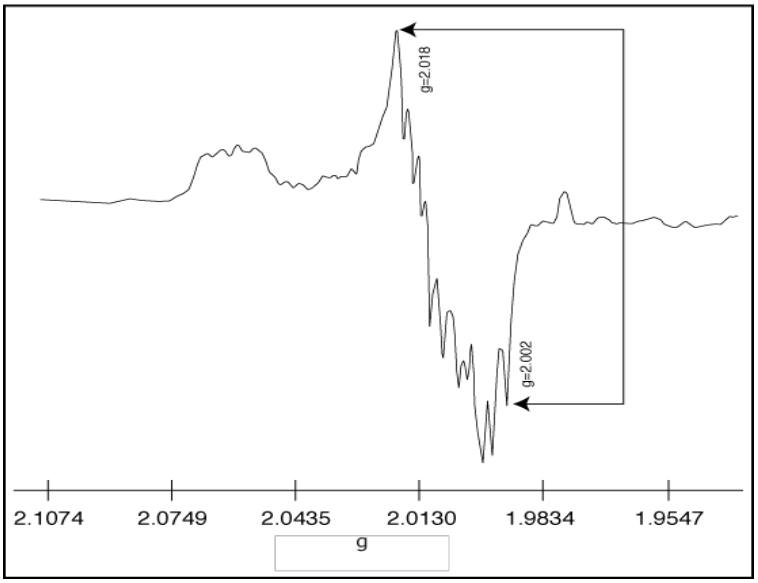

Figure II. 9. Example of ESR signal in Al centre obtained at low temperature from natural quartz (adapted from Toyoda and Falguères, 2003).

The intensity of the Al centre (Fig. II.9) is measured taking the height from the top of the peak (g = 2.018) to the bottom of the peak at g = 2.002 (Yokoyama et al., 1985).

To measure the Al centre, a microwave of 9.440 GHz frequency and 3.2 cm wavelength is used under a field of 339 mT. The power of the microwave is 5 mW and amplitude modulation is 2 G. The measurement is performed at a temperature (-180 °C) close to the liquid nitrogen temperature (-196 °C), (Voinchet, 2002).

II.6.2. Titanium Centre

A Ti atom replaces a silicon atom in the crystalline lattice of quartz without any charge compensation, creating a defect usually written as $[TiO4]^0$ (Weil, 1984) and precursor of the so-called Ti centre. When irradiation at room temperature induces some electron movements in the crystalline lattice of quartz, Ti^{4+} may trap an electron and an alkali ion for charge compensation (usually called M^+) to form a Ti centre. The paramagnetic centre is usually defined as $[TiO4/M^+]^0$, where M^+ is an alkali ion of Li^+, Na^+ or H^+ with different g factors. There are three kinds of Ti centres frequently observed, which may be called Titanium-Lithium (or Ti- Li), $[TiO_4/Li^+]$ O_2, Titanium-Sodium (or Ti-Na) $[TiO_4/Na^+]$ O_2 and Titanium-Hydrogen [Ti O $_4$ / H $^+$], (or Ti- H) centres.

The fundamental species of diamagnetic centres related to the replacement of a silicon atom by a titanium atom (Fig. II.9) of the TiO_4^{4-} is: $SiO_4^{4-} + Ti^{4+} \rightarrow TiO_4^{4-} + Si^{4+}$

Li centre has four hyperfine lines due to ^7Li (I =3/2) induces a nuclear spin (Rinneberg and Weil, 1972). Similarly, the Ti-Na centre has a sodium ion with a nuclear spin (^{23}Na I = 3/2) and is very rarely observed in natural quartz (Toyoda, 2015). The Ti-H centre has a set of two hyperfine lines due to ^1H ($I=\frac{1}{2}$) (Rinneberg and Weil, 1972). The titanium centre disappears as soon as the temperature exceeds 300°C and can regenerate by irradiation after annealing.

The practical application using Ti-Li and Ti-H centres for dating of sediment was first made by Tissoux et al. (2007) and used for date river terraces in China with an age range of 60-400 ka (Liu et al., 2011).

In this study, ESR measurement was done in both centres with the same microwave frequency, wavelength, and field. The measurement was performed at a temperature (-180 °C) close to the liquid nitrogen temperature (-196 °C). However they could be read at different measure conditions (e.g., power of the micro-wave, amplitude modulation), (Voinchet, 2002).

It is possible to separately measure Ti-Li, Ti-Na and Ti-H centres (Fig. II.10). These intensities are estimated as follows.

Each centre has a specific ESR signal: the Ti-H center is defined by three main absorption lines g1 = 1.986, g2 = 1.931, g3 = 1.915, where each one is split into a doublet due to the proton; Ti -Li is defined by a g factor with three different components: g1= 1.979, g2 = 1.931, g3 = 1.913, as well as Ti - Na, with g1= 1.968, g2 = 1.954, g3 = 1.899 (Rinnenberg and Weil, 1972; Toyoda et al., 2000;

Duval, 2015).

Ti centre may potentially offer two advantages in geochronology applications: its ESR intensity may be fully reset to zero by optical bleaching (i.e., no residual ESR intensity), and its bleaching kinetic is significantly much faster than that of Al centre (Toyoda et al., 2000), and therefore there is less uncertainty about the complete bleaching of the signal prior to burial. The Ti–Li centre takes 72 or 168 h for complete zeroing while 24 h is sufficient for the Ti–H and Ti–Na centres.

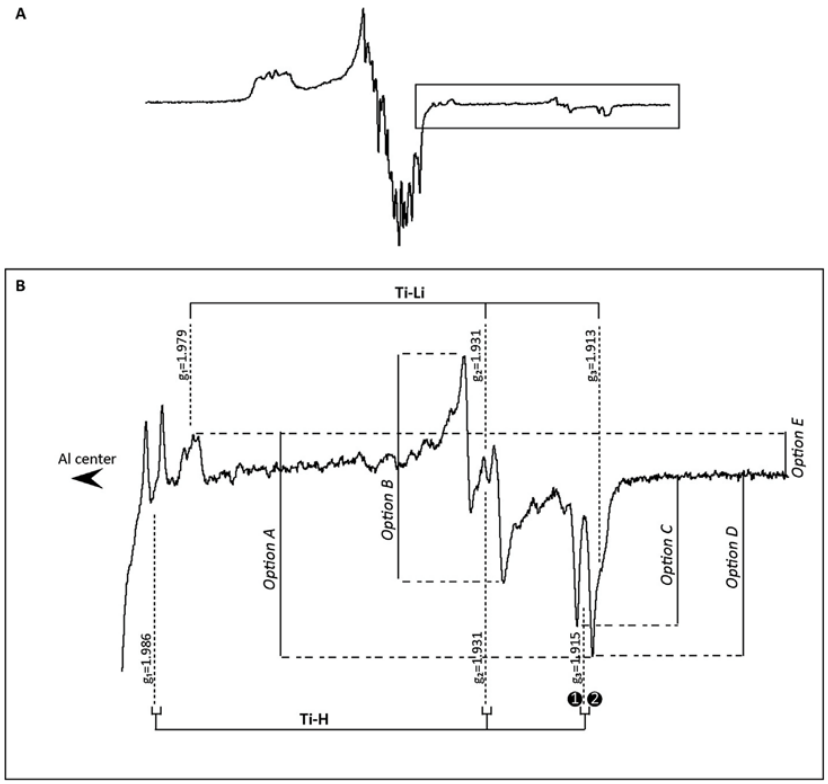

Figure II. 10. Example of ESR signal from natural quartz samples. A. ESR spectrum showing the signal in Ti centre. B- Zoom on the ESR signal of the Ti centre, except the Ti-Na signal (Duval et al., 2015).

The Ti–H and Ti–Na centres are the most sensitive to Light (Toyoda et al., 2000). However, this centre is rapidly saturated and can only be used for samples with weak palaeodoses, i.e., recent site samples and/or low annual dose (Miallier et al., 1994) and the way of measuring the ESR intensity may vary from author to other (e.g. Tissoux et al. 2008; Liu et al. 2010; Rink et al., 2007). According to Toyoda (2015), Ti centres are not always present in the quartz. Quartz in tephra and granite usually shows both Al and Ti centres, but some sedimentary quartz does not show the signal of Ti centres (e.g. loess of Chinese origin). It is usually proposed a new criterion for ESR optical dating: The D_e (in Al and Ti centres) most agree to insure accurate burial ages.

Moreover, when Al signals age is lower than Ti signal age, the Al signal may be considered the minimum burial age. According to Duval et al. (2015), from a methodological point of view, it is very important to measure both Al and Ti centres for dating purpose, which is so far the best way to have an idea about whether the Al centre has been fully bleached or not before sediment deposition. Al and Ti –Li centres were observed in all the analysed samples and measured in this work.

II.7. Optically bleached quartz for ESR

Among the available materials, the potential of quartz is essential for dating, by the presence of various paramagnetic ESR centres in its structure that allows dating different types of geological and archaeological events (Yokoyama et al., 1985; Falguères et al., 1988; Voinchet et al., 2004, 2010). As quartz is one of the most abundant minerals on the earth, many dating applications are possible in sedimentary context, (fluvial, lacustrine, marine, aeolian sediments) (Falguères, 2003; Voinchet et al., 2003, 2010; Duval, 2012). Quartz dating by ESR was proposed in the early 1970s (McMorris, 1971) but the first sedimentary quartz dating was done by (Yokoyama et al., 1985) on the sites of the Caune de l'Arago (Tautavel) and Terra Amata (Nice) in the south of France. Since then, several studies (PhD) have been devoted partly or totally to quartz (Falguères, 1986; Laurent, 1993; Voinchet, 2002; Duval, 2008) within the geochronology laboratory of the Department of Prehistory of MNHN.

The age of the sample is related to the dose of radiation that it has absorbed during its history under the effect of natural activity (D_t). ESR dating of optically bleached quartz grains is based on the same principle as Optically Stimulated Luminescence (OSL) dating: resetting the signal under sunlight exposure during the transport phase before the deposition. This reset is called *optical bleaching* (Voinchet et al., 2007). If this is incomplete, a residual dose (D_r) added to the accumulated dose since the deposit, known as post-deposit dose or equivalent Dose (D_e), will contribute to overestimating the age value (Fig. II.11). As younger is a deposit, higher will be the residual dose impact on the age (overestimation) (Voinchet et al., 2015).

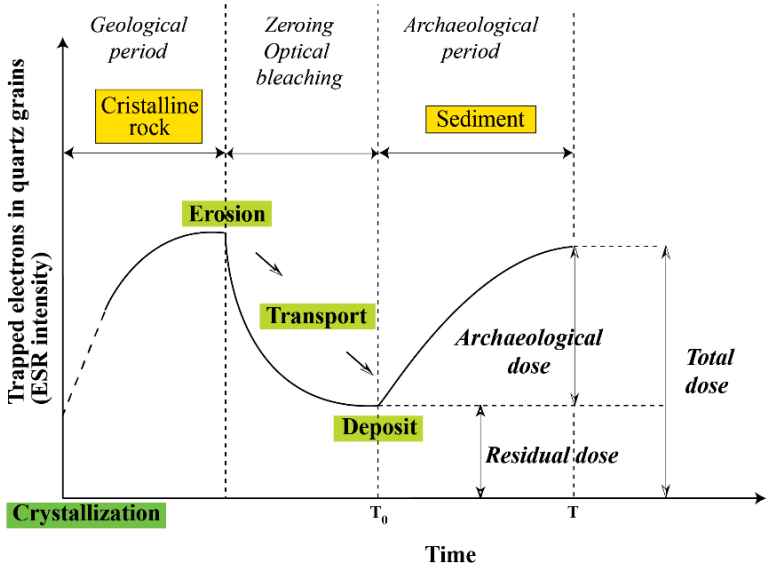

Figure II. 11. Evolution of the Al-centre ESR intensity along with the geological history of quartz grain (adapted from Bahain et al., 2007).

II.8. Grain size dependence

According to Voinchet et al. (2015), the quartz's bleaching quality depends on the selection of the grain size fractions. Very fine and coarser grains should be avoided because they are less exposed to light during transport phases (Fig. II.12). The identification of transportation modes is very important to provide the best sediments bleaching, too. The sands carried out by water are usually better bleached at the time of deposition than aeolian sands. Nevertheless, quartz grains' bleaching is insufficient in opaque water, where the U.V. cannot pass deeply through. For each transportation mode, different temporal zones were identified by Voinchet et al. (2015) (Fig. II.13).

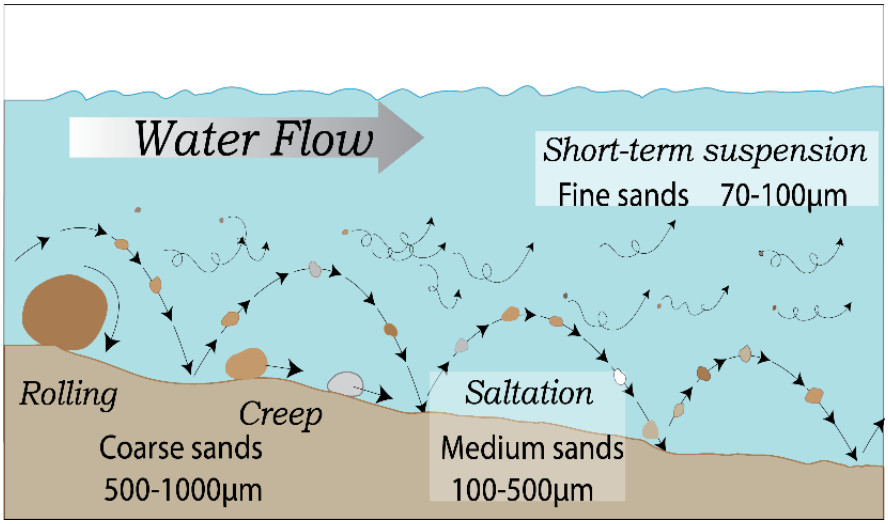

Figure II. 12. Transport modes of different grain size sand by water (modified from Voinchet et al., 20015).

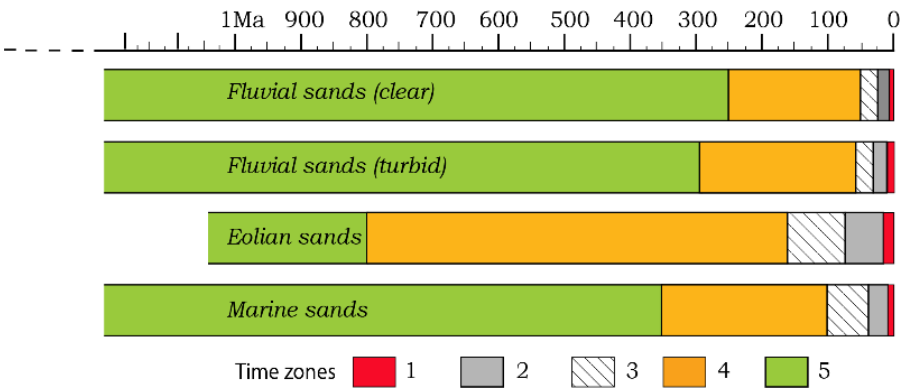

Figure II. 13. Temporal zones defined by fluvial, aeolian and marine sediments in which ages should be more accurate for ESR dating method. Legend: 1- Dr represents more than 25% of the total dose; 2- Dr ranging between 10-25% of the total dose; 3-Dr represents between 5-10% of total dose; 4 - Dr represents between 1-5% of total dose; 5- Dr represents less than 1% of the total dose (modified from Voinchet et al., 2015).

II.6. Principle of Palaeodosimetric method

II.9.1. Residual dose calculation (Dr)

The residual dose is evidenced in optically bleach quartz using Al-centres and is one contribution to D_e uncertainty. This dose is explained by the partial bleaching of a previously acquired burial dose that was not fully reset before deposition (Voinchet et al., 2003; Smedley et al., 2019) resulting from that only a part of trapped electrons is released, even after a long-time light-exposure. The ESR-intensity decreases until a plateau-value corresponds to the electrons, which cannot be "extracted" by light's energy. The "residual dose" hence obtained must be subtracted from the total dose to obtain the sample's dose since its burial (paleodose), used for age determination. As a precaution, it is not recommended to work on samples whose age would be younger than 75 ka by ESR. (Voinchet et al., 2015).

The overestimation of the ages will greatly impact sediments having a recent burial age, (e.g., Late Pleistocene sediments).

II.9.2. Age calculation with ESR

For the calculation of an ESR age is used the equation:

$$TD = \int_0^T da(t).\, dt \qquad (4)$$

where T.D. is the *total dose* of radiations received by the sample, d_a is the *annual dose rate* of natural radiations and T the age of the sample.

The total dose T.D. is proportional to the trapped electrons concentration in the sample and so to the ESR signal intensity.

Both parameters must be determined independently; hence they will be discussed separately.

II.9.2. Annual dose assessment

Annual dose (D) is the irradiation dose absorbed by the sample in one year and can be expressed as follows:

$$D = D_{int} + D_{ext} + D_{cosmic} \quad (5)$$

Where D_{int}, D_{ext} and D_{cosmic} are the internal, external and cosmic dose-rate components, respectively.

The rate of trapped electrons accumulated is proportional to the energy absorbed by a grain from the flux of radiation to which it is exposed. The energy absorbed per kilogram is defined as dose, and its unit of measurement is the grey (Gy). The natural dose-rate or annual dose is expressed as grey per thousand years (Gy Ka $^{-1}$) or milli-grey per year (mGy a^{-1}).

By determining the concentration of radioelements in sediment, it is necessary to assess the dose-rate from alpha, beta particles, gamma rays and cosmic radiation. Figure II.14 illustrates the different penetrating powers of these radiations.

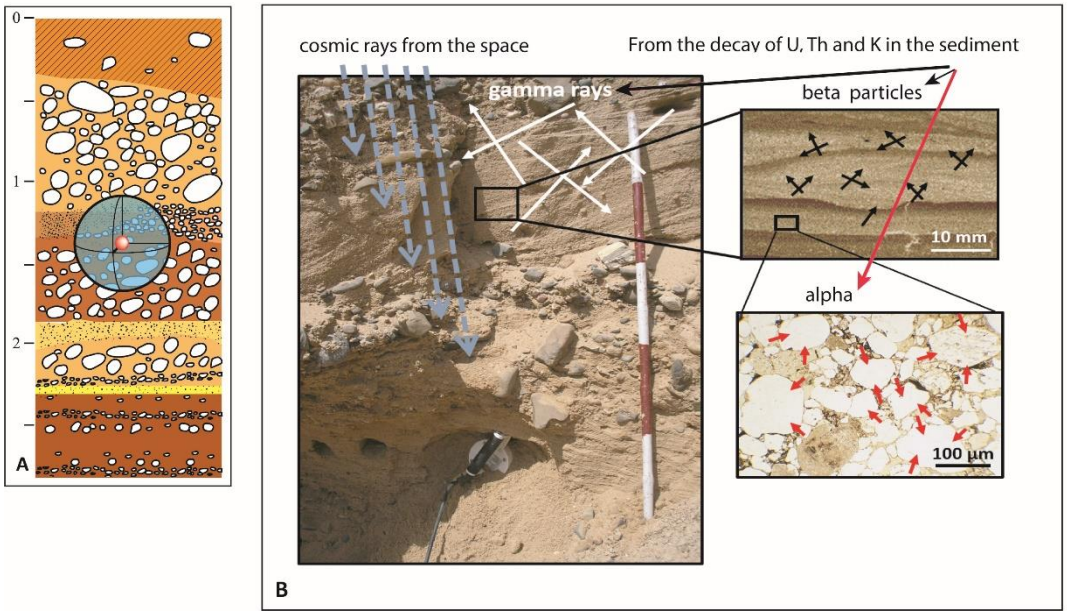

Figure II. 14. A- Schematic representation of dose rate, considering all the ionising radiations within a sphere of ~30 cm-radius (the penetration range of gamma rays in the matter); B-schematic representation of the various components involved in the natural irradiation. Radioactive interaction of a sample with its surroundings (Grün, 2006) (alfa, beta particles, gamma and cosmic rays).

In ESR dating of quartz, the gamma-ray dose rate is often the main contributor to the external dose rate and can be measured in the laboratory and on the field. The laboratory high-resolution low background gamma spectrometer can provide a dose rate measurement with precision for homogeneous deposition. Nevertheless, it is preferable to use in situ gamma spectrometer, where the uniformity of radioactivity within the 30 cm sphere of the surroundings is more representative (Fig. II.14A).

The effect of alpha particles is highly localised to within the order of 25µm (sediment) of the emitting nucleus; the beta (β) particles have a maximum penetration depth in the matter of 2-4mm and gamma (Y) rays reach a few tens of centimetres, respectively (Fig. II.14B). It is because alpha particles ionise heavily and hence lose their energy rapidly; this contrasts to the highly ionising nature of the β, γ and cosmic radiation (Aitken, 1998).

The external alpha contribution is considered negligible for the sand-sized grains by etching away alpha–irradiated rind with hydrofluoric acid to avoid uncertainties resulting from partial penetration.

Alpha contribution takes account of an etching of 10–20 μm of the grains. This difference of 10 μm in the thickness removed by the acid attack induces an age variation of 1–2% depending on the samples and on its radioactive environment (Voinchet et al., 2020).

Therefore, the dose received by the sample is mainly the result of exposure to the nuclear radiations from potassium, thorium and uranium. There are also minor contributions from cosmic rays, but it is dominant unless the overall radioisotope contribution is low, or the sample is from an altitude exceeding 1 km. $_{40}$K emits beta particles and gamma rays, while uranium and thorium chains emit alpha particles (Fig. II.14B).

The annual dose rate can be written as:

$$Da = kD\alpha + D\beta + D\gamma + Dcos \quad (6)$$

According to equation 6, the annual dose rate results from the sum of the dose rate contributed by alpha, beta and gamma rays. A correction factor (called alpha-efficiency or k-value) is applied to the measured or calculated alpha dose rate, because of the higher recombination rates, the saturation of traps close to alpha-tracks and the extensive structural damage in this area (Jonas, 1997). The k-value can be determined by the ratio of an equivalent dose of alpha rays to that by gamma rays, which is equal to the rate of defect production of the two types of radiations. For ESR dating of quartz, the k-value applied was the same as in luminescence dating, but the effect of alpha rays can be eliminated as described above.

Table II. 2. Dose rate contribution of U, Th and K (data from Guerin 2011).

Guerin et al., 2011	**alpha (a=0.1)**	**beta+IC**	**gamma**
U natural	0.2795	0.1457	0.1116
Th-232	0.07375	0.0277	0.0479
K	0	0.7982	0.2491

The internal alpha dose rate can be calculated from the content of ^{238}U and ^{230}Th.

Experimental and theoretical estimates for the attenuation within the sample and from the soil indicate that removing the outer 2 mm is adequate to avoid the influence of beta-radiation from the surrounding soil. The defect production efficiencies by the absorbed energy of beta and gamma rays are nearly the same. The external beta-rays produce radiation damage at 1 mm surface, while a part of internal beta-rays goes out of the sample 1 mm superficial.

Therefore, the average dose rate of both the internal and external beta-dose rate must be used for the surface 0.5 – 1mm of the sample. If this part is removed, only the internal dose rate may be used. However, for thin samples (less than 2 mm), the removed part should be considered in the beta dose rate determination. The β attenuation, according to the grain size and the part removed of the grains used in this work is from Brennan et al., 2003.

Table II. 3.The β attenuation according to the grain size (data from Brennan et al., 2003).

	β attenuation			
Brennan et al., 2003	50-100 μm	100-200 μm	200-315 μm	315-500 μm
U(+IC)	0.91947	0.87855	0.832	0.8912
Th (+IC)	0.8783	0.8239	0.7713	0.8408
K	0.9734	0.9472	0.9123	0.9551

II.9.3. Radioactive equilibrium and Radon loss

The contribution from naturally U and Th are provided by the radioactive chains (Fig. II.15). In one close system, each daughter formation rate is the same and equal to that of the parent. If the system is open, being an addition or removing one of the daughters by some process such as geochemical leaching, the condition is one of radioactive disequilibrium, and some of the relationships between dose-rate and concentration become incorrect. This fact is crucial and has to be considered for the age calculation. The release of gaseous daughter radon is a typical process during the radioactive equilibrium.

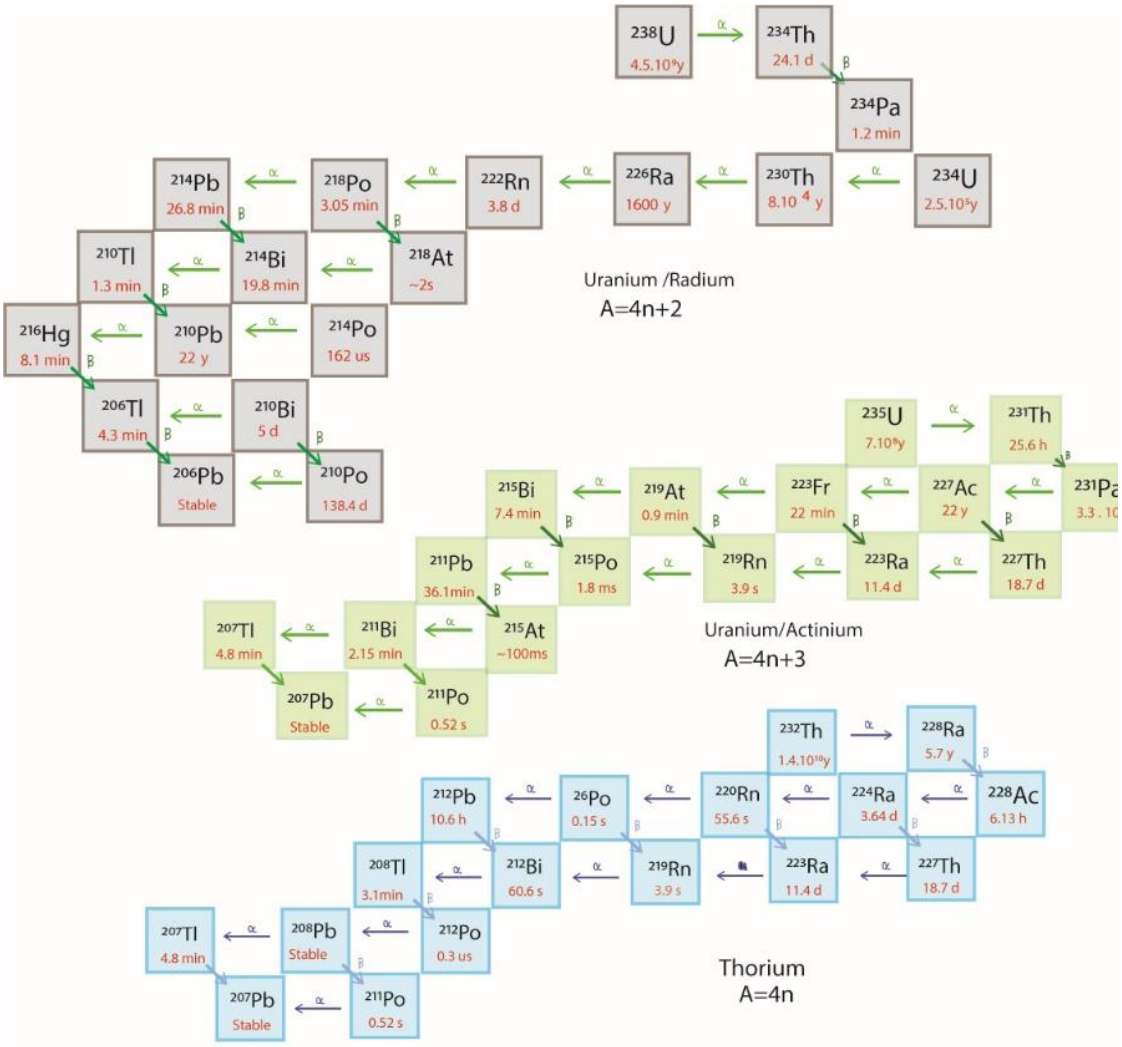

Figure II. 15. The three main decay chains (or families) observed in nature (adapted from Bourdon et al., 2003).

II.9.4. Cosmic rays

The cosmic radiation is originating outside the Solar System. Its dose contribution is attributed to two components. The top half-metre of sediment absorbs the "soft" component, and the more penetrating "hard" component is composed mostly of muons, and it is what we concerned. The hard component is slightly affected by the magnetic fields of earth and Sun than the softly. The intensity of cosmic rays has a weak dependence on the latitude at sea-level and rising from equator to 40° latitude and remaining constant for higher latitudes.

The cosmic dose rate attenuation is calculated for average sediment densities of 2 g/cm^3 and burial depth of the sample with equation 7. The intensity will rise appreciably when the altitude is above 1 km and a more strongly latitude dependent. In dose rate determination of ESR dating, the contribution of cosmic rays was roughly calculated with the following equation (Prescott and Hutton, 1988, 1994):

$$D_{cosmic} = 0.21 \times e^{(-0.07 \times (d \times \rho) + 0.0005 \times (d \times \rho) 2)} \quad (7)$$

Where: D_{cosmic} – cosmic dose; d – burial depth of the sample; ρ – the density of the sediments.

II.10. The irradiation methods

In ESR and luminescence dating, two methods are used for paleodose determination: the additive dose method and the regeneration method. The first one needs the measurement of natural ESR signal, and several aliquots of the sample are submitted to various artificial gamma-ray doses (*multiple aliquots method*) to obtain a dose-response curve, (Fig. II.16). The sample's paleodose is then extrapolated from the fitting growth curve back to zero, using a mathematical function with the least-square method.

The regeneration method needs to bleach the natural aliquot to near zero and give laboratory irradiation doses. The paleodose is obtained by comparing the natural ESR signal with the ESR signal growth curve defined from laboratory irradiation (Fig. II.16).

The additive dose method (Fig. II. 16 up) is the most used in geological and archaeological contexts because, in some datable materials, such as tooth enamel, the signal cannot be zeroed by annealing or optical bleaching methods without permanent alteration of its structure. The intensity of the ESR signal is enhanced by laboratory γ-irradiation of the natural sample.

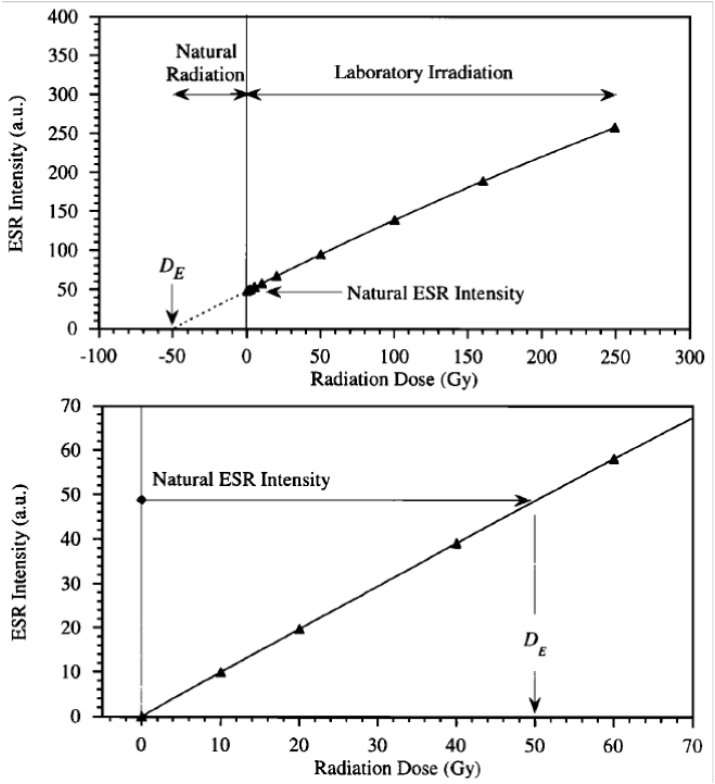

Figure II. 16. Two experimental methods for paleodose determination: additive dose method (up), regeneration method (down) (Grün et al., 1999).

II.11. Fitting functions and equivalent dose

When using the additive dose method, it is crucial to choose the most appropriate function to accurately extrapolate the paleodose. The models should be based on the energy transfer's fundamental physical mechanisms, charge transport, trapping and defect formation (Jonas, 1997). In the low dose range, the dose-response curve supralinearity may occur due to the competition between traps, but it is difficult to identify it because of the unknown model parameters (trap-concentration, cross-section) and the large uncertainties in signal measurements in that dose range (Fattibene and Callens, 2010). The Fig. II.17 shows a hypothetical dose-response curve in the case of a competing trap.

In the first's geological studies of ESR dating, linear extrapolation was used widely for fitting experimental dose points.

It describes a linear relationship between the intensity of the ESR signal (I) and the dose (D), and the linear fitting function is written as:

$$I = I_0\left(1+\frac{D}{D_e}\right) \quad (8)$$

I – measured ESR intensity; I0 – ESR intensity of natural sample; D – artificial radiation dose; De – equivalent dose (paleodose).

Previous studies concluded that the linear fitting would cause strict systematic errors when applied to a dose-response curve following a single saturating function and should be abandoned entirely in ESR and TL dating studies (Grün, 1996).

Another simplest and most common fitting function for paleodose determination in ESR dating is a single saturation exponential (SSE). This function can be explained by a simple model, that there are a given number of possible trap sites that can be filled, and the radiation sensitivity is proportional to the number of remaining unfilled trap sites. The fitting function can be written as:

$$I = I_{max}\left(1-e^{-(D+De)/D_0}\right) \quad (9)$$

Imax – saturation intensity; D – artificial radiation dose; De – equivalent dose; D0 – characteristic saturation dose

In the case of more than one trapping or if recombination centre is involved, an exponential plus linear fitting function (ESP+LIN) can be applied (Berger, 1990; Grun 1990) for paleodose determination when the radiation-induced trap production in a material is assumed to be proportion to the dose (Voinchet et al., 2007).

Exp+Line equation is done by:

$$I(D) = Isat\left(1 - e^{-D_0(D+D_e)}\right) + B(D + D_e) \quad (10)$$

ID – ESR intensity (arbitrary units); D – artificial radiation dose; De – equivalent dose; lsat – saturation intensity; B – coefficient of sensitivity

The Exp+Line and SSE fitting model are suggested for dating quartz samples.

However, the fitting results of conventional SSE fitting functions decrease with reducing dose points in high dose range. This may indicate that the SSE function does not reflect the dose-response in a high dose range (e.g., more than 10000Gy in this study).

The equivalent doses are determined by fitting of the experimental data, including the bleached, natural and irradiated points, to zero (Fig. II.17), using an Exponential+linear (ESP+LIN) function with a least-square method (Voinchet et al., 2013) and with a single saturating exponential function (SSE), using the Microcal Origin Pro 8 software and weighted by the inverse of the squared ESR intensities,1/I2 (Yokoyama et al., 1985). The ESR intensity for Ti - Li centre was measured according to Duval and Guilarte (2015). For the Ti-centre, the SSE functions were used to obtain De values of the younger deposits.

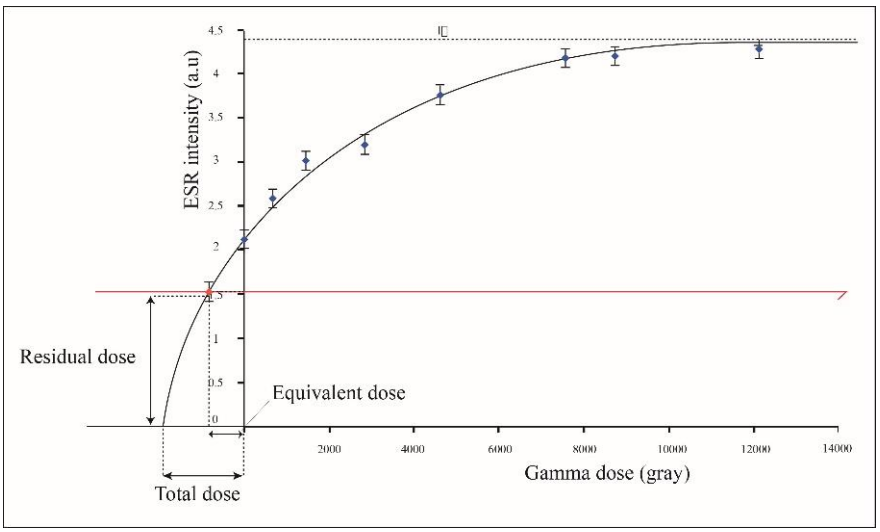

Figure II. 17. Growth curve of the natural, bleached and irradiated aliquots at different ESR intensities. The red line presents the De by subtracting Dr.(Voinchet et al., 2013)

II.12. Office Work

The office work consisted of the preliminary bibliographic analysis of previous work already done on the subject, followed by the analysis and interpretation of geological maps 1/50 000 (nº 19-C, 22-B, 22-D, 26-B, 26-C, 30-A, 30-C, 34-A, 34-C, 38-B), geomorphologic (at different scales), topographic (nº 238-A, 239, 248B, 249, 260, 272, 284, 296, 306B, 316, 326, 337, 349, 361, 374, 388, 401A, 415, 429, 430, 441B, 442, 453) and Digital Terrain Models (MDT), as well as Google Earth images of the study area for regional geological and geomorphological characterization.

II.13. FieldWork

The fieldwork was done in a phased manner to recognise the extension of the study area, using advanced field data collection and mapping methods as well as standard methods. The field investigation of the terraces to be studied was first done in the coastal staircases of Mondego Cape and the vestibular section of the Mondego River (Coimbra, Conchada, Ingote, Tentúgal and Figueira da Foz, Ervidinho) followed by surveys in the UBS 13 outcrops of Barracão, Silveirinha, N.Sra. Vitória beach and Rio Maior during September of 2017 and May of 2018. Later, the identification followed by collecting samples in Peniche, Abano beach, Espichel Cape and the vestibular part of the Tejo River was made during October of 2017 and April of 2019 (Fig. II.18;19). The sites were all photographed and georeferenced using a GPS (global position system) and, in Peniche with precision GPS, GPS-RTK (Fig. II.20C), after the recognition of each study site and surroundings, using geological (1/50 000) and topographic maps (1/25000).

As the efficiency of sediment analysis depends on the sampling method, the field data and observation were all recorded relative to location, date and sample identifier (number and name), for the careful control between field and laboratory process. Records of field measurement as textural variation, stratification, thickness, colour observations and fossil record were done.

Figure II. 18. Field view of some of the studied areas. A - N. Sra.Victória beach; B- Rio Maior; C-Ingote, D-Barracão; E- Peniche; F-vestibular section of the Mondego River.

Figure II. 19. Material and methods used in the fieldwork. A, B- PVC or metal tubes, ziplock bag (C) metal cap, hammer and hand trowel, measuring tape, portable GPS.

Figure II. 20. Material and methods used in the fieldwork. A-photo camera et A - aerial vehicle (UAV); B.;C-GPS-RTK; D-portable spectrometers gamma-ray (Nal probe connected to an Inspector 1000 (Canberra) and RS230).

To ESR sampling, conditions are very similar to those for another luminescence sampling, although it should be mentioned that ESR signal is much less light-sensitive than the OSL signals (see fig. 1 in Duval et al., 2017). Samples for D_e analysis must be collected in a light-proof container such as pre-sharpened (only sharpened on one end) PVC or metal tubes of about 30 cm in length by 6.5 cm in diameter (Fig. II.19A). After a previous cleaning of the ~5 cm section to make a freshly exposed surface, the samples could be collected (Fig. II.18; 19).

Smaller tubes can be used, but one should keep in mind that the amount of pure quartz required for ESR measurements is of ~3-4 g, i.e. somewhat higher than that for quartz-OSL dating (see an example in section 6.5 from Duval et al., 2017). A metallic cap may be used so that the tube can be quickly hammered horizontally into the outcrop (Fig. II.19B).

Following the sample collection, both ends of the tube should be sealed with tape to prevent light exposure and sediment loss. Clearly label the sample (using a permanent dark-coloured pen preferably by indicating, for example, the acronym obtained from the name of the site, year of collection and sample number (e.g., RMAI1; 2017).

Finally, the tube (sealed and labelled) should be introduced into an opaque ziplock bag labelled with the same code). If the sediment is too hard or compact to insert a tube, other sampling techniques can be used. As used in this study for Peniche marine staircase, a sediment block was carved and securely wrapped with aluminium foil and tape. Then it was placed in opaque plastic bags and bigger containers for transport to the laboratory where it was prepared under controlled light conditions. In the case of coarse-grained alluvial deposits where sand lenses are too thin to sample with a tube or a block, the sandy matrix within the gravel (or loose sediment) can also be collected in a light-proof container under an opaque plastic cover. The sediment collection surrounding the deposit for Dr calculation is equally important for accurate age determination (Fig. II.19B).

Stratigraphic columns were raised in the main outcrops, and their description was made (Fig. II.19B). In the most representative stratigraphic sections, the different architectural elements (lithofacies) were described and distinguished based on each section's sedimentological study.

The maximum pebble size (MPS) was determined, calculating the arithmetic mean of the major axes of the ten largest clasts present in each conglomerate deposit and its composition. The depositional facies and architectural elements identified were analyzed (Table II.4).

Recent faults and other tectonic deformations of the sedimentary units as the Plio-Pleistocene culminating unit and the terraces in the selected locations have been identified.

The main relief forms were interpreted from the contour lines' analysis from the analysis of the geomorphological maps. Then, this acquired information was superimposed through MDT and shaded relief models with oblique orientation. The data collected allowed the elaboration of detailed maps at several scales (e.g., Peniche, Mondego river valley and Espichel Cape).

Table II. 4.Lithofacies type (facies code based on Miall, 1985; Miall et al., 1996).

Facies code	Textures	Structures	Interpretation	Facies association
Gm	Pebble to boulder supported conglomerates (clast supported)	well-cemented sandstone and sandy grainstone	horizontal bedding stratification, imbrication	debris flow deposits; floodplain deposits; sand bed braided fluvial; longitudinal bars
Gms	Matrix supported	grading or massive (no internal stratification)	lower flow regime subaqueous traction deposits	debris flow deposits gravel-bed braided fluvial; Shallow, sand-bed braided fluvial; Proximal Sheetfloods; Intermediate Sheetfloods; Floodplain deposits (planicie aluvial); Tide Influenced Shallow, sand-bed braided channels; Upper flow regime Sand Flats
St	Very fine to coarse grained may be pebble	low angle cross stratification	dunes, lower flow regime; migration pf longitudinal bars in the channels	debris flow deposits
Sc	Very fine to coarse grained with pebble	Massive	upper flow regime with high solid charge	Broad, shallow scours
Sr	Fine grained sandstone	ripple cross lamination	Lower flow regime subaqueous traction deposits	Proximal Sheetfloods; Intermediate Sheetfloods; Floodplain deposits; Tide-influenced braided fluvial; Tide Influenced Shallow, sand-bed braided channels; Upper flow regime Sand Flats; Shoreface
Fm	Very fine-grained sandstones to siltstone	Massive, may be mudcracks and rain prints	Deposition from suspension and flocculation, subaerial exposure	Floodplain deposits with fast energy declination

II.14. Sedimentological and textural analyses

Analysis of grain size in sediments is commonly used to identify sedimentary environments, transport and facies in various depositional settings (e.g., Folk and Ward, 1957; Friedman, 1961).

The textural analysis was performed on the samples of fluvial terraces that have not yet been studied and on the coastal staircase sediment samples of Peniche, Cascais - Abano platform and Espichel Cape. The samples were labelled and placed in bags, for laboratory sedimentological characterisation as described above.

In the DCT-UC Sedimentology Laboratory, the texture and compositional analyses were performed with the following methodologies:

a) Drying of the samples in an oven for a minimum period of 48 h at ≤ 40ºC;

b) granulometric analysis, using the sieve column sieving of 1⁄2 Ø of the fraction greater than 63 μm (4 Ø), allowing to obtain the weight distributions and calculate the statistical variables – mean, grain size, standard deviation (sorting) and skewness - by the arithmetic method of the moments (Blott and Pye, 2001).

Median grain-size and mode were measured from grain size distribution curves (Fig.II.22). Laser diffraction for particle size distribution analysis of sediments was also done using a Beckman Coulter. The laser diffraction provides a precise method for the analysis and comparison of sediments. Running samples is a three-step process. The first background is measured, and then the samples are added to the instrument. Third, the data output is grouped according to standard outputs, including standard sieve size fractions for correlation statistic; percentage volume data are also used.

c) The cemented samples (e.g., Peniche; Espichel) after decarbonation with HCl (total sample), were sieved although counting on the loss of the smaller fraction (clay and silt) due to the washing of the sample after the acids attack.

d) The fractions resulting from the sieving were based on a binocular microscope observation (50x), using the methods described by Shepard and Moore (1954), establishing for each fraction, by identification of 100 grains, the percentages of each of the following classes: quartz, mica, rock aggregates /fragments and beach-rock and shells.

e) The silt and clay fractions were analysed, through the preparation of the suspension and later analysis through the laser granulometry, model LS230 (dimensional analysis from 0.04 to 2000 μm), by using a Beckman Coulter laser granulometer (I.4 D).

Before sieving, the sample was homogenised. Deionised water was used to wash the sediment.

For colour identification of dry sediments, the Munsel colour chart (5YR, 7YR, and 10 YR) was used.

The meaning of the granulometric parameters took into account Folk and Ward (1957). The mean represents the average size distribution of the entire sediments. The sand size is a direct indication of the medium of transportation and deposition. Coarse sand has the phi values between -1 and +1, medium sands vary from +1 to+2, and fine grains sand ranges from +2 and +4.

Standard deviation measures the degree of sorting that can be homogeneous or heterogeneous. Homogeneous sorting occurs when there is a very minimal level of deviation from the mean. The skewness is also related to sorting and shows the degree of asymmetry of the grains population or entire sediments distribution, and finally, kurtosis shows the degree of reworking of sediments.

To prepare the clay sediment-oriented slides, it was necessary to prepare a fine material suspension. For this purpose, ~ 100 g of sample was weighed, and the organic matter was removed with the help of tweezers, to achieve complete dispersion of the clay (Fig. II.21 A).

Then, the sample was placed (about 30g in each time) in Stirrer and added about 120 ml of deionised water. It was then left to shake for ~1 minute (Fig. II. 21B).

The liquid fraction was passed through the 63 μm mesh sieve, and the fine fraction shaken and then separated in the centrifuge until the fraction smaller than 2 μm (Fig. II. 21 C, D) (material consisting of clay only) was obtained for X-ray diffractometry.

The coarser fraction was dried in an oven and then stored for later dry sieving.

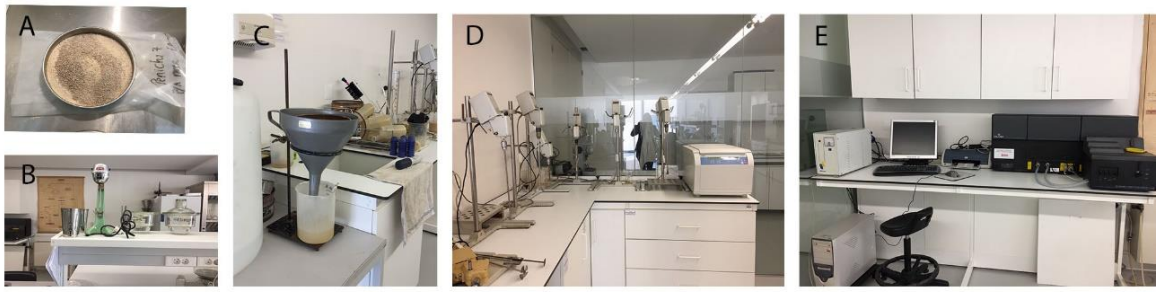

Figure II. 21. Methodologies used in sedimentological and textural analyses A. sample for granulometric analysis in an analytical sieve; B- Stirrer equipment; C-63 μm mesh sieve to separate the fine fraction from coarser ones; D- centrifuge; E-Beckman Coulter laser granulometer.

To make the silt and clay separation all the pipes must have the same weight in the centrifuge (Fig. II.21D), then it is necessary to check which is the appropriate program (normally about 2.36 minutes, at 4000 rpm rotation). After removing the < 4um fraction, we should repeat the process with 10.000 rpm until we obtain the desired concentration for DRX and clay mineral fraction analyses.

The glass slides have to be clean with alcohol and left to dry. After, the material should be pipetted from the centre of the slide not to create air bubbles. Finally, it should be placed to dry in a clean space, and after that, with the help of a needle, the slide should be labelled (Fig.II.22C).

The mineralogical analysis was carried out through the diffractometer of RX PW3710 available in the DCT-UC (Fig. II.22A). The clay mineral fraction of each sample (< 2μm), namely kaolinite (k), illite (i), smectite (s) and chlorite (c) and vermiculite (v) was identified, and the semi-quantification was made according to Reis (1983), with the following equation:

$$T = k + i + s + v + c + p + t \quad (11)$$

where,

k – half area read from the peak position of 7 Å (natural layer);

i = area read from the peak position of 10Å (ethylene glycolate layer);

s = 1/3 of the area read from the peak position between 17-18Å (ethylene glycolate layer);

v = total area read from the peak position of 14Å (ethylene glycolate layer);

c = total area read from the peak position of 7Å (warmed layer)

p= total area read from the peak position of 10.5Å (natural layer);

t = total area read from the peak position between 12- 14Å (ethylene glycolate layer).

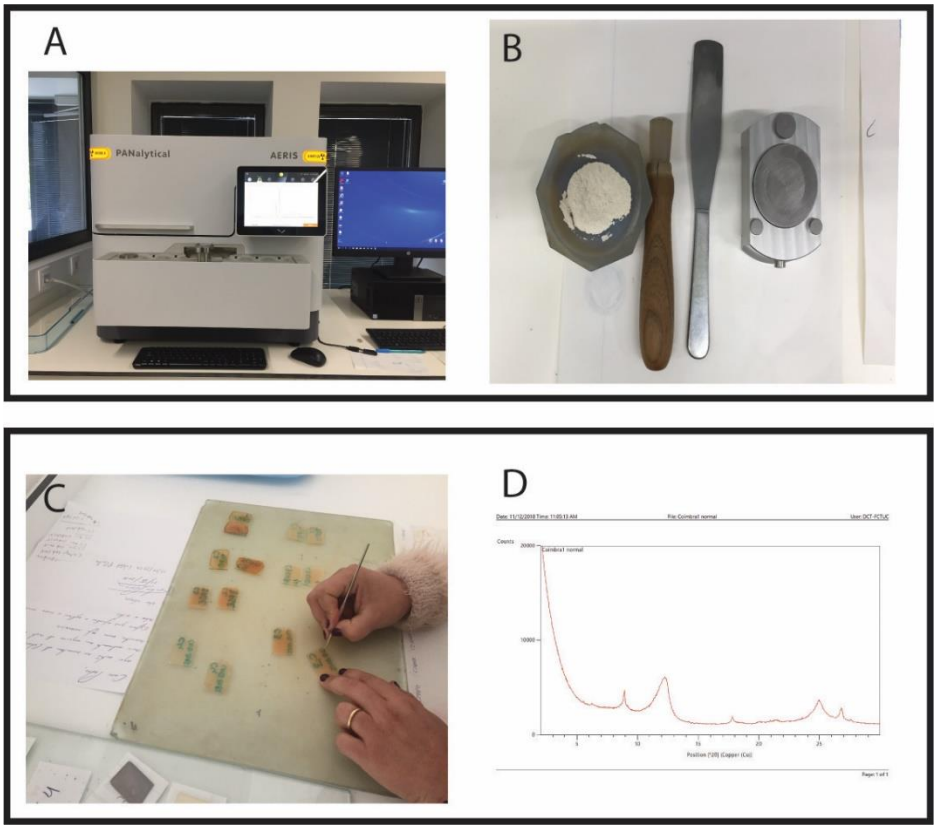

Figure II. 22. A- Analytical Aeris XRD diffractometer; B- sample preparation for measurement; C- clay slide preparation; D- example of x-ray powder diffraction.

Analyses of sediment mineral composition were also done with an X-ray powder diffraction using an Analytical Aeris XRD diffractometer manufactured by Panalytical, with a Cu tube in a 2θ range, at a scanning rate of 3º min-1, 40 kV and 15 nA (Fig. II.22D), (Department of Earth Sciences of the University of Coimbra). The mineralogical composition in non-oriented subsamples was obtained using the analytical software Highscore plus, provided with the instrument. According to the standardised Panalytical backloading system, the subsamples were prepared, which provides a nearly random distribution of the particles.

II.15. Physic-chemic preparation of the mineral fractions for absolute dating

II.15.1. Analytical Protocol

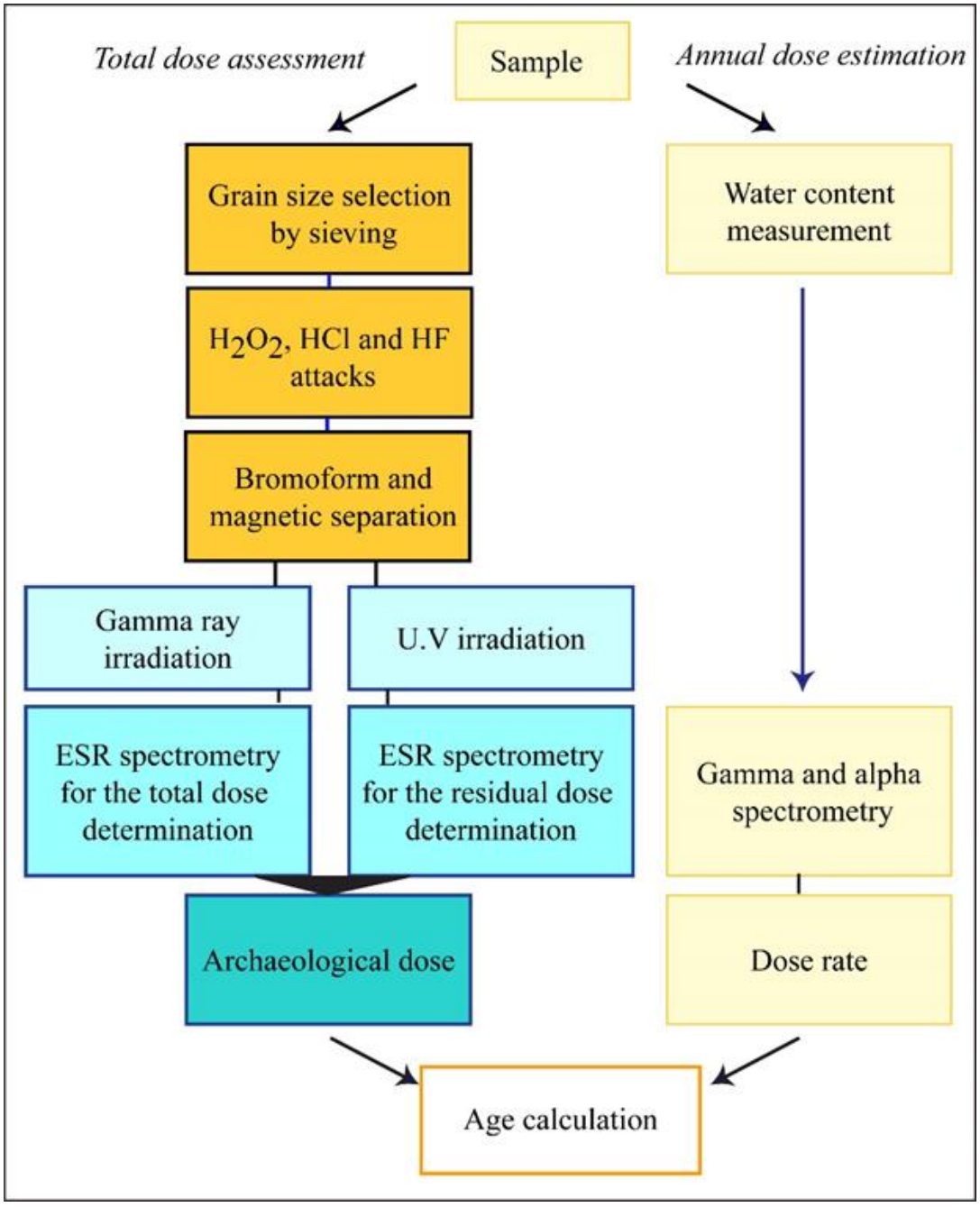

Figure II. 23. Organogram of the analytical protocol used for ESR dating method in quartz sediment samples.

II.15.2. Samples Irradiation, bleaching and ESR signal measurements

II.15.2.1. Samples Irradiation

After the sample preparation, the Multiple Aliquots Additive method (MAA) dose approach was applied. Each sample was divided into 12 multiple grain aliquots (Fig.II. 24; 25). Ten aliquots of each sample were irradiated at CENIEH (Burgos, Spain) with a calibrated Gammacell-1000 Cs-137 gamma source) emitting a 1.25 MeV γ-ray with a dose rate of 200 Gy/h, at different doses ranging from 150 to 20.000 Gy. Each tube's weight must be the same and between 50 to 200 mg (Table II.5; Fig. II.25).

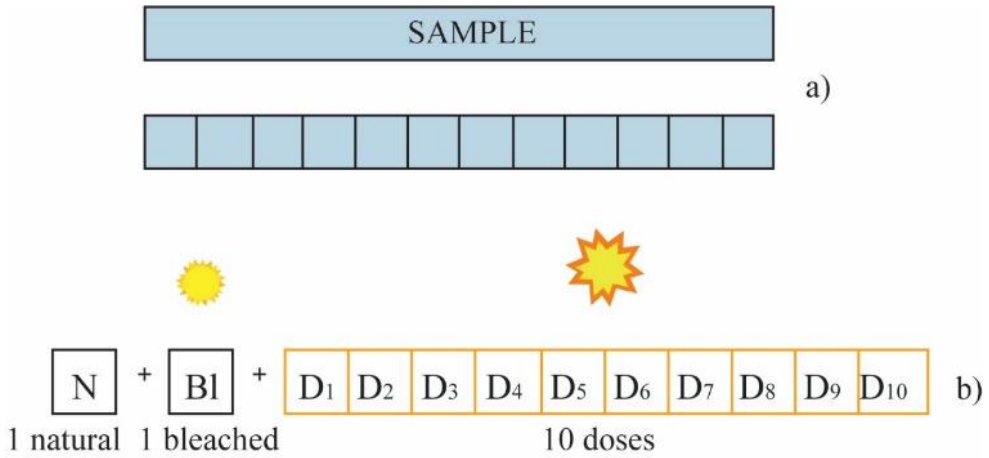

Figure II. 24. Schematic representation of sample preparation for MAA. a) sample is divided into 12 aliquots with the same weight; b) irradiation of ten samples with different doses.

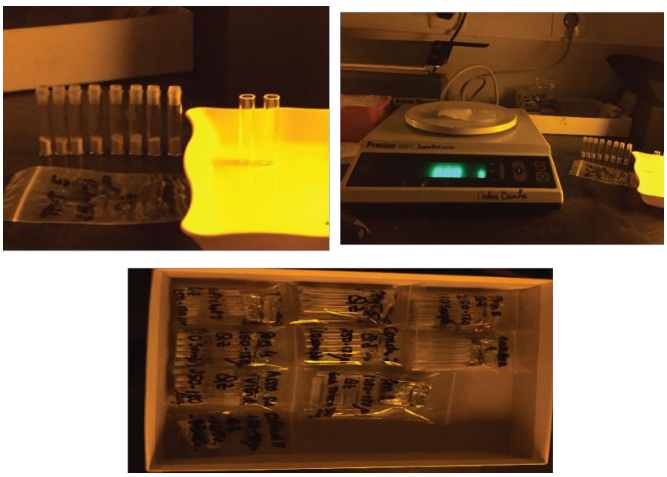

Figure II. 25. Example of quartz grain weights and separation in properly registered and packages for further irradiation process.

Table II. 5. Samples code and weight for tube irradiated in CENIEH by MAA (10 tubes/sample).

N.º	Samples code	Weight (mg)/tube	Fractions (µm)	N.º	Samples code	Weight (mg)/tube	Fractions (µm)
1	Granho1	50	250-180	**17**	Pen 1	130	250-180
2	Malhadios1	60	250-180	**18**	Pen 2	180	250-180
3	Ervi 4	200	180-90	**19**	Pen 3	130	250-180
4	PC9	70	250-180	**20**	Pen 4	116	250-180
5	Peso VG	110	180-90	**21**	Pen 5	200	250-180
6	Far8	150	250-180	**22**	Pen 8	197	250-180
7	VRV5	200	250-180	**23**	Coimbra 1	130	250-180
8	Silv1	200	250-180	**24**	Tentugal 5	171	180-90
9	Ervi1	200	250-180	**25**	Abano 6	60	300-250
10	RMaior1	200	250-180	**26**	Espichel 7	200	250-180
11	RMaior2	200	250-180	**27**	Espichel 8	200	250-180
12	Ingote1	200	250-180	**28**	Conchada 2	166	250-180
13	Bar1	200	250-180				
14	Bar2	200	250-180				
15	PVit1	200	250-180				
16	PVit2	200	250-180				

II.15.3. Bleaching

For each sample, one aliquot was preserved (natural) was optically bleached for 1000 h in a Dr Honhle SOL2 solar simulator to determine the unbleachable part of the ESR-Al signal of quartz (Voinchet et al., 2003). Three halogen lamps and one UV lamp imitating the solar spectrum were used to illuminate the quartz grains. The light intensity then received by each aliquot range between 3.2 and 3.4 105 Lux. The maximal bleaching is attempted after exposure of around 1000 hours (Fig. II.26).

The bleaching rate δbl (%) is then determined by comparison of the ESR intensities of the natural and bleached aliquots as,

$$\delta bl = ((Inat-Ibl)/Inat) \times 100 \quad (12)$$

Figure II. 26. The Dr Honhle SOL2 solar simulator equipment, scheme of each sample location and sample preparation.

II.16. ESR intensities measurements

In the Lab of MNHN, the ESR measurements were performed at 107K with a Bruker EMX spectrometer (Fig. II.6) using the experimental conditions proposed by Voinchet et al. (2004) and already described in the methodology used in each chapter. For each sample, Al and Ti centres were corrected by the corresponding receiver gain value, number of scans and aliquot mass.

The experimental conditions employed for Al centre were: 5 mW microwave power, 100 kHz modulation frequency, 1 G modulation amplitude, 40 ms time constant, and 1 scan. The angular dependence of the ESR signal due to sample heterogeneity was taken into account, measuring each aliquot three times after a 120º rotation in the cavity. This protocol was repeated 4 times over distinct days to check the reproducibility of the Al signal. A mean ESR intensity was extracted for De calculation. The ESR intensity of Al centre was extracted from peak to peak, according to Toyoda and Falguères (2003).

To obtain the De values was used the Microcal Origin 8 software, where were tested two fitting functions for Al and Ti-Li centres; the single saturation exponential function (SSE) and the Exp+lin. The data were weighted by the inverse of the squared ESR intensity ($1/I^2$).

II.17. Dose rate evaluation

The Gamma spectrometry analysis has been used to calculate the dose rate and radon loss of the samples in the present study. Utilising the method of pulse height analysis makes it possible for the direct determination of individual radionuclides in a γ-emitting sample. The gamma rays emitted by nuclides of U, Th and their daughters are counted. Since gamma rays are more penetrating than alpha particles, they can be measured as they are emitted from bulk samples, without any chemical separation. This allows the use of non-destructive gamma-ray analyses for the dating of sediments. However, some correction must be made for the effect of the shape of the object on the absorption and counting of the weaker gamma rays. The precision of this method is about ±10%.

In the Sedimentology Laboratory (University of Coimbra), the total sample was dried, ground to a particle size of < 2 mm, homogenised, and then quartered to obtain a representative sample of the material to be analysed.

At the "Département de Préhistoire du Muséum National d'Histoire Naturelle" in Paris, the radiation was measured from the knowledge of the radioisotope activities of the U-238, U-235, Th-232 and K-40 and determined by high-resolution low background gamma-ray spectrometry to derive external alpha, beta dose rate components using the dose rate conversion factors from Guérin et al. (2012). For that, ~100 g of raw sediment from all samples were analysed (Fig. II.27) and values were corrected for α and β attenuation of spherical grains (Brennan et al., 1991; Brennan, 2003). The cosmic dose rate was determined according to Prescott and Hutton (1994).

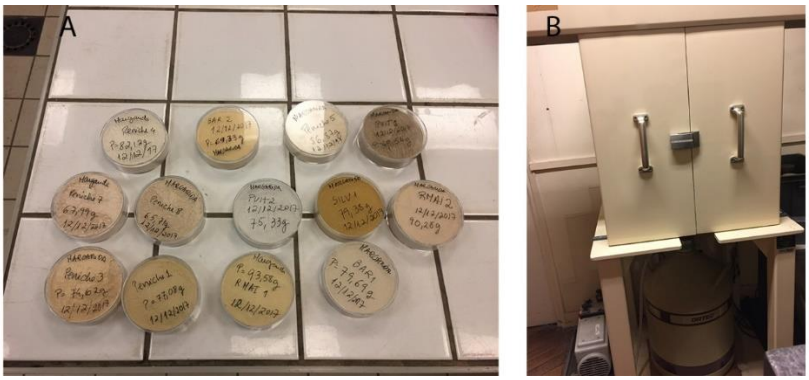

Figure II. 27. A - Samples weighed and labelled for the gamma-ray spectrometry measurements; (B) - gamma spectrometer.

Due to the size of the grains used for dating (the most with 180-250 μm) and the fact that quartz contains very few radioactive impurities, the internal dose was considered negligible, and only the external dose was considered.

The same procedure with a high-resolution gamma-ray spectrometer Ortec equipped with a Ge detector, protected by a lead castle with a NaL spectral analysis software GammaVision v8 was done in the Natural Radioactivity Laboratory, to compare the data in some samples (namely from Rio Maior, Peniche, Barracão, Espichel). The samples after screening at a granulometry of less than 2 mm were placed in Marinelli type beakers with 1000 g, where they stayed approximately 21 days in order to reach the balance in the decay series to obtain the spectrum.

Marinelli beakers are made of plastic and complying the requirements of the standard: low absorption of gamma radiation; transparent, volume to achieve maximum efficiency, impermeable to water and also to gases, wide opening and non-breakable (Fig. II.28A). The top of the sample has to be perfectly horizontal and closed hermetically to extract the air.

All the samples were packed to avoid variations in volume over time.

For each sample, a data acquisition time corresponding to 36 000 seconds (10 hours) was used. The uncertainties are dependent on the concentrations of the radioisotopes being estimated sample by sample.

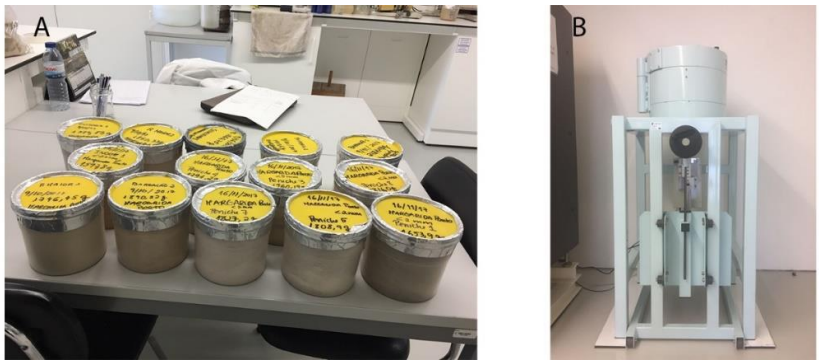

Figure II. 28. A. - Marinelli type beakers filled with each sample. B - high-resolution gamma-ray spectrometer of Radioactivity Laboratory (University of Coimbra).

II.10. Water content

The wetness degree in the sediment was measured, and the average wetness during the whole burial history of the sample was estimated, to minimise the error on the age estimate. In this study, the deposition's moisture was variable due to the environmental changes and the fluvial and filling process. The effect of estimated water content to the sample age was considered. For this purpose, the sample was dried by the natural environment, crushed and quartered to obtain the necessary amount of sediment. The sample was weighed, and water was added until the entire interstitial space be completed. After that, it was reweighed against the water, and the value was recorded. Water contents (W%) were estimated by the difference in mass in the sample with water and after dried for a week in an oven at 50 °C.

Water in the sediments absorbs part of the radiation that would reach the grains, so the dose rate in the sediment containing water is less than that when it is dry, and if this effect is not take in account, may cause inaccuracies in the age calculation. In the DATA program (an ESR age calculation software), the calculation of water attenuation coefficients is according to the formula of Grün (1994).

CHAPTER III. ELECTRON SPIN RESONANCE DATING OF THE CULMINANT ALLOSTRATIGRAPHIC UNIT OF THE MONDEGO AND LOWER TEJO CENOZOIC BASINS (W IBERIA), WHICH PREDATES FLUVIAL INCISION INTO THE BASIN-FILL SEDIMENTS

Adapted from: Electron spin resonance dating of the culminant allostratigraphic unit of the Mondego and Lower Tejo Cenozoic basins (W Iberia), which predates fluvial incision into the basin-fill sediments

Gouveia, M.P., Cunha, P.P., Falguères, C., Voinchet, P., Martins, A.A., Bahain, J.J., Pereira, A. 2020.

Accepted: 14 November 2019

Abstract

The Cenozoic basins of western Iberia have a culminant allostratigraphic unit (referred as UBS13) which records the beginning of Atlantic drainages and predates the stage of fluvial incision that led to the development of the present drainage networks. However, the available numerical dating is quite limited and restricted to the lower-level deposits. Therefore, this study uses for the first time the electron spin resonance (ESR) method to date this culminant unit in the Mondego and Lower Tejo Cenozoic basins of Portugal. The depositional age of this unit is supposed to lie between c. 3.8 Ma (basal deposits) and, probably, c. 1.8 Ma (top deposits). The Al centre provided reliable ESR data. According to the results obtained and considering the existing independent dating of the Vale Farpado site (3.8-3.6 Ma), the ESR ages obtained for the UBS13 basal deposits (3.0 to 2.3 Ma) underestimate the probable burial age. The ESR ages (Al centre) obtained for the UBS13 top deposits indicate a very probable age of c. 1.8 Ma, even if the ESR age of some of the studied samples may underestimate their burial age. Thus, this result assumes an international relevance, as it constitutes the first numerical age obtained for the uppermost levels of the Cenozoic basins of the western Iberia, which predate the stage of fluvial incision in response to the Atlantic Ocean base level.

Keywords: ESR dating; transition infill/dissection; Pliocene; Lower Pleistocene; western Iberia.

III.1. Introduction

For the foreseeable future, the forecast of an increased intensity of global warming raises concern about sea-level rise, as the primary outcome of the melting process of large fractions of Greenland and Antarctica ice sheets. Despite its apparent novelty, there have been previous warming periods in geological time, as in the interglacial periods, (Roucoux et al., 2006; Jiménez-Moreno et al., 2010; 2019) which offer guidance for understanding the magnitude of a possible sea-level rise in the future. In this context, the Iberian Western Margin preserves a good record of glacial-interglacial climate change (Pedoja et al., 2018). Furthermore, the Pliocene represents the final shift from warmer paleoclimates, to the glacial-interglacial periods of the Quaternary (e.g. Dowsett et al., 2012; Loutre and Berger, 2003) and the Western Iberian Margin is an excellent natural laboratory for exploring coastal to fluvial Earth systems.

Climatically, the Pliocene can be divided into two periods, Early and Late, the first with the warmest temperatures, centred at c. 3.7 Ma, and subsequent climatic cooling during the Late Pliocene, resulting in a high-magnitude climate variability, pre-empting the Pleistocene glacial/interglacial cycles (Haywood et al., 2011). In general, the Pliocene represents an accessible example of a world that is similar in many respects to what models estimate that Earth could become in the future (Jansen et al., 2007; Haywood et al., 2011; Raymo et al., 2011). Moreover, the Mid-Pliocene is sufficiently recent for the continents and ocean basins to have nearly reached their present geographic configuration.

A major research line of global-scale reconstruction has been focused on atmosphere−ocean interaction (Lisiecki and Raymo, 2005; Roucoux et al., 2006; Rodrigues et al., 2011). However, terrestrial records also offer a promising alternative proxy data, providing relevant insights to understand the climatic and environmental changes that occurred during the Pliocene and Pleistocene (e.g. Rodrigues et al., 2011; Salzman et al., 2013; Rohling et al., 2014; Haywood et al., 2016;Panitz et al., 2016).

The location of the Cenozoic basins of western Iberia, near the East Atlantic margin (c. 40º N 9ºW), has a significant geological importance, as it allows the use of detailed sedimentary and biostratigraphic information, critical to the study of the major tectonic, climatic and eustatic events affecting the North Atlantic margin (Martín et al., 2009; Cunha et al., 2016). Western Iberia, due its geographic position, transitional between Northern Europe and Africa, and part of the Western Mediterranean environment, is a strategic area for the analysis of the processes associated with climate variability in different regional contexts.

In the Mondego and Lower Tejo Cenozoic basins, located in Portugal, (Fig.1) the allostratigraphic unit UBS13 (Upper Pliocene - Lower Pleistocene; Cunha, 1992a, 1992b) is culminant unit of the sedimentary infill and consists of marine and continental sediments (e.g., Cunha et al., 1993; Pais et al., 2012; Cunha, 2019).

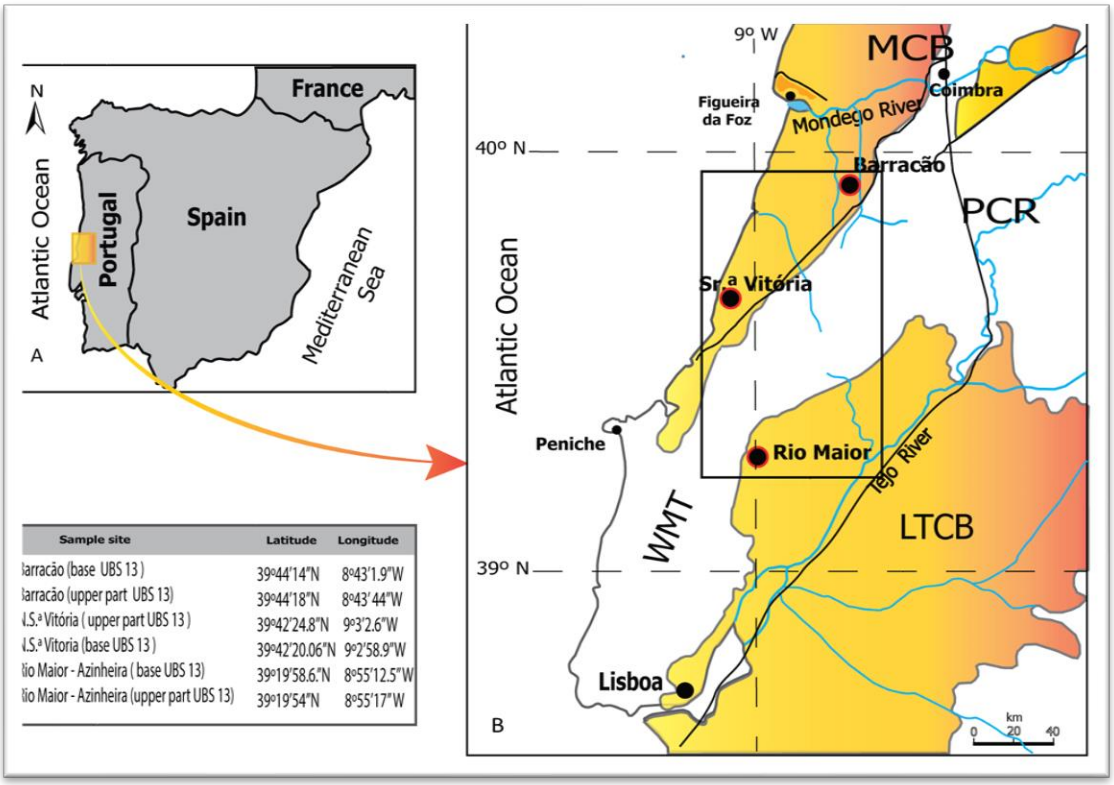

Sample site	Latitude	Longitude
Barracão (base UBS 13)	39º44'14"N	8º43'1.9"W
Barracão (upper part UBS 13)	39º44'18"N	8º43'44"W
S.ª Vitória (upper part UBS 13)	39º42'24.8"N	9º3'2.6"W
S.ª Vitoria (base UBS 13)	39º42'20.06"N	9º2'58.9"W
Rio Maior - Azinheira (base UBS 13)	39º19'58.6"N	8º55'12.5"W
Rio Maior - Azinheira (upper part UBS 13)	39º19'54"N	8º55'17"W

Figure III. 1. Study area, comprising the sampled sites (red circles) of Barracão (Pombal) and Sr.ª Vitória (Marinha Grande), in the Mondego Cenozoic Basin (MCB), and of Rio Maior, in the NW margin of the Lower Tejo Cenozoic Basin (LCTB and the respective table with the geographical coordinates of the sampled sites; W.M.T – Western Mesozoic Terrains; P.C.R. – Portugal Central Range (modified from Silva et al., 2010).

The base of UBS13 is a sedimentary discordance recorded in the Iberian Cenozoic basins and resulting from a tectonic phase at c. 3.7Ma (e.g., Cunha, 1992b; Calvo et al., 1993). The top of the UBS13 unit, which records the reversal of the sedimentary basin infilling and the beginning of fluvial incision (Cunha 2 019). The later incision stage is mainly recorded by Pleistocene marine and fluvial terraces that are inset into the culminant surface to lower levels than that of the UBS13 unit.

Notwithstanding this, the chronostratigraphic framework of the UBS13 unit needs to be significantly improved. For the basal deposits of UBS13, the chronological data are supported by biostratigraphy based on calcareous nannofossils and molluscan assemblages from the Vale do Freixo site (near Carnide; Mondego Cenozoic Basin), which indicate for this basal level an age of c. 3.65 Ma (Cachão, 1989, 1990). However, some pectinid shells from the same level, analyzed for 87Sr/86Sr isotopes, were dated to 3.79 ± 0.27 Ma (Silva, 2001) and 4.38 ± 0.27 Ma (Silva, 2010. Moreover, in the Mondego and Lower Tejo Cenozoic basins are persist other sites containing the lowermost deposits providing mollusc shells ascribed to the Late Pliocene, such as Praia da Vitória, Águas Santas (Choffat, 1889, 1903; Dollfus and Cotter, 1909; Cachão, 1989; Silva, 2001), Alfeite (Dolfus and Cotter, 1909), Fonte da Telha; (Zbyszewsky, 1943), Carnide, Vale Cabra and Vale Farpado (Teixeira and Zbyszewsky, 1951; Rocha and Ferreira, 1953).

In contrast, the age of the UBS13 uppermost deposits is supported only supported by (i) a palaeomagnetic study at Rio Maior (Lower Tejo Cenozoic Basin, which at observed a major magnetostratigraphic reversal assimilated to the Gauss – Matuyama boundary (2.58 Ma) at a stratigraphic level located c. 17 m below the top surface of the unit (Diniz and Mörner, 1995), and (ii) a probable age estimate of c. 1.8 Ma, obtained by extrapolation based on dated terrace staircases of the Lower Tejo and Mondego Cenozoic basins (Cunha et al., 2016). Cosmogenic dating (burial isochron) was used previously to date the UBS13 at the Alvalade Cenozoic Basin, namely at Vila Nova de Mil Fontes (c. 4 Ma; Ressurreição, 2018) and Sagres promontory (c. 1.8 Ma; Figueiredo, 2014). Palynological studies also proposed the latest Zanclean to Gelasian age for the aggradation interval of UBS13 (Diniz, 1984; Vieira, 2009, 2018).

The present work uses ESR dating of samples collected from the UBS13 unit, being the first attempt using this palaeodosimetric method for Late Pliocene to Gelasian deposits in Iberia. In Portugal, a single previous study used ESR dating on terraces of the Lower Tejo River (Rosina et al., 2014). The aims of this study are (i) to obtain ESR ages from the uppermost and basal sedimentary deposits of the allostratigraphic unit UBS13 in selected outcrops of the Mondego and Lower Tejo Cenozoic basins (in coastal and inland SW sectors), (ii) to verify if the age of the UBS13 is identical both in the two basins and (iii) to provide an ESR age for the beginning of incision.

III.2. Geological setting

During Lutetian times, in western Iberia, the Pyrenean orogeny started to generate the Mondego Cenozoic Basin and the Lower Tejo Cenozoic Basin (e.g., Cunha, 1992a, 2019; Pais et al., 1992). Until the middle Tortonian (c. 9.6 Ma), their evolution was marked by the slow and gradual erosion of the Hesperian Massif, under continuous tectonic deformation and climatic conditions (semi-arid to subtropical climate with long dry season) that favoured the planation of the basement and the transport of feldspathic sands to the basins. In the Late Miocene, the climate was hot with strong inter-seasonal amplitude, and the sedimentation was expressed by endorheic and alluvial fans at the scarps foots of active faults (Cunha et al., 2019).

According to the records of fossil pollen content of the UBS13 sedimentary succession (Diniz, 1984, 2003; Vieira, 2009, 2018; Pais, 2010; Vieira et al., 2017), the hot and wet climate prevailed during the latest Zanclean and the Piacenzian, with little seasonal contrast and precipitation that should exceed 1000 mm per year in the less hot seasons. The pollen content in the upper part of the succession records a transition to a less forested environment and cooler climate during the Gelasian.

A marine incursion took place on the Atlantic coast of Portugal during the latest Zanclean – earliest Piacenzian, reaching inland areas located c. 28 km from the present coastline (e.g. Zbyszewski, 1949; Teixeira and Zbyszewsky, 1951, 1954; Teixeira, 1979; Ferreira, 1981; Cunha, 1992, 2019; Cunha et al., 1993; Ramos, 2008).

This incursion can be related with a high eustatic sea level of 40–60 m above the present sea level (a.s.l.) (Dowsset et al., 1996) or 20–25 m (Miller, 2005, 2011). During the following high-stand sea-level conditions, a large shallow sandy littoral zone developed, with fan-deltas environments sourced by an abundant siliciclastic sediment supply. In the Mondego and Lower Tejo Cenozoic basins, the main fluvial drainage axes became the ancestors of the modern rivers (Pais et al., 2012).

According to Cunha et al. (2012, 2016), the incision stage began by 1.8 Ma (Gelasian-Calabrian) when the climate became colder, with the regional tectonic uplift due to Iberia-Africa convergence (Cunha et al., 2012, 2016; De Vicente et al., 2011, 2018) and the eustasy (sea level-lowering) constituting primal determinants for the progressive evolution of the river systems draining to the Atlantic Ocean, (strong incision, regressive erosion and stream piracy).

Onshore, the Mondego Cenozoic Basin is c. 180 km large and extends inland ca. 90 km (Fig. III.1). In general, the UBS13 unit (Pliocene and Lower Pleistocene) is well represented (Fig.III.2) with, approximately, 20 m of thickness at south of the Mondego River, but syn −depositional tectonic activity was responsible for local tilting, vertical fault displacements and the development of fault bounded small sub-basins where this units can reach a thickness of 40 -70 m.

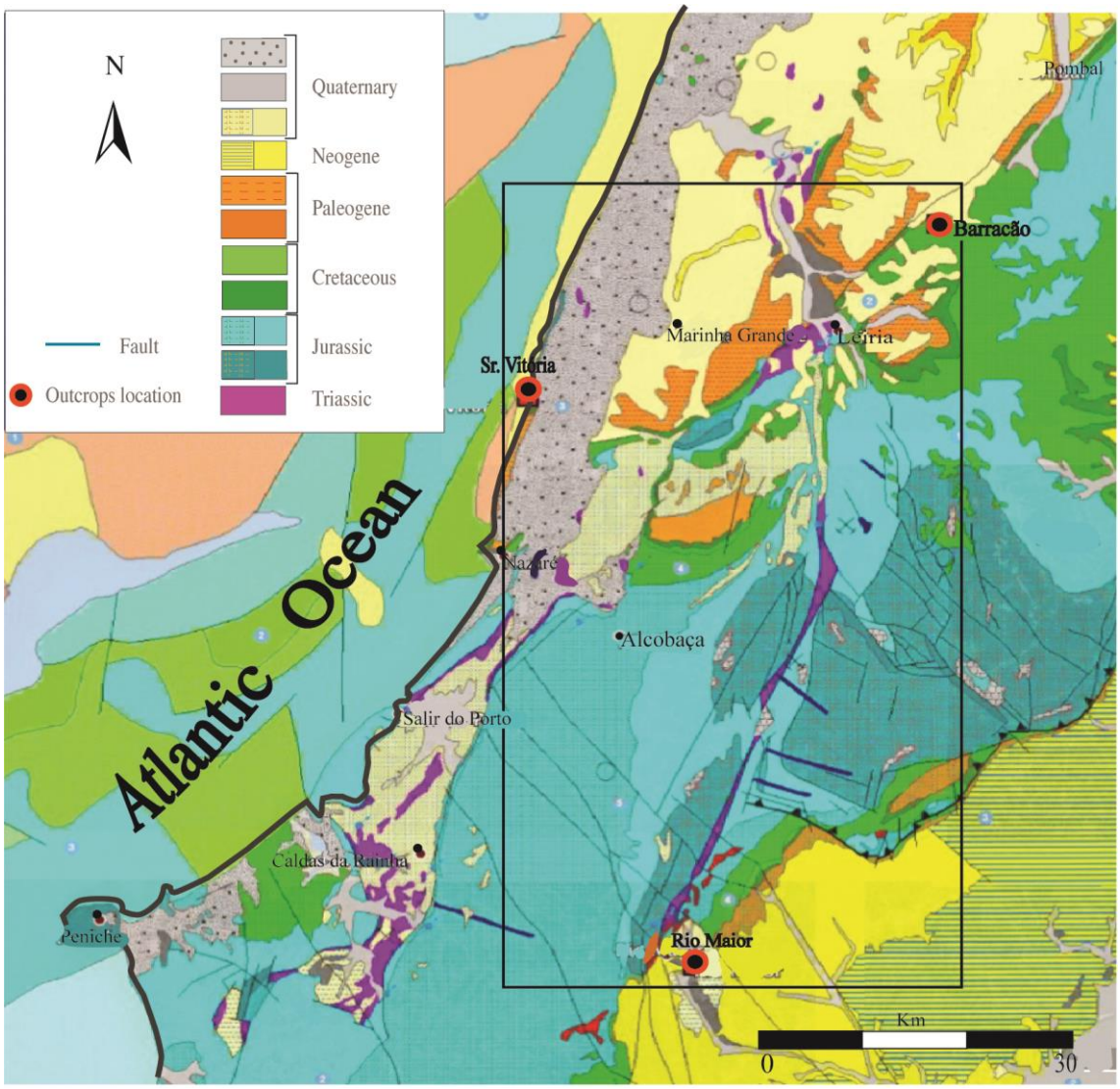

Figure III. 2. Geology of western Central Portugal with the location of the sampled sites (Geology adapted from Geological map of Portugal, 1:500 000, LNEG).

In the region, the UBS13 sequence unit is generally composed of shallow marine sediments, nearshore sediments and continental sediments documenting a regressive succession that comprise three lithostratigraphic units (Barbosa, 1983; Cachão, 1989; Cunha, 1992a; Cunha et al., 1993, 2009; Ramos and Cunha, 2004; Ramos, 2008) (Fig. III.3):

1 - Carnide Formation, consisting of a lumachella followed by fine to very fine yellowish silty micaceous sand, of marine sublittoral environment; some levels of well-rounded pebbles are interbedded with a low angle, planar stratification coarse sands, of beach face environment.

2 - Roussa Formation, composed by medium to fine whitish sands, with large scale planar or trough cross-stratification, of deltaic environment.

3 – Barracão Group, consisting of clays intercalated with sands (palustrine) to sands and gravels deposits (upper fan-delta and fluvial environments) (Cunha et al., 1993; Ramos, 2008; Pais et al., 2012; Dinis and Oliveira, 2016). The Barracão Group has a tabular geometry, with its thickness increasing gradually towards the west. Syn-depositional tectonics seems to have been responsible for local variations in thickness (up to 40–70 m) and facies.

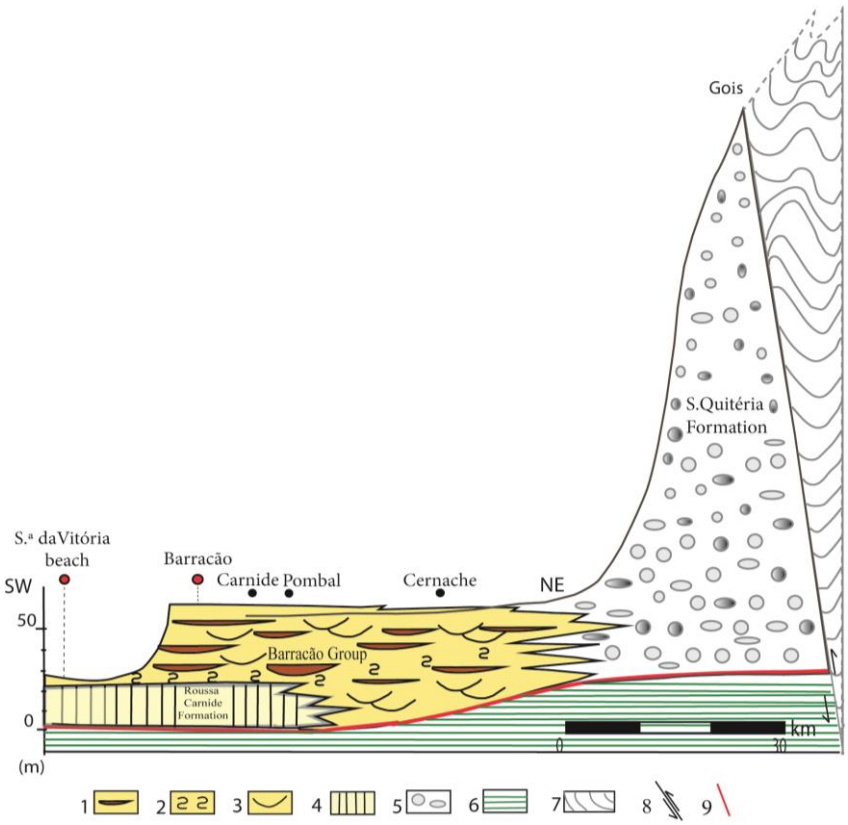

Figure III. 3. Schematic geological cross-section through the uppermost part of the Mondego Cenozoic Basin infill, showing the lithostratigraphic units that constitute UBS13. Legend: 1- alluvial silts and clays; 2 - marsh and swamp sediments (sands and silty clays); 3 - alluvial sandstones; 4 - marine sandstones; 5 - alluvial gravels and sands; 6 - Mesozoic and Cenozoic substratum; 7- metamorphic rocks; 8- Lousã fault; 9 - discontinuity (adapted from Cunha et al., 1993).

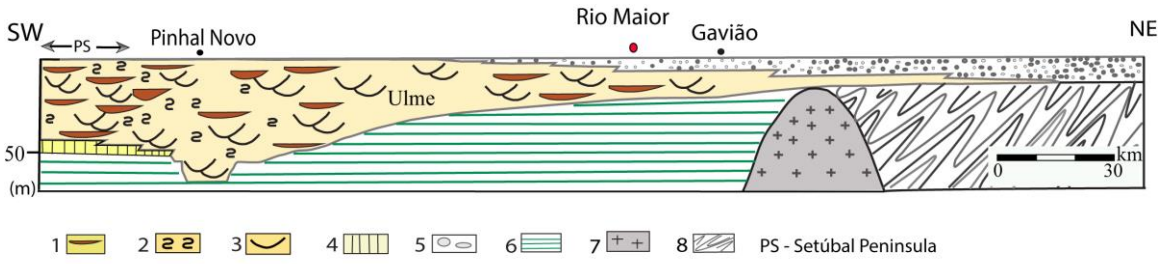

Figure III. 4. Schematic geological cross section of the upper part of the Lower Tejo Cenozoic Basin, showing the lithostratigraphic units that comprise the UBS13 on this section. Legend: 1 - alluvial silts and clays; 2 - marsh and swamp sediments (sands and silty clays); 3- fluvial sands; 4 - marine sandstones; 5 - alluvial gravels and sands; 6 - Mesozoic and Cenozoic substratum; 7- granitic basement; 8- metamorphic basement (adapted from Cunha et al., 1993).

III.3. Material and methods

III.3.1. Field Work

Selected outcrops of the UBS13 unit were studied in detail to improve the characterisation of the local stratigraphy and sedimentology. Fieldwork included stratigraphic logging and sedimentological characterisation of the sediments in order to obtain data on the depositional facies, including sediment colour, texture and clast lithological characterisation.

The Barracão site

At a claypit (39º49'N; 8º43'W) located near the village of Barracão, the culminant basin-fill unit UBS13 is formed by a succession of continental deposits: overlying Miocene mudstones, an alternation of 0.5 – 1 m thick beds of sand and silts (sometimes organic and containing fossil timber) grade upwards to fluvial gravels (Fig. III. 5 A; Fig. III. 6 A, B).

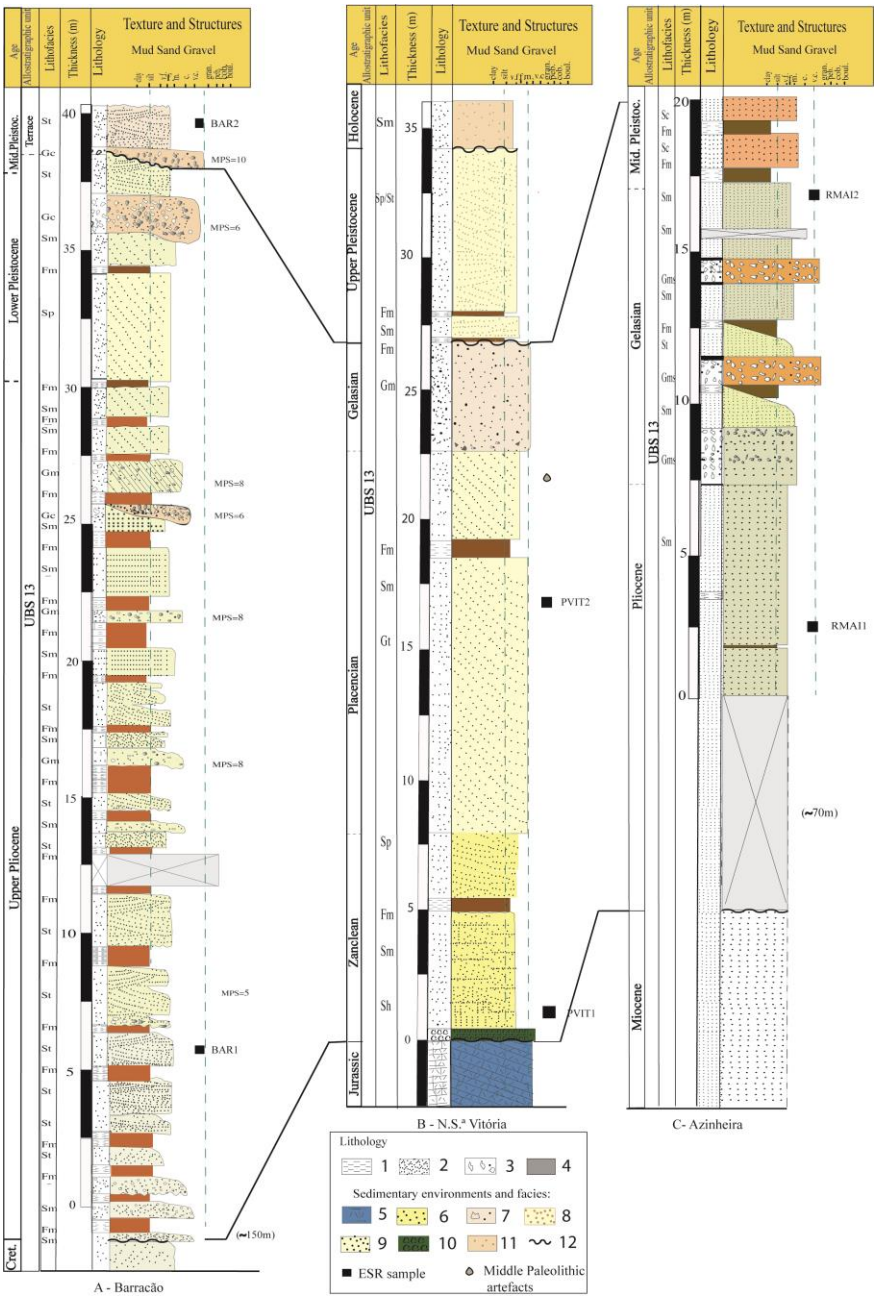

Figure III. 5. Stratigraphic logs of UBS13 at the studied sites (Barracão claypit, Sr.ª da Victória beach outcrop and Azenheira village sandpit - near Rio Maior). The locations of the samples collected for ESR dating are indicated (black squares). Legend: 1 – Siltite; 2 – Sand; 3 – gravel; 4 – Clay; 5 - Substratum, faulted and brechiated limestones; 6- Well sorted and laminated, fine to very fine yellow sands rich in quartz and mica (marine to sublittoral) – Carnide Formation; 7 - Small channel filled gravelly coarse sand containing quartz and quartzite clasts – fluvial; 8 - Late Pleistocene sand dunes – aeolian formation; 9 - Medium to fine whitish sands, with large scale planar or trough cross stratification - delta front (Roussa Formation); 10 - Lumachella levels - interbedded in fine and medium sands ; 11 - Holocene sand dunes – aeolian; 12 - discontinuity. Layers colours are according to Munsell Soil classification. (A and B adapted from Cachão 1989, Ramos and Cunha 2004).

Locally, the base of the unit comprises a sequence of very coarse sands, gravels and grey silts with a thickness of c 3 m. Immediately above, a thin layer of greyish silt passing upwards into medium to fine yellow sands with c. 4 m thickness. This well-sorted sand is interspersed with a layer of coarser sand. The sequence continues with an alternation of coarse-grained yellow sands with concave cross structures (St) and thin dark grey silts. In the middle part, the sands have a larger clay fraction and are better sorted. In the upper part, whitish sands and gravels include round and angular quartz and quartzite clasts. Two samples were collected for ESR dating respectively, near (approximately 6 m above) the base and close to the uppermost of the UBS13 succession.

The Sr.a da Vitória beach

At Sr.a Victória beach (39º42'N; 9º3'W), the UBS13 unit contacts directly with upper Triassic to Hettangian evaporitic marls and silty clays, having been significantly folded and fractured (Choffat, 1889; Cachão, 1989; Ribeiro, 1998; Ribeiro and Cabral, 1998; Ramos, 2008; Cabral et al., 2018). The Carnide and Roussa formations are folded into a broad syncline. The syncline is truncated in the upper part of the beach cliffs (at a height of ca. 25 m a.s.l.) by a Late Pleistocene (c. 40−30 ka) unit of aeolian sands (Benedetti et al., 2009), followed by a cover unit of Holocene aeolian sands (Fig. III. 6B).

Here unit UBS13 is c. 22 m thick. The presence of fine yellow sands, laminated and rich in muscovite at the base, reflects a calm environment (Carnide Formation, c. 12 m thick), (Fig. III. 5 B); the uppermost part of the UBS13 unit consists of thin beds of coarse sands with some mica, while above there are layers of whiter sands intercalated by thin beds of reddish silt and fine to coarse yellow sands (Roussa Formation) (Fig. III. 6B, Fig. III. 6C, D). In this study, two sediment samples were collected for ESR dating, from near the base and close to the top of UBS13.

The Azenheira (Rio Maior) site

At Rio Maior (39º19'N; 8º 55'W), the UBS13 unit is thick (up to 120 m), and comprises (from the base to the top) kaolinitic fine white sands followed by yellow gravelly sands, passing into medium sands and lignites intercalated with diatomite. Its uppermost part is composed of sandy-clay deposits with some gravelly layers (Zbyszewski, 1943, 1967; Pais et al., 2010).

A large sandpit located near the village of Azenheira (Fig. III. 1) was sampled for ESR dating. Sample RMAI1 was collected 18 m from the top of the UBS 13 unit and RMAI2 c.3 m from the top of the outcrop (Fig. III. 6 E, F).

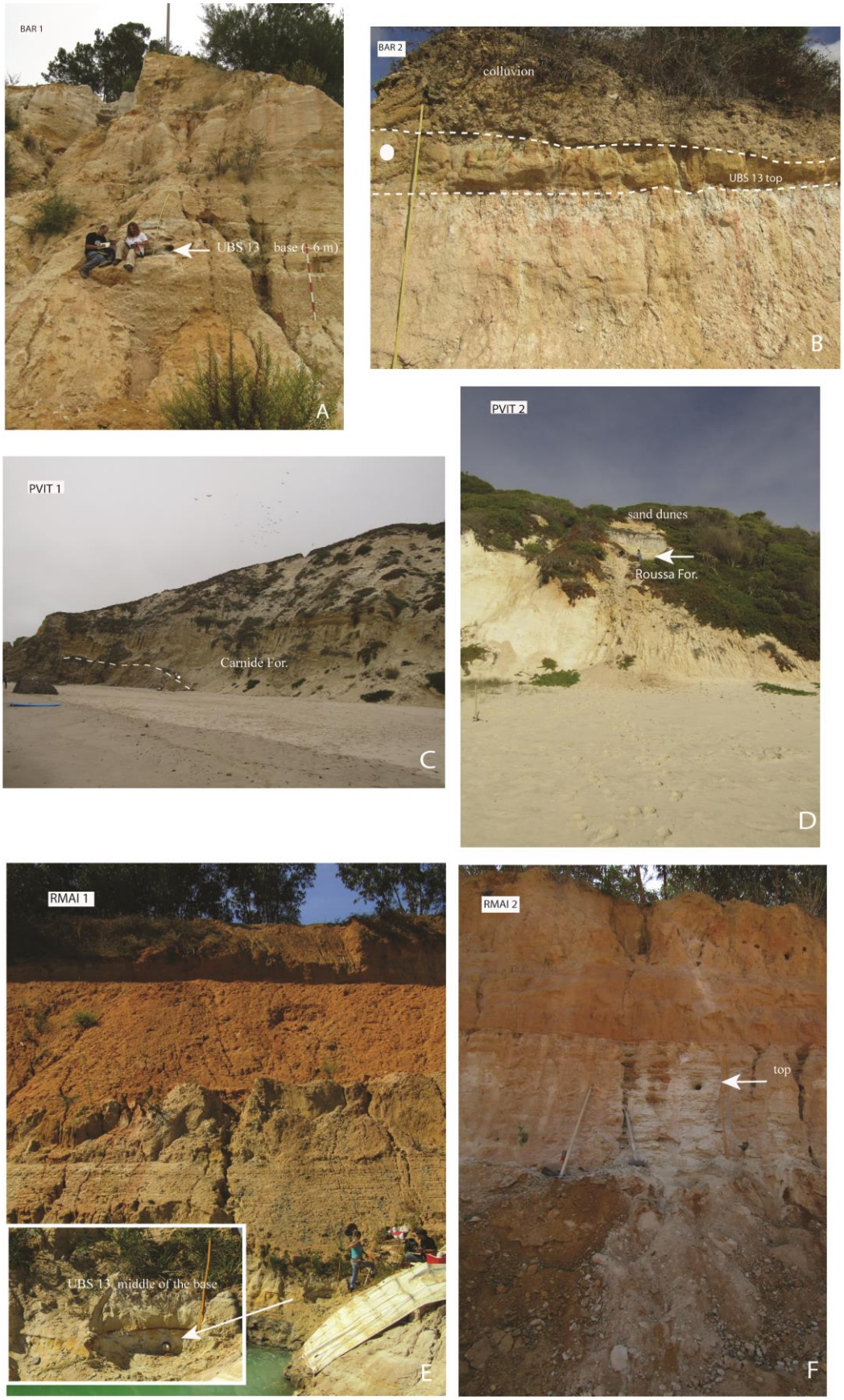

Figure III. 6. Sections from which the six sediment samples for ESR dating were collected (symbols: circle and arrow) at the Barracão site (A, B), Sr.a Vitória Beach (C, D) and near Azenheira (Rio Maior, E, F).

III.3.2. Electron spin resonance dating method

Electron spin resonance dating is a palaeodosimetric method, i.e. the sample is used as a dosimeter for dating, having recorded the total radiation dose received since the event of interest, namely the time of deposition of quartz grains within the sediment (Grün, 1989; Ikea, 1993).

Since the end of 1960s, this method has been used to date materials such as tooth enamel (Falguères et al., 2015), fish scales, aragonite and calcite in corals, molluscs, travertine, marine and continental carbonates (Bahain et al., 1995, 2007), as well as quartz from ash and fluvial deposits, and some flints (Ikeya, 1994; Falguères and Bahain, 2002). The dating of quartz by ESR was proposed in the early 1970s (McMorris, 1971) based on the presence of diverse paramagnetic ESR centres in its structure with the first sedimentary quartz dating undertaken by Yokoyama et al. (1985). ESR dating of quartz is considered one of the best methods able to produce numerical ages for older formations.

The age calculation implies the determination of two main parameters: the total dose (TD), also referred to as the paleodose or equivalent dose (De), and the dose rate (Da), which is an estimation of the mean dose annually absorbed by the sample. The radiation causes a charge to be trapped at defects in the crystal lattice.

$$TD = \int_0^T da(t).dt \quad (13)$$

where TD is the *equivalent dose* of radiation received by the sample over time, da is the *annual dose rate* of natural radiations and t the age of the sample.

Th

e total dose TD is proportional to the concentration of trapped electrons in the sample and so to the ESR signal intensity.

Three paramagnetic centres are frequently used as potential dosimeters of ionising radiation: the Germanium centre (Ge), the Aluminium centre (Al) and the Titanium centre (Ti). Each centre has different characteristics (e.g. differences in optical bleaching kinetics and/or radiation sensitivity), so it is useful to combine studies of more than one centre (e.g. Al-Ti centres are usually present in most of the quartz grains) in the same investigation to evaluate the reliability of the De obtained (Toyoda et al., 2000; Rink et al., 2007; Tissoux et al., 2007; Duval and Guilarte., 2015).

Exposure of the quartz grains to sunlight leads to a release of trapped electrons and the zeroing of the corresponding ESR signal (known as optical bleaching). Concerning the Al-center in the quartz structure, this is not fully bleached during exposure to sunlight and thus corresponds to a 'residual' ESR signal at the time of deposition of the quartz grains after their transportation. It is, therefore, necessary to determine this residual dose and to subtract it from the total dose, in order to determine the dose accumulated after the deposition of the unit under consideration. According to Voinchet et al. (2015) the bleaching quality of quartz is dependent on the selection of grain size fractions and the identification of transportation modes, especially about the Al centre (Al).

ESR is a dating method that has a considerable time-range potential, c. 30 ka to 2−5 Ma (Voinchet et al., 2010). The ESR signal correlated with the Al centre usually has a high radiation-saturation level and thermal stability (e.g. Toyoda and Ikeya, 1991; Duval, 2015) so that it could be used to date Lower Pleistocene (e.g. Rink et al., 2007; Duval et al., 2015), or even older materials (Laurent et al., 1998). In this context, ESR dating of optically bleached quartz has the potential to yield reliable numerical ages for the UBS13 sedimentary unit.

III.3.3. Sediment samples

Six sediment samples were collected for ESR dating during 2016 and 2017, at approximately the base and top of the UBS13 unit, at the Barracão, N. Sr.a Vitória beach and Azenheira (Rio Maior) sites (Fig. III. 1).

After careful cleaning of each section, a sediment sample of around 1 kg was collected in an opaque and watertight tube to prevent light exposure and loss of sediment. Systematic in situ gamma-ray measurements were performed for each sediment sample, using a portable gamma spectrometer (Canberra Inspector 1000 coupled with a 1.5*1.5 inch NaL(Tl) probe) to evaluate the γ dose rate (Mercier and Falguères, 2007), calculated according to Guérin et al. (2011). For external dose rate (D) analyses and evaluation of water content, around 1 kg of sediment was collected from the ESR sampling point and bagged for High-Resolution Low background Gamma-ray Spectrometry in the Laboratory of the Muséum National d'Histoire Naturelle (MNHN, Paris, France) and the Laboratory of Natural Radioactivity of the University of Coimbra.

III.3.4. Samples preparation

Quartz grains were extracted from sediment by chemical analyses. Quartz grains were sieved to separate the 100-200 μm fraction (cf. Voinchet et al. 2003).

Sample preparation for ESR analyses was carried out in darkroom conditions, at the Department of Earth Sciences of the University of Coimbra following the protocol proposed by Voinchet et al. (2003). Material from both ends of the tubes was discarded (not used for paleodose measurements). Samples were wet-sieved to separate the 180–250 μm grain-size fraction and rinsed using HCl (10%) and H2O2 (10%) to remove carbonates and organic matter, respectively. Heavy minerals and the K-feldspar fraction were removed using a heavy liquid solution of sodium polytungstate (r = 2.72 g/cm3 and r =2.58 g/cm3, respectively). Then magnetic minerals were eliminated using a powerful magnet. The quartz fraction was treated with 40 % HF for 40 min to remove the remaining feldspars and the outer parts of quartz grains. After etching in this way, the fraction was treated with HCl (10 %) to dissolve any remaining fluorides. Each quartz sample was divided into 12 aliquots.

III.4. ESR measurements

The Multiple Aliquots Additive (MAA) dose approach for dating quartz grains was applied. Ten of these aliquots were irradiated with a calibrated 137Cs Gammacell-1000 gamma source (dose rate= 200 Gy/h) at different doses ranging from 150 to 20.000 Gy, carried out at CENIEH (Burgos, Spain). Each series of 12 aliquots was measured for ESR low−temperature cavity (107−109 K) using a Bruker EMX spectrometer at MNHN. One aliquot was kept as a natural reference, and one aliquot was illuminated for 1000 h in a Dr Honhle SOL2 solar simulator to determine the unbleachable part of the ESR-Al signal (cf. Voinchet et al., 2003).

The intensity of Al signal was evaluated from peak-to-peak amplitude measurements between the top of the first peak (g=2.0185) to the bottom of the 16th peak (g=2.002) of its hyperfine structure (Toyoda and Falguères, 2003). Details of the experimental conditions employed for the Al and Ti centres are provided in the supplementary material. The angular dependence of the ESR signal was taken into account, measuring each aliquot three times after a 120º rotation in the cavity. This protocol was repeated 2 to 4 times over distinct days to check the reproducibility of the Al signal.

The ESR intensity for Ti – Li centre was measured from peak to baseline amplitude around g=1.913-1.915 (option D) according to Duval and Guilarte (2015), with an excellent dose-response to irradiation. The Ti centre showed a complete resetting of the ESR signal after the artificial bleaching.

A mean ESR intensity value and a standard deviation were derived from all the measurements and also used to evaluate the precision of the ESR data obtained from each centre (available in supplementary material).

The equivalent dose (De) was then determined by subtraction of the residual intensity evaluated through the maximum bleaching value from the total dose, which was obtained by an Exponential fitting function and with a single saturating exponential function (SSE) (for details see Voinchet et al., 2013), using the Microcal Origin Pro 8.1 software and weighted by the inverse of the squared ESR intensities,1/I2 (cf. Yokoyama et al., 1985).

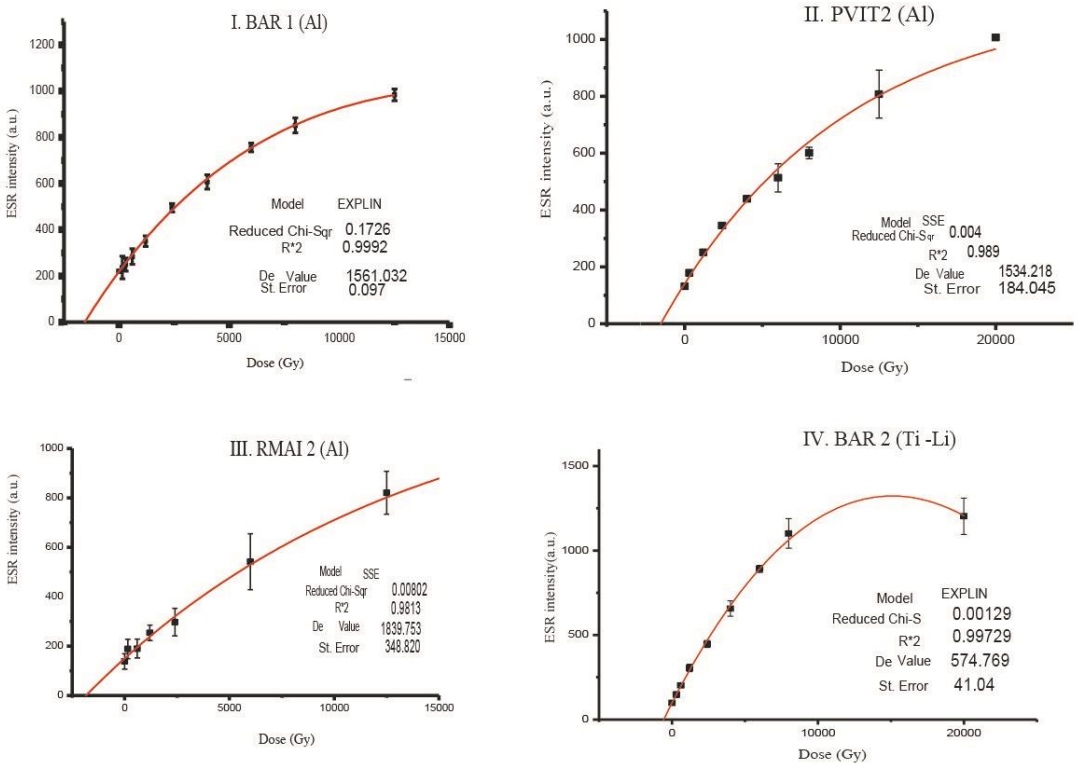

Figure III. 7. Examples of D_e curves obtained from the Al centre of BAR1, RMAI1, PVIT2 and D_e curves obtained from the Ti-Li centre of BAR 2. Errors in every point correspond to the three measures standard deviation (see Table IIISM.2).

III.5. Dose rate evaluation and age calculation

Radioelements contents (U, Th and daughters, and K) were determined by high-resolution low-background gamma-ray spectrometry to derive external alpha and beta dose rate components using the dose-rate conversion factors from Guérin et al., (2012).

The dose rate D is expressed as $D = D_{int} + D_{ext} + D_{cosmic}$ (14)

where D, D_{int}, D_{ext} and D_{cosmic} are the total, internal, external and cosmic dose-rate components, respectively (Duval et al., 2017).

The grain thickness removed after HF etching was assumed to be 20 μm so that the external alpha contribution was considered to be negligible because these particles only penetrate about 25 μm in the mineral. Values were corrected for α and β attenuation of spherical grains (Brennan et al., 1991; Brennan, 2003). Water content was determined by measuring the difference in mass between the natural sample and the same sample dried for one week in an oven with the water attenuation correction based on Grün (1994). The cosmic dose rate was determined according to Prescott and Hutton (1994), based on the altitude, latitude and longitude of each section.

In the age calculation, the annual dose rate (Da) was calculated from the radionuclide activity in the sediments, taking into account both in situ and laboratory gamma-ray spectrometry measurements (see Table IIISM.4).

III.6. Laboratorial characterisation of texture and mineral composition of the samples

III.6.1. Grain-size analysis

Grain-size analyses of sediment samples were carried out by integration of the following: (i) for the fraction > 63 μm, sieving with a sieve tour with ½ Φ increments, and (ii), for the fraction < 63 μm, by using a Beckman Coulter LS230 laser granulometer (measurement range of 0.04 to 2 000 μm). Visual inspection of grain-size distribution curves allowed the identification and interpretation of unimodal or multimodal subpopulations.

III.6.2. Mineral composition

Analyses of sediment composition were based on binocular microscope observation and X-ray powder diffraction (Department of Earth Sciences, University of Coimbra) using a Philips PW 3710 X-ray diffractometer with a Cu tube, at 40 kV and 20 nA. The mineralogical composition of the <2 μm fraction was obtained in oriented samples before and after ethylene glycol treatment and heating up to 550 °C. The percentages of the clay minerals in each sample were determined through the peak areas of mineral presence, with the use of specific correction parameters.

III.7. Results

III.7.1. Texture and mineral composition of the samples

From the Barracão site, the samples BAR1 and BAR2 have light grey (10 YR 8/1) and light yellow (10YR 8/3) colours, respectively. The mean grain size of BAR1 is dominated by medium-coarse sand, is 0.39 mm. The average grain-size fractions and parameters (Table 1) consist of 84% sand, 5% silt and 1% clay, very fine skewed (1.36), leptokurtic (6.01) and poorly sorted (1.88). BAR2 is a medium to coarse sand, with average grain – size components of 72% sand, 13% silt and 6% of clay. The mean grain size is c. 0.28 mm, very poorly sorted (3.04) and mesokurtic (3.66) with very fine skewed (1.36) distribution. The clay-mineral composition of this sample (Table 2) is dominated by kaolinite, followed by illite, although the sample collected at the base of the UBS13 (BAR1) has a higher illite percentage (30%) than that BAR2 from the top (11%). The sand fraction is composed of quartz, quartzite and feldspar detrital grains.

From the N. Sr.a Vitoria site, samples PVIT1 and PVIT2 have a light grey (10 YR 8/3) and light yellow (10 YR 8/2) colour, respectively. PVIT1 is fine sand composed of quartz hyaline and phyllosilicates (muscovite), with a mean grain size of c. 0.13 mm. The average grain-size fractions are 82% sand, 15% silt and 1% clay (Table 1); it is moderately well sorted (1.46), very fine skewed (1.88) and very leptokurtic (7.55). The clay fraction is composed of smectite (54%), illite (37%) and kaolinite (8%). PVIT2 is medium sand, comprising quartz (50%), feldspar (30%), phyllosilicates (15%) and oxides (5%), with average grain – size components of 93% sand, 5% silt and 2% of clay. The mean grain size is c. 0.31 mm, poorly sorted (1.51) with very fine skewed (3.33) distribution and very leptokurtic (15.04). Clay minerals present (Table 2) are kaolinite (70%) and illite (30%).

Regarding the samples collected from the Azenheira site (Rio Maior), the light grey (10YR 8/2) colour samples RMAI1 and RMAI2 are fine and medium sands (mean grain size c. 0.17 and 0.28mm, respectively), both being poorly sorted (1.44; 1.95), very leptokurtic (12.59) and leptokurtic (5.66), very fine skewed (2.98) in the case of RMAI1 and fine skewed (1.11) for RMAI2 (Table 1). On average, the sediment comprises 92% sand, 6% silt and 2% clay (RMAI1) and 74% sand, 14% silt and 6% clay (RMAI2). The sand minerals present are quartz, feldspars, with phyllosilicates (e.g., muscovite) and iron oxides. The clay fractions (Table III.2) in RMAI1 and RMAI2 (respectively), comprise kaolinite (91/71%) followed by illite (9/19%).

Table III. 1. Descriptive and statistical analyses of grain size parameters.

Sample code	Gravels (%) >2 mm	Sand (%) 2mm-63µm	Silte (%) 63-4µm	Clay (%) <4µm	Fines (%) <63µm	Mean (mm)	classification	Median (mm)	Mode (mm)	S.Deviation value	classification	Skewness value	classification	Kurtosis value	classification
BAR 1	9.81	83.59	5.07	1.15	6.6	0.387	m. sand	0.355	0.25	1.99	poorly sorted	1.36	ver.fin. skew.	6.01	leptokurtic
BAR 2	5.37	72.37	13.16	6.04	19.2	0.275	m. sand	0.5	0.71	3.04	very poor.sort.	1.37	ver.fin. skew.	3.66	mesokurtic
PVIT 1	<l.d.	82.24	14.52	1.09	0,00	0.131	fine sand	0.125	0.18	1.46	poorly sorted	1.88	ver.fin. skew.	7.55	ver. leptok.
PVIT 2	<l.d.	92.89	4.63	1.53	0,00	0.306	m. sand	0.355	0.355	1.51	poorly sorted	3.33	ver.fin. skew.	15.04	ver. leptok.
RMAI 1	<l.d.	92.044	5.74	1.88	7.95	0.166	fine sand	0.18	0.18	1.44	poorly sorted	2.98	ver.fin. skew.	12.59	ver. leptok.
RMAI 2	<l.d.	74.15	13.81	5.76	19.57	0.284	m. sand	0.09	0.09	1.95	poorly sorted	1.11	fine skewed	5.66	leptokurtic

<l.d. - limit detetion; m.sand- medium sand;m.coar.sand- medium coarse sand

Table III. 2. Clay mineralogy and clay percentages of the samples collected at the Barracão, N.S.a da Vitória and Azenheira sites.

Laboratory code	Illite (%)	Kaolinite (%)	Smectite (%)
BAR 1	30	70	<ld
BAR 2	13	87	<ld
PVIT 1	37	8	**54**
PVIT 2	30	70	<ld
RMAI 1	9	91	<ld
RMAI 2	19	71	<ld

<l.d. - limit detetion

III.7.2. ESR dating of optically bleached quartz grains

The ESR analytical data are listed in Tables 3 and 4. The Ti−Li centre signal intensities of quartz grains were determined only for top layers.

Table III. 3. Sample information, external β dose rate, dose rate in situ, cosmic dose and bleaching.

UBS 13	Laboratory code	External β dose rate (Gy/Ka)	Dγ in situ (Gy/Ka)	Cosmic dose rate (Gy/Ka)	Bl (%)
Barracão - base	BAR1	0.344 ± 12	0.339 ± 20	0.021±0.001	54±1.5
Barracão - top	BAR2	0.426 ± 12	0.516 ± 26	0.155±0.008	60±2.7
Sr.ª Vitoria beach - base	PVIT1	2.565 ± 21	1.137 ± 57	0.023±0.001	50±0.5
Sr.ª Vitoria beach - top	PVIT2	0.460 ± 11	0.241 ± 12	0.068±0.003	62±2
Rio Maior - base	RMAI1	0.576 ± 14	0.332 ± 17	0.0025±0.001	62±1.4
Rio Maior- top	RMAI2	1.114 ± 17	1.267 ± 63	0.109±0.005	60±2

The final De values for each sample were calculated from the average ESR intensity values, with the errors for each point corresponding to the nine measures. The relative bleaching component values (Table III.3) vary within a narrow range (around 60 ± 5%), suggesting similar bleaching conditions for all samples, which is a finding consistent with previous observations (Voinchet et al., 2007; del Val et al., 2019). The quality of fit is good overall for these samples, with adjusted r2 values of > 0.98.

According to Duval (2012), the reliability of the fitting results obtained from the Al centre should be questioned if the relative errors for the fitted parameters are >25%. All studied samples have relative De errors of less than 14%.

For the Ti centre, the De obtained in this study had a high quality of the fit, with adjusted r2 values > 0.99 and relative errors < 50%, as described by Duval and Guilarte (2015), except for PVIT2 (Table 4). In the studied samples, younger ages were obtained using the Ti centre than using the Al centre, except for BAR2. The De obtained for samples from Rio Maior (RMAI2), and Sª da Vitoria (PVIT2) was similar (Table III.4).

Radionuclide activity values, (with γ dose measured in situ and in the laboratory) provide consistent results at 1σ (Table SM III.4).

The ESR - Al age obtained for the base of UBS13 at the Barracão site (BAR1) is 2188±73 ka. The age estimates for the top of UBS13 at Barracão (BAR2) are 417±35 ka and 517±19 ka, for the Al and Ti−Li centres, respectively. As described above, the Ti−Li signal saturates with lower doses (see Fig. III.7.IV) than the Al signal. For Bar 2, only eight aliquots could be well fitted with the ESR Al centre.

From the N.S. ª da Vitória beach site, the ESR age of the lower sample (PVIT1) collected at the base of the Carnide Formation provided an ESR–Al age of 632±241 ka, which greatly underestimates the probable burial age. This is probably due to an anomalous annual dose rate value (Table 4) because the De is much higher than in the sample collected at the top (PVIT2) and the fitted curve of the ESR signal intensity showed the behaviour described by Voinchet et al., (2013) for old sediment samples. It will need more investigation to understand the behaviour of the environmental radiation dose in this basal part of the UBS13 unit at this site and the parameters that compose it (U, Th, K).

The ESR age of the PVIT2 sample, collected near the top of UBS13, is 1988 ± 121 ka based on the Al centre and 1599 ± 60 ka based on Ti-Li centre (Table III.3).

The lower sample collected at Rio Maior (RMAI1) gave an ESR age of 2894 ± 314 ka, based on the Al centre.

The sample (RMAI2), De of 1839 ± 174 Gy from the Al centre had a well-fitted, and defined curve (SSE fitting curve) and the total annual dose of 2515 ± 71 μGy/yr resulted in a final ESR age of 731± 69 ka. From the Ti−Li centre, the ERS age obtained was about 33% lower (Table III.4) and also seems to be underestimated. However, the De in Ti−Li centre is similar for the samples PVIT2 and RMAI2, but in RMAI2, with a high dose rate, the ESR Ti age obtained is much younger than for PVIT2 notwithstanding the same geological context.

Table III. 4. Sample information, dosimetry and ESR age from the Al and Ti centres. Depth from which sample was taken is given in (m) below the outcrop top. Field water content was calculated as mass water/mass*100%.

UBS 13 Unit	Barracão Base	Barracão Top	Sr.ª Vitoria beach Base	Sr.ª Vitoria beach Top	Rio Maior Base	Rio Maior Top
Laboratory code	**BAR1**	**BAR2**	**PVIT1**	**PVIT2**	**RMAI1**	**RMAI2**
Depht (m)	36	1.5	21	8	17	3.6
Elevation (m)	160	190	4.5	21	73	87.5
Grain size (µm)	250-180	250-180	250-180	250-180	250-180	250-180
Water Content (%)	12	21	25	18	22	22
^{238}U (ppm)	2.10 ± 0.07	1.95 ± 0.07	1.54 ± 0.087	0.61 ± 0.06	0.93 ± 0.065	3.97 ± 0.096
^{232}Th (ppm)	3.78 ± 0.09	8.13 ± 0.11	6.66 ± 0.14	1.14 ± 0.08	2.21 ± 0.09	17.32 ± 0.16
^{40}K (%)	0.10 ± 0.01	0.20 ± 0.006	4.82 ± 0.02	0.87 ± 0.02	0.84 ± 0.01	0.96 ± 0.02
Da (total) (µGy.a^{-1})	713 ± 26	1110 ± 31	3734 ± 63	772 ± 18	938 ± 24	2515 ± 71
De Al center (Gy)	1561 ± 49	458 ± 35	2360 ± 900	1534 ± 92	2713 ± 293	1839±174
Adj. Square	0.99	0.99	0.94	0.98	0.98	0.98
Al center Age (ka)	2188 ± 73	417±35	632 ±241	1988 ± 121	2894 ± 314	731 ± 69
De Ticenter (Gy)	-	574 ± 20	-	1232 ± 45	-	1233±60
Adj. Square	-	0.99	-	0.988	-	0.998
Ti-Li center Age (ka)	-	517 ±19	-	1599 ± 60	-	490 ±24

III.8. Discussion

The ESR age estimates (Al centre) calculated for the UBS13 basal deposits are 2894 ± 314 ka for RMAI1 and 2188 ± 73 ka for BAR1. It was expected that the PVIT1 ESR age would be similar to the biostratigraphic age of the Vale Farpado site (c. 3.6 Ma). For the BAR1 and RMAI1, which are located significantly inland (c. 20 km, Fig. III. 1), their expected burial age is c. 3.0-2.5 Ma. This age coincides with the MIS 103, a slightly warmer interval, the onset of the Matuyama Chron (interval of reversed geomagnetic polarity). Thus, it seems that the ESR age obtained for RMAI1, was in the expected period of time (assuming the error range) and stratigraphic position.

For Barracão (BAR1), the ESR age obtained may underestimate the probable burial age of the respective stratigraphic level but can support the view that the beginning of UBS13 deposition was between the Zanclean and Piacencian times, as in the Tejo Cenozoic Basin.

For the uppermost UBS13 deposits, the obtained ESR-Al age estimates are: 417 ± 35ka (BAR2), 1988 ± 121 ka (PVIT2) and 731 ± 69 ka (RMAI2).

According to our results, the agreement between ages determined from Al on these sediments indicates estimated ESR ages that range between the Pliocene and the Lower-Middle Pleistocene transition (Fig. III. 5).

The De values derived from Al (EXPLIN) and Ti option D (SSE and EXPLIN) are mostly 1σ consistent.

As in other studies, the ESR signal from the Al centre shows no saturation effects at high irradiation doses (e.g. Duval and Guilarte, 2015). In PVIT2, Ti-Li signal could be used to determine whether the sediment has been well bleached at the time of deposition. The "radiation bleaching" phenomenon is observed in the ESR signal of Ti-Li centre at high irradiation doses (e.g. Fig. III.7 IV) and the relative error is > 50 % for the higher doses (> 8000 Gy) in almost irradiated aliquots (Table SM.3). The differences between the values resulting from both centres suggest bleaching in Al-centre at the time of deposition satisfy for all the samples, except for the sample BAR2 (Table 3). In this sample, the De calculated from Al centre is lower than from the Ti-Li centre, but the chronologies provided by each centre are scattered (Table 4). This may be due to different thermal stabilities of Al and Ti centres (Toyoda and Ikea, 1994). The ESR ages obtained for BAR2 seem too young to be from the UBS13 buried sediment but can be explained if the sediment had two different times of deposition. Field data (demonstrating a culminant position and the sedimentary facies) indicate that this sample was collected from the UBS13 deposits (Fig. III. 5, A and Fig. III.6, B). However, it is possible that more recent sediment, embedded in the top of UBS13, may represent a reworking of the culminant unit (Fig. III.5, Fig.6 B) and consequently, should not be considered to give the absolute age of the unit.

Unfortunately, there are still no other absolute ages in Portugal for the uppermost deposits of the UBS13 sedimentary unit. Regarding the expected age for these deposits, c. 2.0-1.8 Ma, the ESR-Al age obtained during the present work from the sample PVIT2 is as expected. The result is according to another field data studies in oldest terrace levels, dated in Lower Tejo (Rosina et al., 2014) and in fluvial culminant levels studied in the Iberian Peninsula, as in Ebro Basin, with a first terrace dated to 1.3 Ma (Duval et al., 2015) and 1.14 Ma in the Duero Basin (Moreno et al., 2012).

The RMAI2 ESR data underestimated the probable burial age of the stratigraphic levels and gave unreliable ages for the uppermost UBS13. The too-high annual dose present in this sediment (Table 4) had a direct consequence on the age underestimation. The presence of clay can have an impact on adsorbing mobile radioactive elements in the environment. If we assume that adsorption is more recent than deposition, or even that it has been continuous throughout the history time of the sediment, this may induce an overestimation of the Da and therefore an underestimation of the age.

It is interesting to see large differences in values of the environment annual dose from the top and the base at the same outcrops and can be explained by different sediment sources.

For PVIT1, a more rigorous approach is required to calculate ages. A study is needed to determine whether dose rate study to know if this is or is not constant with time (e.g. Tsukamoto et al., 2014) and whether signal losses are involved (see Liu et al., 2016 for thermal loss correction). This sample has a value of external β dose much higher (table 3) than all the others. This can be justified for the values of feldspar-K in and from the large amount of muscovite present in the sample with a homogeneous source that increase the β dose values. Another hypothesis is the sample location. PVIT1 was collected near a fault (there is evidence of post-depositional faulting and the limestones are strongly fractured) and is possible that we are in the presence of different time-temperature history or of an apparent age of this unit that corresponds to the probable age of the fault (caused by quartz in fault gouges being exposed to shearing). PVIT 1 contains more muscovite than PVIT 2, as revealed in the clay composition, with 54% of smectite (Table III.2), mainly through chemical weathering of parent aluminosilicate under warm and humid conditions. Therefore, the experimental analysis will be necessary as part of future work.

The present study confirms that the Ti-Li centre ESR signal intensities of quartz grains is consistent and grew with the artificial doses for samples from the Middle Pleistocene (some beyond 8000 Gy), but this seems to result in underestimated ESR ages for successions from the Pliocene and Lower Pleistocene (Tissoux et al., 2007). It also demonstrates that ESR ages are yielded with large error ranges for time older than 3-2.5 Ma if the De is not very high (up to 3000 Gy is required for increased age reliability). The difficulties in obtaining reliable ESR age estimates for the Pliocene and Lower Pleistocene deposits result from the low De values (< 2700 Gy) for the annual dose present in these sediments, which has had a direct consequence on the age determination.

III.9. Conclusions

ESR dating has been used by the first time in this study to date the allostratigraphic unit UBS13 which represents the culminant the sedimentary infilling of the Lower Tejo and Mondego Cenozoic basins, having a depositional age between c. 3.7 Ma (basal deposits) and, probably, c. 1.8 Ma (top deposits).

For the first time, age estimates could be obtained for the basal deposits at the Rio Maior site, approximating 3 Ma. This study shows that the ESR method using the Al signal, in optically bleached quartz, is available for dating deposits as old as the Late Pliocene periods older than 2 Ma.

It has been confirmed that the Ti-Li centre provides unreliable ESR data for successions having Pliocene and Lower Pleistocene burial ages.

The ESR ages (Al centre) obtained for the UBS13 basal deposits indicate a Piacenzian to Gelasian age, notably in the Lower Tejo Cenozoic basin. However, the obtained numerical age of 2.2 Ma underestimates the probable burial age from the Barracão site, taking into account the previously independently dated Vale Farpado site (3.7 Ma).

The ESR ages (Al centre) obtained for the uppermost UBS13 deposits indicate as very probable age of c. 1.8 Ma, even if the ESR age of some of the studied samples could underestimate their burial age, and also shows that ESR dating can provide accurate and reliable absolute ages for the whole Quaternary interval, demonstrating the applicability of this method for the dating of Upper Pleistocene sediments. This result is internationally important because it represents the first numerical ages obtained in western Iberia for the uppermost levels of the Cenozoic basins, which predate fluvial incision into the basin-fill sediments.

This research should be developed in the immediate future, by using ESR dating (Al and Ti centres) to date these uppermost stratigraphic levels, not only in other sites of the Lower Tejo and Mondego Cenozoic basins but also in other Iberian Cenozoic basins. This dating is crucial to investigate the role played by tectonic activity, climate and eustasy in the transition to the incision and to establish the precise timing of this transition.

Supplementary Material

Table SM III. 1. ESR mean data (9 measurements) collected from the measurements of Al centre in the samples of the base (RMAI1, PVIT1, BAR1).

Dose (G)	*ESR (a.u.)* **RMAI1**	*d.s.*	*ESR (a.u.)* **PVIT 1**	*d.s.*	*ESR (a.u.)* **BAR1**	*d.s.*
0	222.11	8. 71	199.455	48.34	219.479	5.02
150	198.876	8.18	247.982	1.48	236.699	48.7
300	281.976	24.06	298.933	27.3	248.517	28.16
600	219.885	27.51	334.495	1.16	283.478	33.76
1200	300.534	23.33	393.906	0.50	349.987	22.64
2400	398.948	43.02	555.435	10.7	495.474	18.51
4000	498.668	36.74	598.758	49.8	606.372	30.94
6000	498.631	28.65	730.863	7.07	755.751	18.39
8000	732.039	31.48	845.502	49.27	851.031	31.89
12500	844.676	31.18	1087.347	35.18	983.168	25.28
20000	1211.11	105.19	1207.478	54.41	1042.46	146.95

Table SM III. 2. ESR mean data collected from the 9 measurements of Al centre in the samples of the top (RMAI2, PVIT2, BAR2).

Dose (G)	*ESR (a.u.)* **RMAI2**	*d.s.*	*ESR (a.u.)* **PVIT 2**	*d.s.*	*ESR (a.u.)* **BAR2**	*d.s.*
0	137.706	31.36	*131.398*	*6.05*	59.472	6.69
150	188.127	38.74	*72.9221*	*2.73*	96.446	11.55
300	214.087	10.29	*178.904*	*11.01*	105.699	*22.29*
600	243.361	38.06	*199.835*	*5.726*	*148.821*	*14.54*
1200	381.399	26.45	*251.341*	*4.385*	*182.940*	7.855
2400	373.983	19.49	*345.847*	*2.485*	259.984	12.110
4000	446.130	40.97	*439.381*	*6.192*	376.089	15.46
6000	715.216	98.59	*533.064*	*50.533*	*481.633*	18.36
8000	824.305	53.50	*600.808*	*20.21*	*621.638*	33.37
12500	911.070	86.38	*852.098*	*46.12*	720.455	*15.84*
20000	1091.667	192.19	*1006.76*	*10.164*	*1162.382*	75.85

Table SM III. 3. ESR mean data collected from the measurements of Ti-Li centre in the samples of the top (RMAI2, PVIT2, BAR2). The protocol was repeated 3and 4 times in each aliquot (9 measurements), only for Bar 2 was possible to use 6 measurements).

Dose (G)	***ESR (a.u.)*** **RMAI2**	***d.s.***	***ESR (a.u.)*** **PVIT2**	***d.s.***	***ESR (a.u.)*** **BAR2**	***d.s.***
0	151.341	19.69	215.483	27.092	98.042	11.725
150	189.612	33.04	260.768	77.439	128.462	18.080
300	196.809	16.04	298.677	67.095	147.658	17.225
600	239,329	45.40	369.072	27.548	201.837	15.01
1200	397,793	72.95	543.323	39.957	304.624	21.352
2400	450,769	123.88			446.681	20.52
4000	651,292	92.03	1011.76	134.380	656.553	45.20
6000	1021,408	148.13	1206.84	127.203	891.584	20.52
8000	1125,749	112.09	1700.54	87.600	1101.35	87.10
12500	1348,0595	144.38			983.445	237.75
20000					1202.26	107.45

Table SM III. 4. Total dose (DT) concentration obtained with gamma dose measured in situ (NaI detector) and in Laboratory analyses (Ortec low background noise germanium spectrometer. The repeatability of the ESR intensities was assessed through the variability of the mean ESR intensity obtained after each day of measurements.

Samples	**ESR int. Repeatability (% Ti center**	**ESR int. Repeatability (%) Al center**	**D total (α+β+γ situ)**	**D Total (α+β+γ Lab)**
BAR 1	-	1.03	696 ±21	702 ±8
BAR 2	0.92	0.91	1099±28	1076±11
PVIT 1	-	0.54	3687±58	3685±14
PVIT 2	0.56	0.87	772±14	790±7
RMAI 1	-	1.58	925±19	902±9
RMAI 2	0.65	0.96	2467±64	2218±16

CHAPTER IV. COASTAL UPLIFT IN WESTERNMOST IBERIA INDUCED BY COMPRESSIVE REACTIVATION OF THE WESTERN IBERIAN MARGIN: DATA FROM GEOMORPHOLOGY AND ESR DATING OF THE PENICHE MARINE TERRACES (PORTUGAL)

This chapter mainly corresponds to a research paper in preparation. Pedro P. Cunha and António A. Martins were involved in the fieldwork. António A. Martins done a new DEM. Margarida P. Gouveia performed the new Geomorphological map of the Peniche Peninsula, all figures presented, ESR dating and sedimentological analyses. All data interpretation was supervised by Pedro P. Cunha, António A. Martins and Alberto Gomes. Christophe Falguères, Pierre Voinchet and Jean-Jacques Bahain supervised ESR dating. The U-serie analysis were done samples in both Paris and Nanjing laboratories.

IV.1. Introduction

Marine terraces (or strandlines) are coastal landforms comprising an erosional bedrock surface (shore platform) overlain by coastal sediments of the beach and/or shoreface origins and sometimes buried by terrestrial deposits (aeolian, fluvial, slope) (Bradley and Griggs, 1976; Anderson et al., 1999). Morphologically, marine terraces typically display a flat to gently dipping surface seawards unless buried terrestrial sediments (e.g. Stokes and Garcia, 2009). Marine terraces reflect the interplay between the temporally and spatially variable climatic and tectonic drivers of eustacy (e.g. Lajoie, 1986). Conceptually, shore platforms are cut during rising sea level, with a notch or sea cliff formed during the sea-level highstand, followed firstly by coastal and then terrestrial sediment deposition as the sea level begins to fall (Bradley and Griggs, 1976). Uplifted coasts, by either active tectonic or isostatic adjustments, can record multiple marine terrace levels in a staircase configuration (e.g. Bull, 1985). Staircases are important as they can provide quantitative assessments of surface uplift rates, giving insights into coastal landscape development over a range of spatial and temporal scales (e.g. Lajoie et al., 1992). Uplift rate calculation requires knowledge of: 1) the elevation of the shoreline angle (landward limit of sea-level highstand) for each marine terrace level; 2) a geochronological framework of the marine terrace levels that comprise a staircase; and 3) the elevation and timing of a eustatic highstand unaffected by tectonic activity (Lajoie, 1986). Whilst all have inherent complexities and challenges (e.g. Pedoja et al., 2011), geochronology of a staircase is perhaps the most problematic. Dating limitations of marine terraces are well known. Older approaches relied on relative techniques, matching terrace levels to respective interglacial highstands (e.g. Zeuner, 1952).

Early adopters of absolute dating for marine terrace applications typically involved the U-Series technique (e.g. Hillaire-Marcel et al., 1986; Muhs et al., 1992). This approach provided chronology for

lower terrace levels, especially those associated with the Late Pleistocene Marine Isotope Stage (MIS) 5e, but with a low resolution for higher, older levels (Early - Middle Pleistocene, i.e. MIS 7 and older).

Although new and updated methods are now routinely applied (e.g. U-Series TIMS: Zazo et al., 2003; OSL: Normand et al., 2019) and age range and accuracy limitations still exist. Literature database modelling approaches have been used to overcome technical dating challenges, where better age constrained lower and younger levels (e.g. MIS 5e) have been used to produce different scenarios of uplift rate (Pedoja et al., 2011; 2014). These rates then inform on timings of higher-older levels via uplift rate extrapolation and integration with eustatic highstand elevations/timings (Pedoja et al., 2011; 2014). Such approaches suggest an acceleration of Pleistocene global uplift rate (Pedoja et al., 2011) as well as providing deeper time (Quaternary-Neogene) perspectives on high elevation marine terrace levels and erosion surfaces (Pedoja et al., 2014).

The Pedoja et al. (2011, 2014, 2018) database approaches highlight 1) a need for improved marine terrace age control spanning the entirety of a given staircase configuration to avoid problems inherent with the assumptions of modelling approaches; and 2) a need to fill regional geographical gaps that lack study of dated marine terrace staircases. These issues commonly occur with low-moderate uplift rate coastlines which often preserve marine terrace records but lack the research attention when compared to tectonically active high uplift rate coastline regions (e.g., SW USA, Mediterranean.) where seismic hazard assessment requirements provide a more urgent need for marine terrace analysis (e.g. Hanson et al., 1994).

Low-moderate uplift rate coasts are common along the passive margins of rifted oceanic basins (Pedoja et al., 2011, 2014, 2018). Within the Atlantic Ocean, the west-facing Iberian passive margin coastline of Portugal and Spain, some 700 km in length, is an example of where marine terrace staircases are variably preserved along the entire coastline length. Early research was descriptive and followed classical marine terrace-climate cycle matching approaches using various coastal sites along the Iberian margin (e.g. Zbyszewski, 1949; Teixeira, 1979). This approach continues in recent years, for example, along the SW Iberian margin, where Figueiredo et al. (2013) have used an assumed MIS5 marine terrace that lacks direct age control to inform on spatial variations of surface uplift linked to active tectonics. Only recently have studies routinely started to apply absolute dating methods (e.g. OSL, TL, U/Th, 14C) to marine terraces. Much of the work focuses on Late Pleistocene coastal sequences associated with the MIS5 highstand (e.g. Carvalho et al., 2006; Alonso and Pages, 2007) to inform on paleoenvironmental change associated with climatic-eustatic variability. In central Iberia, Late Pleistocene marine terraces with MIS5 and MIS3 contexts yielded important insights into early human (Neanderthal) coastal occupation and coastal resource exploitation (Benedetti et al., 2009; Haws et al., 2009). In NW Iberia, Carvalhido et al. (2014) dated a marine terrace staircase comprising five levels, using the results to on Late Pleistocene climatic-eustatic change and uplift rate variability. In SW Iberia, the MIS 5c marine terrace was dated with pIRIR method, k-feldspar (Figueiredo, 2015).

Some common themes emerge from marine terrace studies along the Iberian Atlantic passive margin. 1) Despite a large body of ongoing research since the 20th Century, much of it is descriptive. 2) Dating studies are few and where undertaken the temporal relationship to a given highstand is often the best

estimate based on stratigraphic bracketing. For example, sediments dated to MIS4-2 suggest that the underlying shore platform and any beach sediments are related to the MIS5 highstand.

3) Dating studies of marine terrace staircases, especially those that preserve levels older than MIS5, are rare. Where dating has been attempted, issues with the quality of the sampled material and the limitations of the dating technique often provide minimum ages or large age error bars that span multiple climate parts of the climate-eustatic cycle(s).

Within this study, we describe and date an impressive marine terrace staircase developed onto the rocky headland of the Peniche Peninsula (south-central Portugal). The staircase spans the Early, Middle and Late Pleistocene stages, thus providing a unique and key reference site of passive margin coastal landscape development. Firstly, we describe the staircase sequence through remote sensing and field-based mapping, surveying, and characterisation of marine terrace morphological and sedimentary components. We then apply ESR dating technique to the beach components of the component terrace levels. Terrace elevation and geochronological data are then assessed alongside global Pleistocene eustatic highstand positions and timings. The marine terrace sequence is then used to quantify temporal variations in tectonic uplift. Results are then collectively considered in climatic—tectonic-eustatic contexts with local-regional Iberian marine terrace research and more broadly to low-moderate uplift passive margin coastal landscape development.

IV.2. Geographical, geological and geomorphologic setting

Mainland Portugal is located at westernmost Europe, in the Iberian Peninsula western sector, facing the Northern Atlantic Ocean (Fig. III.1.A). The study area comprises the Peniche Peninsula, with ~5 km^2, located in central Portugal, at about 75 km north of Lisboa (Fig. III.1.B).

Regarding the geological setting, the study area is located on the Eurasian Plate, at the Western Iberian Margin. The successive phases of compression between Iberia, Europe and Africa, dominantly NW-SE oriented since ~9.7 Ma (late Tortonian), are recorded in the Cenozoic basins of Western Iberia, in the form of tectonic structures and allostratigraphic units (Ribeiro et al., 1990; De Vicente et al., 2008, 2011, 2018; Cunha et al., 2019). During the latest Zanclean (~3.7 Ma), a penetrative marine incursion took place at mainland Portugal, evidenced by the marine deposits of the allostratigraphic UBS13 unit (Cunha, 2019). This incursion is related to a high-eustatic sea level of +10-20 m (with error up to ± 15 m) above the present sea level (Miller et al., 2019).

The active compressive stresses during the last ~4 Ma still prevail and point to a WNW-ESE oriented compression under a general crustal uplift, expressed by Pleistocene marine terraces, widespread deformation of Pliocene to Quaternary strata and historical seismicity (Cabral, 1995, 2012; Araújo, 2014; Cabral et al., 2018, 2019; Cunha et al., 2008). Geodynamic models show the existence of an NW-SE to WNW-ESE oblique convergence at a rate of about 4 m/ka, between the African and Eurasian plates (e.g., Stich et al., 2006).

At the western coast of mainland Portugal, this research team already identified staircases of marine terraces at several sites (e.g., Mondego Cape, Raso Cape and Espichel Cape; Cunha et al., 2015). However, the novel characterisation of the Peniche terrace staircase documents a lower uplift rate data and contributes to the evaluation of differential uplift and of the associated active faults.

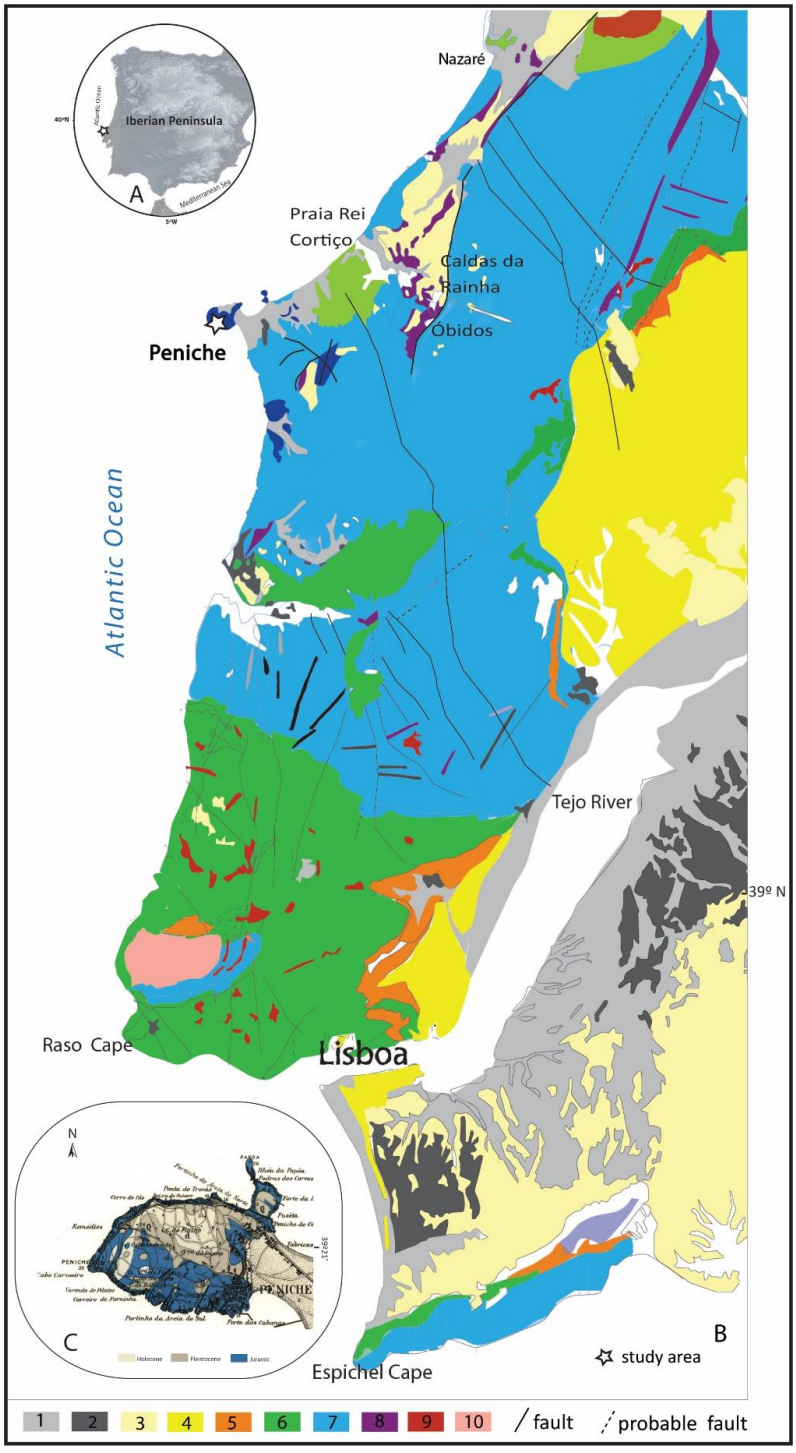

Figure IV. 1. A - Geographical setting of the study area (black star); B - simplified geological map, (1/500,000) of central-western mainland Portugal, adapted from Geological map of Portugal, LNEG; C - geological map of Peniche (modified from the Geological map (26C, 1/50,000). Legend: 1 – Holocene; 2 - Pleistocene; 3 - Pliocene; 4 – Miocene; 5 - Paleogene; 6 - Cretaceous; 7- Jurassic; 8 – Triassic; 9 – volcanic rocks; 10 –granite.

The main tectonic structure located near the study area is the NNE-SSW trending Pombal-Leiria-Caldas da Rainha fault (Fig. IV. 1B), an active fault (Cabral, 2012). Middle Pleistocene coastal deposits were already reported at ~11 km towards NE of the study area, at Praia do Rei Cortiço (Fig. 1B) (Haws et al., 2009). The Peniche Peninsula is one of the best geological heritage sites of Portugal, due its excellent outcrops, palaeontological record and scenic value (e.g., Duarte, 2004; Brilha et al., 2005; Romão, 2009, Rilo et al., 2010). It has diverse Mesozoic lithologies composed by Lower Jurassic marine carbonates, mainly calcarenite limestones (França et al., 1960; Duarte and Soares, 2002), and the Papôa Cretaceous volcanic breccia, in the NW sector. Documented by levels between 33-6m a.s.l., the Cenozoic record comprises a culminant wave-cut platform and a Pleistocene terrace staircase of five wave-cut platforms and associated sedimentary deposits (Cunha et al., 2017). Late Pleistocene and Holocene aeolian sands, but also modern beach deposits, ranging from sands to boulders, are mainly located between the NE sector of the Peninsula and the mainland (Henriques and Neto, 2002) (Figs. IV.2).

The topography of Peninsula decreases from 33 m (a.s.l.), near the Carvoeiro Cape at WNW, to 5 m in the isthmus at SE (Fig. IV. 2). The survey and cross-sections document several wave-cut platforms, cut in Jurassic limestones; some have a veneer cover of marine sandstones and aeolian sands. A small stream channel, consequent with the topographic gradient of the ancient island, cuts down the Jurassic limestone, while others, of minor category, dissect mainly the south coastal cliff (Fig. IV.2). Small faults in the Jurassic limestones coincide with the path of these little streams, which develop gorges and associated blowholes. Because the Jurassic limestones are well-jointed and the waves undercut the base of the cliffs, mass movements, especially rock falls, and toppling are frequently. A considerable amount of debris (mainly boulders), especially in the western end of the Peninsula, cover the shore platform. Near the Carvoeiro Cape, a sea-stack stands a ca. 15 m. Some caves are developed in the face of plunging cliff in the south coast, with more than 20 m in height (e.g. Furninha Cave). Notches and palaeoshore platforms can be seen in the south coastal cliff (Fig. IV.2). Sandy beaches only occur near the small Papoa Península and are probably related to the processes that led to the island's connection to the mainland.

At the westernmost sector of the Peniche Peninsula, the Carvoeiro Cape shows active scarped cliffs. Until the end of XVI century, this Peninsula was an island; currently, it is connected to the mainland through a tombolo, due to the silting promoted by the S. Domingos River mouth (Dias and Bastos, 2017; Fleming et al., 2017).

On the isthmus, field dunes up to 8 m in height, are sourced from the nearby beaches. In the summertime, a coastal low-level wind jet (CLWJ), a northerly wind, is especially frequent and intense. The frequencies of wind occurrence on the western coast of the Iberian Peninsula can reach 40% in summer and ~ 70% in the other days of the year. Its speed has a mean around 15 m/s, reaching maximum speeds of 25 m/s (Soares et al., 2014). We place particular emphasis on the movement of sands in the dry season (summer).

Rock dissolution and salt weathering processes have developed lapies (marine karren) in the area between the N. Sra. dos Remédios chapel and the Carvoeiro Cape. The lapies form small ridges and pits with more than 1 m deep.

The cliffs have some marine caves of different sizes and, locally, adjacent pocket beaches (Figs. IV.1C and IV.2), mainly at the SW of the peninsula, as the Furninha Cave (Fig. IV. 2). In the late 19th century, complete archaeological excavation of the sedimentary infill of this cave allowed the identification of two main lithostratigraphic units (Delgado, 1884) (Fig. IV.3): (i) a 1-3 m thick Holocene succession, of clayish-sandy layers; and (ii) a 9.3 m thick Pleistocene succession (levels I to VII), comprising a basal layer (I) of a bioclastic marine conglomerate (with Patella and Littorina) at ~5-8 m (a.s.l.) followed by aeolian yellowish fine sands containing limestone clasts, fossils of vertebrates (e.g. carnivorous mammals, herbivores, flying mammals, amphibians, turtles, lizards and birds) and Mousterian (Middle Palaeolithic) artefacts (Delgado, 1884; Harlé, 1910; Breuil and Zbyszewski, 1942; Zilhão, 1997; Bicho and Cardoso, 2010; Cardoso and Carvalho, 2011; Brugal et al., 2012; Figueiredo, 2010). A U-series date of 81+42/-31 ka was obtained from a bone collected in a lower level of the Mousterian succession (Raposo, 1995) (Fig.IV.4). The fossil vertebrates of the older succession allow an interpretation of paleoclimates (comprising wet-temperate, wet-cold, dry-temperate and dry-cold conditions) and regional paleoenvironments (coastal areas, wetlands, rocky areas, freshwater lakes, open field areas, woods, forest areas and relief areas) (Figueiredo et al., 2017).

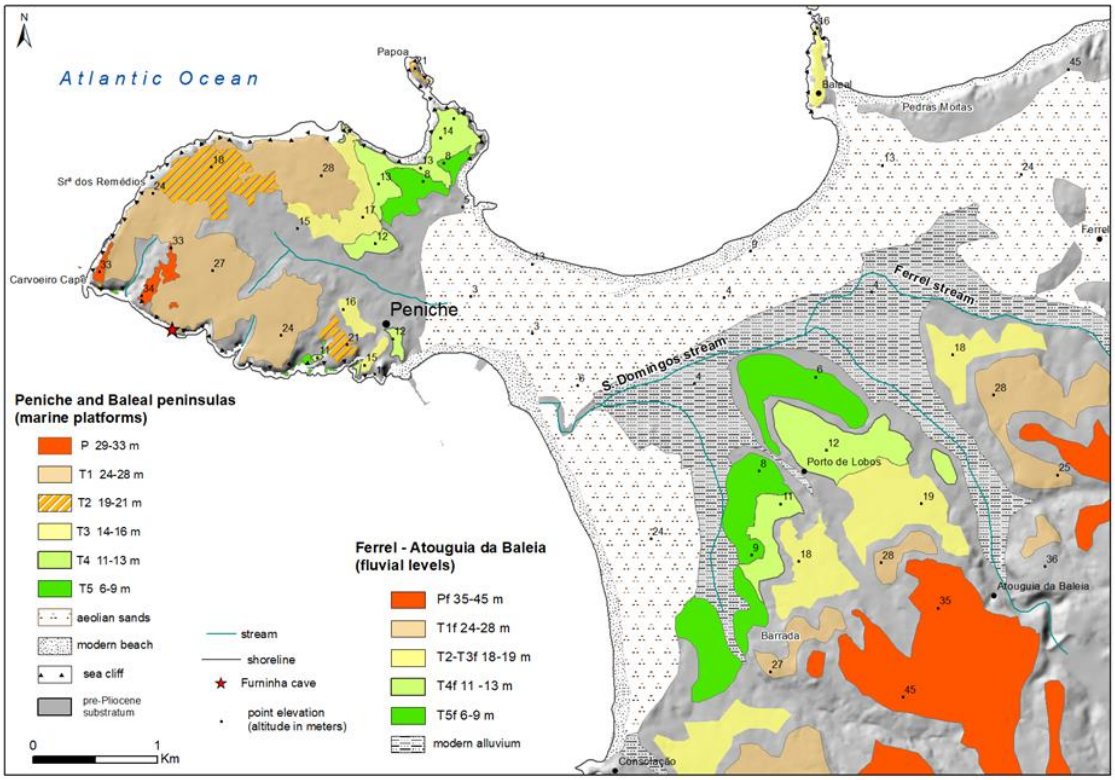

Figure IV. 2. Geomorphological map of the Peniche Peninsula (identification of the several wave-cut platforms – Pm and Tm) and of the adjacent inland area (marine/ fluvial levels at higher altitudes – Pf and Tf).

The 1940's, during the production of the geological map of Portugal in the 1/50,000 scale, hundreds of lithic artefacts in the Peniche Peninsula and adjacent inland area (Fig. IV.2) were collected and classified according to the intensity of patina and elevation (Breuil and Zbyszewski, 1945; França et al., 1960; Zbyzewski, 1970).

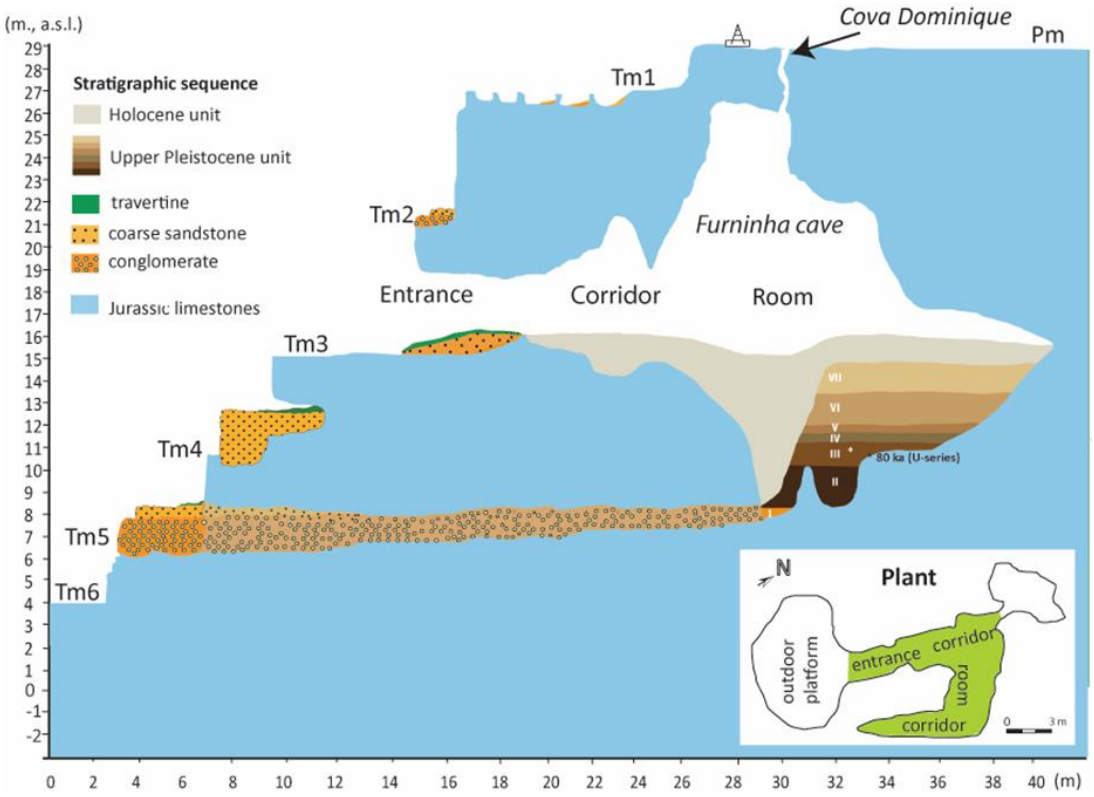

Figure IV. 3. Schematic representation of the geometry and lithostratigraphy of the Furninha Cave (the location of the cave is presented in figure 2). Pm (culminant wave-cut surface); Tm (1 to 6) are wave-cut platforms and associated marine deposits; the Early Pleistocene unit comprised a lower marine conglomerate (I) and upper layers of aeolian sands (II to VII); the Holocene unit consisted in clayish sands. In the late 19th century, the Early Pleistocene and Holocene units were completely excavated (Delgado, 1884). The continuity between the Tm5 deposits at the cliff and the marine bioclastic conglomerate (I) is proposed (a paleo sea connection by a sea cave and karstic gallery).

IV.3. Present climate and oceanography

The climate in mainland Portugal is the Mediterranean with Atlantic influence, Csa type according to the Köppen-Geiger classification (Peel et al., 2007), with dry and hot summers and mild winters (Mota and Pinto, 2014). Atlantic swells from the NW are dominant, and less energetic conditions characterize the wave regime during the summer (~2 m high waves) and energetic conditions (~4.5 m high waves) in the winter, with annual average periods of 9-11s (Mota and Pinto, 2014).

There are some periods of extreme wave conditions (wave height >5m) promoted by storms, associated with prevailing southerly winds and downwelling conditions (Vitorino et al., 2002; Bruneau et al., 2011). The regime is mesotidal, with semidiurnal tides. The average neap tidal range is 1.0 m, and the average spring tidal range is 2.8 m (Fernández-Salas et al., 2015).

IV.4. Material and methods

The information presented in this study derives from geomorphological, stratigraphical, sedimentological and chronological data using a standard approach (e.g., Stokes et al., 2012), combining field and laboratory work.

IV.4.1. Mapping and surveying

The Peniche marine terraces were firstly investigated by remote sensing, and field-based mapping and surveying. Geomorphological mapping was undertaken at 1/10,000 scale using topographic base maps provided by the Peniche Municipality (1/10,000 scale) in conjunction with (2 m/pixel) LIDAR-derived DEM data (DGT, 2011) to characterise the broad morphological configuration of the island. A 1/50,000 geological map (França et al., 1960) was used to establish relationships between the island morphology and its underlying bedrock geology (lithology, stratigraphy, structure). Coastal cliff areas with well-developed marine terrace levels (e.g. Furninha Cave site) were documented by drone aerial photogrammetry and field-based differential GPS survey. The GPS surveying used real-time kinematics with a GNSS Epoch 50 RTK system for centimetre location and elevation accuracy. Survey data from less accessible vertical cliff sections were supplemented with handheld tape measure values. The mapping and surveying results allowed a relative stratigraphic framework of marine terrace levels to be established, providing a context for detailed analysis of the geomorphology, stratigraphy, sedimentology, and geochronological sampling of the component levels.

Special attention was paid to the elevations of the innermost shore platform edges and shoreline angles of each terrace level, since these components provide important data inputs into surface uplift rate quantification (e.g., Lajoie, 1986).

IV.4.2. Marine terrace sediments

Fieldwork included the study in detail of each marine terrace, which consisted in the stratigraphic logging and sedimentological characterisation of the sedimentary deposits, as sediment colour, texture, maximum particle size, clast lithology characterisation, fossil and archaeological content.

Figure IV. 4. Field sections at the Furninha Cave site, roughly parallel with the modern shoreline, were collected from most marine sediment samples. A – Tm3 wave-cut platform; B – Tm2 wave-cut platform; C – Tm1 wave-cut platform; D – Tm4 wave-cut platform; E – Tm5 wave-cut platform; F – Furninha cave entrance; G – in situ dose rate measurement; H – travertine sample collected from the Tm3 top deposits; I – Tm5 conglomerate (the sample Pen7 was collected just above); J – sample Pen1 being collected from Tm3 deposits; L – sampling Pen2, from a sandstone lens included in the Tm3 lower conglomerate division; M – sample location (Pen3); N – Pen4 sample location; O – Tm1 inner-edge; P – shore angle of the Tm4 wave-cut platform.

IV.5. Grain-size analysis and mineral composition of the sediment samples

Sedimentary deposits were described and interpreted in terms of sedimentary and depositional process based on the facies analysis approach, lithology, textures (shape, grain size; roundness; sorting) and composition characterisation. The thickness of each deposit and lateral distribution were represented in the marine staircase profile.

Grain-size analyses of sediment samples were carried out in the Sedimentology Laboratory of the University of Coimbra, by sieving with a ½ Φ increment for the fraction > 63 μm.

Analyses of sediment mineral composition were based on binocular microscope observation (50x) and X-ray powder diffraction using an Analytical Aeris XRD diffractometer manufactured by Panalytical, with a Cu tube in a 2θ range, at a scanning rate of 3º min-1, 40 kV and 15 nA (Department of Earth Sciences of the University of Coimbra). The mineralogical composition in non-oriented subsamples was obtained using the analytical software Highscore plus, provided with the instrument. According to the standardised Panalytical backloading system, the subsamples were prepared, which provides a nearly random distribution of the particles.

IV.6. Numerical dating

IV.6.1. ESR dating of optically bleached quartz grains

In the present study, eight blocks of siliciclastic sandstone cemented by calcite (usually with ~50 x 50 cm), representing beach facies (Pen1 to Pen8, at least one for each marine terrace of Tm1 to Tm5), were collected for ESR dating. The thickness and development of the Tm3 allowed the collection of three samples for ESR dating. However, due to its younger age, sample Pen7 was not selected for ESR dating and is currently being dated by pIRIR290. Pen6 is a boulder of beach sandstone, cemented on the top of Tm5 and probably representing the erosion of Tm4, during Tm5 formation; this sample was also not selected to be dated by ESR.

According to the standard conditions for sample preparation for ESR dating, the core of each block of siliciclastic sandstone was extracted under red light (Yokoyama et al., 1985).

At the Department Earth Sciences-University of Coimbra laboratory facilities for the preparation of mineral fractions for OSL and ESR dating, the 250-180 μm fractions of pure quartz grains were extracted from sediment by sieving, chemical treatments, including fluohydric (HF) acid attack, dense liquid separation and magnetic separation, following the standard procedure (e.g., Voinchet et al., 2004).

The multi-aliquot additive (MAA) dose procedure was employed for De determination. Ten of twelve aliquots with quartz grains were irradiated with a calibrated 137Cs Gammacell-1000 gamma source (dose rate= 200 Gy/h) at different doses ranging from 100 to 25.000 Gy, carried out at CENIEH (Burgos, Spain). After irradiation, each series of 12 aliquots was measured by ESR at low-temperature cavity (~107K) using a Bruker EMX spectrometer at MNHN, Paris. One aliquot was kept as a natural reference, and one aliquot was illuminated for 1000 h in a Dr Honhle SOL2 solar simulator to determine the non-bleachable part of the ESR-Al signal (Voinchet et al., 2003).

Equivalent dose values were calculated considering the average ESR intensities obtained from the three repeated measurements, carried out over three days in each aliquot. Fitting procedure and De calculation were performed with Microcal OriginPro 8.5 software using a Levenberg-Marquardt algorithm by chi-square minimisation (Hayes et al., 1988). Al ESR intensities were fitted with both the exponential+linear (EXPLIN) and single saturation exponential (SSE) functions, according to Duval (2012) and Voinchet et al. (2013). Data points were weighted by the inverse of the squared ESR intensity (1/I) to reduce the leverage of high dose points. Ti ESR intensities were fitted with both functions when SSE described the decreasing behaviour of the ESR intensity at high doses. The goodness-of-fit is assessed through the adjusted r-square (r) value, which accounts for the system's degree of freedom. According to these factors, the fitting curve was chosen.

According to Duval (2012), the reliability of the fitting results obtained from the Al center may be reasonably questioned when the adjusted r2 value is <0.99 and the relative errors on the fitted parameters >25%.

Analytical uncertainties and ages are given with ± 1σ. When possible, weighted average ages were calculated using isoplot 3.0 software (Ludwig, 2003).

Equivalent dose (De) was obtained by an exponential+linear fitting function (EXPLIN) and with a single saturating exponential function (SSE) (for details, see Voinchet et al., 2013), using the Microcal Origin Pro 8.1 software and a data point weighting by the inverse of the squared ESR intensities, 1/I2 (Yokoyama et al., 1985).

To determine the annual dose rates (Da), roughly 1 kg of material corresponding to the dated sediment was extracted. The radioelements contents (U, Th and daughters, and K) were determined by a high-resolution low-background gamma-ray spectrometry measurement and external alpha, and beta dose rate components were derived from the radioelement contents hence obtained using the dose-rate conversion factors of Guérin et al. (2012). Therefore, the grain thickness removed after the HF etching was assumed to be 20 μm and external alpha contribution was consequently considered negligible. Values were corrected for β attenuation of spherical grains (Brennan et al., 1991; Brennan, 2003).

Water content value during burial was estimated, according to Grün (1994). According to Prescott and Hutton (1994), the cosmic dose rate was determined based on altitude, latitude, and longitude of each section.

IV.6.2. ^{230}Th/U dating

The U-series decay chain methodology (Bateman, 1910) was first used in studies of sea-level changes with the dating of corals from continental passive margins and tectonically uplifted reef complexes (Chappell, 2002; Muhs, 2002). Speleothems generally behave as closed systems to uranium uptake after calcite precipitation, so will achieve secular equilibrium, and the number of radioactive decay events in the decay series will equal that of the long-lived uranium parent isotope, and the measured age can be regarded as real (Normand et al., 2019). The travertine deposition usually constrained the time of interglacial high sea-level stands (El Kadiri et al., 2010) linked to warm and wet climatic conditions and sub-aerial cave formation.

At the Furninha Cave marine terrace staircase, one travertine sample was collected at the Tm3 topmost deposits (Fig. III.5) and another one at the Tm4 top. a) Analysis using Q-ICP-MS (Musée de l'Homme, Paris)

Chemistry: U-Th separation using anion exchange resins, performed at the U-series chemistry lab at the Musée de l'Homme, Paris (protocol according to Bischoff et al., 1988, modified by Shao Q., Ghaleb B. & Tombret O.).

Analysis: Thermo iCAP-RQ (ICP-Q-MS), measurement lab at Musée de l'Homme, Paris.

b) Analysis using MC-ICP-MS (Nanjing Normal University, Chine)

Chemistry: U-Th separation using anion exchange resins, performed at the U-series chemistry cleanlab at **Normal Nanjing University, Nanjing, Chine** (protocol according Bischoff et al., 1988, modified by Shao Q., Ghaleb B. and Tombret O.).

Analysis: Thermo NEPTUNE Plus (MC-ICP-MS), measurement lab at Normal Nanjing University, Nanjing, Chine.

Figure IV. 5. Mechanical sampling.

The sample was extracted from the upper part of the travertine using a dentist diamond saw. The

regions of interest were selected, and small pieces were sampled and then cleaned several times, using Milli-Q water and ultrasonic bath for 30 minutes. Finally, less than 1g was selected.

IV.6.2.1. U-series chemical treatment

The sample was extracted from the upper part of the travertine using a dentist diamond saw. The areas of interest were selected, and small pieces were sampled and then cleaned several times, using Milli-Q water and ultrasonic bath for 30 minutes. Finally, less than 1g was selected.

A small quantity of spike (^{229}Th-^{233}U-^{236}U with well-known ratios) was weighted and dried in a PFA beaker. The sample was then weighted and added to the beaker and dissolved by HNO3 7M. H_2O_2 was added to eliminate the organic matter. Iron hydroxides were precipitated to eliminate most of the carbonate matrix and pre-concentrate uranium and thorium. The solution was then eluted on AG-1x8 and UTEVA resins for separation and purification, using appropriate acids. Uranium and Th fractions were kept separately, dried and dissolved in HNO_3 2% for adjusted dilutions and isotopic analysis in a quadripole inductively coupled mass spectrometry, ICP-Q-MS. Uranium and thorium were measured separately. The MNHN laboratory uses an ICP-Q-MS (quadripolar ICP-MS) Thermo iCAP-RQ coupled to a CETAC Aridus III desolvator. The interface has been configured for a high-sensibility and the signal was tuned for both ^{238}U and ^{235}U. The signal intensity of ^{229}Th, ^{230}Th, ^{232}Th, ^{233}U, ^{234}U, ^{235}U, ^{236}U are measured under the pulse counting mode. U and Th elements were measured separately.

In Nanjing laboratory, the sample underwent a similar chemical protocol. However, the uranium-thorium separation and purification were performed using only one resin column UTEVA, according to Douville et al. (2010).

The Paris laboratory uses an ICP-Q-MS (quadripolar ICP-MS) Thermo iCAP-RQ coupled to a CETAC Aridus III desolvator. The interface has been configured for a high-sensibility and the signal was tuned for both ^{238}U and ^{235}U. The signal intensity of ^{229}Th, ^{230}Th, ^{232}Th, ^{233}U, ^{234}U, ^{235}U, ^{236}U are measured under the pulse counting mode. U and Th elements were measured separately. The Nanjing laboratory uses a MC-ICP-MS (multi-collector inductively coupled plasma mass spectrometer) Thermo NEPTUNE coupled to a CETAC Aridus II desolvator. All the elements ^{229}Th, ^{230}Th, ^{232}Th, ^{233}U, ^{234}U, ^{234}U, ^{235}U, ^{236}U are measured on faraday cups and ^{230}Th, ^{234}U on SEMs as well to increase the measurement precision for low signal isotopes.

IV.6.2.1. Mass spectrometry analysis (ICP-Q-MS and MC-ICP-MS)

The laboratory in Paris uses an ICP-Q-MS (quadripolar ICP-MS) Thermo iCAP-RQ coupled to a CETAC Aridus III desolvator. The interface has been configured for a high-sensibility and the signal was tuned for both 238U and 235U. The signal intensity of ^{229}Th, ^{230}Th, ^{232}Th, ^{233}U, ^{234}U, ^{235}U, ^{236}U are measured under the pulse counting mode. U and Th elements were measured separately.

The Nanjing laboratory uses a MC-ICP-MS (multi-collector inductively coupled plasma mass spectrometer) Thermo NEPTUNE coupled to a CETAC Aridus II desolvator. All the elements ^{229}Th, ^{230}Th, ^{232}Th, ^{233}U, ^{234}U, ^{235}U, ^{236}U are measured on faraday cups and ^{230}Th,^{234}U on SEMs as well to increase the measurement precision for low signal isotopes.

Each session measurement includes an internal laboratory standard and a blank for both laboratories.

IV.7. Mean sea-level curves and uplift rates

Interpretation of geomorphological, sedimentary and isotopic data allowed to obtain “global” sea-level curves for the Quaternary. Because of different uplift rates, even very low, in areas assumed as tectonically passive and variations in seawater salinity, temperature and uncertainties regarding the relationship between the δ18O record, ice volume and eustatic sea level, many different sea-level curves that estimate global mean sea level (GMSL) have been published from multiple archives (e.g., Normand et al., 2019). However, very well-dated sedimentary archives suitable for this analysis are very limited (e.g., Suganuma et al., 2018). The last maximum sea-level highstands are the Marine Isotope Stage (MIS) 5 (85-128 ka), with tree sub-stages (MIS5a, 85±5 ka; MIS5c, 105±5 ka; MIS5e, 116-128 ka); MIS7 (190-245 ka), with tree sub-stages (MIS7a, MIS7c and MIS7e); MIS9 (306-334 ka); MIS11 (360-420 ka), MIS13 (480-530 ka) (Thomson et al., 2003) and earlier interglacials, as MIS15 (560-620 ka), MIS17 (650-720 ka) and MIS19 (775-785 ka) (Anderson et al., 2008; Murray-Wallace and Woodroffe, 2014). During MIS21 (final stage of the MPT), the 100 ka cyclicity dominance began with a significant change in climatic variability (Kitaba et al., 2011).

As a marine terrace does not constitute a horizontal reference, the elevation of the shoreline angle (inner edge) of a marine terrace provides a useful marker for the relative sea level and location of a former shoreline (e.g., Lajoie, 1986) (Fig. IV.6).

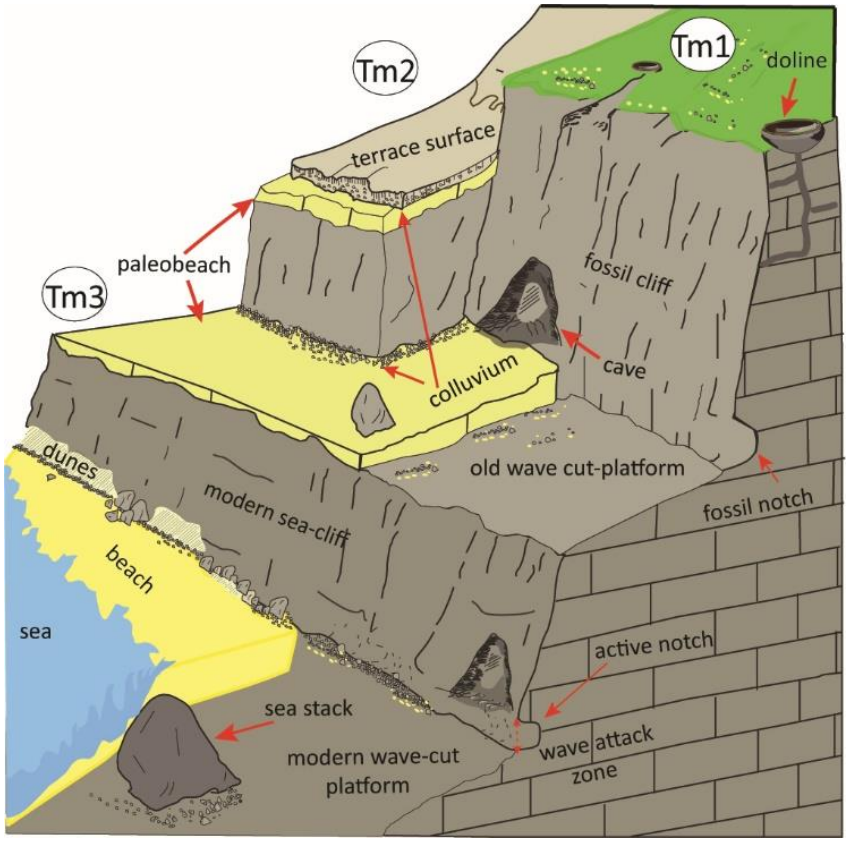

Figure IV. 6. Drawing that conceptually describes the component parts of a marine terrace staircase. Tm1 to Tm3 are the emergent marine terraces, which are located above the modern wave-cut (shore) platform and associated beach deposits.

Based on the measured inner edge of each marine terrace precisely obtained at the SW sector of the Peniche Peninsula (Furninha Cave staircase), it was possible to estimate the uplift rates. All measurements were related to mean sea level. The assignation of terrace MIS ages allows for calculating the uplift rate (U) with the formula of Lajoie (1986):

$$U = \frac{(E-e)}{A} (15)$$

where E is the present-day elevation of the terrace, A is the age of the correlated high stand and e is the eustatic sea-level estimates, at the time of the terrace formation (eustasy correction).

This equation considers only the mean uplift rate from today until age A. In this study, the marine deposits of each dated terrace were correlated to the eustatic sea-level high stands obtained from available sea levels curves (e.g., Labeyrie et al., 1987; Waelbroeck et al., 2002; Siddall et al., 2003), (15).The apparent uplift (Ua) rates were also calculated, without considering the eustatic correction (e.g., Pedoja et al., 2018).

IV.8. Results

IV.8.1 Geomorphological and sedimentological characterisation of marine terrace staircase

As a consequence of carbonate rocks dissolution during the Cretaceous and Cenozoic, several areas with limestones shows karst topography, with small dissolution sinkholes, small basin pools with walls, fringes, lapiás, sometimes better developed along fractures, and caves. These features are well observed from the Carvoeiro Cape until Sra. dos Remédios, in some places covered by aeolian sands (Fig. IV.7).

Near the almost vertical slope cliffs of the Carvoeiro Cape, a sea stack with a caravel shape, named Nau dos Corvos can be observed, with its top at 31 m (a.s.l.). The higher level of the Peniche Peninsula is a wave-cut platform at 29-33 m (a.s.l.), preserved at the Carvoeiro Cape sector and the top of the Furninha cave site (39º21´21" N; 9º23'54.8" W*)* (Figs.IV. 2 and IV.7). This shore platform cut on limestones is affected by karsification.

Along the SW cliffs of the Peniche Peninsula, there is clear evidence of an inset of six marine levels supported by the existence of wave-cut platforms and associated marine siliciclastic deposits (Figs. IV.7, IV.8 and IV.9). Minor normal faults are locally present but with vertical displacements ≤ 0.2 m.

Based on the detailed fieldwork at the area of the Furninha Cave site, a sequence of six marine terrace levels (called Tm1 to Tm6, from the higher to the lower) have been recognized bellow the culminant wave-cut surface (Fig. IV.5, 7, 8 and 9), described in the following paragraphs. All the wave-cut platforms are cut in hard limestones.

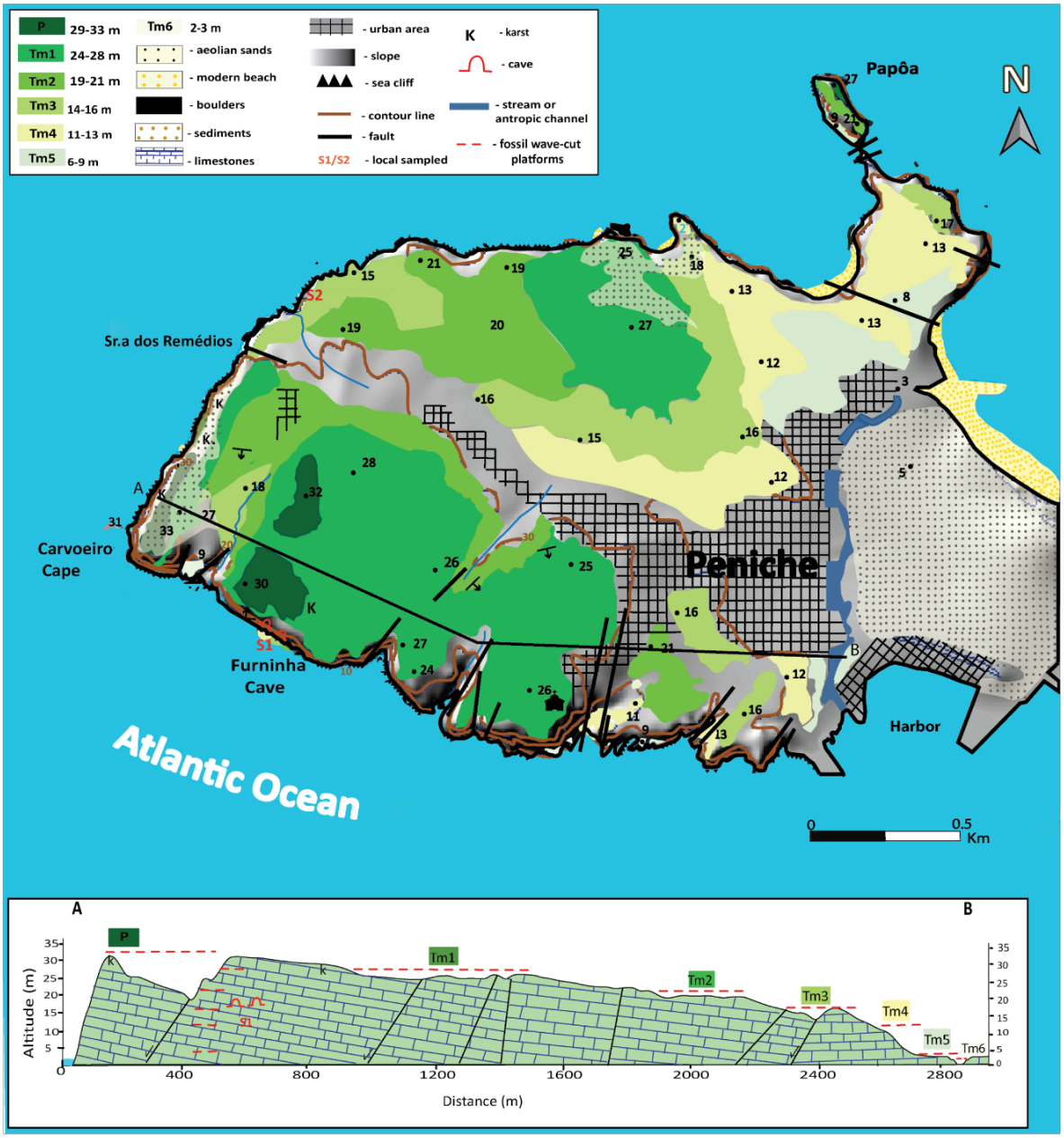

Figure IV. 7. Geomorphological map of the Peniche Peninsula, showing the main wave-cut platforms (the wave-cut platform of Tm6 is too small to be represented at this scale) and other geomorphological information. Site location of the samples dated by ESR: S1 – Furninha Cave, samples Pen2 (Tm3), Pen3 (Tm3), Pen4 (Tm2) and Pen5 (Tm1); S2 – At ~500 m NE of N. Sra. dos Remédios, sample Pen1 (Tm3).

The Tm1 is at 26.9 m a.s.l. (inner-edge), documented by a wave-cut platform developed on a siliciclastic (quartz-rich), with some marine shells, Jurassic limestone. The wave-cut platform is affected by karsification features. For ESR dating, a sample of sandstone was collected (Pen5).

The Tm2 wave-cut platform is represented at 20.0-20.7 m a.s.l. This marine terrace comprises: (i) at the base, a ~0.5 m thick layer of gravels with cobbles and some boulders, with a medium pebble size (MPS) of ~1.0 cm; (ii) at the top, a ~1.0 m thick layer of very coarse to coarse sands, with well-rolled

detrital grains. For ESR dating, a sample of sandstone (Pen4) was collected at ~0.5 m above the inner edge (at ~20.7 m) (Fig. IV.4 N).

Figure IV. 8. Three-dimensional model, with high-resolution (3D model with the texture of the photographs and resolution of 4.6 cm/pix and a high precision Digital Surface Model (MDS) with a resolution of 9, 2 cm/pixel) of the coastal terrace staircase at Furninha Cave site, located at ~850 m SE of the Carvoeiro Cape. The several marine terraces (Tm1 to Tm6) and other geomorphological elements are indicated.

The Tm3 is represented by a wave-cut platform, laterally almost continuous from the Carvoeiro Cape to the Furninha Cave site, showing a ~6 m preserved width, at elevations of 13.5 to 15.5 m (this latter value, the inner-edge) (Fig. IV.8). The sedimentary infill, with a maximum thickness of 3.0 m, comprises: (i) a basal well-cemented beach conglomerate, composed of rolled boulders with a matrix of gravelly very coarse yellow sands, followed by ~1.5 m thick coarse to medium sands; (ii) a thin travertine layer occurs at the top (dated by U-series). The Tm3 is associated with the Furninha Cave marine entrance and small cavities formed by wave action (notches) (Fig. IV. 7). The thickness of the outcrop showing the Tm3 terrace allowed collecting two samples, one near the top and another from the sedimentary sequence base (respectively, Pen3 and Pen2). At a site located ~500 m NE of N. Sra. dos Remédios (NW sector of the peninsula) another sample (Pen1) was collected at the base of the same terrace level, for ground control.

Despite its short extension, the Tm4 wave-cut platform is well-represented at an elevation of 10−13 m a.s.l. This terrace has a sedimentary deposit well preserved in the NW part of the Furninha Cave site cliff (39º21'23" N; 9º24'W). Here, the sedimentary sequence is 2.5 m thick and comprises thin gravels at the base with MPS=1.5 cm, a layer of coarse sands (sample Pen8) and a topmost layer of travertine with fossil bones. The shoreline angle is observed at 12.9 m a.s.l. Some recesses and holes located along the SE part of the cliff are visible too, with very similar elevations (11.3±0.5 m a.s.l.).

The Tm5 marine terrace is observed at altitudes of 6.0 to 9.4 m, consisting of a: lower layer (1.4 m thick) of well-rounded gravels of quartzite, quartz, and some granite pebbles (MPS=7 cm); followed by a pebbly coarse sandstone, 0.6 m thick and from which sample Pen7 was collected; at the top, some boulders of sandstone, fossil bone fragments and thin travertine were identified. The basal layer of marine conglomerate can be correlated to the basal layer of bioclastic conglomerate (with Patella and

Littorina), at ~7-8 m a.s.l., found at the Furninha Cave, which predates a dated level of 81(+42/-31) ka (U-Series) included in the upper aeolian sands.

The lowermost emergent marine terrace (Tm6) is represented by a wave-cut platform at an altitude of 4.0 m.

At the Furninha Cave staircase, fossil bone remains were found at several terrace deposits. At the topmost part of the sedimentary deposits of Tm2, Tm3 and Tm4, bone remains of terrestrial mammals, probably perissodactyl and artiodactyls, were identified. However, they do not provide some age control because the artefacts were found only at the terrace surface.

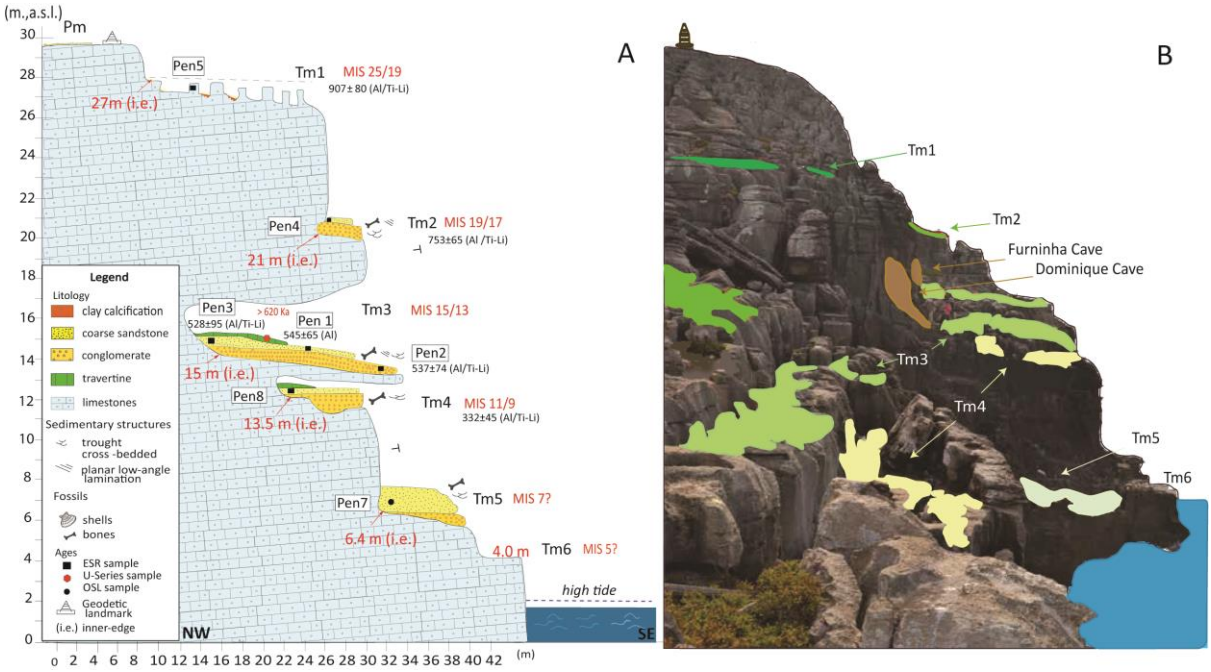

Figure IV. 9. A - Profile of the marine terrace staircase at the Furninha Cave site, presenting the topography and lithostratigraphy; B - Location of each marine terrace (wave-cut platform and sedimentary deposits) (Tm1 to Tm6).

IV.8.2. Texture and mineral composition of the sediment samples

Terrace Tm1

The Tm1 ESR dated sample (Pen5) has a dull yellow-orange colour (10 YR 7/4), consisting of 57% of the sand fraction (medium to very coarse sands) and 39% of gravel fraction. The mineral composition

consists of hyaline and milky quartz, calcite, feldspars (microcline and albite) and minor phyllosilicates (mainly muscovite) (Fig.IV.10). The mean grain size is 1.19 mm, poorly sorted (1.72), symmetrical (0.60) and platykurtic (2.42).

Terrace Tm2

The Tm2 sample (Pen4) has a light grey colour (10YR 8/1) and is composed by 78% of sand (53% of the particle sizes are larger than 300 μm) and 22% of gravels. The sand fraction comprises quartz, feldspar (microcline), calcite, quartzite, granite, muscovite and traces of clay minerals. The mean grain size is 1.34 mm, moderately sorted (0.84), fine skewed (0.96) and leptokurtic (6.15). The quartz grains are usually sub-rounded.

Terrace Tm3

With 0.5 m of thickness, the well-cemented basal conglomerate of Tm3 has a light grey colour (10YR 8/2) (sample Pen2); the sand matrix is composed by subangular grains of quartz, quartzite, feldspar (orthoclase), calcite bioclasts, granite and accessory muscovite. At the terrace upper-division (where sample Pen3 was collected), the sediment has a dull yellow-orange colour (10YR7/2) and is composed by very coarse sand (Fig. IV.9) with the following mineralogy: quartz, K-feldspar (microcline), plagioclase, calcite and accessory muscovite.

Shell fragments and bones are observed, overlaid by a travertine deposit ~17 cm thick. The sample comprises very coarse sand (92%) and gravels (8%), symmetrical (-0.03), poorly sorted (1.31) and platykurtic (2.31). With grey colour (7.5YR8/2), the sample Pen1 is well-sorted medium sand composed by well-rolled quartz, quartzite, feldspars and clay (Fig. IV.4J).

Terrace Tm4

The Tm4 deposit has 2.3 m of thickness and dull yellow orange colour (10YR6/4). The Pen8 sediment was collected about 0.8 m above the wave-cut surface and is composed of medium sand (84%) and gravels (16%) (Fig. IV. 4P). The sample is comprised by well-rounded gravel clasts of quartzite, quartz, granite and schist, and the sand fraction mineralogy contains quartz, K-feldspar (orthoclase and microcline), plagioclase (albite), ankerite/calcite and muscovite (Fig. IV. 9). At the upper part of the sedimentary sequence, fossil bones and travertine were found.

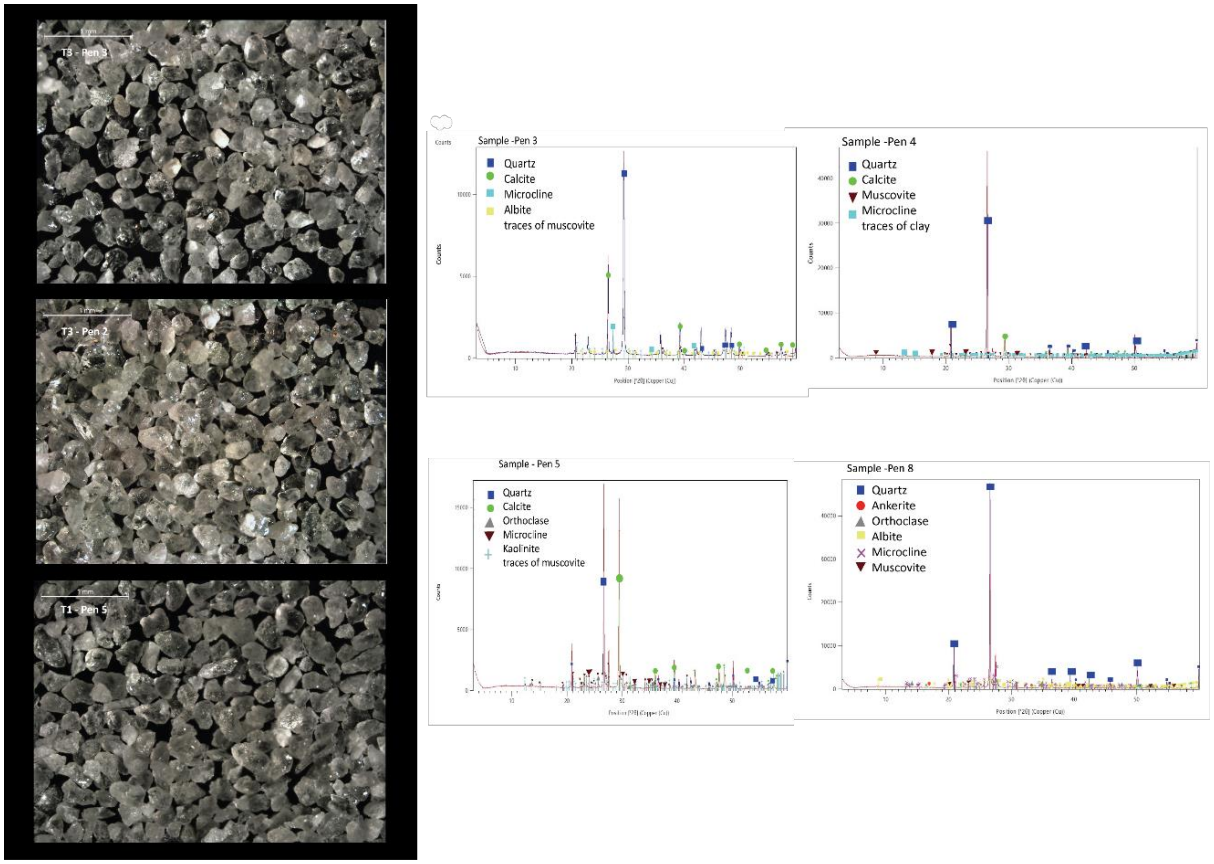

Figure IV. 10. Photomicrograph of some quartz grains (250-180 µm) and examples of the mineral composition of sandstone samples collected from the studied marine terrace deposits.

Terrace Tm5

The base of this deposit is composed by well-rounded clasts of quartz, quartzite, pink granite, limestone, schist and some silex (Fig. IV.4I). The Tm5 deposit has 2.0 m of thickness and at the upper part was found a fossil bone. The sand sample has light grey colour (10YR8/2) and is dominated by medium sand.

IV.9. Interpretation of the depositional environment and sediment provenance

The sedimentary characteristics of the deposits associated with the terraces (rolled siliciclastic clasts, good sorting and pebbly sands), indicate a paleo-depositional setting of very narrow beaches near the related paleo-shore coastal angle. The high wave dynamics is expressed by a predominance of very coarse sands and gravels. The Tm3 deposits (Fig. IV.4L, M, J) locally comprise a lower conglomerate of limestone boulders. All samples have carbonate cement.

The transport of the siliciclastics (sand grains and gravels) that constitute the studied paleo-beach deposits is interpreted as made mainly by littoral drift, from northern river mouths discharges and coastal cliff erosion. Some clasts (granite and schist) have local provenance from the near Berlengas archipelago (at W), which is composed by Palaeozoic and Proterozoic rocks of the Iberian Massif.

IV.10. ESR dating of optically bleached quartz grains

The ESR analytical data are listed in Tables IV.1 and IV.2. Repeated measurements of Al and Ti−Li centres over different days were carried out. Due to the younger age, the Tm5 sedimentary deposits were not dated by ESR and later will be date using OSL dating (pIRIR protocol).
Repeated measurements of Al and Ti centres over different days, with De variability between 5.0 % and 22.0 %, show the reliability of the fitting results (Duval, 2012). The De values derived from Al (EXPLIN) and Ti option D (SSE and EXPLIN) are mostly 1σ consistent (functions described in Chapter II).

Table IV. 1. ESR means data (9 measurements) collected from the measures of Al centre in the samples of the Marine terrace T1 (Pen5), T2 (Pen4) and T 4 (Pen8).

Dose (G)	**ESR (a.u.)**	**d.s.**	**ESR (a.u.)**	**d.s.**	**ESR (a.u.)**	**d.s.**
	Pen5		**Pen4**		**Pen8**	
0	81.681	2.653	71.303	6.767	70.516	11.700
100	102.416	4.099	86.479	23.443	85.214	7.306
200	105.892	5.243	89.672	18.106	106.647	11.104
400	132.649	6.382	107.274	17.841	124.200	7.636
800	159.638	4.226	135.493	19.407	167.833	12.342
1600	196.124	9.942	183.287	53.878	230.743	21.674
3200	252.942	3.819	249.289	35.927	321.235	16.634
6000	345.363	9.553	422.934	64.769	518.686	39.913
10000	359.378	35.553	501.182	80.849	639.263	16.272
15000	430.132	26.436	539.431	65.446	759.038	43.852
25000	617.573	57.442	920.092	97.772	748.894	54.459

The final D_e values for each sample were calculated on the average of ESR intensity values. The relative bleaching component values suggest similar bleaching conditions of all samples, except Pen1 and consistent with previous observations (Voinchet et al., 2007; Duval, 2008; del Val et al., 2019). The goodness of fit is overall good for these samples, with adjusted r^2 values of > 0.98. The D_e values for Al and Ti−Li centres are very similar for almost samples.

Table IV. 2. ESR mean data collected from the 9 measurements of Al centre in the samples of the T3 marine terrace (Pen1, Pen2, and Pen3).

Dose (G)	ESR (a.u.)	d.s.	ESR (a.u.)	d.s.	ESR (a.u.)	d.s.
	Pen1		Pen 2		Pen 3	
0	143.494	13.097	101.977	14.688	76.740	15.930
100	160.610	18.391	120.869	8.033	113.985	12.575
200	184.461	29.437	132.071	11.835	108.352	4.399
400			159.329	7.563	140.821	23.307
800	239.174	29.344	194.920	28.474	195.440	9.105
1600	299.795	44.171	278.051	14.374	250.565	16.423
3200	368.969	44.293	411.204	50.151	320.377	28.222
6000	452.887	94.848	523.921	45.153	342.344	16.191
10000	525.887	76.184	593.302	59.751	473.905	37.561
15000	722.312	41.787	838.543	57.430		
25000	887.619	33.310	1092.253	77.415	865.712	30.805

The weighted average age was obtained for all samples using both centres, using IsoPlot 3.0 (Ludwig, 2003) and given 95% of confidence. Repeated measurements of Al and Ti centres over different days, with D_e variability between 5.0 % and 22.0 %, show the reliability of the fitting results (Duval, 2012). The D_e values derived from Al (EXPLIN) and Ti option D (SSE and EXPLIN) are mostly 1σ consistent. Pen 1 result revealed higher D_e values in Ti−Li centre (927±51) than in Al centre (486±50). In that regard, the difference in Al and Ti ages for this sample is usually interpreted as incomplete bleaching of the Al. In this case, the samples Pen 2 and Pen 3 presents Al ages consistent with the Al age of this sample and not with the age value of Ti−Li, (more articulate with the age of Tm2) so, as they are all of the same levels, the Al value was used.

Table IV. 3. ESR mean data collected from the measurements of Ti-Li centre in the samples of the marine terraces (T1, T2, T4). The protocol was repeated 3 and 4 times in each aliquot (9 measurements).

Dose (G)	ESR (a.u.)	d.s.	ESR (a.u.)	d.s.	ESR (a.u.)	d.s.
	Pen 5		Pen4		Pen 8	
0	146.565	12.549	136.191	23.176	113.219	9.051
100	179.050	27.787	156.755	15.895	150.650	5.443
200	199.264	20.081	172.425	21.400	167.024	8.880
400	251.250	19.451	224.431	33.109	235.705	16.511
800	319.662	19.985	287.489	72.100	265.718	14.005
1600	395.326	24.140	430.700	79.817	358.873	19.073
3200	551.412	43.858	640.596	89.884	538.358	25.763
6000	627.013	34.262	1067.496	197.600	795.086	46.587
10000	713.874	52.640	1164.825	135.110	984.790	44.152
15000	719.722	71.150	1120.218	105.117	792.441	69.352
25000	671.403	56.964	1000.741	132.661	798.713	65.345

Table IV. 4. U content (ppb), isotopic ratios and age of the Furninha Cave T3 travertine.

Sample	^{238}U (ppb)	^{232}Th (ppb)	^{234}U/^{238}U	^{230}Th/^{234}U	^{230}Th/^{238}	^{230}Th/^{232}Th	Age (Ka)
Furn A (Paris)	114±1.5	29.9±0.39	1.054±0.01	1.024±0.032	1.078±0.032	13±0.3	>438
Furn B (Nanjing)	92±0.08	7.23±0.02	1.033±0.003	1.018±0.004	1.052±0.002	41±0.15	>620

According to the intensity growth for ESR-Al signal curve responses (Fig. IV.11), the youngest samples had a rapid growth of the first doses and a much slower for high doses, as described in another study (Voinchet et al., 2013). For the older samples (e.g. Pen5) the growth is slower.

Table IV. 5. Sample information, external β and γ dose rate, cosmic dose and bleaching. External α was considered negligible. The water content (W.C.) for the burial time was estimated considering the field water content and the saturation water content.

Marine terrace	Sample code	Estimated W.C. (%)	External β dose rate (Gy/Ka)	External dose rate (Gy/Ka)	Cosmic dose rate (Gy/Ka)	Bl (%)
Tm1	Pen5	5 ± 2	318 ± 27	211±31	169.1±8.4	61.0±1.3
Tm2	Pen4	11±5	460±22	279±25	177.7±8.8	46.0±8.8
Tm3	Pen3	11±5	352±25	231±29	163.1±8.2	44.0±2.9
Tm3	Pen2	5±2	385±26	249±30	177.7±8.8	53.0±6.6
Tm3	Pen1	15±5	705±29	469±33	163.1±8.2	42.0± 5.0
Tm4	Pen8	10±2	456±29	280±34	180.5±9.1	50.0±2.3

Table IV. 6. Dosimetry and ESR age in Al, Ti−Li centres of sedimentary samples collected from the marine terraces. The depth from which sample was taken is given in (m) below each sedimentary sequence top.

	Tm1 terrace	Tm2 terrace	Tm3terrace (top)	Tm3 terrace (base)	Tm3 (base)	Tm4 terrace
Sample code	**Pen5**	**Pen4**	**Pen3**	**Pen1**	**Pen2**	**Pen8**
Depth (m)	0.8	0.5	0.2	0.1	0.2	2
Elevation (m)	26.9	18.5	16.5	15.0	15.0	13.1
Grain size (µm)	250-180	250-180	250-180	250-180	250-180	200-100
^{238}U (ppm)	0.55±0.07	0.76±0.06	0.59 ± 0.06	1.49±0.08	0.92±0.06	1.07±0.07
^{232}Th (ppm)	1.73±0.45	2.12±0.40	1.89 ± 0.43	4.18±0.55	1.68±0.48	1.90±0.52
^{40}K (%)	0.31±0.02	0.53±0.01	0.35 ± 0.01	0.79±0.02	0.39±0.02	0.45±0.20
D_a (total) (µGy.a^{-}	706±42	987±36	756±38	1716±60	821±42	941±45
D_e Ti centre (Gy)	585±30	687±77	384±76	899±66	431±33	281±49
Adj. Square	0.99-	0.99	0.97	0.99	0.99	0.98
D_e Al centre (Gy)	582±59	716±38	356±38	694±80	437±45	338±31
Adj. Square	0.98	0.98	0.98	0.99	0.99	0.98
Ti−Li centre Age (ka)	896±350	733±35	508±103	684±43	525±47	298±54
Al centre Age (ka)	987±120	773±49	548±87	545±65	588±60	366±37
Mean Age (Al and Ti−Li)	977±110	753±65	528±95	-	537±74	332±45

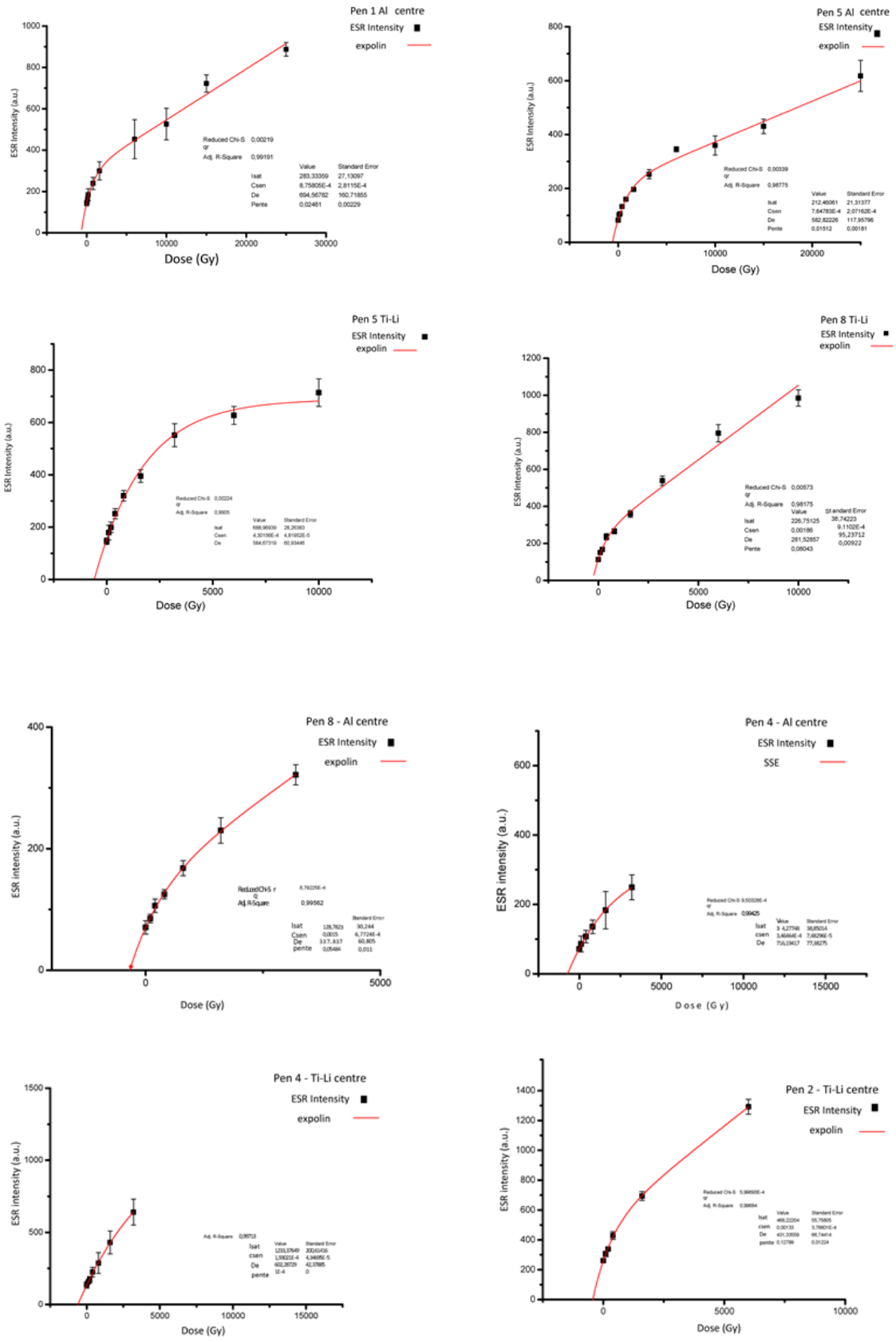

Figure IV. 11. Examples of the fitting curves of Peniche samples (Pen1, 2, 4, 5, 8) in Al and Ti-Li centres.

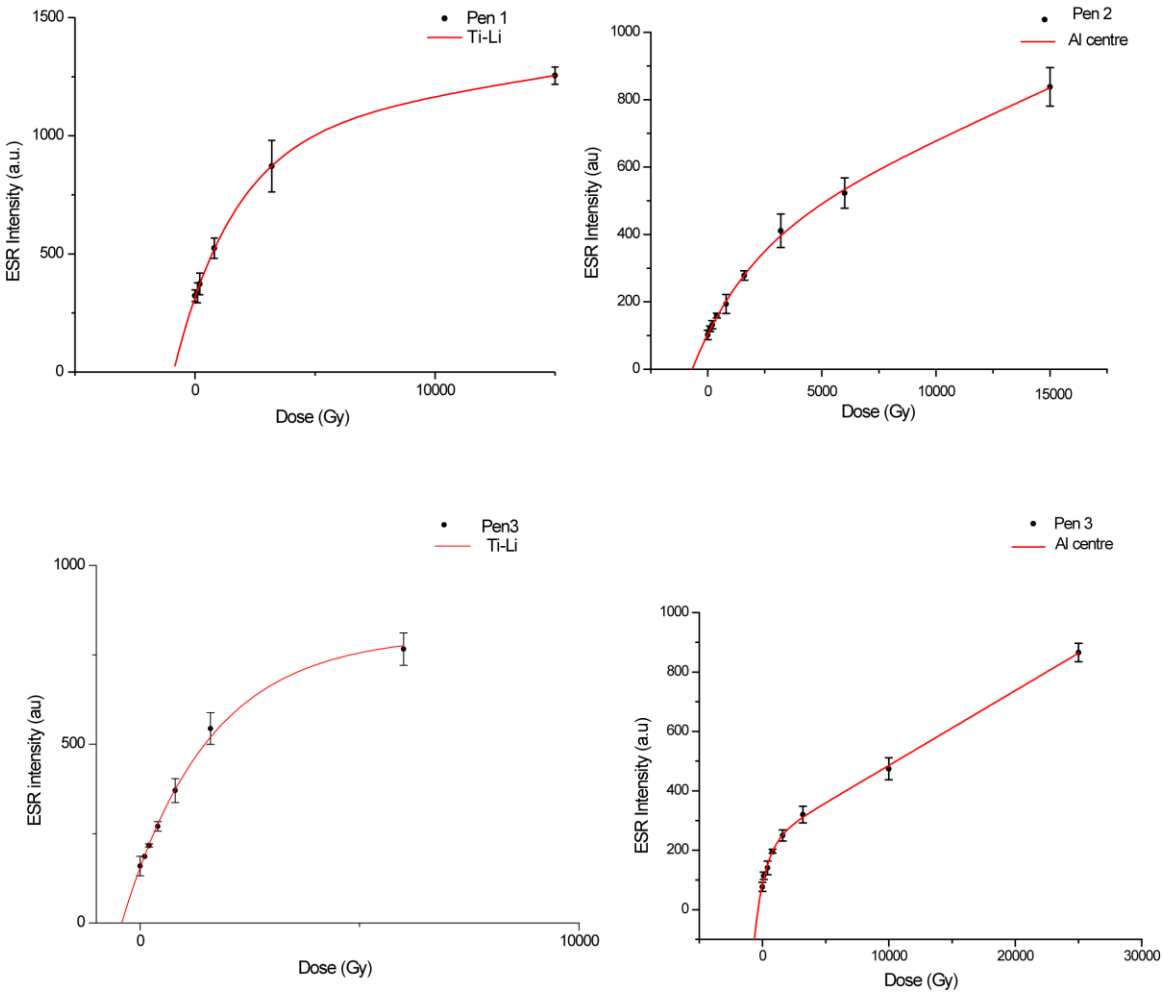

Figure IV. 12. Examples of the Fitting curves of Peniche samples (Pen1, 3, 2) in Al and Ti-Li centres.

IV.11. U-series dating of travertine levels

A sample of the travertine level located at the topmost deposits of the Tm3 was collected at the Furninha Cave entrance. U-series have analysed sub-samples in both Paris and Nanjing laboratories, and the data agree. The uranium content ranges between 90 and 115 ppb according to the heterogeneity of the analysed sample (Table IV.4). Isotopic ratios agree for both laboratories at 1-2 %. The $^{230}Th/^{232}Th$ ratio is higher than 41 at Nanjing laboratory showing that the sample is free of exogenous thorium. The measurement performed in Nanjing with MC-ICP-MS is expected to be more accurate, and the obtained age (>620 ka) can be used without any correction.

Another travertine sample was collected from the topmost deposits of the Tm4 at the Furninha Cave terrace staircase, but it provided an age (19±0.5 ka; Table IV5) much younger than the Tm4 terrace formation.

Table IV. 7. U content (ppb), isotopic ratios and age without correction of the Furninha Cave Tm3 and Tm4 travertine samples.

Sample	^{238}U (ppb)	^{232}Th (ppb)	$^{234}U/^{238}U$	$^{230}Th/^{234}U$	$^{230}Th/^{238}U$	$^{230}Th/^{232}Th$	Age (ka)
Tm3travertine **(Paris)**	114±1.50	29.9±0.39	1.05±0.01	1.02±0.02	1.08±0.03	13±0.30	>438
Tm3travertine **(Nanjing)**	92±0.08	7.23±0.02	1.03±0.00	1.02±0.00	1.05±0.00	41±0.15	>620
Tm4 travertine **(Paris)**	465.0±9.6	28.10±0.57	1.143±0.024	0.160±0.004	0.182±0.004	9.00±0.10	19±0.5

IV.12. Correlation of the marine terraces with available eustatic curves and Marine Isotope Stages

The ESR ages obtained presents the standard chronological pattern for the stepped terraces, the oldest being the highest. The obtained ESR ages for each marine terrace (Lower and Middle Pleistocene) were compared to the available global mean sea level curves and to the established MIS's (Labeyrie et al., 1987; Murray-Wallace, 2002; Waelbroeck et al., 2002; Siddall et al., 2003) (Fig. IV.13).

The ESR mean age obtained for Tm1 is 977±110 ka, suggesting that is terrace is probably correlated with the high sea-level conditions spanning 950-820 ka (MIS25-19) (Early Pleistocene). When the uplift rate is low, it is possible that a marine terrace records two or more marine isotope stages (e.g., Muhs et al., 2002; Zomenia, 2012).

For the sample collected from the Tm2, the ESR dating values of Al and Ti centres are similar, with a weighted mean age of 753±65 ka with 95% confidence, (2σ, MSWD=0.084, P=0.77). It is possible to propose that the Tm2 could correlate to the MIS17 high stand sea level conditions (740-680 ka).

For the three ESR dated samples of the Tm3 terrace (Table IV. 6), similar results on Ti−Li and Al centres were obtained for Pen3 (528±95 ka) and Pen2 (537±74 ka), but Pen1 has a similar age on the Al centre (545±43ka). The Tm3 terrace age with all the weighted age values of the samples (without Pen1 in Ti-Li) is 526±31, with 95% of confidence (2σ, MSWD=7.5 and P=0.001). The U-series age of >620 ka (Nanjing laboratory) of the travertine at the Tm3 topmost level is higher than expected, probably due to the proximity of the secular equilibrium with an age ratio in excess. In conclusion, this terrace probably records aggradation during MIS15 and MIS13 (620-540 ka and 495-460 ka, respectively).

For Tm4, the ESR values of both centres (Table IV.6) are within the error range (366±37/298±54 ka), and the weighted mean age was of 332±45 (2σ, MSWD=4.7 and P=0.001). Considering that there are high stands comprised in the age error range, this marine terrace could represent the MIS11 and the MIS 9 intervals (430-390 ka; 330-270 ka, respectively).

Regarding the lower emergent marine terraces, Tm5 probably correlates to the high stand conditions during 240-180 ka (MIS7) and the Tm6 wave-cut platform to the 128-85 ka interval (MIS5).

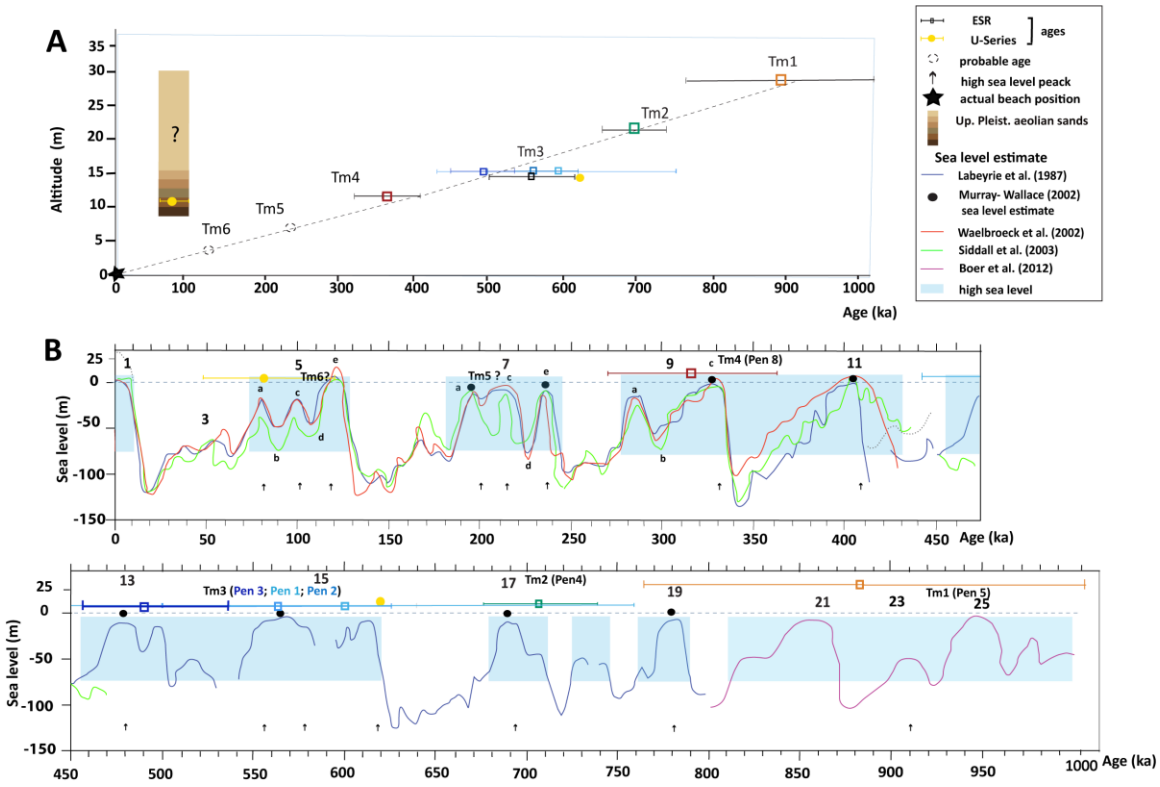

Figure IV. 13. A – Plot of the altitude versus the respective age of each terrace dated sample of the Peniche staircase (elevations are not corrected for eustatic changes). B - Global mean sea level curves (modified from Labeyrie et al., 1987), ESR mean and U-series ages obtained and the most probable age of the sedimentary deposits of the terraces indicated in grey shading. Black circles indicate the Murray Wallace (2002) sea-level estimates for MIS7, 9 and 11; the red and green curves show the ones proposed by Waelbroeck et al., (2002) and Siddall et al. (2003), respectively. Terraces (Tm) are displayed with the respective altitudes of their inner edges. The data indicate that under a low uplift rate, the sedimentary deposits of a marine terrace could record a continuous aggradation interval comprising high stand sea-level conditions of successive MISs or that the same level can be re-occupied by several high sea-level peaks (a complex terrace, with sedimentary discontinuities, comprising several aggradation intervals).

IV.13. Uplift rates

The studied marine sequence is a precious tool for understanding coastal behaviour and identifying the uplifting Quaternary trend in the studied area. Because the fossil sea cliff (shoreline angle/strandline) of each terrace is a good approximation of sea level during the peak of a highstand (Lajoie, 1986), these were measured in the field with a GPS RTK and the $E \pm \Delta E$ values were obtained (Figs. IV.8 and IV.9).

As defined by Bull (1985), the inferred corrected uplift rate involves subtracting the marine terrace shoreline angle, relative to modern sea level from the shoreline angle altitude of global paleo sea level at the considered age; the corrected height is then divided by the age of the marine terrace. For the study area, using the elevation of the culminant wave-cut platform (34 m) as the geomorphic reference of the Pliocene sea-level peak (+10-20 m; Miller et al., 2019), a long-term corrected uplift rate of 0.005±0.001 is obtained for the last 3.7 Ma. For the previous ~1 Ma, the apparent short-term uplift rates (eustatic changes in sea level are not corrected) vary between 0.03 and 0.05 m/ka (means of 0.03 to 0.04 m/ka) and the corrected short-term uplift rates between -0.05 and 0.05 m/ka (means of -0.02 to 0.05 m/ka) (Tables IV.8 and IV.9). If for Tm6 (ascribed to MIS5) a eustatic correction of +2 m is used (Galve et al., 2019), the obtained uplift rate is 0.02 m/ka, a more suitable value.

Table IV. 8. Apparent uplift rate calculation using the altitude of the shoreline angle (inner edge) of the studied several marine levels (relative sea-level (RSL) reconstructions); for those values of U_a, eustatic changes in sea level are not considered. For the terraces that could represent two or more marine isotope stages, it was used the age of the younger MIS. WCN - wave-cut notch; IE- inner edge; *sediment thickness at the shoreline angle; altitude at the shoreline angle (E±ΔE); assigned Age (A); apparent uplift rate ($U_a = E/A$).

Marine level	**Probable Marine Isotope Stage**	**Type of marker**[a]	**Sediment thickness*** (m)	**Altitude of shoreline angle** (m)	**Assigned age** (ka)	**Apparent uplift rate** (m/ka)		
						U_{max}	U_{min}	U_{mean}
Pm	**-**	Wave-cut platform	0	33	3700	01	0.01	0.01
Tm1	**MIS25-19**	IE	0.8	27±0.5	875±130 (ESR) 1000-820	0.04	0.03	0.03
Tm2	**MIS 19-17**	IE	0.5	21±0.5	707±32 (ESR) 720-670	0.030 0.03	0.03 0.030	0.03 0.03
Tm3	**MIS15-13**	WCN	0.8-2.5	15.5±0.01	558±52(ESR) 620-450	0.03 0.04	0.030 0.04	0.04 0.03
Tm4	**MIS9**	IE	2.5-3.0	13.5±0.01	327±30 (ESR) 370-275	0.03 0.04 0.05	0.03 0.04 0.03	0.04 0.04
Tm5	**MIS7**	IE	2.0	7±0.01	not directly dated (MIS7, 240-180)	0.04	0.03	0.04
Tm6	**MIS5**	IE	0	4.0±0.5	not directly dated (MIS5, 128-85)	0 0.05	0.03	0.04

Table IV. 9.Relative uplift rate calculation, taking into account the altitude of the shoreline angle (inner edge) and the respective paleo-sea level. WCN- wave-cut notch; IE- inner edge; *sediment thickness at the shoreline angle; altitude at the shoreline angle (E±ΔE); assigned Age (A); relative uplift rate ($U = E/A$). The following sea-level peaks were used: +10-20 m for Pliocene (Miller et al., 2019); -0.5 m for MIS7 (Muhs et al., 2012); +6±4 m for MIS5 (Murray-Wallace and Woodroffe, 2014).

Marine level	**Probable eustatic paleo-sea-level** (m)	**Type of marker** [a]	**Sediment thickness*** (m)	**Relative altitude of shoreline angle** (m)	**Assigned age** (ka)	**Apparent uplift rate** (m/ka)		
						U_{max}	U_{min}	U_{mea}
Pm	**+10-20**	Wave-cut platform	0	(33 - (+10-20) 23-13	3700	0.006	0.004	0.005
Tm1	**0**	IE	0.8	26.9	875±130 (ESR) (950-820)	0.04 0.03	0.02 0.03	0.03 0.03
Tm2	**0**	IE	0.5	20.7	707±65 (ESR) 680 (MIS17)	0.03 0.03	0.03 0.03	0.03 0.03
Tm3	**0**	WCN	0.8-2.5	15.0	503±96 (ESR) 550-620 (MIS15) 450-500 (MIS13)	0.04 0.03 0.04	0.04 0.03 0.03	0.04 0.03 0.04
Tm4	**-0.5**	IE	2.5-3.0	(12.9 + 0.5)	359±37 (ESR) 270-340 (MIS9)	0.04 0.05	0.03 0.04	0.04 0.05
Tm5	**-0.5**	IE	2.0	(6.4 + 0.5)	190-240 (MIS7)	0.04	0.02	0.03
Tm6	**+6±4**	IE	0	(4.0) – (6±4)	128 (MIS5)	0.02	0.05	-0.02

IV.14. Discussion

The culminant wave-cut platform should be the record of the important late Zanclean-Piacenzian marine incursion, with a paleo-sea level of +10-20 m (a.s.l.) (Miller et al., 2019), well represented along the Western Iberian Margin (e.g., Cunha, 2019; Gouveia et al., 2020) and in the Mediterranean area (e.g., Müller, 1993; Barnolas et al., 2019). The studied marine terrace staircase is a consequence of the several Pleistocene eustatic sea-level highstands (Anderson et al., 1999; Lisiecki and Raymo, 2005; Stephenson et al., 2013; Normand et al., 2019), on a set of low crustal uplift.

The ESR ages obtained in this study are consistent with the terrace stratigraphic order and with the most relevant sea-level high stands during the Pleistocene that is older than the MIS7.

The ESR signal from Al centre is in accordance in all the samples of the Tm3 (Pen1, Pen2 and Pen3). The chronology provided by Ti−Li centre is in accordance with the other values in Tm3, except for Pen1 with higher value (684±43 ka). The D_e of Pen 1 in Ti-Li can be explained by the intensity values of the first points and the saturation signal at higher doses (15000 Gy).

As previously stated, when the uplift rate of a coastal area is low, an old marine terrace may represent two or more marine isotope stages (e.g., Muhs et al., 2002; Zomenia, 2012). It seems to be the case for Tm1 (MIS25-19), Tm3 (MIS15-13) and Tm4 (MIS11-9). However, the MIS13 could be not represented, as in almost worldwide (Caputo, 2007; Bintanja and Van De Wal, 2008). Some terraces within a sequence could be removed by marine erosion (e.g., MIS11), especially if the next highstand lasted long enough (e.g., Saillard et al., 2009), providing the conditions to make it to collapse and/ or to be eroded.

Below the Pm, the most extensive inland wave-cut platforms are those associated with the Tm1 (implying a long duration of sea-level high stand conditions) and with the Tm3 (both with a probable time of ~160 ka). The moderately inland-developed wave-cut platforms are those associated with the Tm4, Tm2 and Tm5 (possible duration of ~100, 80 and 60 ka, respectively). The less-developed emergent wave-cut platform is the one associated with the Tm6 (~50 ka but favoured by the higher elevation above the present sea level during the MIS5and MIS 11).

The Pliocene recorded a period of global warmth and high sea level. Global surface temperatures during the most recent period of Pliocene warmth at ~3 Ma were 2–3°C warmer than the 20th century (Dowsett et al., 2013). During the Middle and Late Pleistocene, the sea surface temperature (SST) in the Western Iberian Margin, fluctuated between 6ºC and 21ºC, with the warmest temperatures occurring throughout interglacial MIS5e and MIS19c (Rodrigues et al., 2017). The coolest interglacial (17ºC) was MIS23 (with least impact in sea-level fluctuation). Climatically, MIS 11 represents the warmest sea surface temperatures of recent interglacials, followed by MIS9 with the highest sea levels (Spratt et al., 2016).

Summarizing the interpreted coastal evolution of the study area during the Pleistocene, by using the less restrictive probable intervals of aggradation:

- During 1000 to 760 ka (MIS25 to MIS19), generally high sea-level stands generated the Tm1 wave-cut platform; after, low sea levels lead to the retreat of the shoreline;

- During 710 to 680 ka (MIS17), generally high sea-level stands generated the Tm2 terrace, followed by a retreat of the shoreline during 680 to 620 ka;

- During 620 to 450 ka (MIS15-13), high sea-level stand generated the Tm3 terrace, followed by a retreat of the shoreline;

- During 430 to 275 ka (MIS11-9), high sea-level stands generated the Tm4 terrace, later exposed;

- During 275 to 240ka (MIS8), low sea levels lead to the retreat of the shoreline;

- During 240 to 180 ka (MIS7), high sea-level stands generated the Tm5 terrace; followed by a retreat of the shoreline;

- During 125 to 85 ka (MIS5), the relevant high stand generated the Tm6 terrace;

- During 85 to 18 ka (MIS4 to MIS2), sea level has fluctuated following an overall lowering trend characterised by highstand positions at MIS5a (80 ka, -55 m) and MIS3 (60 ka, -24 m), and the low stand of the Last Glacial Maximum (LGM)/MIS2 (18 ka, ~ -120 m). The sites where the 80–18 ka shore platform and marine terraces would have developed are currently located in submerged areas offshore. During the huge retreat of the shoreline, the paleoclimates comprised wet-temperate, wet-cold, dry-temperate and dry-cold conditions and the cold climate conditions (Figueiredo et al., 2017); the latter were characterized onshore by the predominance of energetic aeolian sand dynamics (with deposition inside the Furninha Cave and as a cover unit at the Peniche Peninsula).

- The sea-level rise following the 18-ka low stand was rapid and associated with climatic amelioration during the transition into the current interglacial. This evolution leads to the Holocene sedimentation in gravelly/sand beaches and the associated field of aeolian dunes.

The long-term uplift rate obtained for the littoral areas of Portugal mainland, for the last ~3 Ma are estimated as 0.1-0.2 m/ka (Cabral, 1995) or, considering as geomorphic reference the great wave-cut platform dated as 3.7 Ma, as 0.019-0.071 m/ka for the more elevated setting of Cape Espichel (Cunha et al., 2015), as 0.004–0.055 m/ka for the Figueira da Foz area (Ramos et al., 2012) and as 0.004-0.006 m/ka for the less elevated study area. These values evidence differential uplift along the western Portuguese coast. For the last ~1 Ma, the apparent short-term uplift rates (eustatic changes in sea level are not considered) vary between 0.03 and 0.04 m/ka and the corrected uplift rates between 0.02 and 0.05 m/ka. So, low crustal uplift conditions were determined, that are in agreement to a passive margin setting, but evidencing higher rates during the Pleistocene that should be interpreted as resulting of an increase in intraplate compressive stress affecting the Western Iberian Margin (e.g., Martins et al., 2010; Cabral, 2012; Vilanova et al., 2014; Cunha et al., 2016; Cabral et al., 2018, 2019). As a comparison, along the SE Spanish peninsular and insular coasts, the MIS7 coastal unit is exposed with a maximum height of +10-12 m (a.s.l.) and a minimum of +1.5 m (a.s.l.), also pointing to differential uplift (Zazo, 2013; Galve et al., 2019).

IV.15. Conclusions

The low relief coast of the Peniche Peninsula records a culminant wave-cut platform above a staircase of six marine terraces.

The ESR ages obtained in optically bleached quartz are consistent with the stratigraphic order of the terrace staircase. So, considering the highstands comprised by the ESR ages error range: the Tm1 wave-cut platform could correlate to 1000-785 ka (MIS25-19); the Tm2 marine terrace could correlate to 745-680 ka (MIS17); the Tm3 terrace can be related to 620-460 ka (MIS15-13); the Tm4 terrace could record the interval 365-275 ka (MIS11-9); the Tm5 terrace probably spans 240-180ka (MIS7); in the lowermost emergent position, the wave-cut platform at 4 m (Tm6), probably records the interval 128-85 ka (MIS5).

The paleogeographic evolution of the Peniche Peninsula since the early Pliocene can be explained by the development of several marine shores during sea-level high stands, in a setting of low uplift. The Quaternary coastal landscape development in the study area has been driven by an interplay between tectonics, eustatic and climatic forcing mechanisms. In areas of low uplift rate and tectonics, sea level and climatic changes dominate coastal landscape development.

The Western Iberian Margin is a region where active tectonics plays a significant role in the geomorphic expression and distribution of Quaternary marine terraces, recording in many cases vertical ground motions (uplift/subsidence) superimposed on global sea-level oscillations.

Shoreline angle altitudes associated with identified platforms were used to calculate uplift rate estimates. Using the culminant wave-cut platform as a geomorphic reference, generated at ~3.7 Ma under an estimated sea-level peak at ~+10-20 m, a long-term corrected uplift rate of 0.004-0.006 m/ka is obtained. For the last 1 Ma, the marine terraces of the study area allow estimating a long-term corrected uplift rate of ~0.03 m/ka (mean short-term uplift rates of -0.02 to 0.05 m/ka). These values indicate a low uplift rate, but increasing, which agree with a passive margin under intraplate compression. Comparison with the uplift rates obtained for other areas of the Western Iberian Margin supports differential uplift in a setting of active faults.

CHAPTER V. GEOMORPHIC MARKERS OF QUATERNARY TECTONICS IN WESTERN IBERIA: INSIGHTS FROM THE LOWER MONDEGO RIVER TERRACES, CENTRAL PORTUGAL

V.1.Introduction

In the western sector of the Iberian Peninsula, there are numerous geomorphic evidence of uplift, such as high sea cliffs and raised marine terraces along the coast, plateaus and planation surfaces at high altitudes deeply incised drainage networks inland and terrace staircases along the main river systems.

Marine platforms and river terraces are relevant geomorphic records of vertical crustal movements (either regional uplift or differential uplift) and climate change, contributing to infer apparent sea-level change, rates of the fluvial incision (e.g., Burbank and Anderson, 2001) and providing important insights to understand the long-term landscape evolution (e.g., Bridgland and Westaway, 2014). The influence of tectonics and climate on terrace formation (i.e. alternation of fluvial incision and aggradation) have been widely debated (Kukla, 1975, 1977; Bull, 1991; Li, 1991; Antoine, 1994; Bridgland, 1994, Tyràcek, 1995; VandenBerghe, 1995, Saucier, 1996; Maddy, 1997; Bridgland, 2000; Bridgland and Westaway, 2008). It seems to be consensual that for a staircase of terraces, the river flow areas should have experienced uplift, which driven the valley through an incision tendency. The uplift is considered indispensable to create the vertical space in which the successive terraces are disposed above the present valley floor (Maddy, 1997; Maddy et al., 2000; Westaway, 2002a, b, 2007; Westaway et al., 2009). On the other hand, the intensity of climate change controls the terraces' aggradational or degradational character (Demoulin et al., 2017) through its influence on discharge and sediment supply.

In mainland Portugal, the terraces along the main rivers - Douro, Tejo, Guadiana and Mondego - appear as stepped morphologies on the slopes of the valleys probably driven by cyclic glacio-eustatic sea-level changes, superimposed on a long-term uplift trend (Cunha et al., 2008, 2017; Martins et al., 2009; 2010; Ramos et al., 2012). This stepped arrangement of terraces results from the situation along the western Atlantic border of the Iberian Peninsula, considered a passive margin, but experiencing NW-SE convergence of 4-5 mm/y between Eurasia and Nubia plates (Cabral and Ribeiro, 1988; Cabral, 1995; Ribeiro et al., 1996; Calais et al., 2003; Nocquet and Calais, 2004; Cloetingh et al., 2005; Fernandes et al., 2003, 2007; Cabral, 2012), at least during the Quaternary.

The glacio-eustatic control on the main Portuguese rivers' terrace formation is easily explained by the Atlantic Ocean proximity and the fact that the rivers have lower reaches less than 200 km away from the ocean. Relative sea-level lowstand (e.g., 120 m below the present-day sea level) caused deep incision on the continental shelf, reaching up to 100 km inland, while in the sea-level high stands the valleys were drowned and transgressed by tidal and marine environments near the coast (Vis 2009).

In mainland Portugal, several geomorphological markers have been used to characterise the Quaternary vertical movements. In coastal regions, a regional Pliocene wave-cut platform dated as ca. 3.7-3.6 Ma (Diniz et al., 2016) and some dated Pleistocene coastal units (Benedetti et al., 2009; Ramos et al., 2012; Carvalhido et al., 2014, Ressurreição, 2018; Figueiredo et al., 2014; Cunha et al., 2015; Gouveia et al., 2020b) has been used for this purpose. Inland the most used geomorphological references are the surface of the culminant sedimentary unit, with probable age of ~2 Ma (Cabral, 2012; Cunha, 2019), and Pleistocene fluvial terraces along the major river valleys (Martins et al., 2009; Cunha et al., 2005, 2008, 2012, 2016, 2017). The long-term uplift for the last 3-2 Ma, ranges from 0.1 and 0.2 mm/y with higher values inland relative to coastal areas (Cunha et al., 2005, 2008, 2010, 2016; Cabral et al., 2012).

The LMV is the study area, located between Coimbra and Figueira da Foz (river mouth in the Atlantic Ocean) (~50 km), in the southwest sector of the Mondego Cenozoic Basin (Fig. V.1). This basin records a marine incursion during the latest Zanclean-Piacenzian (Cunha et al., 2019). In the LMV, the Quaternary deposits were first studied by Ribeiro and Patrício (1943) and Soares (1966). Soares et al. (1992, 1997, 1999) grouped the Quaternary deposits of the LMV into four sets according to their marine-fluvial counterparts at Figueira da Foz and Coimbra areas. According to the heights above the alluvial plain and the sedimentary characteristics, the Quaternary deposits were correlated with tectonic pulses and climatic rhythms of the Quaternary, and their age ascribed as: Sicilian (Lower Pleistocene), first group; Mindel/Riss stage (Middle Pleistocene), second group; Riss/Würm interglacial, third group; and Holocene, fourth group.

Up to now, the study area lacks a detailed geomorphological mapping of the terrace staircases and the long-term landscape evolution is not entirely understood. Detailed cartography is needed to establish a longitudinal and transversal correlation of the river terraces along the valley and to assess differential uplift in an area with evidence of active tectonics (http://info.igme.es/qafi/About.aspx; García-Mayordomo et al., 2012).

The goals of this study in the LMV, are: i) to identify the terrace levels, using a detailed geomorphological mapping and cross-sections; ii) to present the sedimentary characteristics of the terrace deposits, through observations of outcrops/exposures; iii) to date some terraces by using the ESR method; iv) to understand and to quantify active tectonics, by using the terraces as geomorphic references and assessing the differential uplift during the Quaternary.

V.2.Geographical, geological and geomorphological setting

The Mondego river has a catchment area of 6671 km^2 and is the longest river entirely comprised in Portuguese territory, flowing for 234 km in a south-westward direction in mainland Portugal, from the Estrela Mountain until the Atlantic Ocean near the Figueira da Foz town (Fig. V.1, V.2).

In the LMV, the Mondego flows over Mesozoic (carbonates and siliciclastics) and Cenozoic (siliciclastics) sedimentary rocks (Fig. V.1C). The LMV can be subdivided in four main reaches limited by main faults (Fig. V.1D), from upstream to downstream: i) reach I, SE-NW, comprises the Ceira River confluence with the Mondego until the Campo do Bolão; ii) reach II corresponds to the NE-SW trend valley, located between Campo do Bolão and Montemor-o-Velho; iii) the reach III, corresponds to the very narrow reach, located between Montemor-o-Velho and Lares gorge; IV) reach IV corresponds to the large lower estuary, located between Lares village and the river mouth. Reach I is a steep valley, controlled by structural scarps cut on Jurassic limestones in its left bank and showing a broad amphitheatre of an abandoned meander, on the right bank (Carvalho, 1951). Reach II is a broad valley filled with Holocene sediments forming an alluvial plain up to 4 km wide. The last includes in the upstream part a remarkable widening of the valley, named Campo do Bolão, that is a subsiding area with a 36 m thick Holocene accumulation (Soares et al., 1985; Tavares, 1999). Campo do Bolão works as a sediment spill area, whose aggradation is visible on the remarkable drop in the alluvial plain gradient (0.10%), between Campo do Bolão and S. Martinho da Árvore (Fig. V.12 A-C). Downstream of S. Martinho da Árvore, the alluvial plain gradient is lower (0.015%). Reach III corresponds to the superimposed Mondego River on the homoclinal ridge of Serra da Boa Viagem, forming a gorge in the hard Cretaceous and Jurassic sandstones and limestones. Reach IV corresponds to the estuary's lower sector, with its tidal flats, salt marshes, adjacent to the aeolian dune field located near the coast.

Several main faults cross the study area: the N-S to NNW–SSE strike-slip Porto – Tomar fault zone (PTf), the SSW-NNE strike-slip Coimbra - Antanhol fault (CAf), the SSW-NNE strike-slip Montemor -o - Velho – Verride fault (MVf) and the WNW-ESE Quiaios - Maiorca thrust fault (QMf). These faults seem to be active. The Coimbra - Antanhol fault contacts a Cenomanian unit with the Pliocene-Lower Pleistocene culminant sedimentary unit (UBS13; Cunha, 2019) (Soares, 2017). The Quiaios - Maiorca thrust fault promoted significant uplift of the Serra da Boa Viagem during the Quaternary (Cabral and Ribeiro, 1988; Cabral, 1995; Ramos et al., 2012). NW–SE to NE–SW fault systems (Rodrigues et al., 1995; Pereira et al., 2004) are responsible for the tectonic uplift of compartments controlled by the Penacova-Verrim and Porto Tomar faults (e.g., Rôxo hill, ~510 m a.s.l.; Logo de Deus plateaux, ~133m a.s.l; Montes Claros – Conchada plateaux,140-90 m a.s.l., but also for the subsidence of the Campo do Bolão depression, evidenced by the vestibular depression of the Fornos stream (Soares et al., 1985).

Tectonics should have played an essential role in the river drainage development in the region, with flexural tilting of the Cretaceous formations at the right valley side (Ribeiro et al., 1979; Soares et al., 1990).

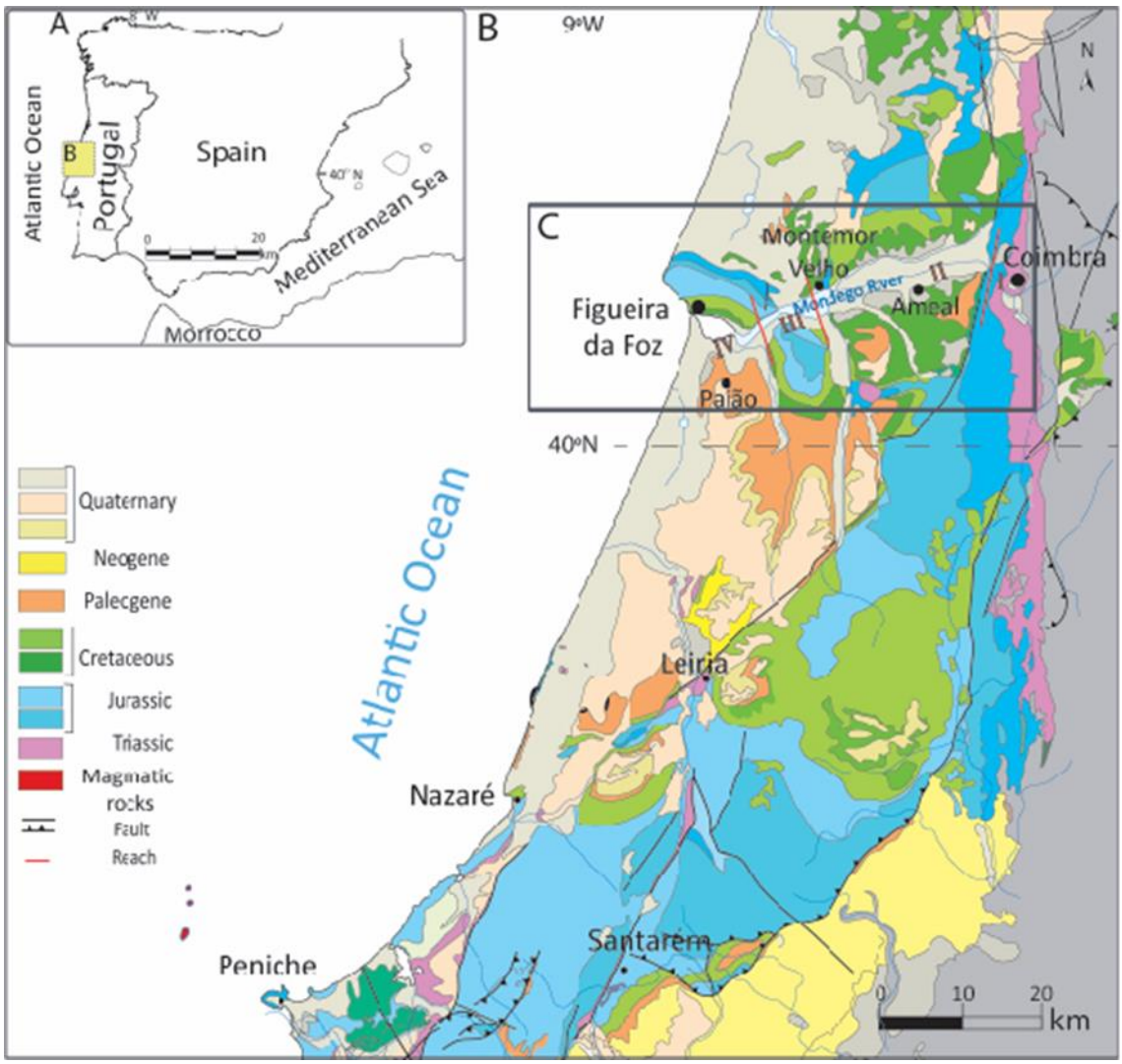

Figure V. 1. Geological framework of the study area (modified from Geological map, 1/500,000, LNEG). A – Geographical setting; B - Geological and structural map; C – Study area (Lower Mondego valley, from Coimbra to Figueira da Foz). Roman numbering indicates the four main reaches of the Lower Mondego Valley.

The Pleistocene deposits are organised in a terrace staircase on both sides of the river. Fluvial terrace deposits are preserved in the right valley margin (e.g., at S. Silvestre, Zouparria do Campo and Tentúgal, the "red sands of Zouparria deposit" and near Tentúgal ("Tentúgal deposit") (Soares et al., 1985). On the left-hand valley margin, the "Ameal and Gabrielos" terraces are represented at ~50 m and 25 m a.a.p., respectively (Soares et al., 1985).

In the lower estuary area, five terrace levels (T1 is the highest one and T5 the lowest one) have revealed successive episodes of river incision followed by aggradation in transition environments (fluvial to shallow marine). The terrace staircase is disposed at different elevations (a.a.p.) in both sides of the river due to differential uplift (Ramos et al., 2012).

The Holocene floodplain, up to 4 km wide, develops downstream Coimbra. The Holocene infilling thickness is between 24 and 33 m at Coimbra, 36 m at Campo do Bolão and 42 m near the stream mouth.

The lack of numerical age control and the influence of active tectonics made the correlation between the Quaternary deposits and the establishment of the timing of landscape modifications difficult. In the estuary area of the Mondego river, luminescence ages were obtained for the lower T5 terrace (120-110 ka), the minimum age for the T4 (>390 ka) and another minimum age (>138 ka) for the T3 (Ramos et al., 2012). The ages for the older terraces (T3, T2 and T1) have been estimated by extrapolation using an elevation-age function, by correlation with the ages of the Lower Tejo River terraces and assuming that the beginning of the incision stage is ~1.8 Ma (Cunha et al., 2012). Recently, the culminant sedimentary unit (which pre-dates the set of the fluvial incision) was dated at the Lower Tejo Cenozoic Basin and in the Mondego Cenozoic Basin by using the Electron spin resonance (ESR) method. At Praia da Victória, in Mondego Cenozoic Basin (MCB), an age of ca. 1.8 Ma was obtained for the top of the culminant unit (Gouveia et al., 2020).

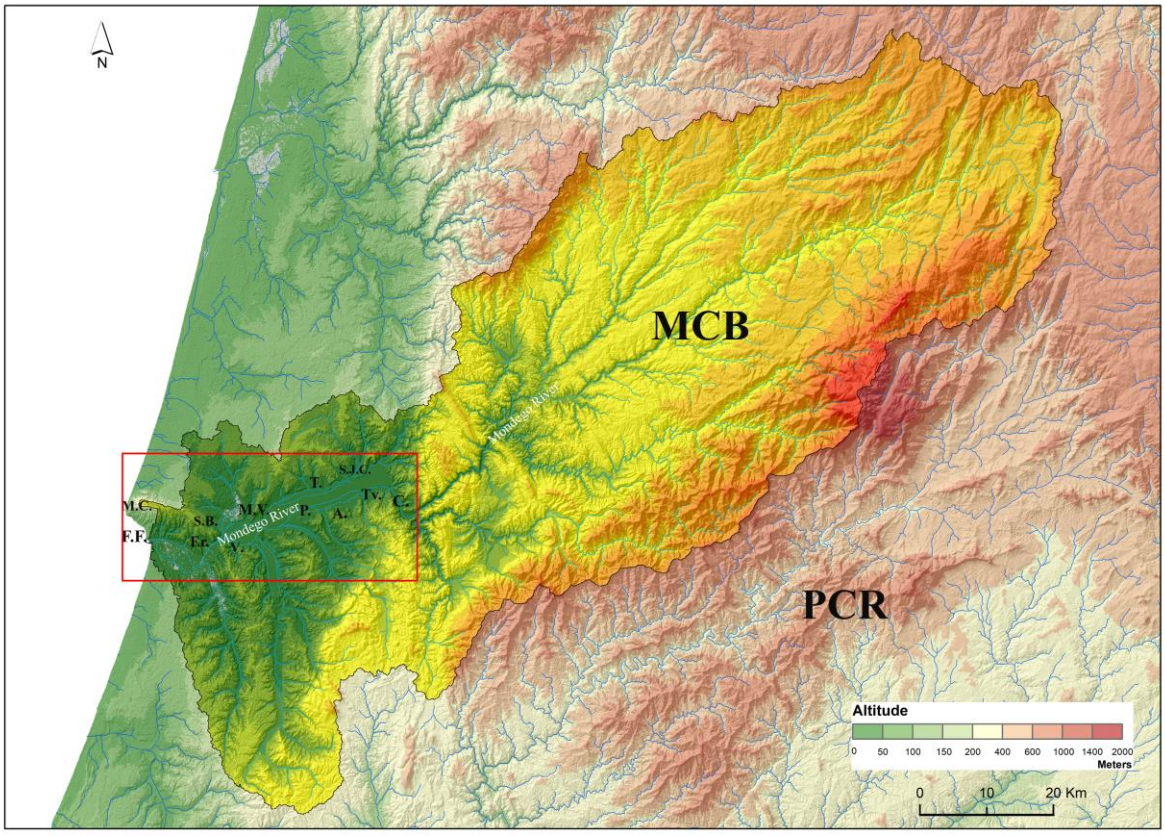

Figure V. 2.The Mondego catchment (black line) and its drainage network (blue lines). MB – Mondego Basin; PCR- Portugal Central Range; C.- Coimbra; F.F.- Figueira da Foz; M.C.- Mondego Cape; S.B.- S. Bento Mountain; M.V. Montemór -o-Velho; Er. - Ervidinho; V.- Verride; P. – Pereira; A.- Ameal; T.- Tentúgal; S.J.C. – S. João do Campo; Tv.- Taveiro.

Serra da Boa Viagem is an E-W to WNW-ESE elongated ridge, composed by Jurassic and Cretaceous limestones and associated marls and sandstones, dipping towards SW and S. The flattened hilltop, ranging 220 to 256 m a.s.l., derives from an uplifted Pliocene wave-cut platform (erosive base of the UBS13 unit). Three lower wave-cut platforms, associated with beach deposits, were recognised at the Cabo Mondego headland: Farol Novo (T1), ~100-90 m a.s.l. (Carvalho, 1964; Soares et al., 2007), T2 at 20 m a.s.l. and T3 (Murtinheira) at 10 m a.s.l. (Soares et al., 1989, 1992; Cunha et al., 2015). Aeolian dune fields are also present at the littoral (Almeida et al., 1997; André et al., 2009).

V.3. Materials and methods

The information presented was obtained from the geomorphological, stratigraphical, and sedimentological study of the terrace sequence using a standard approach (e.g., Stokes et al., 2012), combining field and laboratory work. Additional methods, including sampling for ESR dating and laboratory age determination, are given within relevant data sections for reference facility. In this work, the ESR dating is used to date the T4 and T3 terraces, with sampling limited by finding suitable material to be dated.

V.3.1. Geomorphology

Geomorphological mapping was undertaken with field mapping on geological (1/50,000; 1/25,000) and topographical (1/25,000; 1/10,000 and 1/5,000) base maps, available for the study area. A high-resolution digital elevation model (D.E.M.) based on elevation points of 1/10,000 municipal topographic database, was generated with ArcGIS geoprocessing tools. It was analysed and synthesised a range of geological information. After collecting and combining all geographic information, the identified fluvial terraces in the area were vectorised by creating shp.files with geographic attributes. The delimitation of the river basin, the development of thematic cartographies with fluvial forms and several cross profiles of the river course were performed using geoprocessing tools in ArcGIS and Adobe Illustrator.

V.3.2. Stratigraphy and sedimentology

Fieldwork included the study of terrace deposits at outcrops/exposures, which consisted of the stratigraphic and sedimentological characterisation of the sedimentary deposits, as sediment colour, texture, maximum particle size and clast lithology characterisation. The different fluvial deposits preserved in the sedimentary outcrops used nomenclature and standard methodologies (e.g., Miall, 1996; Moore and Reynolds, 1997). Sedimentary deposits are described and interpreted using sedimentary logs and described based on sedimentary facies analysis approach that integrates lithology, texture and composition characterisation. The thickness of each deposit and lateral distribution were analysed.

At the Sedimentology Laboratory - University of Coimbra, grain-size analyses of sediment samples were carried out by sieving with a ½ Φ increment for the fraction > 63 μm. Analyses of sediment mineral composition were based on binocular microscope observation (50x) and X-ray powder diffraction using an Analytical Aeris XRD diffractometer manufactured by Panalytical, with a Cu tube in a 2θ range, at a scanning rate of 3^0 min^{-1}, 40 kV and 15 nA (Department of Earth Sciences – Univ. Coimbra). The mineralogical composition in non-oriented subsamples was obtained using the analytical software Highscore plus, provided with the instrument. According to the standardised Panalytical backloading system, the subsamples were prepared, which provides a nearly random distribution of the particles.

V.3.3. Numerical dating

V.3.3.1. ESR dating of optically bleached quartz grains

The basis of this absolute dating method is the accumulation of charges in crystal lattice defects of quartz minerals, resulting from natural radiation during their burial history. The number of charges, detected by ESR, is directly proportional to the duration of the burial age of the minerals. As there is no ESR signal intensity saturation up to several kGy and quite good thermal stabilities, the method can date the age range from several thousand years up to 3 Ma (Voinchet et al., 2004, 2010; Gouveia et al., 2020).

The ESR age calculation implies the determination of two main parameters: the total dose ($D_{.T.}$) also referred to as the paleodose or equivalent dose (D_e), and the dose rate (d_a) which is an estimation of the mean dose annually absorbed by the sample, based on the equation:

$$D_T = \int_0^T d_a(t).dt, \quad (16)$$

where T is the age of the sample.

The total dose $D_{.T.}$ is proportional to the trapped electrons concentration in the sample and so to the ESR signal intensity. The paramagnetic centres commonly used as potential dosimeters of ionising radiation in quartz grains are: Aluminium (Al), Titanium (Ti) and Germanium centres (Ge) though hardly observed in natural samples (Falguères et al., 1991). Each centre has characteristic behaviour in optical bleaching kinetics and radiation sensitivity, being useful combining multiple centres approach in ESR dating since each one provides independent dose control (Toyoda et al., 2000; Rink et al., 2007; Tissoux et al., 2007; Duval and Guilarte, 2015). The Al centre signal has a high radiation saturation level and thermal stability, is usually used for ESR dating of Middle Pleistocene to Pliocene deposits (e.g. del Val et al., 2019; Voinchet et al., 2019; Gouveia et al., 2020). Ti centre usually decreases at high dose values, called "radiation bleaching" (Euler and Kahan, 1987), commonly being used for dating more recent materials (e.g., Middle and Late Pleistocene deposits; Tissoux et al., 2007).

In the present study, five samples were taken during a fieldwork campaign along the LMV in March and May of 2018. At Coimbra (reach I), samples were collected from the Ingote, José M. Dias Ferreira street and Conchada sites (Ing1, Coim1 and Concha1). At Tentúgal (reach II), sample Tent5 was taken. At Ervidinho (reach IV), samples Ervi1 and Ervi4 were collected, respectively, from levels near the base and the top of this terrace.

At each site, for ESR dating, the sediment samples were collected by hammering opaque metal tubes (30 cm long with a diameter of 6-7 cm) in freshly cleaned sections of sandy levels, in order to minimise parasite bleaching. The tubes were directly sealed from sunlight with opaque tape and bags. The surrounding material was also collected for water content estimation and laboratory gamma spectrometer analysis.

In the laboratory (Earth Sciences Department-University of Coimbra), the sediments were extracted afterwards under red light, according to the standard conditions of the sample preparation in ESR dating process (Yokoyama et al., 1985). In the preparation of mineral fractions for ESR dating, the 250-180 and 180-90 μm fractions of pure quartz grains were extracted from sediment by sieving, chemical treatments, including fluorhydric (HF) acid attack, dense liquid separation and magnetic separation, following the standard procedure (e.g., Voinchet et al., 2004).

The multi-aliquot additive-dose (MAA) method was employed for D_e determination. Ten of twelve aliquots with quartz grains were irradiated with a calibrated ^{137}Cs Gammacell-1000 gamma source (dose rate= 6.3216 Gy/min) at different doses ranging from 100 to 25.000 Gy, carried out at CENIEH (in Burgos, Spain).

One aliquot was kept as a natural reference, and the other was illuminated for 1000 h in a Dr Hönhle SOL2 solar simulator to determine the non-bleachable part of the ESR-Al signal (Voinchet et al., 2003).

After irradiation, each series of 12 aliquots was measured by ESR at low-temperature cavity (~107 K) using a Bruker EMX spectrometer at Muséum National d'Histoire Naturelle of Paris. The given sample was placed in the centre of the cavity, measured three times after a 120° rotation in order to account ESR signal angular dependence. The ESR measurements were carried out on three different days and repeated 2 to 4 times to evaluate the data repeatability. Baseline correction was applied by

WINEPR Processing software using a quadratic function.

The Al ESR intensity was evaluated from peak-to-peak amplitude measurements between the top of the first peak (g=2.0185) to the bottom of the 16th peak (g=2.002) of its hyperfine structure (Toyoda and Falguères, 2003). ESR intensities of Ti centre were extracted from the peak to baseline amplitude measurement around g=1.913-1.915 (option D, Duval and Guilarte, 2015). Al signal was systematically measured together with Ti-Li one, in order to get a proper background correction (Duval and Guilarte, 2015). The sample preparation and experimental conditions employed for Al and Ti centres are provided in the Supplementary Materials (S.M.). Ti centre showed a complete resetting of the ESR signal after the artificial bleaching and a good dose-response to irradiation (Table 1). The equivalent dose (D_e) was determined for Al centre considering the subtraction of the residual intensity evaluated through the maximum bleaching value from the measured ESR intensities. Al ESR intensities were fitted by an exponential+linear fitting function (EXP+LIN), (Fig. V.2), through the mean ESR intensities (Duval et al., 2009; Voinchet et al., 2013) and Ti ESR were fitted using an SSE and (EXP+LIN) functions, (Fig. V.2 and V.3), using the Microcal Origin Pro 8.1 software and a data point weighting by the inverse of the squared ESR intensities, $1/I^2$ (Yokoyama et al., 1985). Ti-Li signals of the last two fitted points presented a saturated trend and large error magnitude in most samples. They were not used in the D_e extrapolation.

V.3.3.2. Dose rate evaluation and age calculation

The radioelements contents (U, Th and daughters, and K) were determined by high-resolution low-background gamma-ray spectrometry measurements. The external alpha and beta dose rate components were derived from the radioelement contents obtained using the dose-rate conversion factors of Guérin et al. (2012). The grain thickness removed after the HF etching was assumed to be 20 μm and, the external alpha contribution was therefore considered negligible. Values were corrected for β attenuation of spherical grains (Brennan et al., 1991; Brennan, 2003). Water content value during burial was estimated, according to Grün (1994). The water content for marine deposits has changed considerably during the past.

To account for their history of littoral accumulation, the saturated water content of the sample was measured, and the mean value of 7 ±2 % was obtained, accounting for the drying as a consequence of sea-level changes and tectonic uplift. The cosmic dose rate was determined according to Prescott and Hutton (1994), based on altitude, latitude and longitude of each section.

The final D_e values for each sample were calculated on the average of ESR intensity values obtained from the nine repeated measurements carried out over three days.

In the age calculation, the annual dose (D_a) was obtained from the radionuclide activity in the sediments, taking into account both in *situ* and laboratory gamma-ray spectrometry measurements.

V.4. Results

V.4.1. Geomorphological characterisation

V.4.1.1. Geomorphological characterisation of reach I (Coimbra – Campo do Bolão)

Along reach I, six terrace levels were identified and mapped below the UBS13 unit (Fig. V.3, V.4).

In the left margin of the LMV, nearby Cruz de Morouços (210 m) and Antanhol (172 m, Fig. V.3) small plateaus (*mesas*) were identified, remnants of the culminant sedimentary unit (UBS13). Below these plateaus, an erosive surface (N1) cuts the Jurassic limestones and the UBS13 unit, which are strongly faulted. These faults branch upwards to the UBS13 unit, suggesting the structural architecture of a flower structure linked to an NNW-SSE strike-slip fault system, named in this study as an F1 fault system (Fig.V.3). The first terrace level (T1), correlating with the N1 surface, appear slightly inset as a strath. This situation is especially evident on the left margin of the LMV that was uplifted relatively to the right margin (Fig. V.3, V.4A, SM V.2).

In a lower elevation, a gently sloping ramp (strath of the T1) is followed by a flat area where the T2 terrace level is observed in both margins of the river (Fig. V.3D, E). Terraces 3, 4 and 5 are better exposed in the right margin of the valley (Fig. V.4B, D, E).

The heights above the alluvial plain (a.a.p.) of the geomorphic references on the left valley margin are higher compared with their equivalents on the opposite right margin, significantly smaller for all references, namely at Pinhal de Marrocos, in the abandoned meander, and at Lordemão plateaux (Fig. V. 4 A, B, C, D, E).

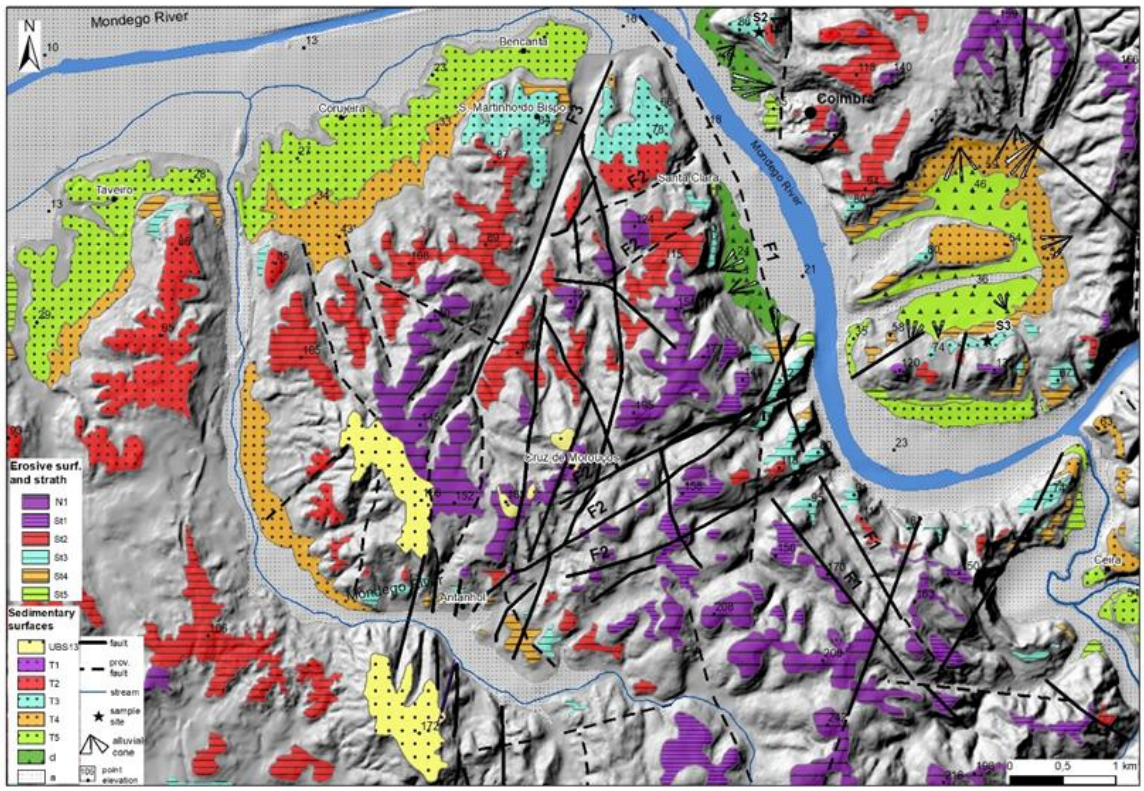

Figure V. 3. Geomorphological map of the LMV reaches I. Sedimentary surfaces: UBS13 culminant sedimentary surface of the Mondego Cenozoic basin; Erosive surfaces and straths: N1 erosive surface, near the base of UBS13 unit, St1 to St5 strath terraces. Sedimentary surfaces: UBS13 - the culminant surface of the Cenozoic basin; T1 to T5 - fill terraces; F1, F2 and F3 - strike-slip faults referred in the text; S3 - studied site at the José M. Dias Ferreira street (sample Coim1).

The elevations of the staircase in the most uplifted left margin are: UBS13 at 210 m a.s.l. (+189 m a.a.p.); T1 at 141 m (+120 m); T2 at 118 m (+97 m); T3 at 91 m (+70 m); T4 at 64 m (+46 m); T5 at 36 (+16 m).

The ENE-WSW F2 fault system caused the left margin to be downthrown compartment at Santa Clara and at the northern end, being the preserved terrace remains of T2, T3, T4 and T5 less elevated than their counterparts on the opposite margin, namely at Conchada and Lordemão (Fig. V.4E).

The transition between reach I to reach II is done through a ~40 m height scarp, associated with an NNE-SSW F3 fault system (V.3, V.5). Along this fault, the Pedrulha compartment, at the west, corresponds to the downthrown block, concerning the uplifted compartment of Ingote, at east. The sudden widening of the valley named the Campo do Bolão constitutes a subsiding area with a 36 m thickness of Holocene alluvium (Tavares, 1999). UBS13 and fluvial terraces on each side of the F3 fault are positioned at different elevations above the alluvial plain. The elevations range from +122 m (UBS13) and +8 m (T5), in the east side, while in the west side the same geomorphic references are at +90 m and +6 m, respectively (Fig. V.3, V.4, SM V.2). On the left margin of the valley, a probable T6 terrace could be present near the surface of the alluvial plain (at ~18 m a.s.l.), at the Sta. Clara Monastery (Fig. V.4C).

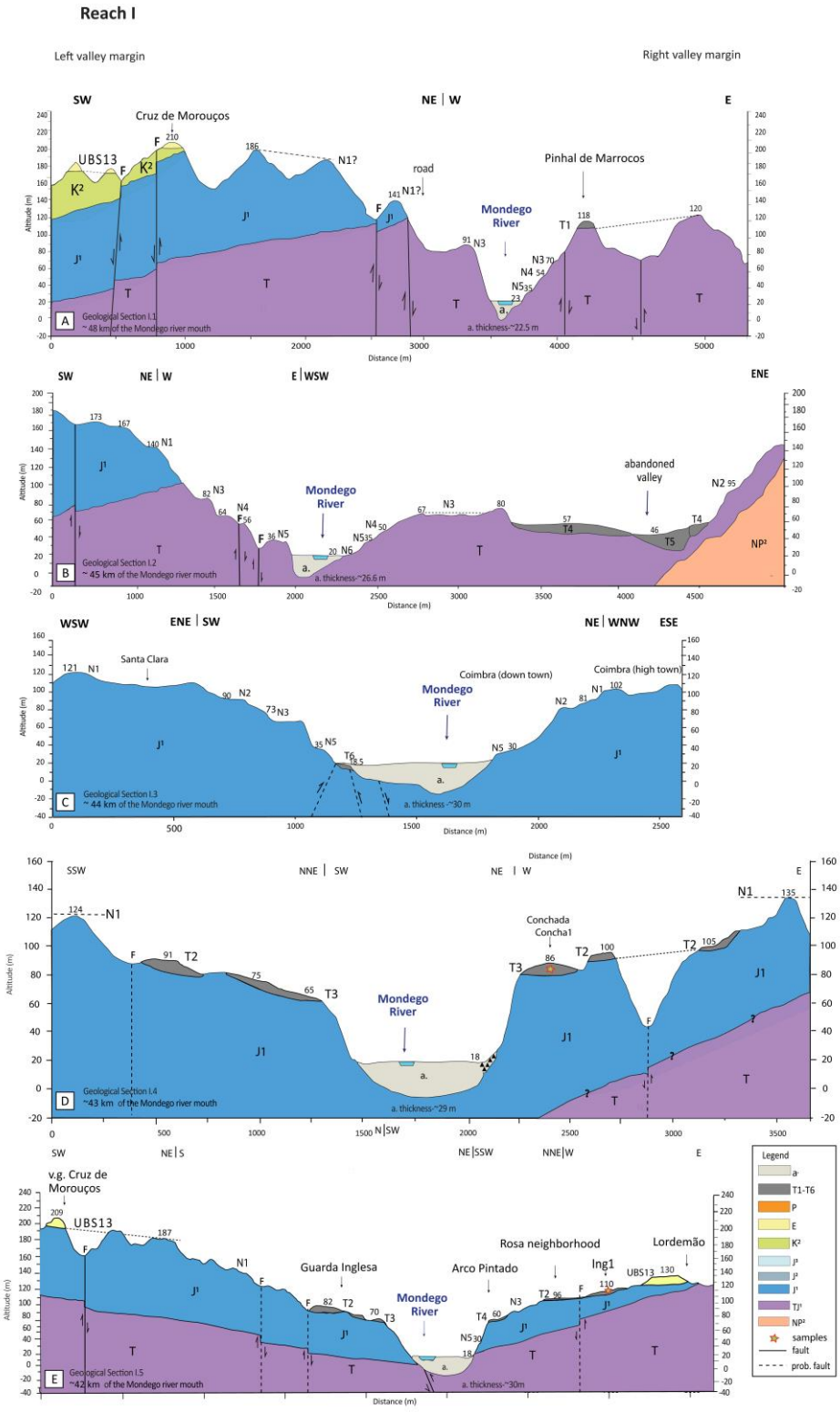

Figure V.4. Transverse profiles to the Mondego River in the reach I. NP2 – Precambrian and Phanerozoic; T - Triassic; J^1 - Lower Jurassic; J^2 - Middle Jurassic; J^3 - Upper Jurassic; K^2 - Cretaceous; E – Paleogene; P - Pliocene; T1-T6 – fluvial terraces (Pleistocene); a – Holocene, (Fig. SM V.2 with profiles location).

V.4.1.2. Geomorphological characterisation of reach II (Campo do Bolão – Montemor)

Reach II has a general ENE-WSW trend, from Campo do Bolão to Montemor-o-Velho, along which five terrace levels have been identified below the UBS13 unit (Figs. V.5, V.6, V.7).

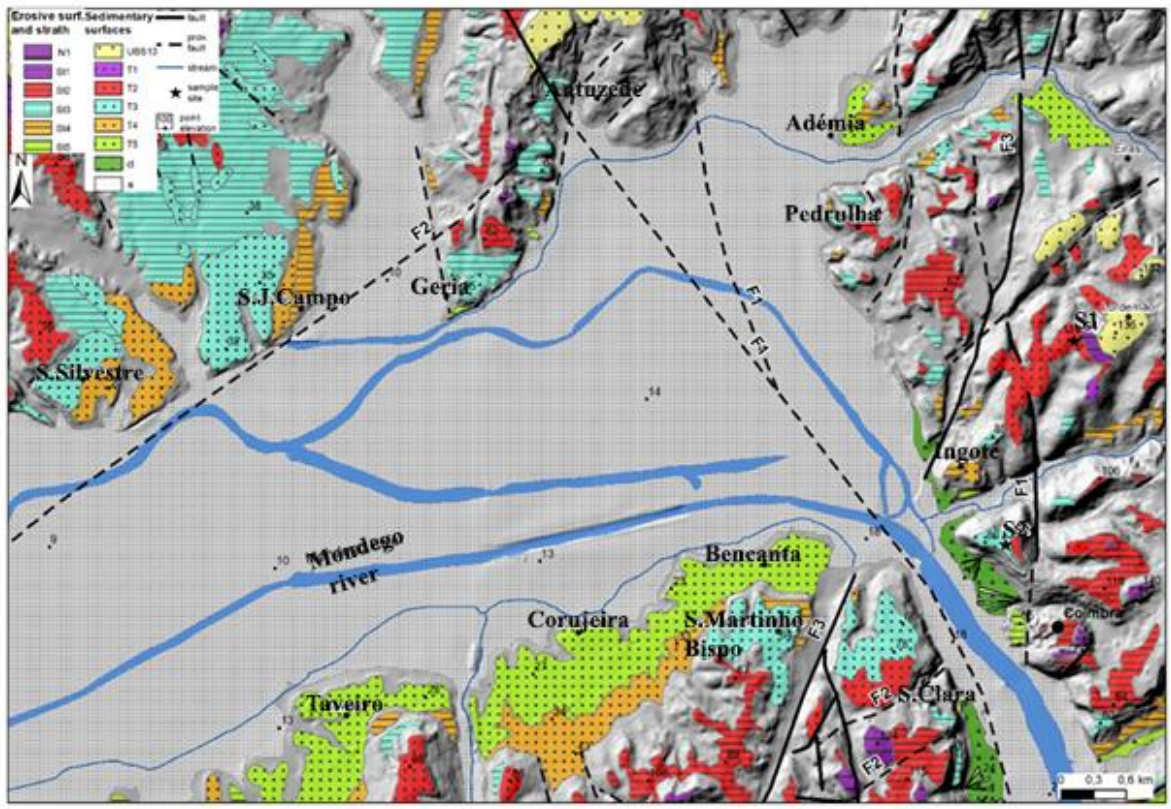

Figure V.5. Geomorphological map of the LMV reach II, upstream part. The NNE-SSW F3 Coimbra - Antanhol fault forms a ~40 m height scarp, in the right margin of the Mondego river. The scarp separates the Ingote - Lordemão upthrown compartment from the Pedrulha downthrown compartment. Sedimentary surfaces: UBS13 culminant sedimentary surface of the Mondego Cenozoic basin; T1 to T5 - fill terraces; cl - colluvium; a - alluvium. Erosive Surfaces: N1 - erosive surface correlated with the T1 terrace; St1 to St5 – erosive surfaces and straths. S2- sample site of Concha1; S1 – sample site of Ing1.

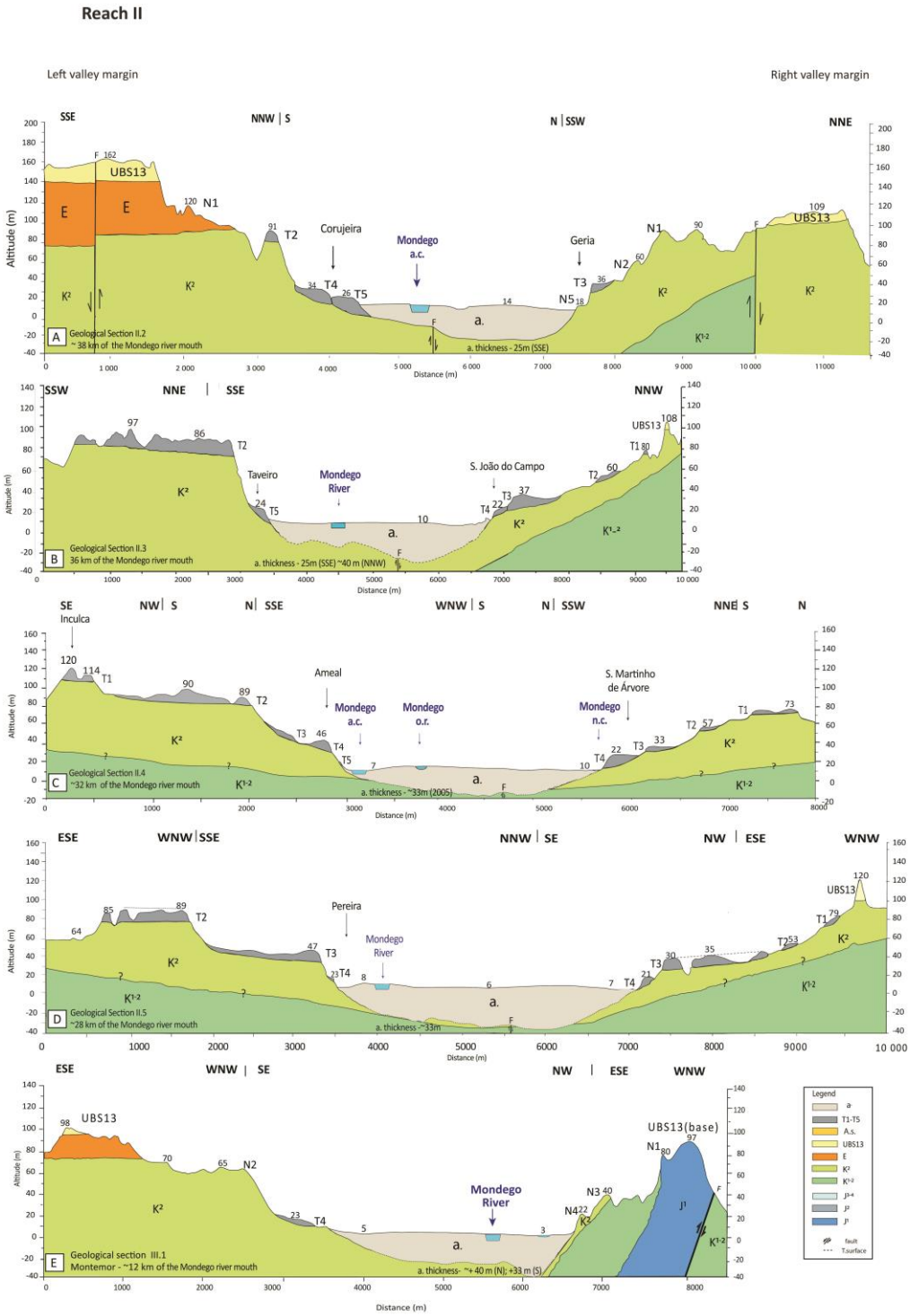

Figure V. 6. Transverse profiles to the LMV in the reach II. J^1 - Lower Jurassic; J^2 - Middle Jurassic; J^{3-4} - Upper Jurassic; K^{1-2} - Lower Cretaceous; K^2 – Cretaceous; E – Paleogene; UBS13 – Pliocene to Lower Pleistocene; A.s. – aeolian sands; T1-T5 – Fluvial terraces (Pleistocene); a – alluvium (Holocene), (see Fig. SM V.2, profiles location).

Reach II is limited in the upstream by the NNE-SSW F3 Coimbra - Antanhol fault (Fig. V.5) and in the downstream end by the "push up" plateau of Montemor-o-Velho (97-112 m) on the right side of Mondego and by the Verride antiform structure on the left side.

Five transverse profiles, comprising the two sides of the Mondego valley, located between Campo do Bolão and Montemor (Figs. V6 B, D, E, SMV.2), reveal that the terraces at the left margin were more uplifted than the terraces on the right margin. This is well observed in the terraced staircase of Ameal, S. Martinho (Fig. V.6C). At the western end of reach II, this difference no longer exists, as observed in the downstream transverse profile at Montemor-o-Velho (Fig. V.6E), where the terrace elevations are almost equal between the two sides of the valley.

The T1 and T2 are present at both sides of the valley, except near Montemor-o-Velho, where they form erosional surfaces (straths).

On the right side, there are small remnants of the T3 and T4 terraces, (in S. João do Campo and S. Silvestre) (Fig. V.6B). The same terrace levels are also observed along the left side of the valley, from S. Martinho to Alfarelos, although they are very anthropised. The T5 level is recognised along the road that connects the villages.

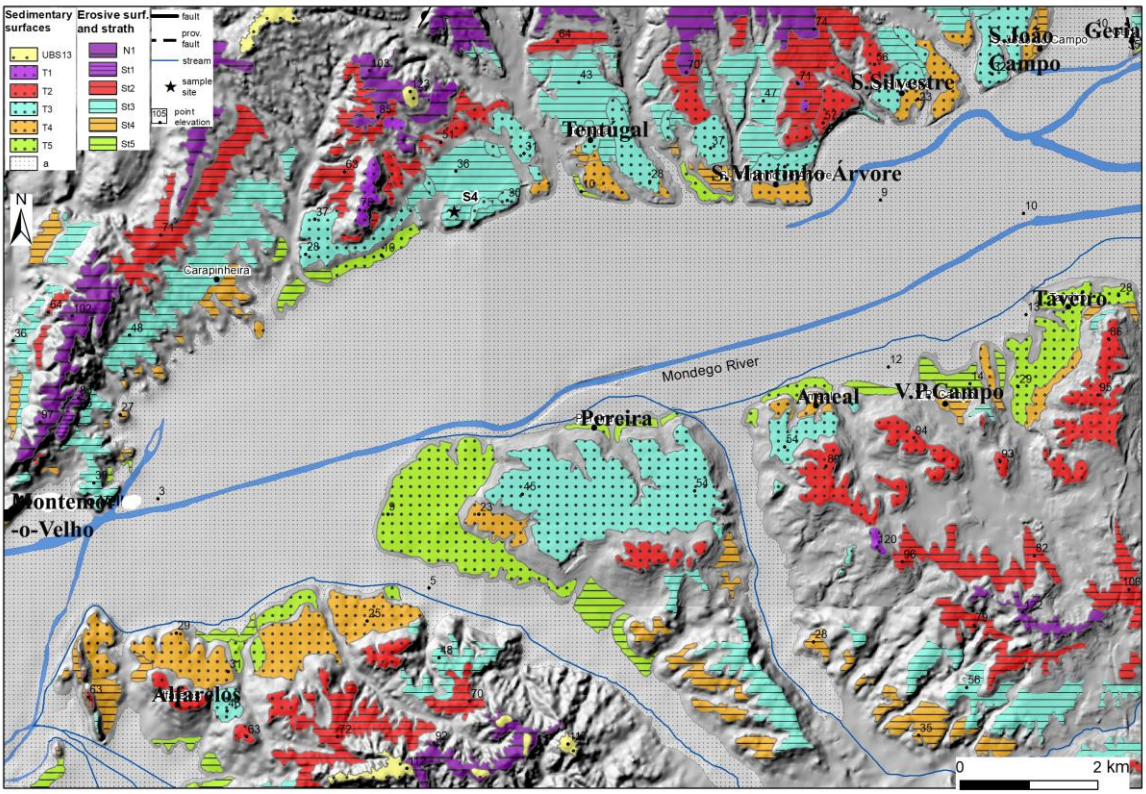

Figure V. 7. Geomorphological map of the LMV reach II, downstream part. Note the enlargement of the Mondego valley and the "push up" plateau of Montemor-o-Velho at 97-110 m, whose surface corresponds to the N1 erosive surface. Sedimentary surfaces; UBS 13 – the culminant sedimentary surface of the MCB; T1 to T5 - fill terraces; cl - colluvium; a - alluvium. Erosive Surfaces: N1 - erosive surface correlated with the T1 terrace; St1 to St5 – erosive surfaces and straths. S2- sample site of Concha1; S1 – sample site of Ing1.

In the selected transverse profiles (Fig. V.6 B, C, D), the average heights of the geomorphic references are estimated. In the valley left side, the UBS13 surface is at ~154 m a.s.l. (+144 m a.a.p.), T1 is at 118 m (+108 m), T2 is at 87 m (+77 m), T3 is at 56 m (+46 m), T4 is at 30 m (+20 m), and T5 is at 18 m (+8 m). In the right side, the UBS13 is at 107 m (+97 m), T1 is at 82 m (+ 72 m), T2 is at 58 m (+48 m), T3 is at 37 m (+27 m), T4 is at 26 m (+16 m) and T5 is at 13 m (+3 m). In some right side locations, the T5 is buried by the Holocene alluvium (Figs. V6D, E).

V.4.1.3. Geomorphological characterisation of reach III (Montemor-o-Velho - Lares)

Reach III is ~6 km long, located between Ereira and Lares villages. From the Lares gorge, the Mondego River crosses the Serra da Boa Viagem - Verride antiform structure. It is formed mainly by Jurassic limestones, marls and sandstones dipping to SW (Fig. V.8 A, V.9). At the crossing by superimposition (Soares et al., 1985; Almeida et al., 1990; Ramos et al., 2012) the SE edge of Serra de Boa Viagem hill, the Mondego river forms a narrow valley where the lower terraces are not well preserved (Figs. V.8B, V.9).

UBS13 unit is preserved at the south of the Reveles village, in the left margin of the valley (Fig. V.8 C). T1 and the T2 have considerable extension in both sides of the LMV (Figs.V.8 A, B; SM V.3). Moreover, the T1 terrace forms a flat landform underlain by alluvial deposits at Serra de S. Bento and Serra de Castros (120 m a.s.l.; +117 m a.a.p). T2 is a strath terrace at 90–70 m a.s.l., at both sides of the Lares gorge. T3, T4 and T5 form small erosional straths carved into the bedrock at 59 m, 32 m and 16 m a.s.l., respectively.

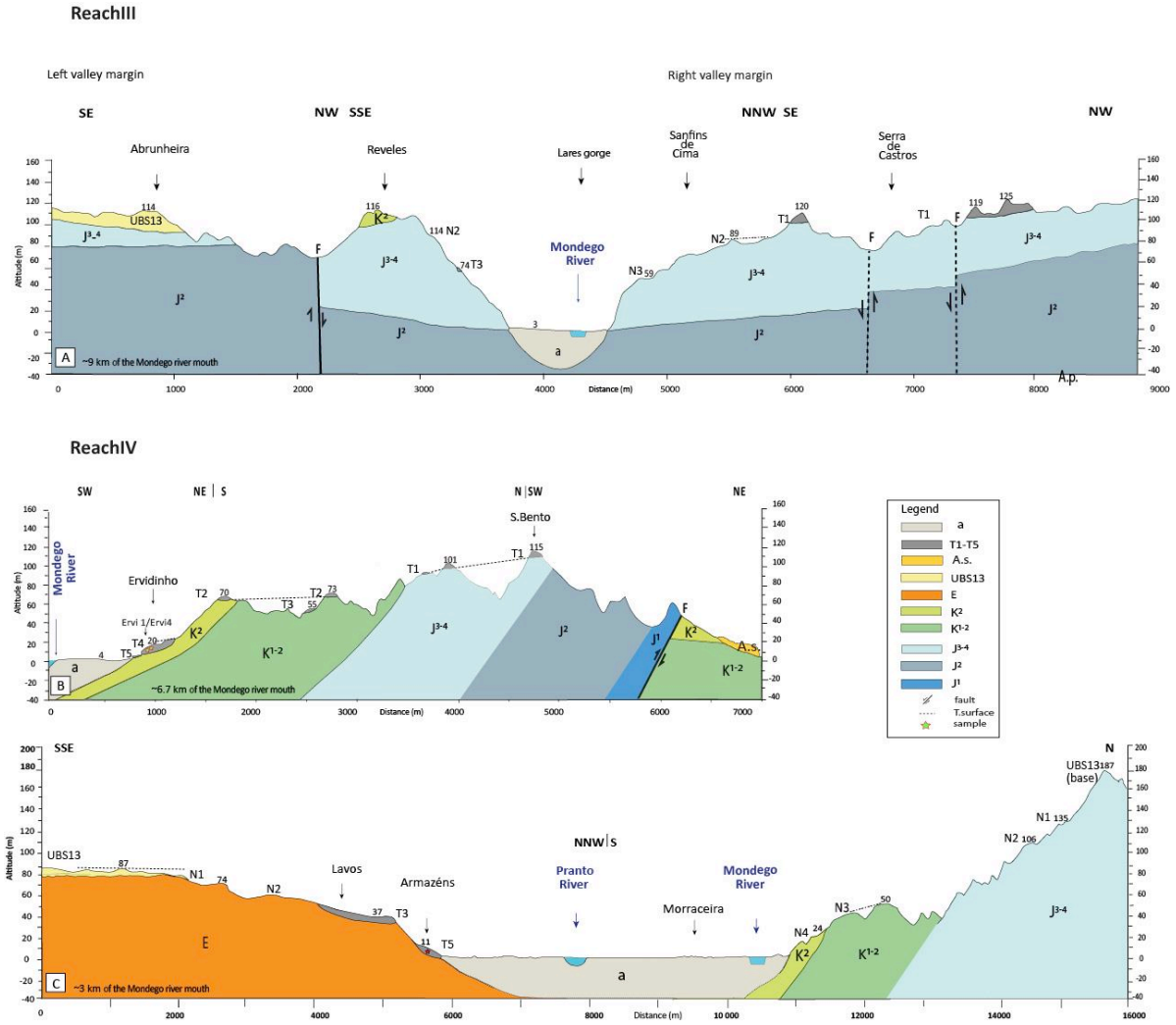

Figure V. 8. Transverse profiles of the LMV reach III (A) and IV (A and B). J^1 - Lower Jurassic; J^2 - Middle Jurassic; J^{3-4} - Upper Jurassic; K^{1-2} - Lower Cretaceous; K^2 – Cretaceous; E – Paleogene; UBS13 – Pliocene - Lower Pleistocene; A.s. - aeolian sands; T1-T6 – Fluvial terraces (Pleistocene); a– alluvium (Holocene), see Fig. SM V.3, profiles location).

The transverse profile at the Lares gorge (profile Abrunheira – Serra de Castros, Fig. V. 8A, SM V.3) does not show significant differences in terrace elevations at both sides of the Mondego valley, except for the UBS13 unit, which top is at 135 m a.s.l. in the left margin and will have reached 160 m a.s.l. in the right margin. We estimate a ~10 m thickness for this unit, considering the left margin thickness observed and its surroundings.

In the neighbouring area of the gorge, several NE-SW lineaments cross the Jurassic and Cretaceous formations. One of these lineaments intersects the Quiaios - Maiorca thrust fault (F4) at the northeast of the Maiorca village, in the valley right margin.

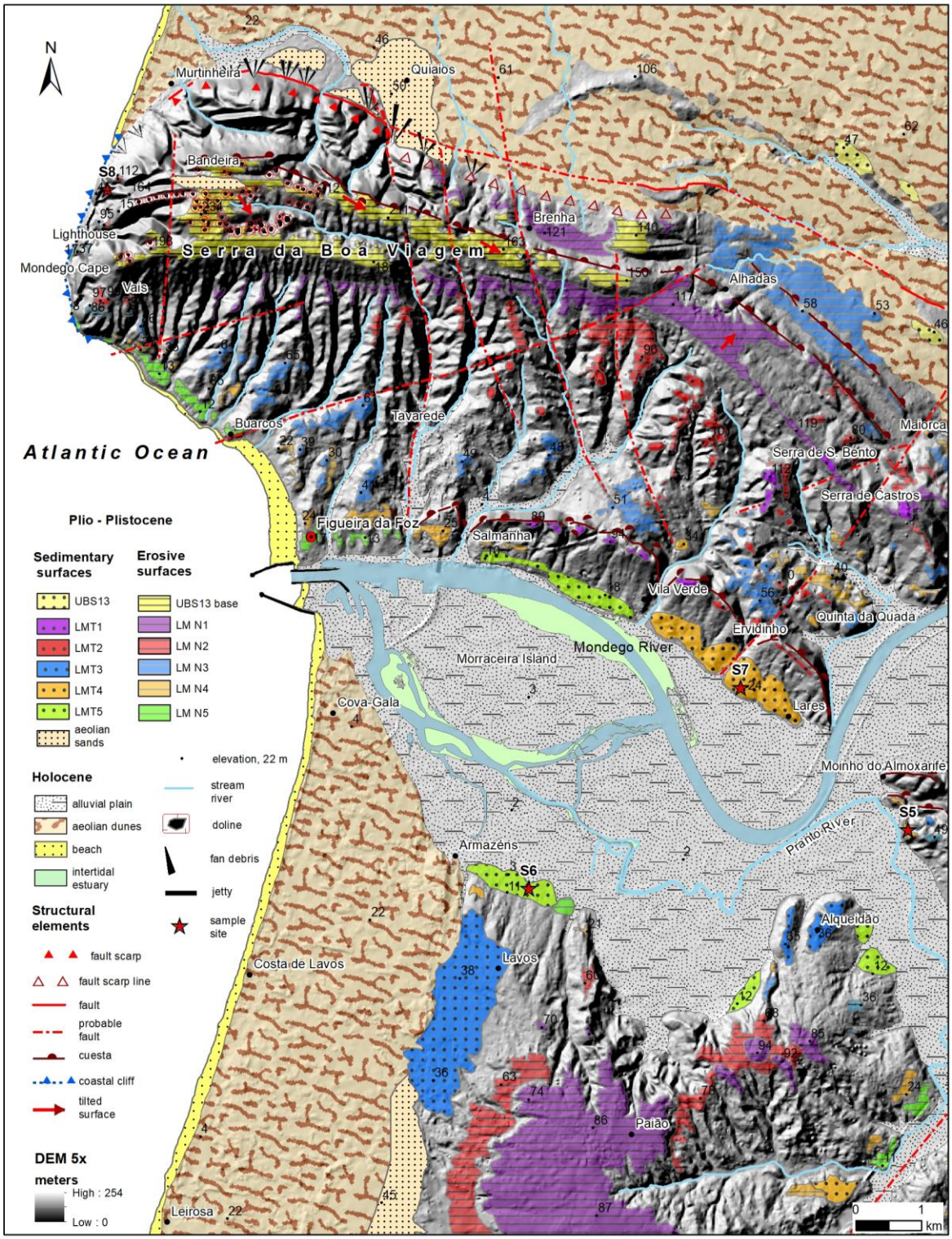

Figure V. 9.Geomorphological map of the LMV reach III, and of the reach IV. In the reach III, the Mondego crosses the homoclinal limb of Serra da Boa Viagem, forming a narrow valley named Lares gorge. Reach IV, lower estuary area. Sedimentary surfaces: UBS13 – the culminant sedimentary unit of the Mondego Cenozoic basin; LMT1 to LMT5 – fill fluvial terraces. Erosive surfaces: UBS13 base – marine platform at the base of the culminant sedimentary unit; LM N1 to LM N5 – erosive surfaces and straths correlated with the fill terraces.

V.4.1.4. Geomorphological characterisation of reach IV (Figueira da Foz)

The lower sector of the Mondego estuary has wide tidal flats and marches near the margins downstream of the Lares gorge. This sector is limited on the north side by the Serra da Boa Viagem hill (257 m a.s.l.) and by the littoral platform covered with aeolian dunes at the south (Fig. V.8). The Serra da Boa Viagem forms an elongated E-W to WNW-ESE curved ridge, limited at the north by the prominent scarp ~240 m of maximum height, related to the Quiaios thrust fault (Almeida, 1997; Ramos et al., 2012).

The Jurassic and Cretaceous successions that form Serra da Boa Viagem are tilted to SW, giving the character of a homoclinal ridges with *cuestas* and water gaps (Fig. V. 9.B, C). Several erosional surfaces (straths) and sedimentary fluvial terraces are inset, on the south slope of the Serra da Boa Viagem, where some sedimentary covers remain are preserved on the top of *cuestas*. They attest the superposition of Mondego and their tributaries on the homoclinal ridges and the transverse character of the drainage regarding the relief.

Above the alluvial plain (at 2 to 3 m a.s.l.) five terrace levels are exposed below a wave-cut platform (at 150-257 m a.s.l.) cutting the Jurassic limestones on top of the Serra da Boa Viagem (Fig. V.9). It corresponds to the discordance at the base of the UBS13 unit dated as ~3.7 Ma at Carnide (Cunha et al., 1993; Pais et al., 2012). The cross profile from the Serra da Boa Viagem to the Mondego (Fig. V.9C) shows the fluvial terrace levels: T1 at 101-115 m a.s.l. (ca. +98 m a.a.p.); T2 at 73 m (+70 m); T3 at 55 m (+52 m); T4 at 20 m (+17 m); T5 at 7 m (+3 m).

In Serra da Boa Viagem five marine platforms are exposed on both sides of the Mondego Cape, all decreasing in altitude to the south (Figueira da Foz), given the basement be tilted to SW.

Tm1 is a wave-cut platform (at 164 -153 m a.s.l.) better preserved at NE of the Mondego Cape; Tm2, held in small remnants at 112-97 m.; Tm3 at 93-86 m, is a terrace deposit with similar elevation levels in the N part of Mondego Cape as near the lighthouse and lower elevation to the south; Tm4 is a platform poorly preserved between 45 and 27 m a.s.l.; Tm5 is the best-preserved terrace deposit in the area, mainly in a semi-protected area with less wave action near Buarcos and under the Lighthouse (13m-8m a.s.l.), respectively.

V.4.2. Characterisation of the studied sites and sedimentary deposits

V.4.2.1. Sites at reach I (Coimbra – Campo do Bolão)

In reach I, the best outcrops of fluvial terrace deposits were selected for sampling and sedimentary characterisation, especially from T2 and T3 levels (Figs V.10A, B, C, D and V.11).

Figure V. 10. Terrace deposits studied in the right valley margin of the LMR. Reach I: A - terrace T1 at Lordemão; B - terrace T2 at Ingote (sample Ing1); C - terrace T3 at Conchada (sample Concha1); D - terrace T3 at the José M. Dias Ferreira street (sample Coim1); Reach II: E - terrace T3 at Tentúgal (sample Tent5); Reach III: F - Terrace T4 at Ervidinho, with samples collected from the base (Ervi4) and top (Ervi1). G - Examples of MPS measures in Lordemão.

Figure V. 11. Exposures studied in the left valley margin of the LMR. Reach I: A - UBS13 unit at Antanhol, comprising white sandstones and conglomerates; B - terrace T1 at Vale das Hortas; C - terrace T1 at St. Clara; D - terrace T2 at St. Clara; E - terrace T3 at St. Clara; Reach II: F - terrace T4 near S. Martinho do Bispo.

Near Lordemão, at 135 m a.s.l., there is a sedimentary deposit with well-identified channels, composed by coarse to very coarse soft sandstones, containing rolled cobbles and pebbles, some imbricated, with MPS=12.1cm (Fig. V.10A). According to the geomorphology, is considered as the UBS13 unit. The first terrace level (T1), appears slightly inset as a strath.

The T2 deposits present orange colour (7.5 YR 6/8) and are formed by conglomerates (MPS ~4.7 cm) at the base and very clayey sand. The pebbles are mainly of quartz and quartzite, with accessory shales. The sample for dating and laboratory characterisation, named Ing1, was collected near the top of T2 (40014'0"N; 8025'33"W), in a sandy-gravel layer ~ 3.5 m thick (Fig. V.10B). This level is well preserved near the road at 98-110 m a.s.l. (+76 to 84 m a.r.b.). The grain size distribution of the Ing1 sample comprises 8% of gravel (>2mm), 64% of sand (2 mm – 63 μm), 23 % of silt (63 – 4 μm) and 3% of clay (< 4μm). The mean grain size is 0.22 mm (medium to fine sand), very poorly sorted (2.79), mesokurtic (2.96) and fine skewed (0.87).

The mineral grain composition consists of hyaline and milky quartz, feldspars, and muscovite. The clay association is Kiv (97% of kaolinite, 1.5% of illite and 1.5% vermiculite).

The terrace T3, ~10 m thick and red colour, can be observed near the Conchada cemetery (40013'01" N; 8025'47" W) at 96-86 m a.s.l. (+70 m to +60 m a.r.b.). The Conchada site shows matrix-supported gravels at the base, grading to pebbly very coarse to medium sands at the top, with some through cross lamination (Fig.V10C). Concha1 sample, collected ~2 m below the top, has a dull orange colour (7.5YR 7/4) and comprises 10% of gravel, 60% of sand and 30% of fines. The sieving results indicated a mean grain size of 0.135 mm, very poorly sorted (2.79), fine skewed (0.87) and mesokurtic (2.96). The quartz grains are usually sub-angular. The sand fraction comprises hyaline and milk quartz, quartzite, feldspars and phyllosilicates (muscovite). The clay minerals present are illite (54%) and kaolinite (46%).

The base of the T3 fluvial sedimentary sequence is represented in an exposure at the José M. Dias Ferreira street (40011'31''N; 8024'15.9''W) at ~70 m a.s.l. (+54 m a.r.b, Fig. V.3D) on the right margin of the river. With a ~6.4 m thickness exposed and showing reddish-orange colour (7.5 YR 6/8). It is very heterometric, with boulders and cobbles at the base, overlying the Triassic substratum. Upwards consists of pebbly coarse to medium sands, with levels of imbricated cobles (MPS ~20.6 cm). The sample (Coimb1) was collected in the middle part of the outcrop (~ 2.30 m below the top) in a sand layer (Fig. V.10D). The grain size distribution of the sample comprises 18% of gravel, 48% of sand, 2% of silt and 1% of clay. The mean grain size is 0.91 mm (coarse sand), poorly sorted (1.58), very leptokurtic (9.46) and very fine skewed (2.18). The mineral composition consists of hyaline and milky quartz, feldspars and phyllosilicates (muscovite). The clay association is Kiv (97% of kaolinite, 1.5% of illite and 1.5% vermiculite).

In the left side of the valley, the T1 was observed at 183 m a.s.l. (Vale das Hortas), on the way to Cruz de Morouços (Fig. V.11 B). Near Santa Clara, an artificial cut made for the opening a new road exposed the T2 terrace (~4 m thickness) (Fig. V.11D). This deposit is composed of two sedimentary units: a conglomerate at the base with large cobbles of quartzite and coarse to very coarse sands at the top. The existing cobbles have different MPS values at the base and the top (24.8 and 12.4 cm, respectively). Nevertheless, there is no certainty that the large pebbles and boulders from the base are all local or removed from the surrounding areas when the road was constructed.

T2 is displaced by two NW 260º SE faults, not yet reported in the literature.

V.4.2.2. Sites at reach II (Campo do Bolão – Montemor-o-Velho)

In reach II, the best outcrops of fluvial terrace deposits found for sedimentary characterisation and sampling belong to the T3 level (Fig V10E). The terrace T3 can be observed in an exposure along the road, at the west of Tentúgal (Fig. V.3E). Near the base, overlying the Cretaceous substratum, a layer of clast-supported conglomerate (~0.5 m thick), comprises well-rounded boulders and cobbles (MPS ~17 cm) of quartz and quartzite (*Gm* facies). This layer is followed by a layer (~0.9 m thick) of grading coarse to finer sandstones (Sc and St facies); with yellow-orange colour (10YR/8.8). On the top of the

fluvial sequence, is a ~1.4 m thick siltite layer, with *Fm* facies and grey colour. The Tent5 sample was collected (+18m a.r.b.) at the sand layer and consist of 9.4% gravel, 86% sand and 4% fines. The mean grain size is 0.16 mm (fine sand), is very poorly sorted (2.27), finely skewed (1.11) and mesokurtic (3.53). The sands consist of well-rounded to angular grains of quartz, feldspars, quartzite and muscovite. The clay fraction is composed of kaolinite (62%) and illite (38%).

V.4.2.3. Sites at reach IV (Figueira da Foz)

T4 is represented near Vila Verde (Ervidinho) by fluvial facies, between 29–24m a.s.l. in the right – hand bank of the river (4008'2'' N; 8047'37''W), (Fig. V.10F). At the Ervidinho site, the T4 deposits were sampled for ESR dating. At this site, this terrace was already dated, which enables an age control for this section. The base of the sedimentary sequence (~4 m) is composed of moderately sorted and well-rounded fluvial gravels of quartzite and quartz, with some granite, limestone, schist and silex; it shows planar and trough cross-stratification (Sp facies). A middle layer, ~6 m thick, comprises fine sands, moderately sorted, with horizontal lamination (Sh facies), followed by moderately to poorly sorted medium to coarse yellow sands. The sample Ervi1 was collected at 1 m above the conglomerate layer. This sand layer has some thin intercalations of gravels with planar cross-stratification (Sp facies), some ripple marks and bimodal paleocurrents. The uppermost layer, ~4.5 m thick, consists of medium sands and silt, with light grey colour (10YR8/2). Sample Ervi4 was collected 2.5 m from the top of the outcrop, in a white fine sand layer.

V.4.2.4. Mondego Cape – The marine terrace staircase

A marine terrace (Tm3) located at the northern quarry of the Mondego Cape, was sampled by Pedro P. Cunha by 2005, at about 1 m below the surface of the sedimentary terrace unit (40º11'26" N; 8º 54' 11" W; ~95 m a.s.l.) from a 1 m thick of yellowish very coarse sands, which are below a layer of old colluvium.

Near the lighthouse, the terrace deposits were studied by Soares et al. (2007) (*Farol deposit)*. This deposit comprises two outcrops at ~95 m a.s.l. and one at 51 m, a.s.l., described as:

1) outcrop at 92-100 m, with ~8 m thickness, composed by a succession of lenticular levels of immature limestone conglomerates, interbedded with whitish to yellowish very coarse sandy levels with rhizocretions and laminated structure. The sample of Far-8 was sampled in this outcrop, at 92m, a.s.l.

2) near the lighthouse at 95m, the outcrop is composed by a brownish polymictic and fossiliferous conglomerate at the base. Above the conglomeratic level, a sandy unit with rounded to sub-angular grains of quartz, limestone, and quartzite presents a cross-stratification structure. The upper part is a conglomerate clas-supported unit, with rounded clasts and some sandy fraction.
3) The third outcrop, at 53m, is a polymitic conglomerate with sandy matrix, that fills some paleokarsts of Jurassic ages and consist of a basal gravel thin layer, covered by a whitish sandy conglomeratic unit, with rounded to well-rounded clasts and coarse sandy matrix, with planar cross-stratification. At the top, the succession is composed by interbedded layers of mature, medium to fine sands with rounded to well-rounded quartz grains, attributed to beach facies, also.

The sample (code Far8), has a dull yellow-orange colour (10YR6/4), is dominated by medium sand (55%) and gravels (29%). The total sample comprises well-rounded gravel clasts of quartzite, quartz, granite and schist, and the sand fraction contains quartz, K-feldspar (orthoclase and microcline), plagioclase (albite), ankerite/calcite and muscovite. The mean grain size is 1.25 mm (very coarse sand), is poorly sorted (2.63), finely skewed (1.25) and mesokurtic (3.65). The clay fraction is composed by kaolinite (73%) and illite (27%) (Table V.1).

Table V. 1. Clay mineralogy and clay percentages of the samples (<ld- limit detection).

Sample code	Illite (%)	Kaolinite (%)	Vermicolite (%)
Ing 1	1.5	97	1.5
Concha1	54	46	<ld
Coimb1	25	75	<ld
Tent 5	38	62	<ld
Far-8	27	73	<ld

Table V. 2. Descriptive statistical analyses of grain-size parameters. In Far 8 was just measured the grains< 2mm.

Sample code	Gravels (%) (>2 mm)	Sand (%) (2mm-63µm)	Silte (%) (63-4µm)	Clay (%) (<4µm)	Fines (%) (<63µm)	Mean (mm)	Median (mm)	Mode (mm)	S.Ds	Skewness	Kurtosis
Ing1	7.98	64.06	21.62	3.52	25.14	0.20	0.25	0.50	2.79	0.87	2.96
Concha 1	10.00	54.81	30.33	4.27	34.60	0.13	0.12	0.50	2.62	0.60	2.64
Coimb 1	17.99	48.05	2.22	31.74	33.96	0.91	0.8	2.0	1.58	2.18	9.46
Tent 5	9.00	65.30	22.26	3.50	25.76	0.16	0.29	0.35	2.27	1.11	3.53
Far8		78.87	12.22	2.38	20.60	0.36	0.7	1.4	2.63	1.25	3.65

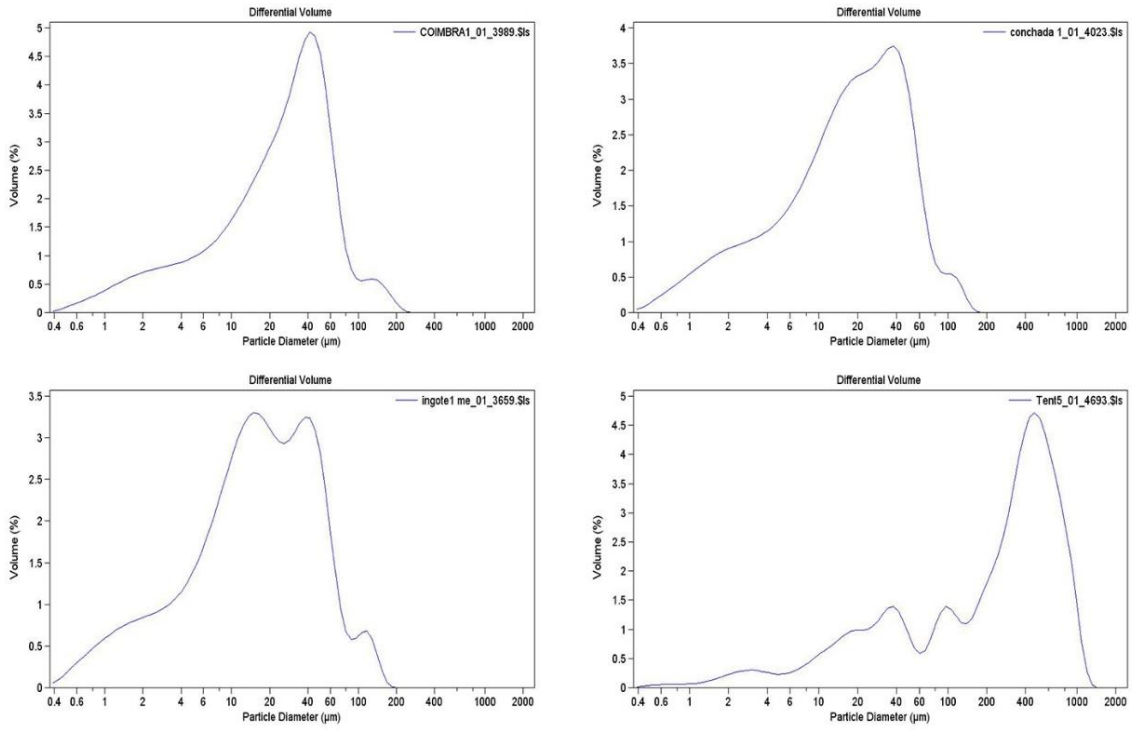

Figure V. 12. Typical grain size curves of the fluvial sediment samples studied.

V.5. ESR dating

The ESR intensities of bleached aliquots of the Al centre suggest similar bleaching conditions for samples of the same stratigraphic level (e.g., Concha1 and Tent5), with higher bleaching rates observed in Ervidinho samples collected near the base (Ervi1) of the fluvial terrace than that of the top (Ervi4), with a bleaching average ranging between 48 and 65% and centred around 58% (Table V.3). These data are comparable to those obtained in most of the fluvial contexts studied in Europe, (e.g., Voinchet et al., 2007; Duval, 2008; Moreno et al., 2017; del Val et al., 2019).

Table V. 3. Bleaching rates (%) of the quartz samples taken in different terraces.

Terraces	**T2**		**T3**		**T4**		**Tm1**
Samples	**Ing1**	**Concha1**	**Tent5**	**Coim1**	**Ervi1**	**Ervi4**	**Far8**
Bleach average %	57	56	48	60	66	51	65
error	1.2	0.1	4.7	3.3	1.2	1.9	0.7

Repeated measurements of Al and Ti centres over different days show the reliability of the signal intensities. The D_e values determined using Al and Ti−Li centres are mostly 1σ consistent, except for samples Ing1 and Tent5. For ESR-Al signal, a specific intensity growth curve response was observed for the youngest samples (e.g., Ervi4) with rapid growth for the first doses and a much slower for high doses (Fig. V.13), as described in other studies (Voinchet et al., 2013).

The ESR analytical data are listed in Tables 2 and 3. Analytical uncertainties and ages are consistent with ± 2σ for most of the samples. When possible, weighted average ages were calculated using Isoplot 4.0 software (Ludwig, 2008).

The ^{238}U, ^{232}Th and ^{40}K concentrations range from 1.58 to 5.04 ppm, 2.20 to 9.75 ppm and 0.54 to 1.73 %, respectively. The results do not show differences in their sources areas, as catchment geology. Overall, comparing the results of the ^{226}Ra, ^{222}Rn and, the ^{238}U measurements, seems to indicate a disequilibrium in the samples Ing1, Concha1 and Ervi1. The spatial heterogeneity could explain the disequilibrium present in the sediment environment of the samples (e.g., the past or active diagenetic processes that lead to a variation of the composition of mobile elements (Guibert et al., 2009). Numerous cobbles of quartzite characterise the sediments within these deposits, and the sand fraction is very poorly sorted, with sandy and silty/clay matrix. The hypothetical past changes in U concentrations were taken into account, and gamma dose rate was calculated using the Pre-radon dose rate conversion factors from Guérin et al. (2012) and attenuated by the measured water content a given sample.

Ing1 sample revealed higher D_e for Al centre (1168±100 Gy) than D_e for Ti−Li (723±32 Gy) while in Tent5 the opposite is observed, with higher D_e values in Ti−Li centre (882±36 Gy) than in Al centre (566±120 Gy), (Table V.2, Fig. V.12, V.13).

The Al D_e values in sample Tent5 are 22% lower than in Ti−Li centre (option D) can be tentatively explained by the heterogeneity of the quartz that makes up the sample. The Tent5 and Ervi1 samples fraction used (180-90 μm) are lower than that used for the other samples (250-180 μm), resulting in more mass of quartz in each aliquot and it could explain a more considerable quartz heterogeneity.

Indeed, this could explain the poorly defined Al growth curve fitting for Tent5, (e.g., Fig.V.13) linked to the fact that some grains of different burial time could be present in the different aliquots. Nevertheless, this sample shows too high goodness-of-fit for the Ti-Li centre (Fig. V.14). The adjusted r^2 is higher than 0.99 and errors ranging < 10%, and the age obtained is the consistent with-it stratigraphic position. The Al signal age should be interpreted as the minimum burial age for this deposit. The ESR Al - age is more consistent for Ervi1, given that Ramos et al. (2012) obtained no finite OSL age for a sample immediately bellow (>390 ka) and even because D_e obtained from the Ti centre seems to saturate earlier with the dose at ~8 kGy (Fig. V.14) which is in line with previous studies (e.g., Duval and Guilarte, 2015; Gouveia et al., 2020). The ESR age estimate is based only in Al centre, so this is considered the maximum possible age (Duval et al., 2015).

Coim1 could not be fitted or calculated by the wide variation present in ESR intensities, without a linear growth match.

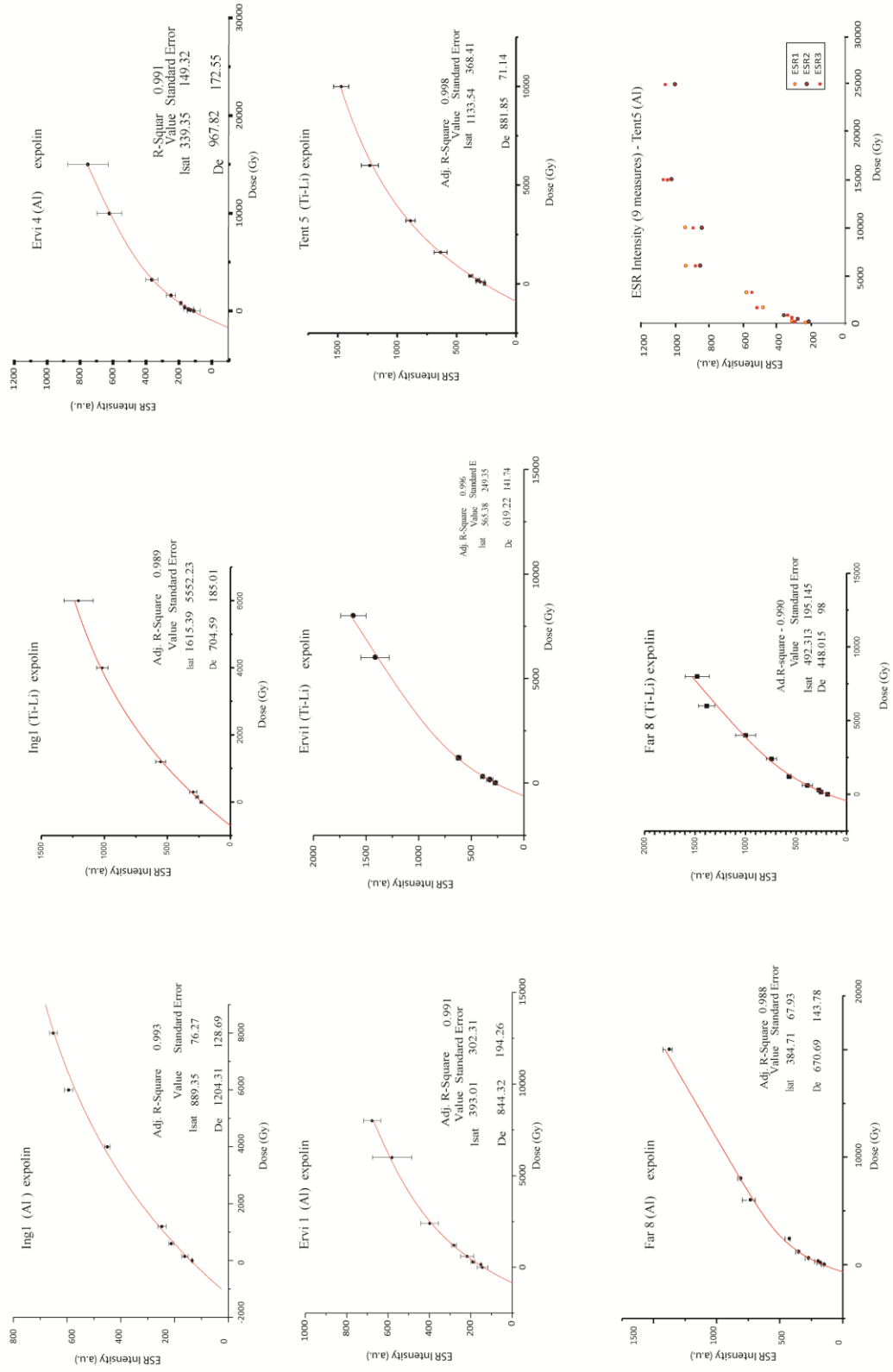

Figure V. 13. Examples of the fitting curves with EXP+LIN of fluvial quartz samples in Al and Ti-Li centres. The last graphic shows the growth-curves for Al-centre based on the average intensities of the sample Tent5 (9 total measures).

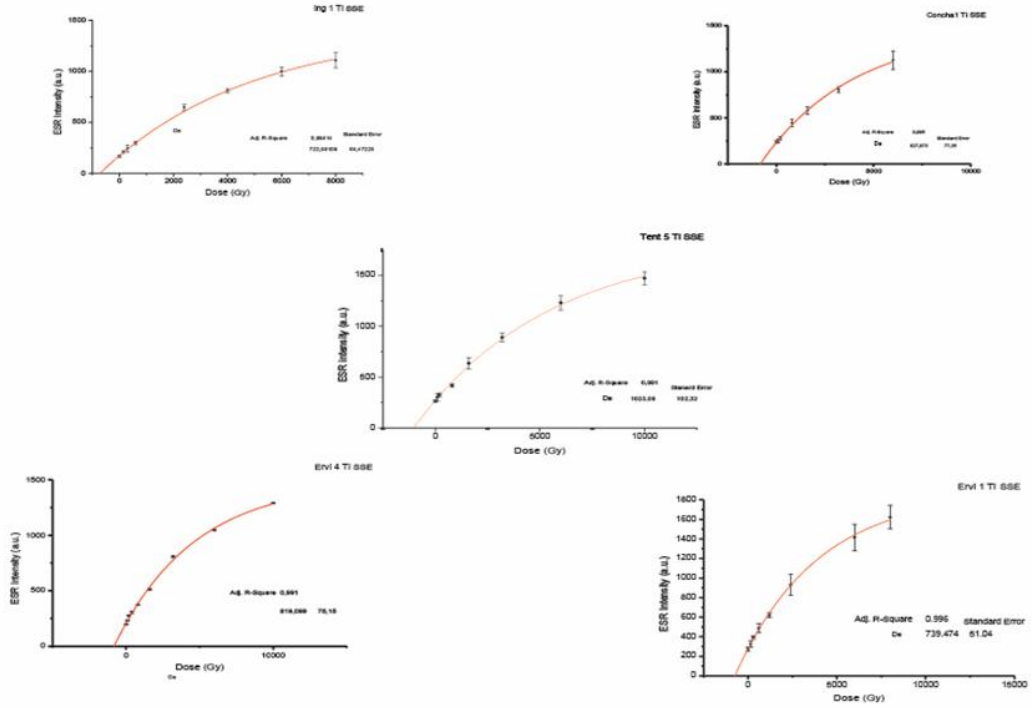

Figure V. 14. Examples of the fitting curves with SSE and EXP+LIN of fluvial quartz samples in Ti-Li centre.

The Al ESR age result of Ing1 sample (670±40 ka) seems an age for T2. This sample also yields a significantly young Ti-Li age of 410±10 ka, which is considered as clearly underestimated, given the geomorphological context. The ESR ages obtained can be explained by the low radioactive activity concentration (Table V.4) and the less stability of Ti-centre than Al-centre in this sample. According to Voinchet et al. (2004), its use seems more reliable for samples of age until Middle -Late Pleistocene.

Table V. 4. Sample information, external β and γ dose rate, cosmic dose and bleaching. External α was considered negligible. The water content (W.C.) for the burial time was estimated, considering the field water content and the saturation water content. *FT - fluvial terrace of LMV; MT - Marine terrace (~100 m a.s.l.) at Mondego Cape.deposits.

Terraces	Sample code	Estimated W.C. (%)	External α dose rate (Gy/Ka)	External β dos rate (Gy/Ka)	External γ dose rate (Gy/Ka)	Cosmic dose rate (Gy/Ka)
FT Reach I	Ing1	20 ± 5	41.5 ± 0.8	939.09 ± 17	832.99±15	165.75±8.3
FT Reach I	Concha1	20±5	33.3 ± 0.7	875.24±17	758.96±16	140.00±7.0
FT Reach II	Tent5	5±2	111.7± 11.3	804.93±61	681.62±53	150.42±7.52
FT Reach IV	Ervi1	5±2	51.1 ± 2.6	1509.02±25	692.30±18	45.99±2.3
FT Reach IV	Ervi4	5±2	32.7 ± 0.9	1352.48±22	872.34±18	58.38±2.9
MT	Far8	15±5	14.36±1.6	345.06±31	310.32±27	140±7

The age results for T3 are consistent with the geomorphological position in each reach of the Mondego valley: they provide a chronology of the fluvial terrace, between 480±21 ka and 536±40 ka (Concha1 and Tent5, respectively). The ESR ages calculated for the Concha1 are consistent in both centres (Table V.5). The adjusted r^2 are higher than 0.99 in both samples (0.995 and 0.991, respectively).

Finally, the samples Ervi1 and Ervi4 (collected in the same T4 sedimentary sequence) are consistent with the stratigraphic position for T4, with ESR ages between 430 ka to 396 ka, respectively. Ervi1 and Ervi4 have an adjusted r^2 higher than 0.99 and an error < 25% for both centres. The D_e in Ervi4 given by Al (862 ±94 Gy) and Ti-Li centres (819 ±37 Gy) are proximal and similar in both functions for Ti-Li centre (795±93 and 819±37) (EXP+LIN and SSE, respectively). Nevertheless, it has always been chosen as the fitting function that gives the least error value. The ages obtained in T4 at Ervidinho are according to the stratigraphy and with the previous chronological data.

The ESR dating of the Mondego Cape marine terrace Tm1 (~100 m a.s.l.) is consistent in both centres, with high goodness of fit and the age average obtain (651±81 ka) is following the stratigraphic elevation. The ESR age seems to support the geomorphological correlation between the Tm1 and the T2 fluvial terrace level of the LMV. Using these ESR ages and the OSL results of Ramos et al. (2012), the ages for the top deposits of T3, T2 and T1 were estimated by extrapolation using the elevation-age function plot on Fig. V.14 as: T5 – 100 ka; T4 – 300 ka; T3 – 450 ka; T2 – 670 ka; T1 – 900 ka (Fig. V.15). The age for the LMV T1 top deposits obtained by extrapolation (~900 ka) is identical to the ESR age in Rosina et al. (2014) for the Lower Tejo T1 top deposits.

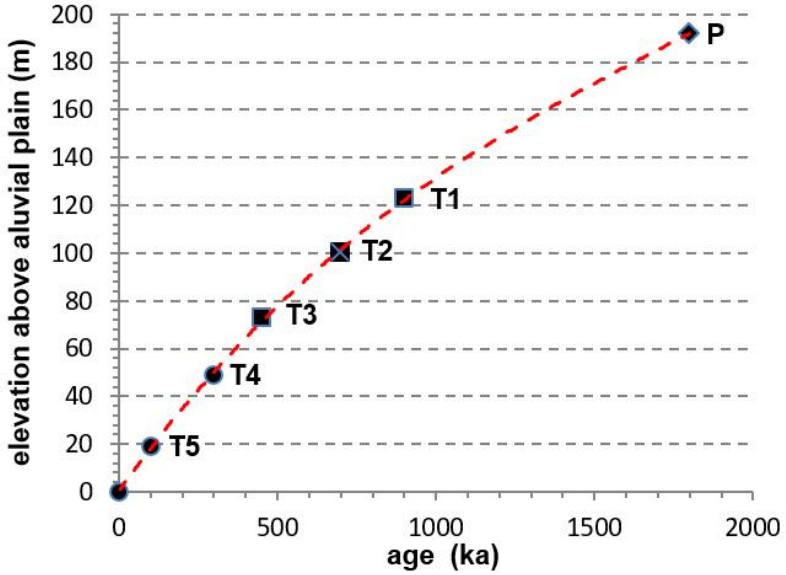

Figure V. 15. Ages of the top sedimentary deposits of the terraces and UBS13 plotted according to the Mondego River alluvial plain height, using the staircase of the reach I right margin. The age of UBS13 (lozenge) of 1.8 Ma is, according to Gouveia et al. (2020), corresponding to the beginning of the incision stage.

Table V. 5. Dosimetry and ESR ages in Al, Ti−Li centre of sedimentary samples collected from the fluvial and marine terraces. The depth of each sample was taken is given in (m) below each sedimentary sequence top. *Tm - marine terrace at ~100 m a.s.l. (Mondego Cape).

Stratigraphic position	**T2**	**T3**	**T3**	**T4**	**T4**	**Tm3***
Sample code	**Ing1**	**Concha1**	**Tent5**	**Ervi1**	**Ervi4**	**Far8**
Depth (m)	1	2	2	10	8	3
Elevation (m)	114.0	83.5	27.0	12.0	18.0	92.0
Grain size (µm)	250-180	250-180	200-100	200-100	250-180	250-180
^{238}U (ppm)	5.045±0.09	3.467±0.01	1.581 ± 0.48	1.749±0.08	2.625±0.08	0.989±0.24
Rn (ppm)	4.230±0.035	2.709±0.034	-	1.343±0.028	2.096±0.07	-
^{232}Th (ppm)	6.78±0.12	9.644±0.15	9.749 ± 0.17	2.197±0.10	6.348±0.12	3.65±0.26
^{40}K (%)	0.543±0.01	0.822±0.01	0.715 ± 0.01	1.732±0.02	1.334±0.01	0.258±0.01
D_a(total) (µGy.a^{-})	1893±43	1824±56	1050±81	2213±43	2118±44	499.5±41
D_e Ti centre (Gy)	723±32	816±45	882±36	742±20	819±37	599±150
Adj. Square	0.99	0.99	0.99	0.99	0.99	0.99
D_e Al centre (Gy)	1168±100	804±61	566±120	844±97	862±94	648±96
Adj. Square	0.99	0.98	0.98	0.99	0.99	0.99
Ti−Li centre Age (ka)	410±10	480±30	**536±40**	339±20	389±20	656±50
Al centre Age (ka)	**670±40**	480±40	340±70	430±30	409±40	641±70
Mean Age (Al and Ti−Li)	-	**480±21**	-	-	**396±31**	**651±81**

V.6. Incision rates and vertical displacements

The mean elevation values of the left and right margins are present in Table V.6. Using the estimated ages for the top deposits of the terraces and UBS13 (T5 – 100 ka; T4 – 300 ka; T3 – 450 ka; T2 – 700 ka; T1 – 900 ka; UBS13 – 1.8 Ma), the vertical movement rates and the differential uplift rates between the left and right margins of the valley can be estimated for the four reaches.

Table V. 6. Vertical displacements (meters a.a.p.) of the UBS13 and the terrace levels in staircases of the four reaches.

Reach I			**Fault F1**			
Stratg. Unit	**UBS13**	**LM T1**	**LM T2**	**LM T3**	**LM T4**	**LM T5**
Right (R)	123	87	70	48	33	14
Left (L)	189	120	98	67	45	16
L-R	**66**	**35**	**28**	**19**	**12**	**2**
Rate (m/ka)	**0.037**	**0.039**	**0.041**	**0.042**	**0.038**	**0.015**
Reach II			**Fault F2**			
Right (R)	97	72	48	27	16	3
Left (L)	144	108	77	46	30	9
L-R	**47**	**36**	**29**	**19**	**14**	**6**
Rate (m/ka)	**0.026**	**0.042**	**0.043**	**0.028**	**0.031**	**0.060**
Reach I to II			**Fault F3**			
East side	122	100	76	63	46	16
West side	90	76	52	41	26	8
E-W	**32**	**24**	**24**	**22**	**20**	**8**
Rate (m/ka)	**0.018**	**0.028**	**0.036**	**0.048**	**0.067**	**0.08**
Reach IV			**Fault F4**			
Right (R)	195	128	109	47	22	11
Left (L)	85	76	72	35	21	9
R - L	**110**	**52**	**37**	**12**	**1**	**2**
Rate (m/ka)	**0.061**	**0.061**	**0.055**	**0.027**	**0.002**	**0.020**

V.6.1. Reach I (Coimbra – Campo do Bolão)

Although not all terrace levels and surfaces are represented in a single profile, the differential uplift between the left and right margins of the valley was estimated at a maximum of ~66 m for the UBS13 unit and a minimum of ~2 m for the T5 (Table V.6). For this reach, the differential vertical movement rates is: 0.037 m/ka for UBS13 (66 m/1800 ka), 0.036 m/ka for T1 (35 m/900 ka); 0.040 m/Ka for T2 (28 m/670 ka); 0.042 m/ka for T3 (19 m/450 Ka); 0.038 m/ka for T4 (12m/300 ka) and 0.015 m/ka for T5 (2 m/100 ka); average =0.034 m/ka. The N-S to NNW-SSW F1 fault system (Fig. V.3) should be responsible for the main vertical movements.

The activity of the F1 fault system seems to increase with time, reaching the maximum at the end of T4 ~300 Ka, but diminishing in the last 100 ka (after the formation of T5). We admit that the last assumption maybe not entirely true, considering that the amount of differential uplift for T5 is only 2 m and by the possibility that T5 aggradation could have extended a little more.

The incision rates follow a similar pattern of the differential uplift rates calculated regarding the F1 system faults, i.e., also increasing to newer times (Fig. V.16), reaching the maximum value at the T4 terrace (0.15 m/ka in the more uplifted left margin and 0.11 m/ka in the right margin). The incision rates of the Mondego River are substantially higher than the vertical movement rates associated with the F1 faults. The ratio uplift rate/incision rate is ca. 0.25 m/ka in the left margin and 0.34 m/ka in the right margin (averaged of the six geomorphic levels ratios). This difference may be understood because the differential uplift in the F1 strike-slip fault system is only a part of the entire crustal vertical movement and does not include the regional uplift, the isostatic component related to surface processes or other mechanisms. However, the similar behavioural pattern between the vertical movement rates on the F1 fault system and the incision rates indicates that, in the long-term, the formation of these terraces should be superimposed on the tectonic component of uplift, responsible by the vertical spacing and staircase disposition.

The difference in the heights a.a.p. of the geomorphic references allows estimating the vertical displacement rate in the F3 fault (Fig. V.17, Table V.6). For the UBS13 unit, ~0.018 m/ka (32 m/1800 ka); for the T1, 0.027 m/ka (24 m/900 ka); for the T2, 0.034 m/ka (24 m/670 ka); for the T3, 0.049 m/ka (22 m/450 ka); for T4, 0.067 m/ka (22 m/300 ka) and for the T5, 0.08 m/ka (8 m/100 ka).

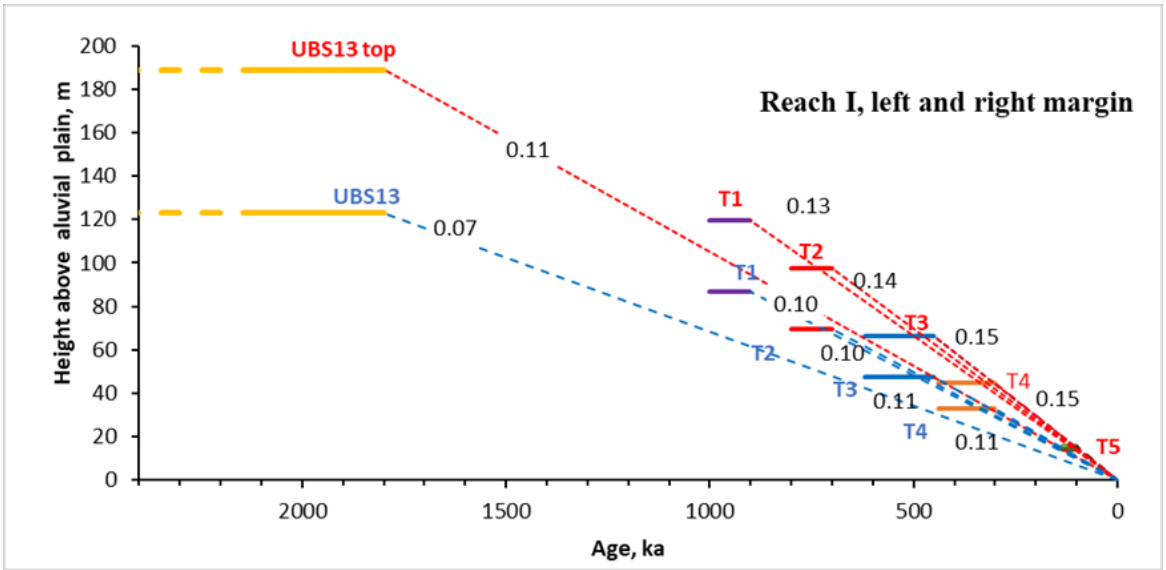

Figure V. 16. Elevations of the UBS13 and terrace levels above the alluvial plain in reach I, at Cruz de Morouços and Pinhal de Marrocos, displaced by the F1 system faults. The slope of the lines matches with the incision rates values. Blue lines correspond to the downthrown compartments and the red lines with the upthrown compartments.

The values indicate an increase in tectonic activity in the F3 fault system until the end of the T4 formation, decreasing after that period (Fig. V.17).

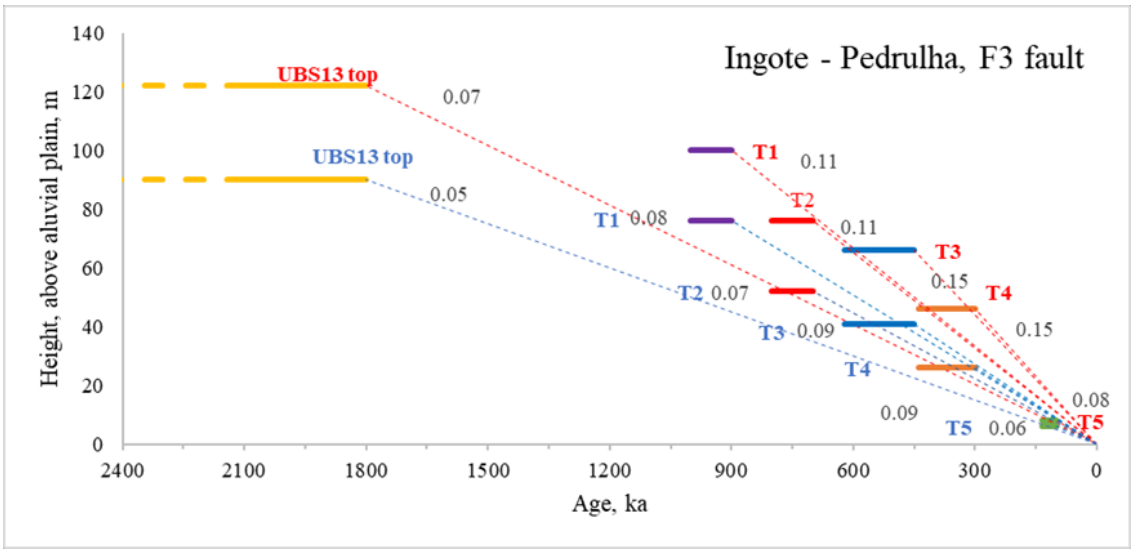

Figure V. 17. Elevations of the UBS13 and terrace levels above the alluvial plain in reach I, right margin, at Ingote and Pedrulha compartments, displaced by the F3 fault. The slope of the lines matches the incision rates values. Blue lines correspond to the downthrown compartments and the red lines with the upthrown compartments.

Incision rates have similar behaviour as the differential uplift rates, increasing from the Lower to Middle Pleistocene, reaching maximum values in the last 300 ka and probably becoming attenuated after the T5 (during the Late Pleistocene).

In valley right side, in the abandoned meander area, the T3, T4 and T5 terraces are well identified. Using the age of ~100 ka for the T5 top deposits, we can assume that the abandoned meander formation should postdate the last interglacial, occurring the neck cut off probably during the last glacial period, when the incision wave triggered by the sea-level drop, reached this area. The würmian incision was filled with up to 33 m of Holocene alluvium, under the Pedro and Inês bridge (Fig. SM.V.1.).

V.6.2. Reach II (Campo do Bolão – Montemor-o-Velho)

The differential uplift calculated through the difference in the elevations a.a.p. of each geomorphic reference between the two valley sides is ~47 m for the UBS13 to ~6 m for the T5 (Table V.6), as an average of the four transverse profiles. We presume that this differential uplift may be caused by an ENE-WSW to NE-SW F2 fault hidden by the Mondego alluvium. This probable F2 fault was not identified in outcrops. However, in the vicinity of Campo do Bolão, in the LMV right side, ENE-WSW to NE-SW faults are mapped near the Antuzede village (Soares et al., 1965). These faults extend outward of the reach II, controlling the Fornos stream valley direction (Fig. V.5).

The vertical displacements associated to the ENE-WSW F2 fault is the following (Fig. V.18, Table V.6): 0.026 m/ka for the UBS13 (47 m/1800 ka); 0.041 for the T1 (36 m/ 900 ka); 0.041 m/ka for the T2 (29 m/670 ka); 0.040 m/ka for the T3 (19 m/450 ka); 0.047 m/ka for the T4 (14 m/300 ka) and 0.060 m/ka for the T5 (6 m/100 ka). Averaged vertical displacement rate = 0.037 m/ka.

Uplift rates show a tendency to increase from the Lower Pleistocene to the Middle Pleistocene (~300 ka, end of the T4 aggradation), up to 0.04 m/ka. The increasing trend of the uplift should have continued in the Late Pleistocene, if the final aggradation of the T5 took place by ~75-80 ka (not as ~100 ka), as seems to have happened in the regional context of central Portugal (Martins et al., 2010a,b; Cunha et al., 2012, 2016).

Incision rates are higher in the LMV left margin (Fig. V.18), and they are considerably higher than the vertical displacement rates associated with the F2 fault. The ratio of the vertical displacement rate/incision rate is ~0.44 for the left margin and ~0.73 for the right margin (averaged for ratios of the six levels). It can be understood because the differential uplift produced by the vertical movement of the strike-slip faults corresponds only to a fraction of the regional uplift.

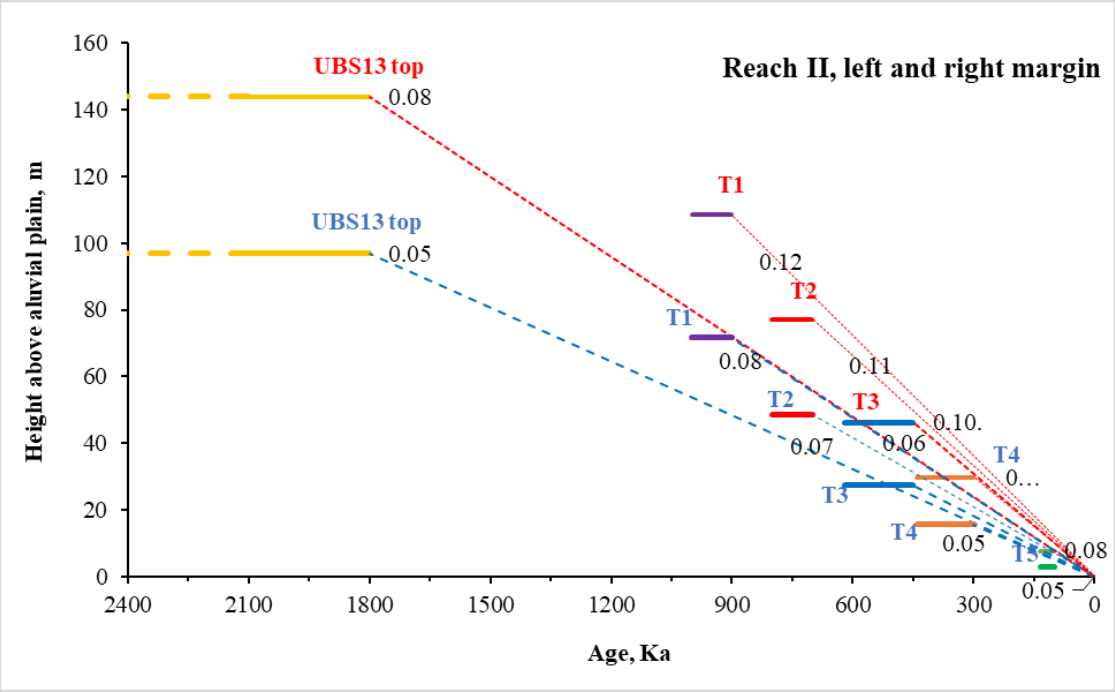

Figure V. 18. Elevations a.a.p. of the UBS13 and terraces in the left (red colour) and right (blue colour) sides of the LMV, reach II. For each geomorphic reference, the average of the four cross-profiles was calculated.

V.6.3. Reach III (Montemor-o-Velho - Lares)

In the Lares gorge, the Mondego River crosses the Serra da Boa Viagem - Verride structure dipping to SW.

As said before, terrace staircase has higher elevations at the right margin (Fig. V.19), resulting from the increase in Serra da Boa Viagem uplift toward NW, determined by the Quiaios thrust fault (Ramos et al., 2012). The superimposition of Mondego on the homoclinal ridge of Serra da Boa Viagem is easily understood, seeing that the UBS13 sedimentary remains still cover the planation surface at 115-130 m a.s.l. in the valley left margin. In the neighbouring area of the gorge are several NE-SW lineaments crossing the Jurassic and Cretaceous formations. One of these lineaments intersects the Quiaios thrust fault (F4) at the northeast of the Maiorca village in the valley right margin. The arching of the Quiaios trace fault, after the intersection by NE-SW lineaments, suggests that these possibly work with a slight left slip component in a compressive regime.

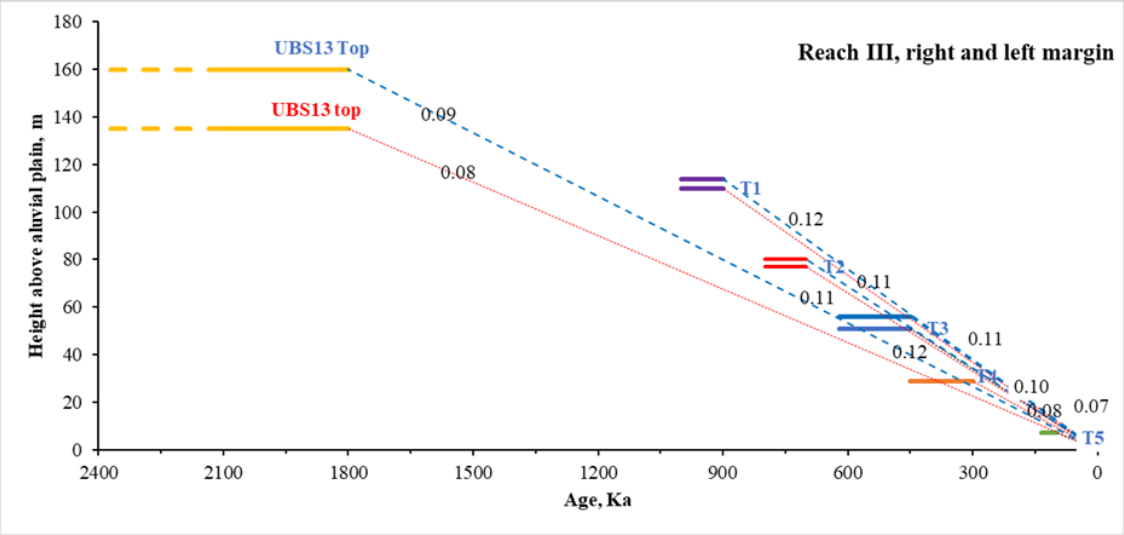

Figure V. 19. Elevations a.a.p. of the UBS13 and terraces in the reach IV upper sector (Lares, A) and at the reach IV lower sector (Figueira da Foz, B). The slope of the blue lines documents the incision rates of the right margin, while the slope of the red lines documents the left margin. In the B sector, the UBS13 at Serra da Boa Viagem is uplifted more than 100 m in relation to the left margin position.

V.6.4. Reach IV (Lares - Figueira da Foz)

As Serra da Boa Viagem was uplifted during the Quaternary (Cabral and Ribeiro, 1988; Cabral, 1995; Ribeiro et al., 1996), the erosional surfaces and terraces became progressively higher in the northwest part of the hill (Fig. V.20).

Due to the uplift promoted by the Quiaios - Maiorca fault, tilting the southern compartment toward the south, the terrace levels at the right valley margin are at higher elevations than the levels at the left margin (Fig. V.21). For the calculations of the incision rates using the Pliocene marine platform (3.7-1.8 Ma) the position of sea level during the Middle Pliocene warm period was considered as ~30 m above the present sea level (+10 - 20 m above the present seal level according to Miller et al., 2005; 2019). The right valley margin comprises the following elevations: for the UBS13 top, that we estimated to have reached locally +195 m, ~0.11 m/ka (195 m/1800 ka); for the T1~0.15 m/ka (128 m/900 ka); for T2 ~0.16 m/ka (109 m/670 ka); T3 ~0.10 m/ka (47/450 ka); for T4 ~0.13m/ka 22/300ka); for T5 ~0,11 m/ka (11m/100 ka).

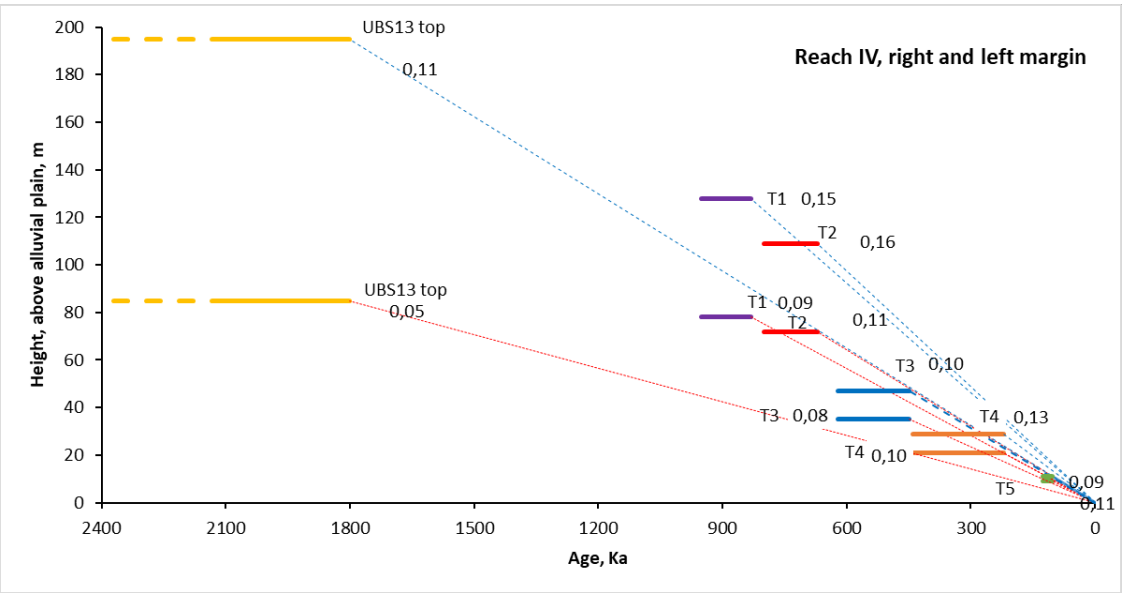

Figure V. 20. Elevations a.a.p. of the UBS13 and terraces in reach IV. The slope of the blue lines documents the incision rates of the right margin, while the slope of the red lines documents the left margin. The UBS13 at the Serra da Boa Viagem is uplifted more than 100 m concerning the left margin position.

Regarding the left valley margin: for the UBS13 top, ~0.05 m/ka (85/1800 ka); for the T1~0.09m/ka (78 m/900 ka); for T2 ~0.11 m/ka (72 m/900 ka); T3 ~0.08 m/ka (35/450 ka); for T4 ~0.10 m/ka (21m/300ka); for T5 ~0.11 m/ka (9 m/100 ka). However, at the NW edge of Serra da Boa Viagem, the Pliocene wave-cut platform, considered of the same age as the base of UBS13, reaches 257 m a.s.l. The incision rate obtained for the older reference is: 0.07 m/ka (257/3700 ka).

The differential uplift for the UBS13 top, that we estimated to have reached locally +195 m (185 m plus 10 m of sedimentary thickness), ~0.05 m/ka (185-85 m/1800 ka); for the T1~0.058 m/ka (128-76 m/900 ka); for T2 ~0.055 m/ka (109-72 m/670 ka); T3 ~0.027 m/ka (47-35/450 ka); for T4 ~0.003m/ka 22-21/300ka); for T5 ~0,02 m/ka (11-9 m/100 ka).

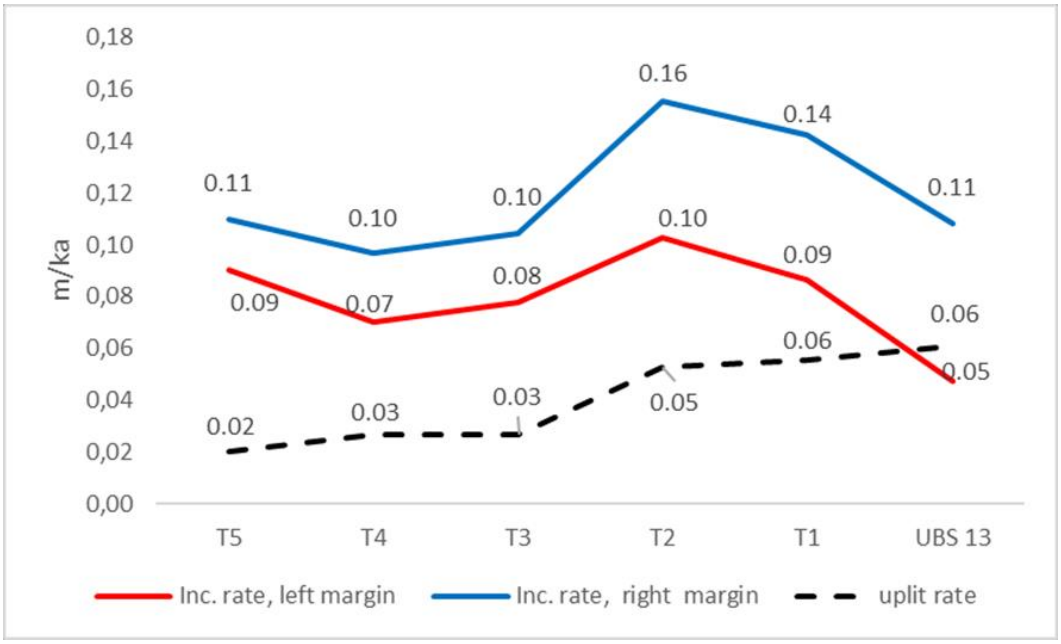

Figure V. 21. At reach IV, the long-term evolution of incision rates in the right and left valley margins and the long-term evolution of the uplift rate are mainly determined by the Quiaios fault.

VI.7. Discussion

The detailed geomorphological mapping, the realisation of transverse geological profiles and some absolute age control, allowed the identification of terrace levels according to their elevation a.a.p. in both margins and the different reaches of the LMV. The LMV terraces can be compared with the Lower Tejo terrace levels, located in a near area under a similar climatic, eustatic and tectonic control.

The oldest terrace level (T1) of the LMV has heights above the alluvial plain up to +63 m in the less uplifted right margin of the reach II, the less uplifted of the four reaches and up to +100 m in the more uplifted left margin (Figs. V6, V7C). The oldest terrace level (T1) of the Lower Tejo, at +76 to +180 m a.r.b., is considered with a probable aggradation interval of ~1000-830 ka (Martins et al., 2009; Cunha et al., 2012, 2017; Rosina et al., 2014).

The ESR age of terrace T2 was obtained from a sample collected in the Ingote plateau at the site S1, with a height of +92 m a.a.p. (Fig. V.3), but the same terrace is only presented at +48 m in the reach II right margin. The active fault systems (F2, F3), that uplifted the Ingote plateau explain the height differences in the same geomorphic reference. As the ESR age of 670 ± 40 ka is considered a probable minimum estimate, we used 700 ka for the top of the T2 terrace in the LMV. At the Lower Tejo, the aggrading top surface of T2, at +57 to +150 m, is considered with a probable age of ~600 ka (Cunha et al., 2016).

The T3 is at +68 m in the right margin of reach I but is only at +27 m in the right margin of reach II. In previous studies (Soares, 1966; Cunha et al., 1999) the T3 remain at Conchada has been considered correlative of the terrace level at Ingote, but without absolute age control. Considering reliable the ESR ages of Tent5 (486±30 ka) and Concha1 (480±40 ka), the probable aggrading interval of the T3 at LMV could be in the range 580-450 ka. In the Lower Tejo, from the T3, two ESR ages were obtained (~405 ka and ~461 ka) with a similar range (Rosina et al., 2014).

The T4 at reach IV, with a height of +30 m a.a.p. in the right margin and +16 m in the left margin, provided minimum ages of >390 ka and >340 ka (Ramos et al., 2012) for middle and basal stratigraphic levels. For ESR dating, this terrace was sampled just above the basal conglomerate level (Ervi1) and near the top (Ervi4), giving ages of 383 ka and 374 ka. The ESR age for the sample at the top of this terrace (Ervi4) seems to overestimate the final aggradation time of T4. In the Lower Tejo, the T4 terrace is considered with an aggrading interval of ~340-155 ka (Cunha et al., 2017), but the beginning of sedimentation could have started by ~440 ka. In the incision rates calculations, we used the age of 300 ka for the T4 top.

The T5 terrace of the LMV, at +8 m a.a.p. in the reach IV, but +3 m in the left side of the reach II, can be correlated to the T5 of the Tejo River, dated as 135-75 ka. Not having the age for the LMV T5 topmost deposits, we used 100 ka to calculate the incision rates.

As in other basins, in the LMV, there is a need for more absolute age control to constrain better the periods of aggradation and for a more precise calculation of the incision rates.

In the study area, active faulting during the Quaternary is responsible by the differential uplift expressed by the vertical displacement of the UBS13 unit and fluvial terraces. The area of reach I was more uplifted than the reach II, given the geomorphic markers heights. In the more uplifted left margin of reach, I, the elevations a.a.p. of the UBS13 unit and the fluvial terraces are even higher than theirs equivalents at the Serra da Boa Viagem (reach IV, right margin), indicating that, in the regional context, the Cruz de Morouços plateaus should have experienced the highest uplift of the study area. In fact, the incision rates of the more uplifted left margin of the reach I, are slightly higher than the incision rates of the more uplift right margin of the reach IV, including the east part of the Serra da Boa Viagem. The western end of Serra da Boa Viagem is the exception.

Under the NW–SE compression that characterises the geodynamic framework of Iberia during the Quaternary, the N-S to NW-SE F1 system faults and the NNE-SSW F3 system faults should act as left strike-slip faults, the WNW-ESE to E-W Quiaios - Maiorca F4 fault should move as a reverse fault with slight right lateral movement, and the WSW-ENE F2 system faults should move as right strike-slip faults.

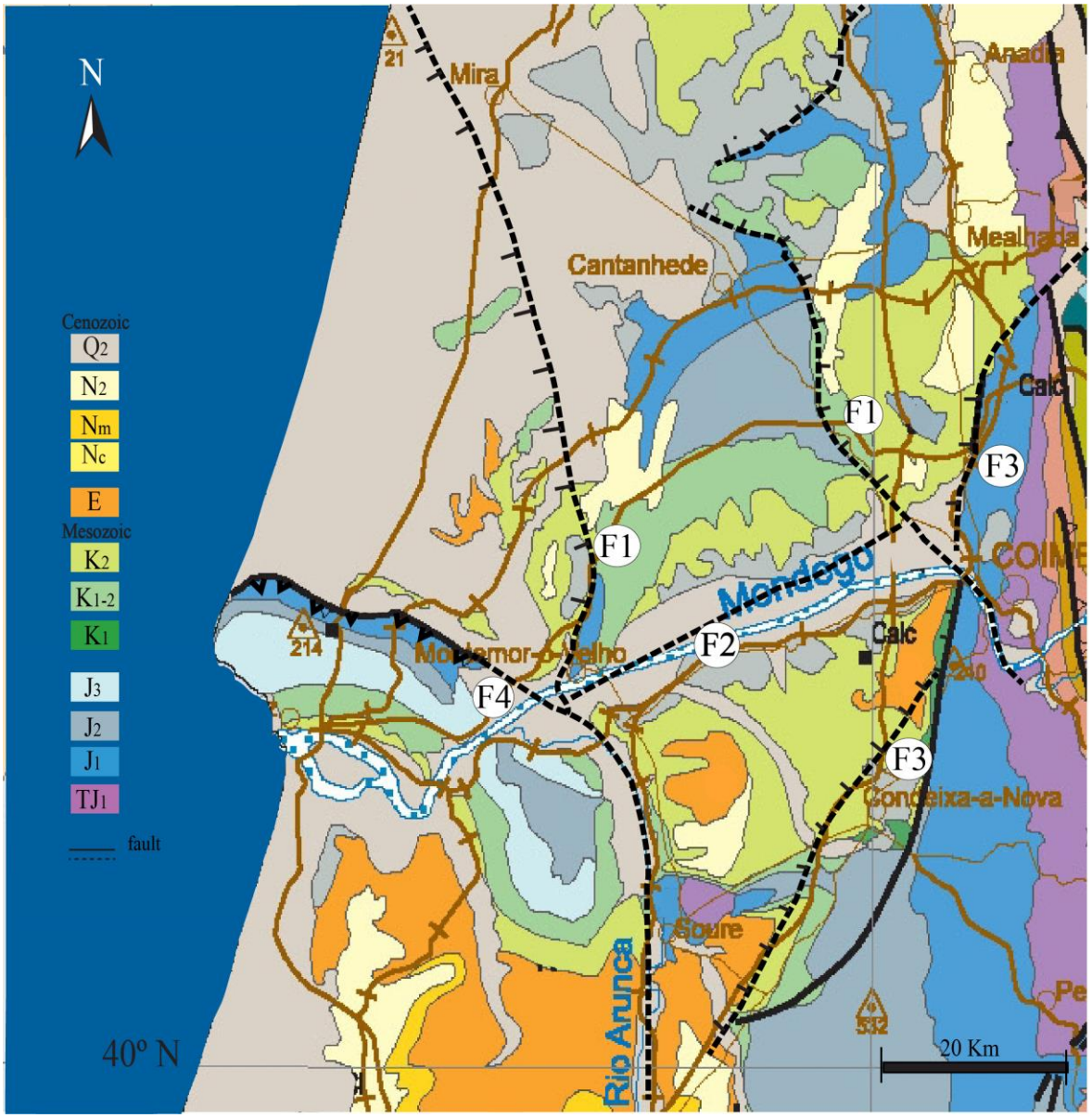

Figure V. 22. Map of faults evidencing activity in the study area. F1-(N-S to NNW-SSE system fault; F2 - (NE-SW - Mondego valley fault); F3- (NNE-SSW – Coimbra - Antanhol fault); F4- Quiaios-Maiorca fault, (modified from Geologic Map of mainland Portugal, 1/1.000.000 scale).

The incision rates may be considered a reasonable proxy for regional uplift (e.g. Merritts et al., 1994; Burbank and Anderson, 2001; Hancock and Anderson, 2002) and both should match if the river incision has graded the longitudinal profile to the lowering base level that results from the continental uplift. This fact only occurs when the incision rate balances the uplift rate of the continent, but this equilibrium probably happens in time scale over millions of years for the great rivers (Whipple and Tucker, 1999; Whipple, 2001; Pazzaglia, 2003; García-Castellanos and Larrasoaña, 2015).

The incision rates are relatively higher in the entire Lower Mondego valley than the vertical displacement rates calculated in the several main faults. In the strike-slip faults, the vertical displacement rates should be lower than the slip rates of the horizontal offset.

The vertical displacement rates measured in different faults of the study area were estimated to be (averaged from the six references): 0.038m/ka in the F1 fault (N-S to NNW-SSE fault; 0.031 m/ka in the main F2 (NE-SW - Mondego valley fault); 0.041 m/ka in main F3 fault (NNE-SSW – Coimbra- Antanhol fault); 0.028 m/ka in the Quiaios-Maiorca fault (F4). These values are within the values of slip rates measured in other active faults in Portugal, whose slip rates change between 0.005-0.5 m/ka (Cabral, 1995; Ressurreição et al., 2011; Cabral et al., 2012).

In the long-term, the activity of the faults F1 is relatively stable and seems to decrease in the lower terrace (T5), F2 and F3 seem to be increasing from the Early Pleistocene to the end of the Middle Pleistocene, having slightly reduced during the Late Pleistocene. The exception is the Quiaios fault (F4) whose activity seems to be decreasing since the Middle Pleistocene to the present (Table V.6, Fig. V.21).

VI.8. Conclusions

In the LMV, five terrace levels were identified below the culminant sedimentary unit (UBS13). In the reach I, a sixth terrace (T6) was placed buried by the modern alluvium.

The lithological and structural characteristics of the substratum, together with the active regional faulting during the Quaternary, give different morphological peculiarities to each of the four reaches of the LMV: a) the reach I is an incised valley carved in a generally hard substratum, whose steep slopes are promoted by continuous uplift and active faulting; b) in reach II, the valley is wide, with extensive flood plain and asymmetric slopes resulting from differential uplift in each side of the valley; c) the reach III is a superimposed narrow gorge on the Serra da Boa Viagem structure; and d) in the reach IV, the valley is much larger and comprises the lower sector of the Mondego estuary; it has a strong structural control in the right side. During the Quaternary, active tectonics is responsible for the differences in the elevations a.a.p. that serve as references to the fluvial landforms along the LMV.

In the reach II, the fluvial terraces show the lowest elevations a.a.p. (mainly on its right bank): T1 +72 m; T2 +48 m; T3 +27 m; T4 +16 m; T5 +3 m; these values should be considered as the minimum elevations a.a.p.

Our interpretation suggests that the T1 terrace would have formed during the Early Pleistocene, probably in the period between ~1000-900 ka. The T2 terrace is perhaps from the transition Early to Middle Pleistocene, with an age of ~800-700 ka; the T3 (probably ~620-450 ka) and the T4 (probably ~440-300 ka) are Middle Pleistocene, the T5 (probably ~135-100 ka) and the T6 (~60-30 ka ?) are Late Pleistocene.

The chronological framework introduced above is similar to that reported for the Lower Tejo, which may indicate common external controls. Since that all the LMV reaches are located less than 50 km from the Atlantic Ocean, we admit that the glacio-eustatic base-level changes will have been the main forcing mechanism of terrace formation, with the aggradation phases occurring during the sea level high-stand periods and incision phases during low-stand periods. However, the terrace levels would encompass more than a single MIS, except the T5 and, probably, the T6, which seem to mainly correlate to the MIS 5 and the MIS 3, respectively.

The disposition in terrace staircases confirms the relevance of the ongoing regional uplift, whose values were estimated indirectly through the incision rates, within the parameters inherent to a passive margin under compressive reactivation. The differential uplift, mainly related to strike-slip faults, created complexity in the terrace staircases' height.

The differential uplift is relatively low, ranging between 0.01-0.05 m/ka using the ~1.8 Ma reference and is 0.09-0.15 using the terraces as references. The vertical displacements deduced at several faults ranged from 0.035 m/ka to 0.044 m/ka, agreeing with the values of slip rates estimated for the last 2.5 Ma in mainland Portugal, ranging from 0.005 and 0.5 m/ka.

This study shows the importance of river terraces in determining the uplift in passive margins with moderate to low tectonic activity during the Quaternary. However, more numerical dating of the terrace sequence is still needed to the chronological framework, particularly for the older terrace levels that encompass various MIS stages. More dating is required, especially at the base and top of each terrace level to evaluate the aggradation interval. The better temporal constrain will allow evaluating the role played by eustasy and climate under an ongoing uplift.

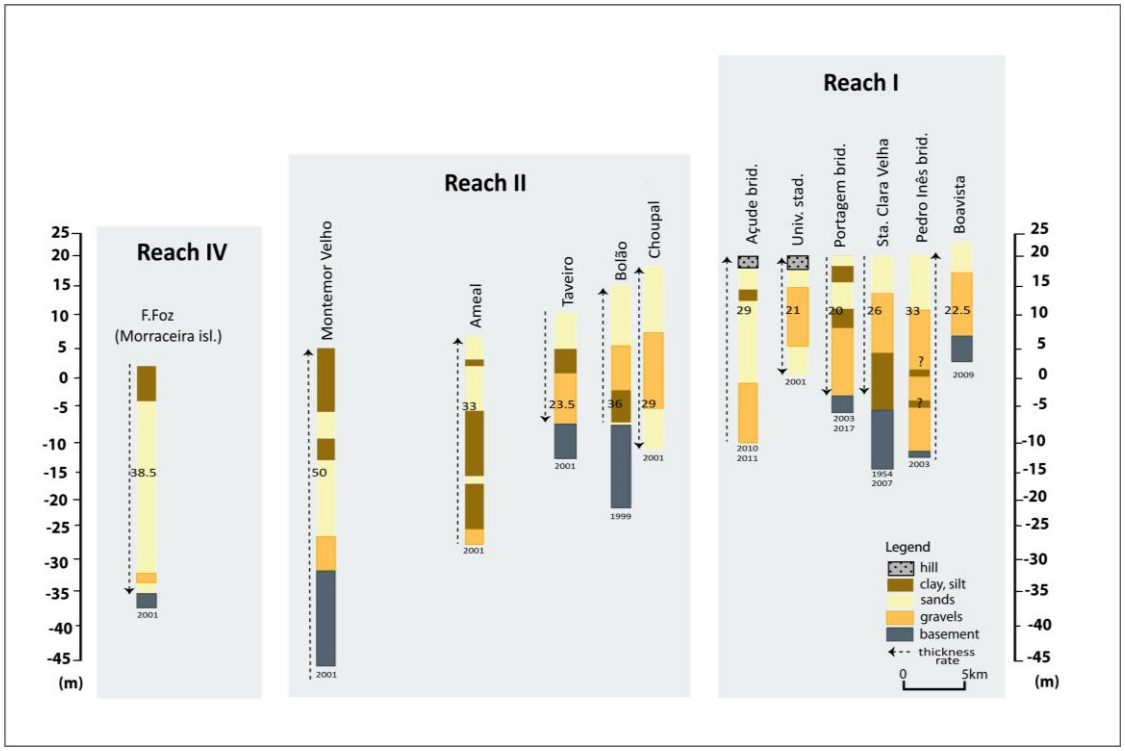

Figure SM. V 1. Alluvial thickness correlation panel of the right-hand bank of Mondego River valley between Coimbra and Figueira da Foz, (borings were taken in different years 1999; 2001; 2003;2010; 2011; 2017, in Andrade, 2005, Tavares and Soares, 2010; Mota, 2019).

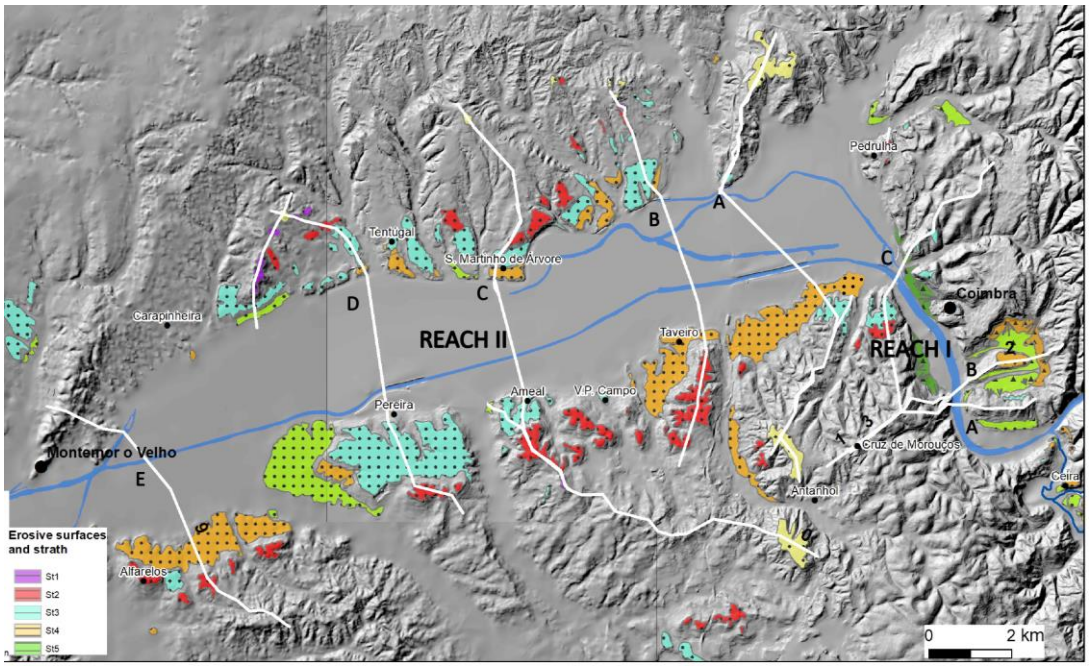

Figure SM.V 2.Transverse profiles location in Reach I and II.

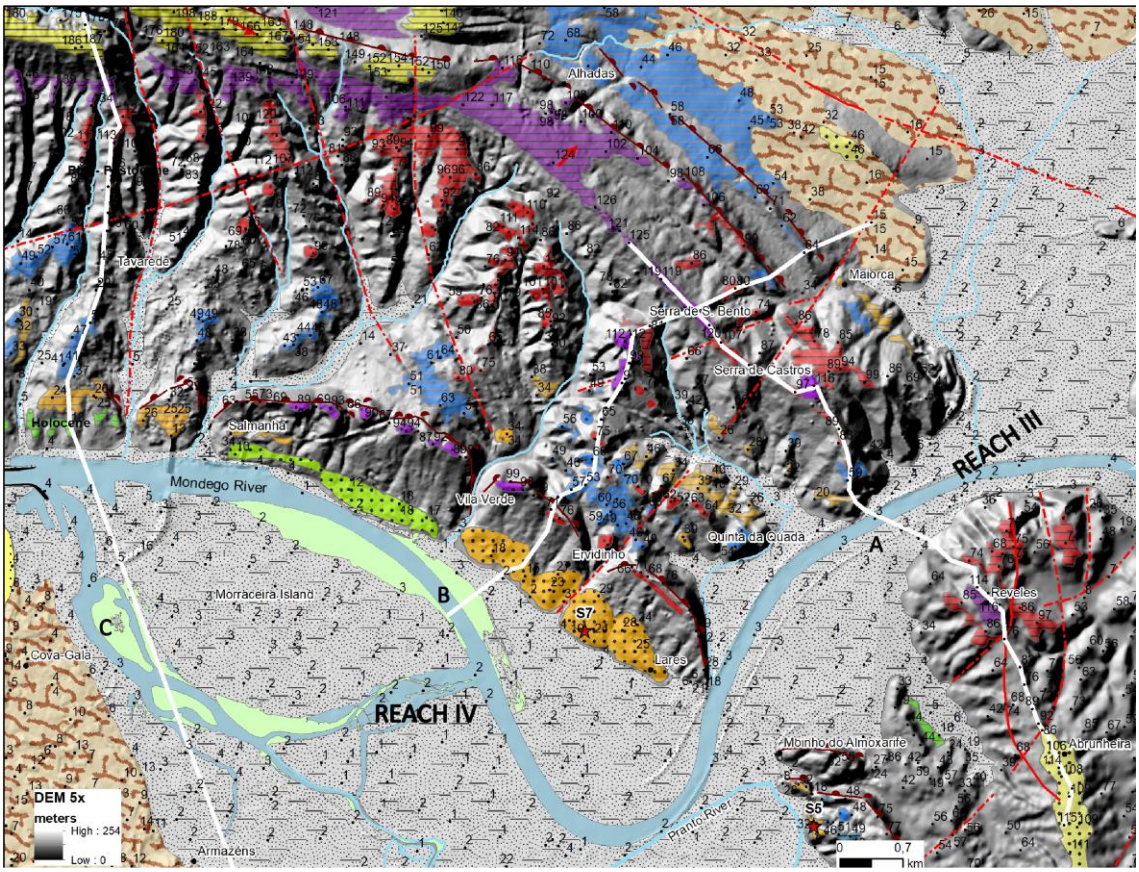

Figure SM.V 3. Transverse profile locations in Reach III and IV.

Table SM V. 1. ESR mean data (4 measurements) was collected from Al centre of the quartz grains of the fluvial sediments Ing1 and Ervi 1.

Dose (G)	ESR (a.u.) Ing1	d.s.	ESR (a.u.) Ervi1	d.s.
0	134.284	0.562	130.142	13.958
150	161.664	11.873	160.350	6.339
300	193.496	34.625	190.619	13.383
600	212.366	9.073	234.902	28.223
1200	247.201	15.443	281.679	14.009
2400	388.580	118.183	400.937	30.005
4000	449.577	9.591	532.890	88.871
6000	593.719	15.696	569.192	52.372
8000	650.920	14.735	692.584	26.376
12500	755.338	38.546	857.223	65.088
20000	954.211	67.365	1139.860	103.134

Table SM V. 2. ESR mean data collected from Al centre of the quartz grains of the fluvial sediments Concha1, Tent5, Ervi4.

Dose (G)	ESR (a.u.)	d.s.	ESR (a.u.)	d.s.	ESR (a.u.)	d.s.
	Concha1		Tent5		Ervi 4	
0	104.800	31.367	243.059	25.726	109.105	38.881
100	117.840	15.449			129.363	22.050
200	125.473	13.279	333.166	7.805	141.849	29.580
400	134.599	33.959	322.888	24.181	164.260	3.527
800	209.623	22.390	356.431	21.953	187.941	6.421
1600	262.894	26.534	503.079	26.745	247.709	27.094
3200	409.831	35.367	601.540	43.762	364.604	36.790
6000	504.806	105.879	925.426	23.470	486.285	90.251
10000			910.067	22.942	621.864	75.371
15000	679.098	109.712	1042.575	68.622	752.712	123.289
25000	773.712	101.075				

Table SM V. 3. ESR mean data (3 measurements) was collected from Ti-Li centre of the quartz grains of the fluvial sediments Ing1 and Ervi1.

Dose (G)	ESR (a.u.)	d.s.	ESR (a.u.)	d.s.
	Ing1		Ervi1	
0	296.698	13.391	272.956	22.037
150	328.890	5.473	325.126	30.159
300	331.629	55.666	393.213	17.104
600	388.328	110.493	486.302	45.097
1200	676.206	75.512	620.960	22.895
2400	936.933	19.818	931.518	108.923
4000	1210.169	49.103	1223.516	260.284
6000	1485.381	122.028	1415.459	134.482
8000	1498.790	242.421	1622.378	119.772
12500	1840.962	240.045	1631.699	104.909
20000	1595.617	170.084	1429.296	140.972

Table SM V. 4. ESR mean data (3 measurements) was collected from Ti-Li centre of the quartz grains of the fluvial sediments Concha1, Tent5 and Ervi4.

Dose (G)	ESR (a.u.)	d.s.	ESR (a.u.)	d.s.	ESR (a.u.)	d.s.
	Concha1		Tent5		Ervi 4	
0	238.501	13.911	264.59	9.82	198.423	25.462
100	243.307	19.232	300.30	36.25	232.787	34.293
200	279.108	18.928	324.00	17.12	275.289	42.041
400	315.095	34.439	381.55	17.36	306.156	47.133
800	443.356	41.600	416.52	12.83	373.935	41.283
1600	579.855	41.276	635.52	54.72	514.470	75.565
3200	807.186	31.767	888.86	40.23	807.042	106.487
6000	1125.938	98.750	1231.15	72.10	1048.654	138.481
10000			1472.06	64.23	1289.046	102.950
15000	1264.039	150.590	1313.91	62.22	1190.286	322.505
25000	931.912	75.900	1337.88	72.04	954.293	161.560

CHAPTER VI. ESR DATING OF FLUVIAL TERRACES AT THE TEJO RIVER LOWERMOST REACH AND OF MARINE TERRACES AT THE ADJACENT COAST (RASO CAPE AND ESPICHEL CAPE)

This chapter mainly corresponds to a research paper in preparation. Pedro P. Cunha and António A. Martins were involved in the fieldwork. António A. Martins done a new DEM for Espichel Cape. Margarida P. Gouveia performed the ESR dating and sedimentological analyses and interpreted the data with Pedro P. Cunha, António A. Martins and Alberto Gomes. Christophe Falguères, Pierre Voinchet and Jean-Jacques Bahain supervised ESR dating.

VI.1. Introduction

In Atlantic coastal areas undergoing crustal uplift, the fluctuations of sea level during the Quaternary left a record of marine terraces (uplifted beaches), caves and groundwater speleothems developed in coastal caves (e.g., Cabral, 2012; Pedoja et al., 2014, 2018; González-Acebrón et al., 2016; De Gelder et al., 2018; Normand et al., 2018). In the western border of the Iberian Peninsula, only a limited number of research have focused the Plio-Pleistocene record, mainly due to limitations in outcrops/exposures and absolute dating. During the last decade, due to technology advances and availability of new methods, there has been an intensification of studies across interdisciplinary fields, such as geomorphology and paleoenvironmental reconstructions of the Pleistocene of W Iberia (e.g., Pérez-Alberti et al., 2004; Desprat et al., 2006; Cunha et al., 2008, 2015; Martins et al., 2010, 2017).

Representative expression of geology and geomorphology of Portugal is the diversity of coastal environments along its 943 km of coastline (Haws et al., 2011; Figueiredo et al., 2014; Moura et al., 2017). A general framework of the Portuguese marine terraces was established by Teixeira (1979) based on the elevation of the wave-cut platforms that were correlated with marine terraces of the Mediterranean Sea, although located in different geodynamic contexts. Further studies of marine terraces focused on localised sectors were associated with the eustatic control and also inferred controlled by the regional and local tectonics (e.g., Pereira, 1990; Ramos et al., 2012; Figueiredo et al., 2013; Ribeiro, 2019). Nevertheless, only a few studies yield reliable absolute ages. Marine terraces are typically constituted by beach deposits (boulders to coarse sands) and in some cases, with aeolian (medium to very fine sands with paleosols), lagoonal (grey muds) and colluvial facies (heterometric angular clasts of local origin).

In the Iberian Peninsula, the Quaternary period (last 2.58 Ma) is characterised by the final installation of the current river drainage network (e.g., Cunha et al., 2005, 2008; Santisteban and

Schulte, 2006; Viveen et al., 2012a, 2014; López and Heydt, 2014). The mapping of fluvial and coastal terraces, the morphometric analyses of longitudinal river profiles, but also the stratigraphic archive and chronological data have been used to constrain the evolution of fluvial and coastal processes throughout Iberia (e.g., Antón et al., 2012; López Recio et al., 2015; Martins et al., 2017). However, absolute dating by Optically stimulated luminescence (OSL) has only been performed in a limited number of locations and almost solely on the lower terraces (e.g., Pereira, 1990; Cunha et al., 2005, 2012; Martins et al., 2009; Ramos et al., 2012; Figueiredo et al., 2013, 2020). Among other methods, ESR dating could be used to date marine and fluvial sediments in the range 100 ka to 3 Ma (e.g., Rosina et al., 2014; Gouveia et al., 2020; Voinchet et al., 2020).

The study area of present work is located in the western Atlantic coast and also includes the more occidental (and lower) reach of the Lower Tejo River. It provides ESR ages of marine terraces near the Tejo River mouth, in Abano beach (near Raso Cape) and Espichel Cape (Arrábida Chain), as well as in the left flank of the Lower Tejo River, in a section of the reach IV, located ~70 km of the river mouth. This dating will be integrated with previous ages of the studied terrace staircases, to support the correlation between the fluvial and marine terraces of the same basin and evaluate the control by eustasy, tectonics and climate.

VI.2. Geological and geomorphological setting

Portugal mainland is located in the Western Iberian Margin, at the westernmost sector of the Euroasian Plate, close to the boundary with the Nubia plate. Iberian had a complex compressive tectonic evolution during the Cenozoic (Ribeiro et al., 1979, 1990; De Vicente et al., 2011, 2018, 2019; Cunha et al., 2019). It developed the Pyrenees and the Betic orogenic chain (e.g., De Vicente et al., 2011; Martin-Gonzalez and Heredia, 2011). Deformation progressively increased, rising the main topographic elements that exist today inside Iberia and the formation of sedimentary basins (Galve et al., 2019, 2020). In the Pleistocene, the convergence between Nubia and Eurasia changed to a WNW-ESE direction (De Vicente and Vegas, 2009; Cabral et al., 2012).

During the Pliocene, the high sea level is supposed to have reached about 25-60 m above the current level (Dowsett et al., 1996; Miller et al., 2011), being responsible for a marine transgression that reached sites located 24 km from the current western coast of mainland Portugal and developed a large wave-cut platform with marine deposits adjacent to deltaic deposits. The main drainage axes of the deltaic systems were the ancestral of the present rivers systems (Cunha et al., 2008). The uppermost allostratigraphic unit (UBS13) that documents the last episode of sedimentary infilling of the Portuguese sedimentary basins has been considered of latest Zanclean to Gelasian age (~3.7 - 1.8 Ma; Cunha et al., 2012, 2016; Diniz, 2016; Gouveia et al., 2020).

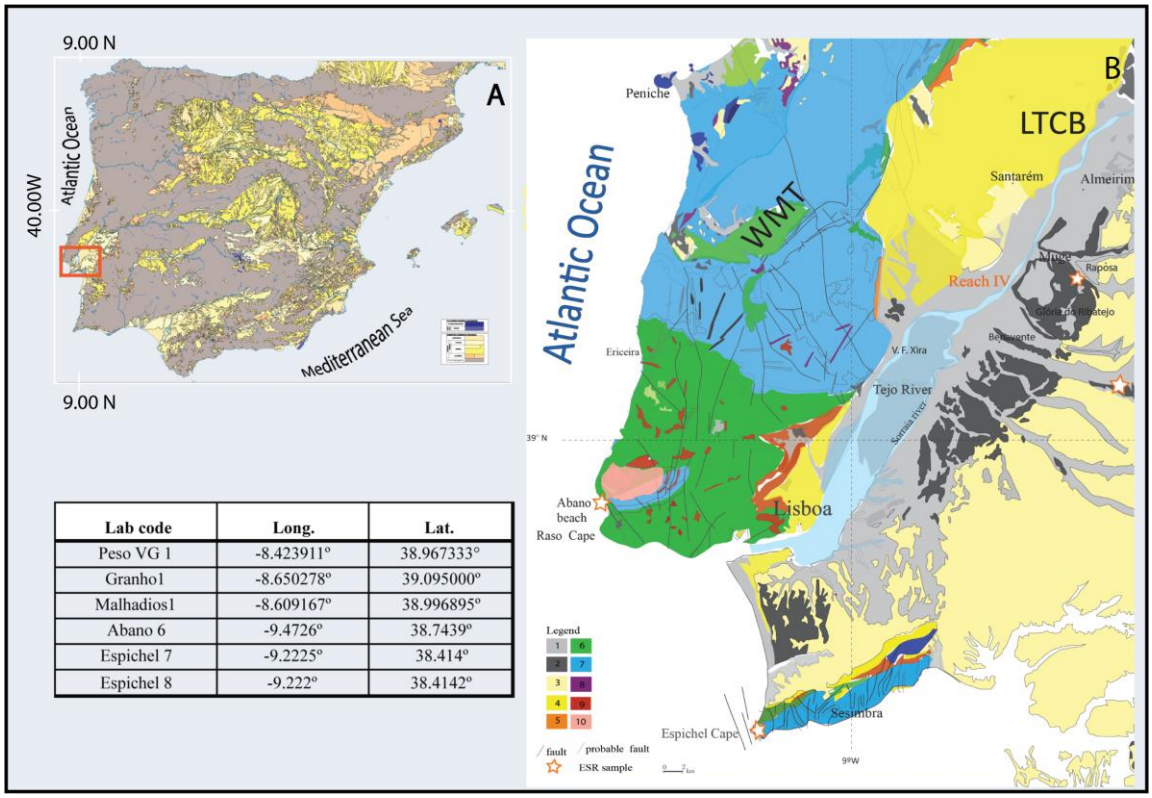

Lab code	Long.	Lat.
Peso VG 1	-8.423911º	38.967333º
Granho1	-8.650278º	39.095000º
Malhadios1	-8.609167º	38.996895º
Abano 6	-9.4726º	38.7439º
Espichel 7	-9.2225º	38.414º
Espichel 8	-9.222º	38.4142º

Figure VI.1. A - Geographical setting of the study area (orange rectangle); B – Geology of the Western Central Portugal (adapted from the Geological map of Portugal 1/500,000, LNEG). Stars indicate the studied sites. Table with geographic coordinates of the ESR samples. Legend: WMT - Western Mesozoic Terrains; LTCB – Lower Tejo Cenozoic Basin. 1 - Holocene, 2 - Pleistocene, 3 - Pliocene, 4 - Miocene, 5 - Palaeogene; 6 - Cretaceous, 7 - Jurassic, 8 - Triassic, 9 - volcanic rocks, 10 - granite.

The next evolution stage was characterised by the predominance of the fluvial incision (e.g., Cunha et al., 2005). Catchments and drainage rearrangements occurred controlled by the long trend of the sea-level drop, lithological anisotropy of the substrate and active tectonics. The eustatic sea-level changes superimposed on the long-term uplift trend of the coast generated coastal and river terrace staircases.

The Lower Tejo Cenozoic Basin (LTCB) is located in the western border of the Iberian Massif, and it is separated from the Mondego Cenozoic Basin by the Central Portuguese Cordillera (CPC). LTCB (Fig.VI.1B) is developed over the Variscan basement (igneous and metamorphic units) and Mesozoic formations. Nowadays, the main faults are the Arrife fault, the Lower Tejo Valley fault and the Arrábida W-E thrust (e.g., Cabral and Ribeiro, 1988; Cabral, 2012).

Tejo River is the longest river of the Iberian Peninsula. It flows westwards from Spain along 1076 km to reach the Atlantic Ocean, in Lisboa.

In the Spanish sector, a sequence of 23 terraces has been identified, stepped between 8 and 195 m a.r.b., where 13 of these belong directly to the Tejo (e.g., Bridgland et al., 2006; Perez-Gonzalez et al., 2008). In the study area, the landscape is dominated by the flatness of the culminant sedimentary unit (UBS13), with altitude decreasing at the east (~ 260 m) to the west (~ 60 m), near the Atlantic coast.

The Lower Tejo River was subdivided into five valley reaches separated by major faults by Cunha et al. (2005b), later characterised (e.g., Martins et al., 2009; Cunha et al., 2017). In reach IV (Fig.VI1B), the Tejo is routed NNE-SSW controlled by the Lower Tejo Valley fault zone. Pleistocene sediments are represented by one extensive staircase of six fluvial terraces (Table VI.1) developed along its valley sides (Martins, 1999), an aeolian cover unit (Carregueira Formation) and colluvium (e.g., Martins et al., 2009). The Holocene sedimentation forms a wide alluvial plain mainly at the Tejo estuary area (Vis et al., 2010). The estuary connects to the Atlantic Ocean by a gorge-oriented E -W.

Adjacent to the Tejo River mouth, two coastal areas can be distinguished: Raso Cape area, at the north, with the UBS13 platform between 100-70 m a.s.l. and a sequence of four marine terraces; and the Espichel Cape area, at the south, with the UBS13 platform at 220-140 m a.s.l. (e.g., Daveau, 1993; Duarte et al., 2004) and a sequence of eight marine terraces (Cunha et al., 2015) (Fig.VI.1B).

VI.3. Previous studies

VI.3.1. The reach IV of the Lower Tejo River

In the Lower Tejo reach IV (between Entroncamento and Vila Franca de Xira towns), previous works focused on the terraces was firstly done by Breuil (1942) and Zbyszewski (1943, 1946) that identified four fluvial terraces based on the altitude of the terrace surfaces. More recent studies have identified up to six fluvial terraces, discontinuously represented along the Lower Tejo valley (T1 is the uppermost and T6 the lowermost; Corral, 1998a, 1998b; Martins, 1998; 1999; Rosina, 2002; Cunha et al., 2008, 2016; Martins, 2009, 2010a, 2010b, 2017). Essential contributions in morphotectonics and OSL dating (quartz-OSL and pIRIR on K-feldspar) of the Tejo River terraces have been achieved (e.g., Martins et al., 2009, 2010; Cunha et al., 2012, 2016, 2017). In the Lower Tejo, the long-term uplift rates were estimated as ~ 0.1-0.2 mm/yr for the last 3 Ma (Cabral, 1995; Cunha et al., 2005, 2008, 2016).

Table VI. 1. Summary of the geomorphological and sedimentological characteristics of the sedimentary terrace units present in reach IV of the Lower Tejo River (adapted from Cunha et al., 2017).

Terrace staircase (Reach IV)	Elevation (a.s.l. and a.r.b.)	Thickness of the associate deposits	Sedimentary characteristics
T1	90 m a.s.l. (+86 m a.r.b.)	5m	reddish gravels (MPS-22 cm)
T2	82-72 m a.s.l. (+74 m a.r.b.)	6-7 m	brown massive clast supported gravels (quartzite and quartz) MPS-17 cm
T3	60-50 m a.s.l. (+52-46 m a.r.b.)	10 m	Gravels with quartzite and quartz MPS- 22 cm
T4	38-20 m a.s.l. (+30-26 m a.r.b.)	23 m	sub-rounded to sub-angular gravels (quartzite and quartz) MPS -20 cm
T5	13-10 m a.s.l. (+3-6 m a.r.b.)	~9-10 m (partially buried)	coarse to fine sands and clays
T6	(-) 4 m a.s.l.	18 m	silty clays and coarse to fine sands

a.s.l. – above sea level; a.r.b. – above riverbed; MPS- maximum clast size

On reach IV, IRSL and pIRIR (k-feldspar) and quartz-OSL ages were obtained for the T4 (~340-155 ka), T5 (136-75 ka) and T6 (62-32 ka) terrace deposits; their genesis was mainly linked with eustatic sea-level changes superimposed on the regional uplift tendency of the continent. Climate may have also influenced the discharge and the sediment characteristic of the terraces (Cunha et al., 2012, 2016; Martins et al., 2010b, 2017). By using ESR dating, ages were obtained for T1 (~903 ka) and T3 (~405-461 ka) (Rosina et al., 2014).

In the upstream part of the reach IV, at Chamusca area, the terrace levels at the east side of the valley are at a higher elevation than the ones presented by the west side, which is explained by the vertical displacement by the Lower Tejo Valley fault zone (Martins et al., 2009; Cunha et al., 2016).

Table VI. 2. Summary of the ages provided by Martins et al. (2009, 2010b) and Rosina et al. (2014), and elevations of each surface for the terrace sequences represented at reaches III and IVa.

	Reaches III and IVa **Gavião- Chamusca**			Reach IVa **VI N. Barquinha and sector IV a**		
Terrace staircase	**Age**	**Elevation (m)**	**Dating method**	**Age**	**Elevation (m)**	**Dating method**
UBS13 Almeirim Form. and Ulme Form.	prob. **3.6-1.8 Ma** Pliocene	142 -210	not dated	prob. **3.6-1.8 Ma** Pliocene	+162	not dated
T1	**~903 Ka** Calabrian?	84- 164	ESR	Calabrian?	+124	not dated
T2	Middle Pleist.?	57-112	not dated	Middle Pleist. ?	+92	not dated
T3 (Pego Terrace)	**~405 - 461 ka** Middle Pleist.	43-73	ESR	**>310 ka** Middle Pleist.	+57	IRSL
T4 (Atalaia Terrace)	**~340 - 155 ka** Middle/ Late Pleist.	26 - 50	IRSL-ESR	**> 190 - 154 ka** Middle/ Late Pleist.	+37	IRSL
T5 (Entroncamento Terrace)	**~125 - 76 ka** Late Pleist.	5 - 28	IRSL-ESR	**125-90 ka** Late Pleist	+16	IRSL
T6 (Azinhaga Terrace)	**~51 - 39 Ka** Late Pleist.	3 - 10	IRSL	**62-30 ka** Late Pleist	+10	IRSL

VI.3.2. The Raso Cape - Abano beach sector

The coastal area adjacent to the Raso Cape has flat topography. There are some limitations in the differentiation of marine terraces by the small thickness of the deposits, the short platform steps, the preservation level, and the existence of an aeolian sands cover unit. Four marine terraces were identified in the Abano beach by Duarte et al. (2014). That cartography was subsequently improved by Cunha et al. (2015), which show morphological continuity from the Abano beach until the Raso Cape area. Different altitudes were also ascribed to each terrace level (Fig.VI. 2).

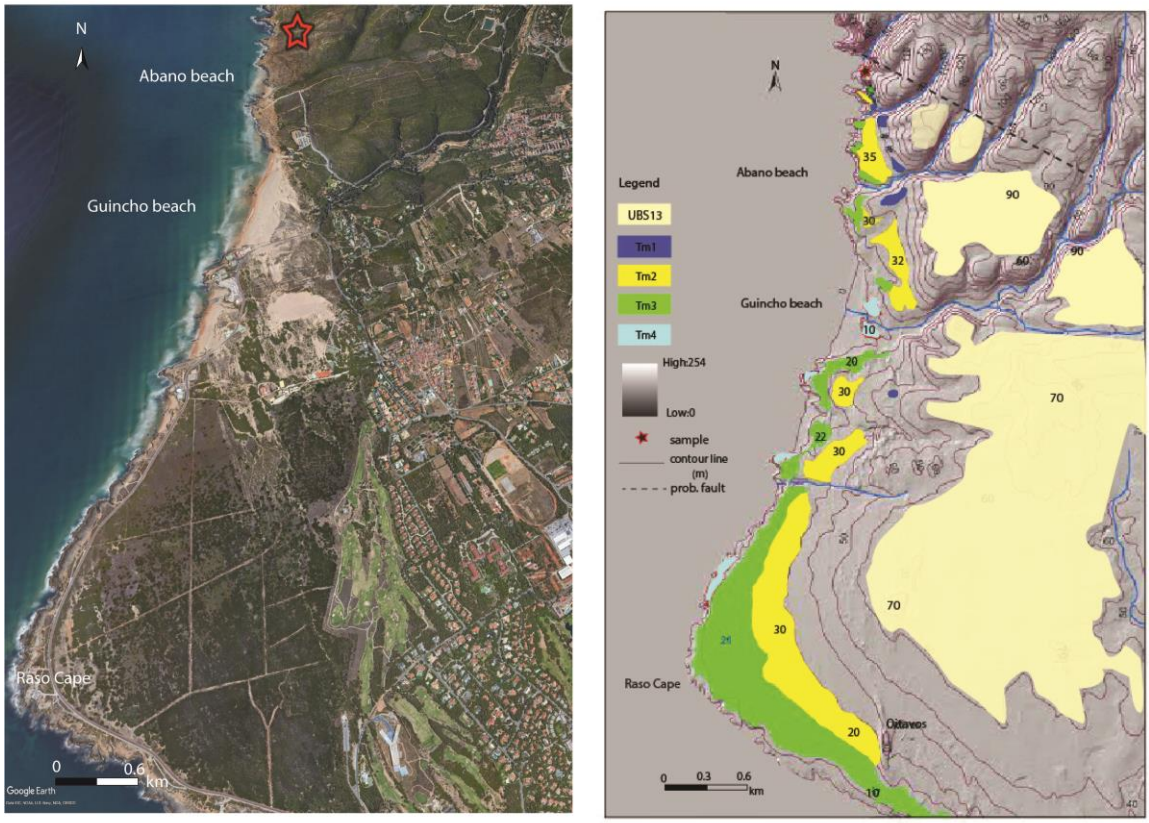

Figure VI. 2. A. Coastal area overview between Abano beach and Raso Cape (Source: Google Earth Pro, October 15, 2020) B. Geomorphological map of the Abano beach and Raso Cape, with identification of several wave-cut platforms (adapted from Cunha et al., 2015).

Immediately below a broader wave-cut platform (at 100 m to 70 m a.s.l.), four wave-cut platforms are preserved, described as Tm1 (uppermost) to Tm4 (lowermost) between 40 m and 4 m a.s.l., respectively (Fig.VI. 2). The best-preserved terraces are the Tm2 and Tm3. The beach sediments of the terrace Tm2 appear in more significant extension to the north of Abano beach, which allowed the identification of this terrace at ~34 m a.s.l. (inner edge). At the south of Abano beach, the wave-cut platform of this terrace is covered by beach siliciclastic pebbles and coarse sands. The Tm3 is mostly a wave-cut platform, without sediments.

The Tm4 is preserved at 9-10 m elevation, from the Guincho beach until the Raso Cape area, but was probably eroded at the north of Guincho beach and is devoid of marine deposits. To the south of the Guincho beach, the Tm4 platform is very evident, cutting the limestone layers and forming a soft slope toward the sea.

Some sectors are flatter, which do not allow a fair recognition of the marine terrace staircase, overlaid by aeolianites and aeolian sands (Cunha et al., 2015). At the Oitavos site, the following aeolianite succession was identified: a basal unit of medium aeolian sands at 32 m a.s.l., with horizontal lamination and rich in muscovite, dated by quartz-OSL as 97 ka (Prudencio et al., 2007).

The age obtained for the middle unit, 1 m thick, containing *Helix shells* and organic matter was 30 ka (C^{14} in Monge Soares et al., 2006). The upper unit, c. 10 m thick, of cemented coarse sands with steep dune foresets was dated by radiocarbon and quartz-OSL and gave ages of 15 to 12 ka (Prudêncio et al., 2007).

VI.3.2. The Espichel Cape sector

The Espichel Cape has a sizeable wave-cut platform with elevations between 220 m to 140 m along the coast (Fonseca et al., 2015), located at the western sector of the Arrábida Chain, reaching the ocean by an almost vertical sea cliff. The Arrábida Chain contains an almost complete sedimentary sequence from the Lower Jurassic to the Pliocene and is one of the best structural examples of the Alpine orogeny in Portugal (Ribeiro et al., 1990; Fonseca et al., 2015; Kullberg and Kullberg, 2017). Tectonic structures limit the chain: at east, the Setúbal - Pinhal Novo Fault (SPNF) (Moniz, 2010); at the south, by the Arrábida W-E thrust; and to the north, by the Lagoa de Albufeira syncline (Fonseca et al., 2020).

During the Pliocene and early Pleistocene, the ancestral Tejo River reached the Atlantic Ocean by the Setúbal Peninsula. In the Pleistocene, active tectonics affected the Cape Espichel wave-cut platform (Daveau and Azevedo, 1981; Moniz, 2010).

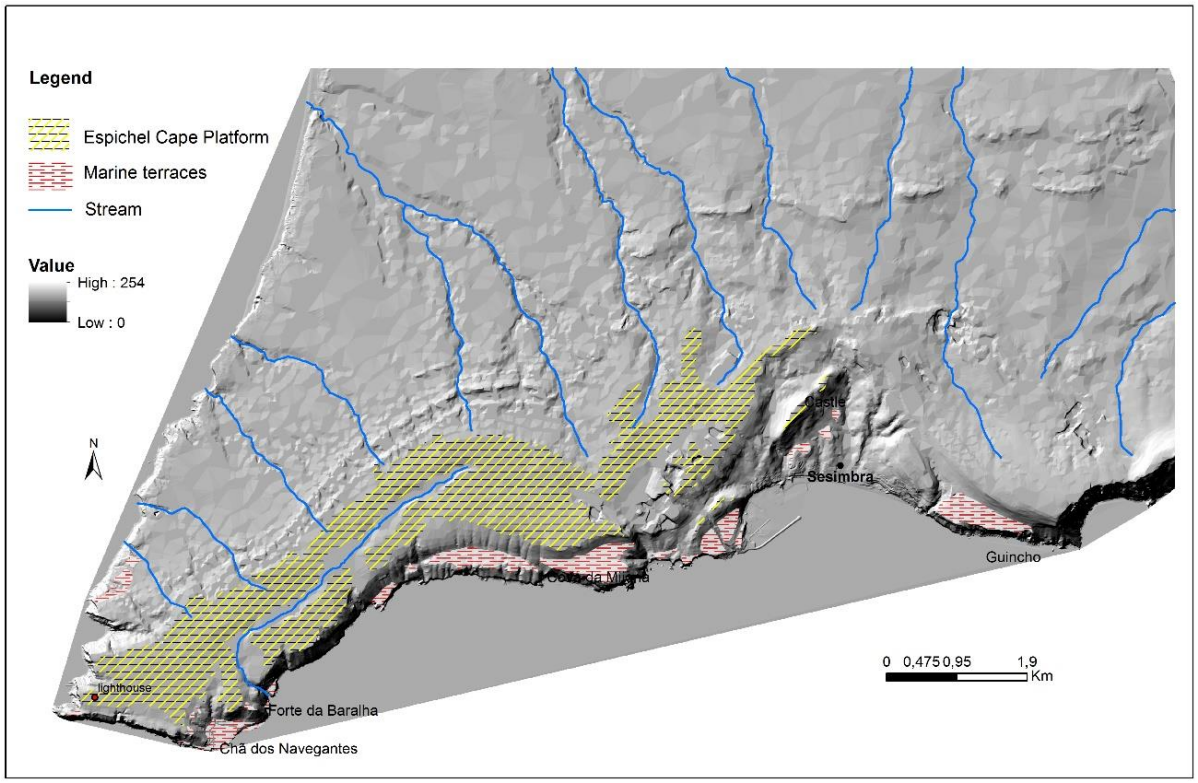

Figure VI. 3. Simplified geomorphologic map of the Espichel Cape - Sesimbra area (Cunha et al., 2015).

During the Pliocene and Pleistocene, high sea-levels produced the Espichel Cape platform and eight marine terraces (Cunha et al., 2015), at different altitudes above the present-day sea-level (Fig.VI.3), expressing the sea-level fluctuations under a context of uplift. At southern and western sectors of the promontory, the terrace staircases comprise levels that are mainly represented by cemented beach sands. The altitude of the terrace levels is different for the two sectors of the promontory, indicating differential uplift.

Further research was done in the surroundings, as in: Lagosteiros beach (with three marine terraces identified); Sta. Margarida and Figueira Brava caves and in Forte da Baralha (Fig. V1.3). Zbyszewsky and Breuil (1945) studied the fossils present in the caves and identified the marine terraces at 12-15 m and 5-8 m a.s.l. At Forte da Baralha, wave-cut platforms with beach sands at 7-8 m and 10-11 m a.s.l. were recognised by Pereira and Regnauld (1994). At the level of 10-11 m, several shells were dated by C14 in a carbonate conglomeratic beach deposit, but without reliable age results (Pereira et al., 2007). In the submerged area, two more levels were identified, one at -20 m and the other at -7 m evidenced by rocky levels, with local cliffs with notch and deposits (Pereira et al., 2020).

VI.4. Materials and Methods

VI.4.1. Fieldwork

Local detailed investigations, as stratigraphic and sedimentological characterisation of the deposits and sampling, were done in several field campaigns conducted between 2011 and 2019. GPS measurements and data collection for the generation of a high-resolution digital elevation model (DEM) were done during February 2019. ESR dating methodology was applied during 2018 / 2019 on MNHN, in Paris.

Fieldwork included the characterisation of the sedimentary deposits studied, as sediment colour, granulometry, texture, fossil content and clast lithology (Fig.VI.5). For ESR dating, after cleaning of each field section, fluvial sediment samples of around 1 kg were sampled in an opaque tube to prevent light exposure and loss of sediment. In the Abano beach section, the samples were collected in stratigraphy from the same terrace (base at 34 m and top at 38 m a.s.l.) at ~1 m distance and identified as Abano-5, 6, 7 and 8, respectively. The Abano-6 sample was selected to obtain numerical ages applying ESR into optically bleached quartz grains (Fig.VI.7). On the western sector of the Espichel Cape, the terrace staircase was surveyed (Tm1 to Tm 8, between 108 m and 10 m a.s.l., respectively). Tm5 (inner edge at 53 m) and Tm6 (inner edge at 30 m) were sampled for ESR dating, granulometry and textural composition, with sample codes Espi-8 and Espi-7, respectively.

The cemented marine deposits were removed using a sledgehammer. The Espichel samples are 50-50 cm blocks, from which the core was extracted under red light, according to the standard conditions for this absolute dating method.

VI.4.2. Geomorphological mapping

Geomorphological mapping was undertaken with field mapping on to topographical (1/25.000; 1/10.000) and geological (1/50.000) base maps, but also by the generation of a high-resolution digital elevation model (DEM) based upon LIDAR surveys (with ~30 cm of mean vertical resolution) and elevation points of 1/10.000 municipal topographic databases (Fig.VI.3). Elevations of the marine terraces were determined with real-time kinematics GNSS system for a very high accurate measurement in a centimetre level. The absolute location of the base station was measured by GNSS RTK rover.

VI.4.3. Grain-size measurements and mineral composition

Grain-size analyses for the fraction > 63 μm were carried out by sieving with a sieve tour with ½ Φ increments of sediment samples in Sedimentology Laboratory of the Department of Earth Sciences - University of Coimbra. Analyses of sediment mineral composition were based on binocular microscope observation (50x) and X-ray powder diffraction using an Analytical Aeris XRD diffractometer manufactured by Panalytical, with a Cu tube in a 2θ range, at a scanning rate of 30 min-1, 40 kV and 15 nA (Department of Earth Sciences of the University of Coimbra). The mineralogical composition in non-oriented subsamples was obtained using the analytical software Highscore plus, provided with the instrument. According to the standardised Panalytical backloading system, the subsamples were prepared, which provides a nearly random distribution of the particles.

VI.4.4. ESR dating of optically bleached quartz grains

This absolute dating method is based on the storage of electrical charges in crystal lattice defects in minerals (e.g. quartz) as a natural radioactivity function. The number of electrical charges detected by ESR is directly proportional to the length of time when the material was last exposed to sunlight. As the ESR signals have dose-response to several kGy and quite good thermal stabilities, the method has potential to date materials in the age range from several thousand years to more than 2.5 Ma (Voinchet et al., 2004; Voinchet et al., 2010).

The age calculation implies the determination of two main parameters: the total dose (TD), also referred to as the paleodose or equivalent dose (D_e), and the dose rate (D_a) which is an estimation of the mean dose annually absorbed by the sample, based on the equation:

$$TD = \int 0 T d_a(t).\, dt \quad (17)$$

where TD is the equivalent dose of radiations received by the sample over time, da is the annual dose rate of natural radiations and t the age of the sample.

The total dose TD is proportional to the trapped electrons concentration in the sample and so to the ESR signal intensity.

Some paramagnetic centres can usually be observed by ESR spectroscopy in quartz, but Aluminium (Al) and Titanium centres (Ti) have the best potential to date Quaternary fluvial sediments (Tissoux et al., 2007) being useful combining multiple centre approach since they provide independent dose control (Toyoda et al., 2000; Rink et al., 2007; Tissoux et al., 2007; Duval and Guilarte, 2015). The Al centre signal has a long-life expectancy due to thermal stability exceeding six million years (Toyoda and Ikea, 1991) being used for ESR dating of Lower Pleistocene materials (Gouveia et al., 2020). Ti centre usually decreases at high dose values, called “radiation bleaching” (Euler and Kahan, 1987) commonly being used for dating more recent sediments (e.g., Late and Middle Pleistocene) (Tissoux et al., 2007).

VI.4.4.1. Preparation of sediment samples

Under darkroom conditions, the sediment samples were wet sieved to separate different grain sizes (< 63 um, 63-180 um, 180-250 um, 250-300 um, and >300 mm), following Voinchet et al. (2007). The 180–250 μm fraction was selected. Quartz was then separated using a chemical and physical protocol already detailed in the literature (Yokoyama et al., 1985; Laurent et al., 1994; Voinchet, 2003).

This protocol first consists in a series of acid attacks: HCl (10%) for 2 hours to remove carbonates, HF during 1hour to remove feldspars, HCl for 2 hours to remove fluorides and H2O2 (10%) treatments to remove organic matter. After that, heavy minerals and K-feldspar fraction were removed using a heavy liquid solution of sodium polytungstate (r= 2.72 g/cm3 and r =2.58 g/cm3, respectively) (Fig.II.28A).

After being placed in the oven at 45ºC for drying, the fraction was ready to be packaged in an opaque tube, with adequately labelled aluminium foil. The quartz fraction was treated with 40 % HF for 40 min to remove the remaining feldspars and clean the grains. After etching, the fraction was treated with HCl (10 %) to dissolve any remaining fluorides. The last step is magnetic separation to eliminate the previous minerals "parasites" (Fig. II.29). After this treatment, the sample was split in several aliquots used for the residual dose and total dose determinations.

VI.4.4.2. ESR measurements

The multi-aliquot additive dose procedure was employed for De determination.

Ten of twelve aliquots with quartz grains were irradiated with a calibrated 137Cs Gammacell-1000 gamma source (dose rate= 200 Gy/h) at different doses ranging from 100 to 25.000 Gy, carried out at CENIEH (Burgos, Spain). After irradiation, each series of 12 aliquots was measured by ESR at low-temperature cavity (ca. 107-109 K) using a Bruker EMX spectrometer at MNHN. One aliquot was kept as a natural reference, and one aliquot was illuminated for 1000 h in a Dr Honhle SOL2 solar simulator to determine the unbleachable part of the ESR-Al signal (Voinchet et al., 2003). The intensity of Al signal was evaluated from peak-to-peak amplitude measurements between the top of the first peak (g=2.0185) to the bottom of the 16th peak (g=2.002) of its hyperfine structure (Toyoda and Falguères, 2003). The angular dependence of the ESR signal was taken into account, measuring each aliquot three times after a 120º rotation of its initial position in the cavity. This protocol was repeated 2 to 4 times over distinct days to check the reproducibility of the Al signal. The ESR intensity for Ti −Li centre was measured from peak to baseline amplitude around g=1.913-1.915 (option D) according to Duval and Guilarte (2015). Both Al and Ti signals have been acquired in a single spectrum with baseline correction (quadratic function). Ti−Li centre showed a complete resetting of the ESR signal after the artificial bleaching and good dose-response to irradiation. As a result, for fluvial and marine quartz samples studied were obtained for each measured signal nine and six intensities values, respectively.

The equivalent dose (De) was determined by subtracting the residual intensity evaluated through the maximum bleaching value from the total dose. De was obtained by an exponential +linear fitting (EXP+LIN) function and with a single saturating exponential function (SSE) (see details in Voinchet et al., 2013) using the Microcal Origin Pro 8.1 software and weighted by the inverse of the squared ESR intensities 1/I2 (Yokoyama et al., 1985). The goodness-of-fit is assessed through the adjusted r-square (r2) value, which accounts for the degree of freedom of the system.

For the dose rate calculation, radioelements contents (U, Th and daughters, and K) were determined by a high-resolution low-background gamma-ray spectrometry to derive external alpha and beta dose rate components using the dose-rate conversion factors from Guérin et al. (2012). Therefore, the grain thickness removed after HF etching was assumed to be 20 μm and the external alpha contribution was considered negligible (α radiation is not considered because it is restricted to the outermost part of the sample). Values were corrected for β attenuation of spherical grains (Brennan et al., 1991; Brennan, 2003). Water content was measured by the difference in mass between the natural sample and the same sample dried for 1 week in one oven and the water attenuation was based on Grün (1994). The cosmic dose rate was determined according to Prescott and Hutton (1994), based on altitude, latitude and longitude of each section.

VI.5. Results

VI.5.1. Geomorphological and sedimentological characterisation of the studied Lower Tejo T1 and T3 terraces

During the Pleistocene, a staircase of six river terraces (T1 to T6 from the upper to the lower) was developed in the LTCB. In this study area, the T6 is buried by Holocene fluvial plain deposits (Fig.VI.4). Lithostratigraphy of the terraces was described by Cunha et al. (2017). In the present study, additional data were collected in the T1 and T3 fluvial terraces.

In the study area, UBS13 is preserved in small patches, in the Serra de Almeirim hill, at 168 m a.s.l. (+158 m a.r.b.) and in small patches to NE of the map (Fig.VI.5). The conglomeratic facies of this unit are about 20-25 m thick in the study area, passing to sandy facies (Ulme sandstones) to the S and SW. The Ulme sandstones unit was partially eroded during the formation of the first terrace of Tejo River (T1), with an altitude of 90 m (+86 m a.r.b.) at Glória do Ribatejo area (Fig.VI.6).

Terrace T1 is composed by reddish gravels near Muge stream and Glória do Ribatejo, where it remains form plateaus standing between 93 and 72 m a.s.l. (+89-68 m a.r.b.). In the sampled site (Peso VG1), the deposit consists of a sand unit at the base with ~3 m thickness and gravels above (Fig.VI.4A, B). This deposit, with a brown colour (5YR/8), has gravel clasts of quartzite and quartz, gravelly coarse sand and a sandy to a clayish matrix.

Terrace T2, at 65-56 m a.s.l (+59-50 a.r.b.), is well preserved mainly on the south side of the Muge stream, being ~ 10 m thick.

T3 terrace is one of the best-preserved terraces of the area (Fig. 4A), being at 47-44 m a.s.l (+41-38 m a.r.b.), in Granho-1 (south of Muge stream) and at 57 m a.s.l (+ 51 m a.r.b.), in the north side of the stream. The T3 terrace is ~ 15 m thick in the outcrops of Malhadios and little less in the Granho. With dull orange colour (7.5 YR/4, dry sediments), the outcrops are mainly composed by clast supported gravels (lithofacies Gp) that display horizontal bedding, with small channel geometries and lenses of massive sand bars with Sc and Sm lithofacies. The gravels are composed by quartzite and quartz cobbles and pebbles (Fig.VI.4C) and have a maximum size of 15 cm. The Malhadios-1 sample was collected in the outcrop located in the north side of the Muge stream, in a sandy channel layer at the middle of the terrace, between two gravelly layers. The Granho-1 sample was collected at the opposite side of the stream at the top of the terrace (Fig.VI.4 E).

Figure VI. 4. A. The Peso VG1 outcrop (T1 terrace). B. Tube extracted from Peso VG1 for absolute dating methods; C. Granho-1 outcrop (T3 terrace); D - E. The Malhadios exposure and location of the sampling (collected near the T3 terrace base).

T4 terrace rises from +23 to 26 m a.s.l. (17-20 m a.r.b.) with the maximum thickness of ~ 23 m near Muge.

The T5 terrace is at 10-12 m a.s.l. (+4-6 m a.r.b.). Downstream of Muge the terrace is almost buried by modern alluvium. However, terrace treads are preserved along the Muge stream, mainly in the right margin (Fig.VI.5).

According to Cunha et al. (2017), the T6 should be present at -4 m a.s.l. being ~18 m thick.

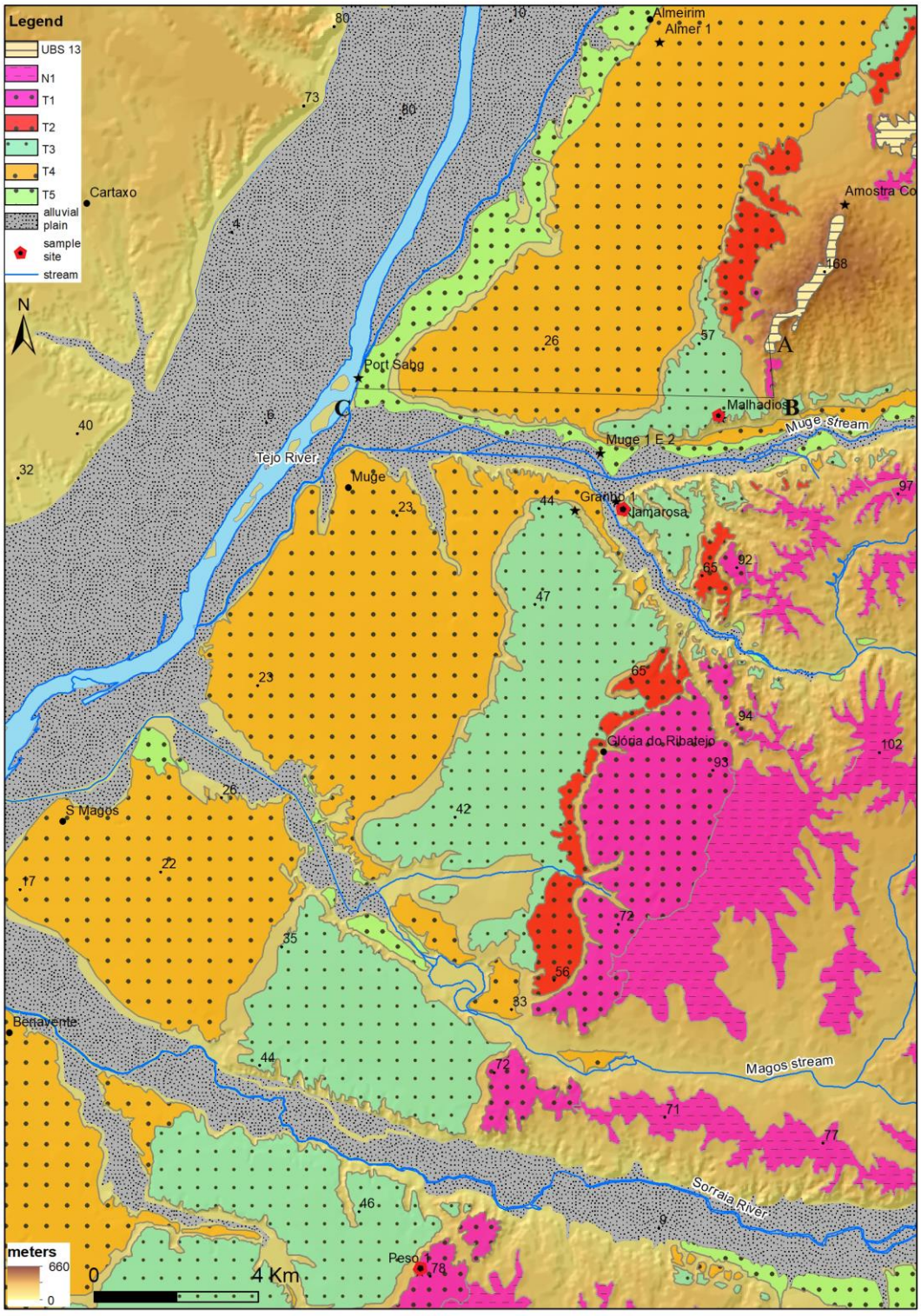

FigureVI. 5. Geomorphological map of the area between Muge and Almeirim, in the reach IV of LTCB.

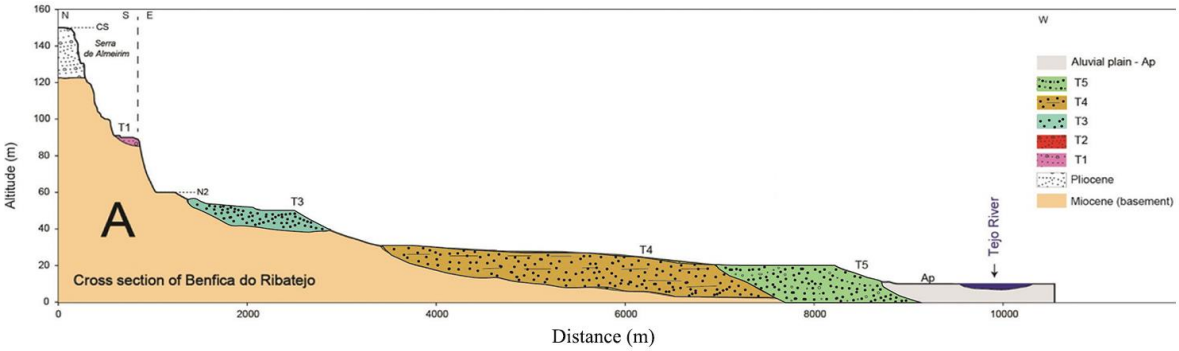

Figure VI. 6. Geomorphological profile of left reach of Tejo River in the vicinity of Muge (modified from Martins et al., 2017).

VI.5.2. Geomorphological and sedimentological characterisation of the studied marine terraces

VI.5.2.1. Cape Raso - Abano beach marine terraces

Four marine terraces have been mapped between the Abano beach, at the north, and the Raso Cape area, named Tm1 to Tm4, from the upper to the lower. Marine terraces are best preserved in the southern sector of the area, except the Tm1 terrace.

Tm1 is at 42-38 m a.s.l. in the Abano beach site. Round boulders are scattered along the slope at this altitude.

Tm2 is between 34-37 m a.s.l. in the northern part of the map (Fig.VI.7A), but only 25-30 m a.s.l. at the southern sector, in the Raso Cape area.

Tm3 is well represented by flattened surface carved in the limestone substrate between the Guincho beach at 22 m a.s.l. and the Raso Cape at 20 m (Fig. VI.2).

Tm4 is represented by small patches along the coast at 10-9 m a.s.l. between Guincho beach and the Raso Cape. This terrace has no morphological expression to the north of the Guincho beach, where it was probably eroded (Fig. VI.7).

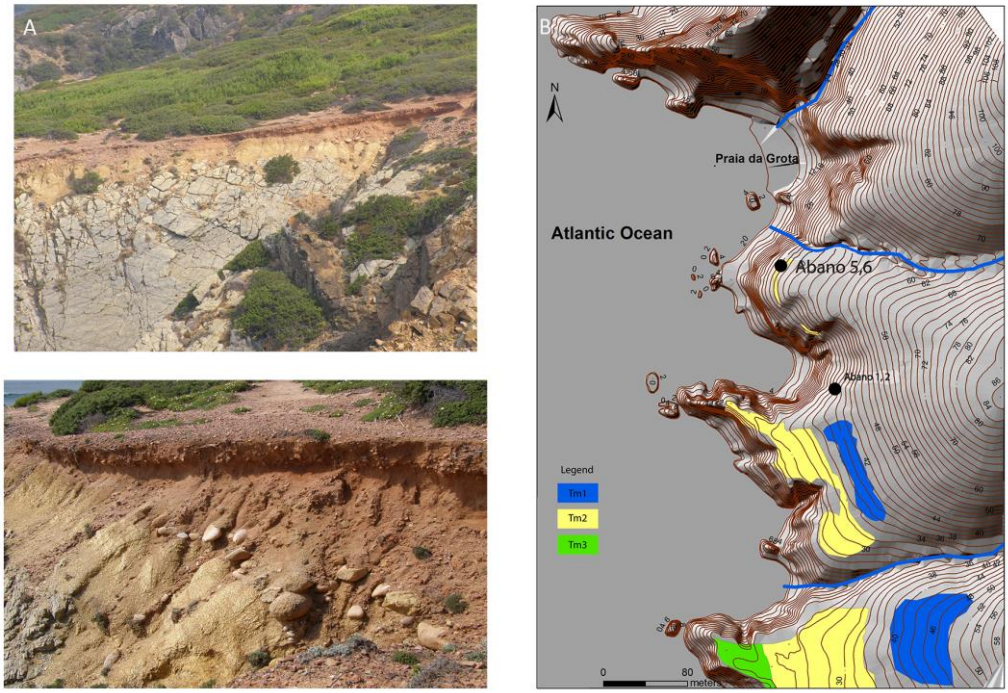

Figure VI. 7. A. Photos of the Abano beach area. B. Geomorphological map (1/40.000) with the location of the dated sample.

The Tm2 is the only one with sediment thickness available for ESR dating. The other terraces are rocky platforms without deposits. The sedimentary sequence of the Tm2 comprises lower gravels with rolled boulders and pebbles at the base, white coarse to medium sands in the middle part and colluviums at the top (Fig. VI.8). The sample Abano-6 was collected from the coarse to medium sands of the middle part of the terrace (Fig. VI.9). The sample Abano-6 has an orange colour (7.5YR 5/6); the mean grain size is dominated by coarse to medium sand (0.5 mm). The grain-size curve of relative frequency is almost symmetric, dominated by medium to coarse grain sand (Fig. VI.8). The average grain-size fractions consist of sand (97.8%), 1.8% silt and 0.4% clay; the sediment is fine skewed (0.6), mesokurtic (2.64) and very poorly sorted (2.62). The sand fraction is composed by hyaline quartz (80%), feldspars (15%) and some dark minerals. The quartz grains are rounded to sub-rounded.

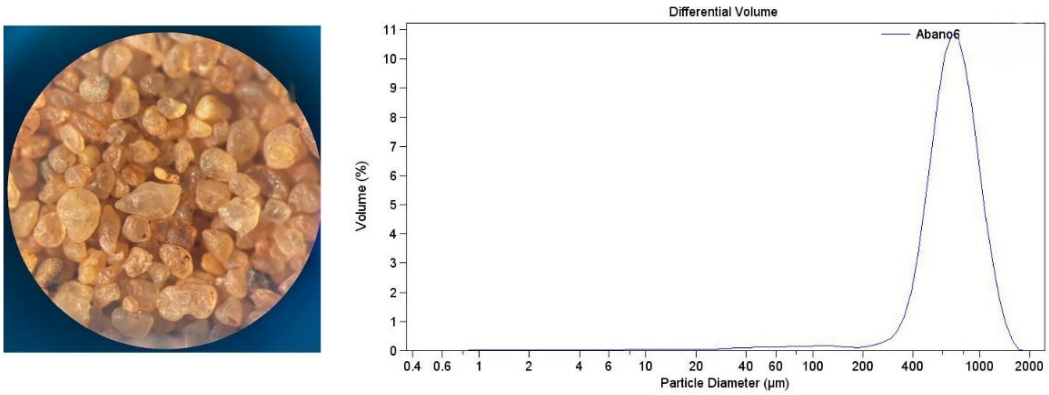

Figure VI.8. Compositional and morphoscopic observation of the sample Abano-6, with a binocular microscope (50x). Grain size distribution of Abano-6 (total sample), by laser granulometry.

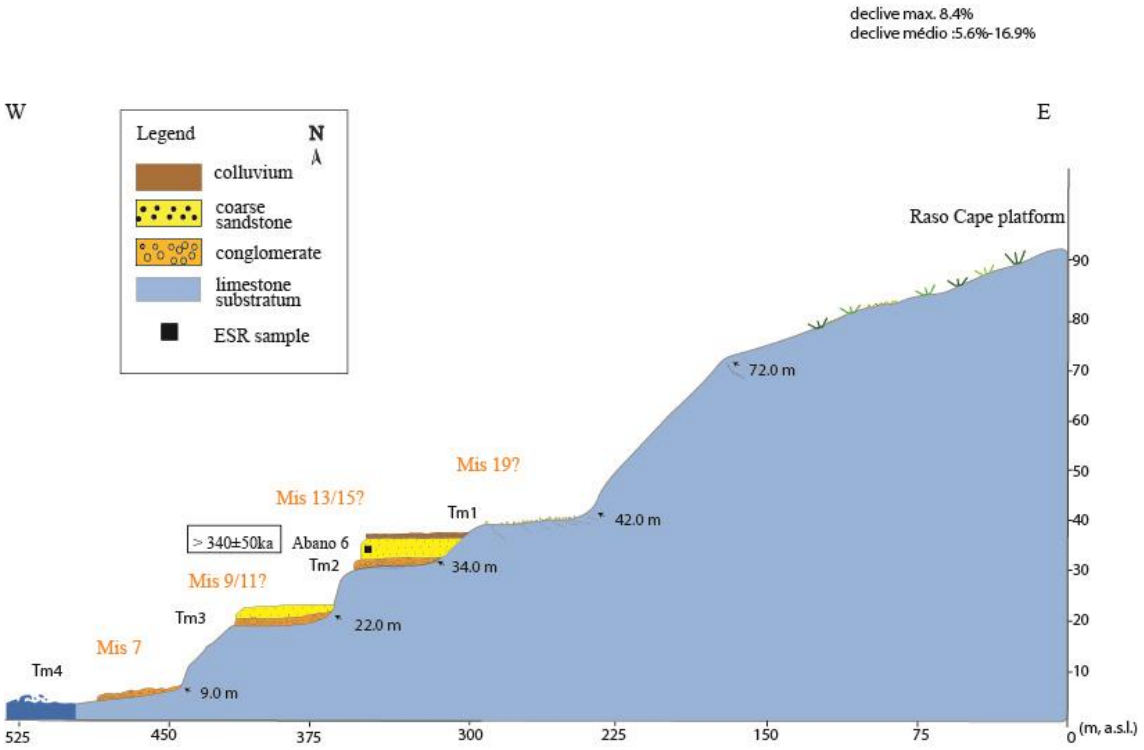

Figure VI. 9. Schematic section of the marine staircase in Abano beach (N of the Raso Cape).

VI.5.2.2. Espichel Cape marine terraces

In the Espichel Cape, bellow the large Espichel Cape platform, a total of nine marine terraces can be identified (Fig. VI.10, VI.11). At the Praia dos Navegantes, the terrace staircase is also documented in the south reach of the promontory. At the W reach of the promontory the different terrace levels are less developed, however, cemented beach sands with shell fragments and gravels, represented by cross-stratified facies at different altitudes, are available for dating and can be summarised as follows:

The Espichel Cape platform, at 137-140 m, probably vertically displaced by a fault (Fig. VI11), to 118-120 m a.s.l.; locally shows a cover of cemented coarse sands, ~ 1 m thick.

Tm1 is represented by a small abrasion platform at 108 m a.s.l.

Tm2 has an abrasion platform at 83 m a.s.l., covered by ~ 6 m of cemented marine gravels at the base and very coarse sand at the top (surface at ~ 89 m a.s.l).

Tm3 has an abrasion platform at 73 m a.s.l., covered by ~ 5 m of cemented marine gravels at the base, followed by very coarse sandstones and colluvial deposits at the top.

Tm4 has an abrasion platform at 65 m a.s.l.; it comprises a basal conglomerate followed by sandstones and a thin layer of cemented colluvial deposits at the top (~ 7 m thick; top surface at ~ 72 m a.s.l).

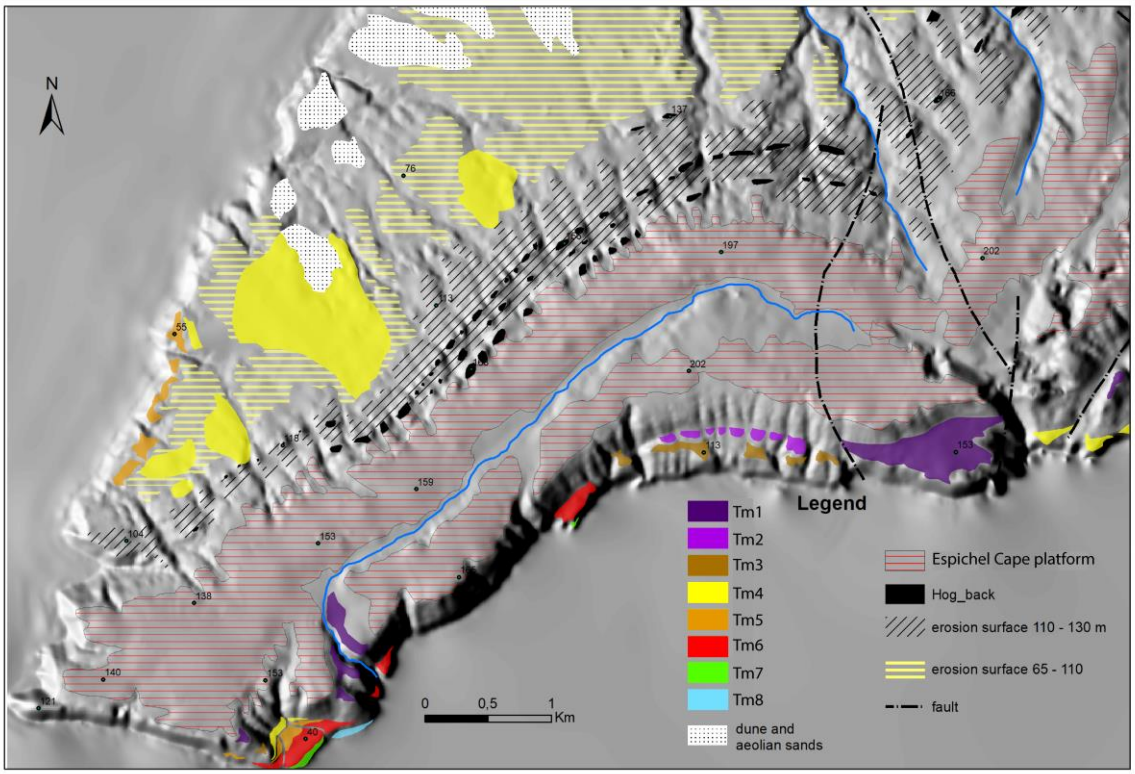

Figure VI. 10. Detailed Geomorphological map at the Espichel Cape area. (1/50.000) with marine terraces identified.

Tm5 has an abrasion platform at 53 m a.s.l.; it comprises a basal conglomerate followed by very coarse sandstones and a thick layer (~5 m) of cemented colluvial deposits at the top (~ 4 m thick; top surface at ~ 57 m a.s.l). The sample Espi-8 (56 m a.s.l.) was collected from the middle-upper part of the Tm5.

Tm6 has an abrasion platform at 30.5 m a.s.l.; it comprises a thick basal boulder conglomerate with lenses of sandstone and a layer of cemented colluvial deposits at the top (~ 10 m thick). Sample Espi-7 was collected from a lense of sandstone (at ~ 36 m a.s.l.).

Tm7 is represented by a small abrasion platform at 16-20 m a.s.l.

Tm8 is represented by a small abrasion platform at 10-12 m a.s.l.

Tm9 platform is not recognised in the field at the study site due to the existence of a vertical cliff but along the SW sector of the Espichel Cape. This marine platform is recognised at ~8 m a.s.l., between the Forte da Baralha and Sta. Margarida and Figueira Brava caves (Fig.VI.11).

In the submerged area, the level identified by Regnault et al. (1995), at -7 m, is evidenced by rocky levels with local cliffs with notch and deposits (Fig VI.12).

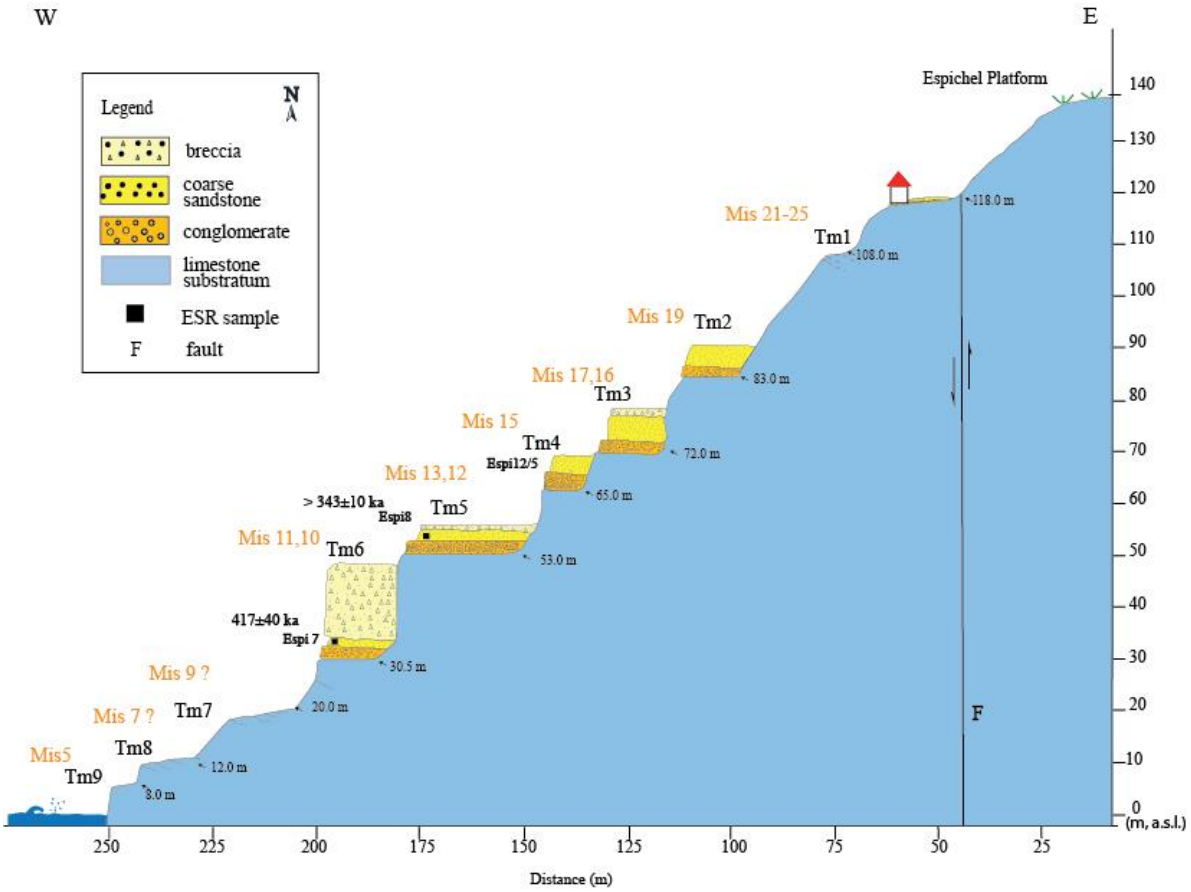

Figure VI. 11. Schematic section of the marine staircase in the western sector of the Espichel Cape.

Figure VI. 12. Interpreted image of the Espichel Cape with Tm9 terrace above the modern counterpart and elevates ~8 m a.s.l. (adapted from the original photo made by Carlos Sargedas).

The sample Espi-8 (Tm5) has a dull orange colour (7.5YR 7/4) and calcium carbonate cement. The sand fraction (Fig.VI.12) is composed by quartz hyaline (80%), feldspars (orthoclase and albite) (15%), granite (5%) and some dark minerals (Fig.VI.13).

The quartz grains are angular to sub-rounded, with medium sphericity. The mean grain size of > 63 μm fraction is dominated by coarse sand (0.59 mm) with the median and mode with the same value (0.50 mm). The grain-size fractions consist of sand (98%) and some gravels (2%). The sediment is unimodal (0.50mm), leptokurtic (4.46), moderately sorted (1.03) and with fine skewness (0.84). The mineral composition of the sand fraction is composed of quartz and some feldspars (microcline and orthoclase), (Fig. VI.14). Observation of the 180-250 μm fraction of the sample indicated that some quartz grains have a cover of manganese oxides (Fig.VI.15).

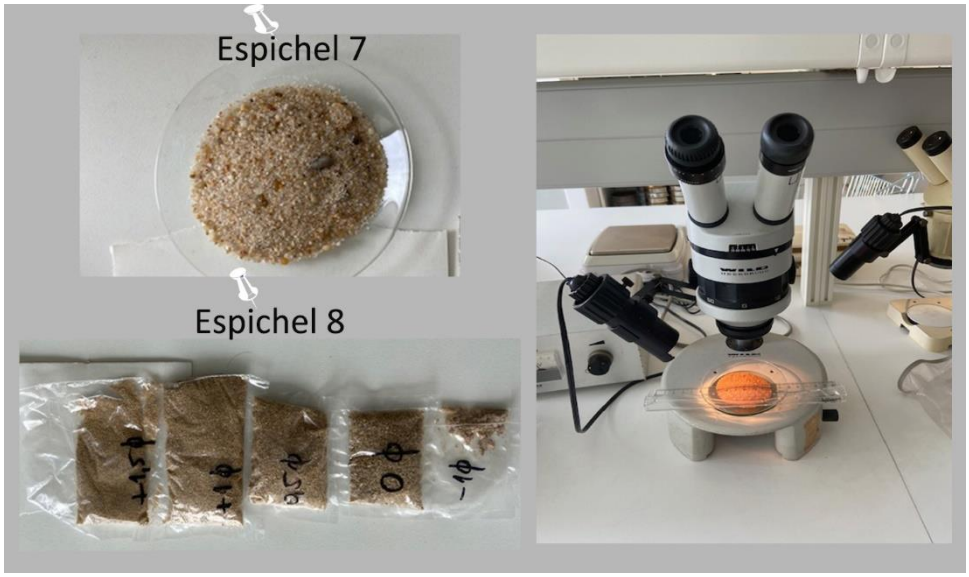

Figure VI. 13. Compositional and morphoscopic analysis of the samples Espi-7 and Espi-8, with a binocular microscope (50x).

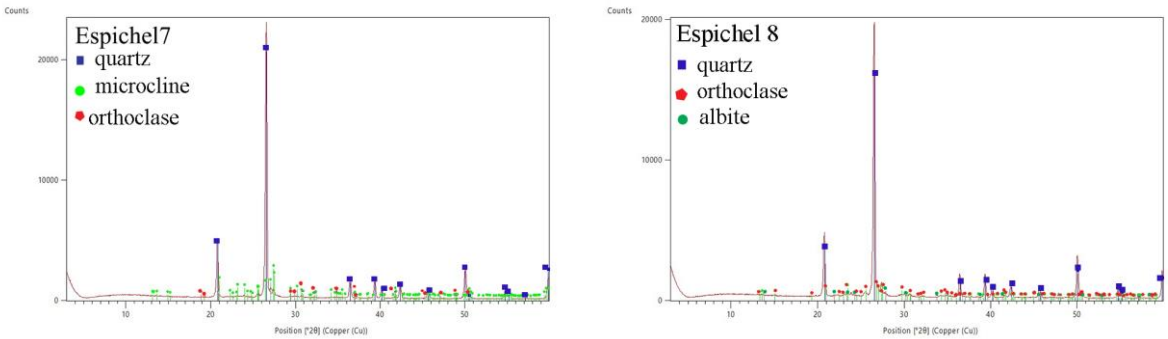

Figure VI. 14. Mineral composition of the sand samples studied from the Espichel Cape marine terraces.

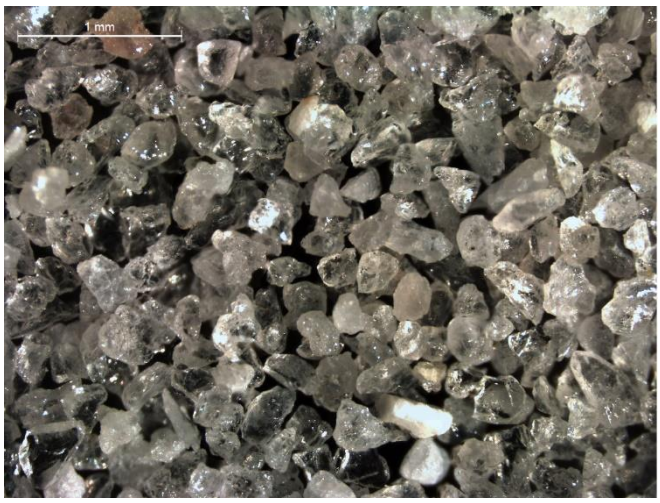

Figure VI. 15. Photomicrograph of the sample Espi-8, in the 250-180 µm grain fraction.

The sample Espi-7 is composed of medium pebbly sand, with light grey colour (7.5YR 8/3) and carbonate cement. The quartz grains are subangular. The sands mean grain size (> 63 μm fraction) is dominated by coarse sand (0.67 mm), with the median and mode with almost the same value (0.55 mm). The grain-size fractions consist of sand (98.3 %) and gravel (1.7 %). The sediment is moderately sorted (0.9), leptokurtic (3.86) and fine skewed (0.7). The sand fraction comprises quartz (hyaline, milky and dark) (80%), feldspars (orthoclase and microcline) (15 %), tourmaline (5%) and some dark minerals (5%) (Fig.VI.14).

V.6. ESR results

The Al centre could be measured in all the samples (Tables VI. 3, 4, Fig. VI.17). Similarly, the Ti-Li centre was measured for all samples, except for Espi-8. For this sample, the signal intensity was too different in each measure to be reliable evaluated, even with two scans. It was not the case for the sample Espi-7, for which the use of multi-centre approach was possible. Bleaching mean values are between 40 and 67% (Table VI.9).

Table VI. 3. ESR medium data collected from the measurements of Al centre of the quartz grains of the fluvial sediments Malhadios1, Granho1, (irradiation data 2018).

Dose (G)	ESR (a.u.) Malhadios1	d.s.	ESR (a.u.) Granho1	d.s.
0	207.839	8.604	187.769	17.36139
150	243.596	4.592	232.611	16.32035
300	271.093	19.055	296.720	12.0839
600	326.097	25.328	333.663	23.2837
1200	411.298	12.121	446.194	28.8704
2400	568.801	39.325	595.224	28.0006
4000	690.363	31.375	849.438	50.8287
6000	881.098	47.519	1030.972	33.8177
8000	962.155	13.511	1212.499	56.1074
12500	1189.836	30.647	1402.072	64.2183
20000	1640.702	29.613	2134.459	75.0523

Table VI. 4. ESR medium data collected from the measurements of Ti-Li centre of the quartz grains of the sediments Peso Vg, Espi-7, Espi-8 and Abano-6 (irradiation data: 2019).

Dose (G)	ESR (a.u.) Malhadios1	d.s.	ESR (a.u.) Granho1	d.s.
0	423.883	7.626		
			371.318	39.896
150	488.961	22.507		
			483.072	35.144
300	563.285	26.305		
			698.991	58.440
600	672.007	54.584		
			808.239	41.327
1200	876.954	70.120		
			1011.009	36.164
2400	1158.653	58.076		
			1379.469	196.771
4000	1456.968	29.380		
			2234.670	64.035
6000	1680.981	114.935		
			2171.480	171.328
8000	1808.584	55.301		
			2442.154	165.085
12500	1982.973	46.663		
			2388.299	171.924
20000	1760.734	48.958		
			2256.362	184.716

Table VI. 5. ESR medium data (3 measurements) collected from the measurements of Al centre of the quartz grains of the fluvial sediments Peso VG, Espi7, Espi8, Abano-6.

Dose (G)	ESR (a.u.) PesoVG1	d.s.	ESR (a.u.) Espi-7	d.s.	ESR (a.u.) Espi-8	d.s.	ESR (a.u.) Abano-6	d.s.
0	171.2149	69.4	62.800	4.378	99.328	21.176	105.988	17.767
100	189.164	56.164	76.103	8.566	128.613	5.473	153.779	31.253
200	227.414	72.131	97.915	8.894	184.035	8.431	172.743	46.944
400	249.437	52.241	94.590	5.961	199.323	27.815	239.324	62.807
800	334.4768	83.523	164.219	4.857	220.596	18.630	353.679	45.919
1600	376.827	81.998	210.885	12.296	348.335	17.994	472.205	65.612
3200	528	71.578	318.408	6.586	512.927	30.616	656.234	165.786
6000	693.3767	52.715	432.816	24.271	694.433	39.073	1177.499	218.802
10000					888.896	67.668	1305.428	220.314
15000			775.353	39.353	1160.874	65.943	1624.713	70.828
25000			1008.001	56.002	1472.115	44.986		

For Ti-Li, equivalent doses (De) were determined following different approaches: the exponential and linear fitting function (Duval et al., 2009; Voinchet et al., 2013) was firstly used and then a single saturating exponential function by limiting the curve to the first six points (from natural to the 4000 Gy) (Fig.VI.15).

The histograms obtained from Isoplot data analyses reveal the frequency distribution of the De in Al centre within the same range for each sample (Fig.VI.16).

The values of radioisotopes measured in two reference laboratories (MNHN - France and Riso - Denmark) showed no significant differences in either sample.

Table VI. 6. ESR medium data (3 measurements) was collected from Ti−Li centre of the quartz grains of the sediments Peso Vg, Espi-7and Abano6.

Dose (G)	ESR (a.u.)	d.s.	ESR (a.u.)	d.s.	ESR (a.u.)	d.s.
	PesoVg1		Espi-7		Abano-6	
0	246.430	49.750	192.968	11.147	207.880	14.256
100	274.029	33.565	219.555	17.297	292.794	33.813
200	300.937	30.424	249.878	12.185	358.056	48.490
400	335.834	60.202	300.143	27.235	450.368	64.858
800	426.983	54.288	432.409	21.920	565.631	24.263
1600	603.202	75.939	578.201	48.416	940.002	11.849
3200	818.480	141.961	926.449	34.395	1711.105	201.261
6000	1139.383	182.617	1268.875	67.106	2356.116	93.445
10000	1244.978	185.881	1392.784	54.625	2432.270	172.428
15000	1285.840	238.739	1572.866	83.772	2297.258	392.123
25000	1313.134	286.755	1215.065	72.301	207.880	14.256

Table VI. 7. Dosimetry and ESR ages in Al and Ti−Li centres of sedimentary samples collected from the fluvial and marine terraces. * ECT – Espichel, Cape terrace; RCT - Caso Cape terrace.

	Fluvial samples			**Marine samples**		
	T3 middle	T3 top	T1?	ECTm7	ECTm6	RCTm2
Sample code	**Malhadios1**	**Granho1**	**Peso VG1**	**Espi-7**	**Espi-8**	**Abano-6**
Depth (m)	1	0.3	0.7	0.2	0.1	0.6
Elevation (m)	59	47	78	38	58	35
Grain size (µm)	250-180	250-180	180-90	250-180	250-180	300
Bleaching (%)	68	60	40	48	50	48
D_e Ti centre (Gy)	898±15	582±66	708±44	444±107	-	334±48
Adj. Square	0.999	0.980	0.993	0.985	-	0.991
D_e Al centre (Gy)	858±35	676±55	622±27	314±30	723±25	321±29
Adj. Square	0.998	0.989	0.999	0.994	0.993	0.995
Ti−Li centreAge	**280±10 320±10***	**290±30 296±10***	**280±10 310±10***	**590±140**	**-**	**340±50**
Al centreAge (ka)	**270±10 310±10***	**340±60 382±40***	**240±10 260±10***	**417±40**	**343±10**	**320±30**

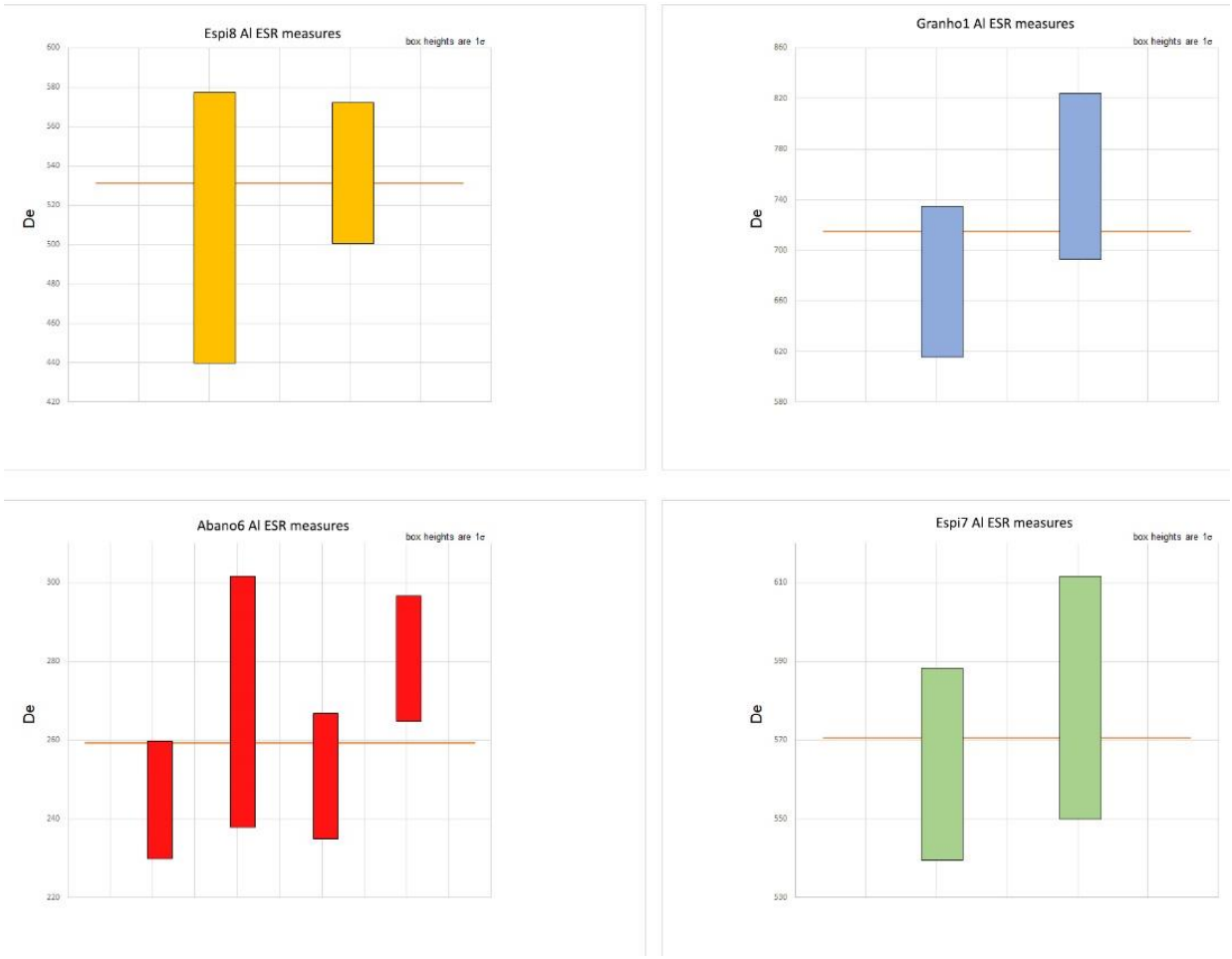

Figure VI.16. Some examples of histograms obtained from Isoplot data analyses software of the frequency distribution in quartz grains of the De in all aliquots (Al centre) of the samples Espi-8 (yellow); Granho-1 (blue); Abano-6 (red) and Espi-7 (green).

Table VI. 8. Sample information, dosimetry, external β and γ dose rate, cosmic dose and water content (WC). External α was considered negligible. The water content for the burial time was estimated considering the field water content and the saturation water content.

Samples	U (ppm)	Th (ppm)	K (%)	D''β	Dcos	Dγ	Dt (µG/a)	W(%)
Peso VG-1 Al	**1.164 ± 0.08**	**5.043 ± 0.117**	**2.971 ± 0.02**	2234.588 ± 25.07	67.112 ± 3.36	865.02 ± 15.124	2.923 ± 0.27	20
Peso VG-1 Ti	1.164 ± 0.08	5.043 ± 0.117	2.971 ± 0.02	2234.588 ± 25.07	67.112 ± 3.36	865.02 ± 15.124	2.923 ± 0.27	20
Granho- 1Al	1.164 ± 0.07	3.236 ± 0.094	1.881 ± 0.02	1464.329 ± 20.88	118.580 ± 5.93	627.16 ± 13.729	2.154 ± 0.24	15
Granho-1 1 Ti	1.164 ± 0.07	3.236 ± 0.094	1.881 ± 0.02	1464.329 ± 20.88	118.580 ± 5.93	627.16 ± 13.729	2.154 ± 0.24	20
Malhadios- 1 Al	1.507 ± 0.09	3.744 ± 0.127	3.649 ± 0.03	2593.308 ± 30.10	46.395 ± 2.32	1032.24 ± 19.310	3.480 ± 0.34	16
Malhadios- 1 Ti	1.507 ± 0.09	3.744 ± 0.127	3.649 ± 0.03	2593.308 ± 30.10	46.395 ± 2.32	1032.24 ± 19.31	4.480 ± 1.34	16
Espi-7	0.291 ± 0.06	0.746 ± 0.077	0.736 ± 0.01	535.413 ± 16.82	163.843 ± 8.19	228.71 ± 12.464	0.932 ± 0.02	8
Espi-8	0.604 ± 0.08	1.869 ± 0.104	2.568 ± 0.02	1833 ± 26.00	164.843 ± 9.19	733.66 ± 17.671	2.739 ± 0.03	7
Abano-6	0.652 ± 0.06	1.757 ± 0.084	1.049 ± 0.01	764.973 ± 17.01	76.152 ± 3.81	371.19 ± 13.075	1.212 ± 0.02	10

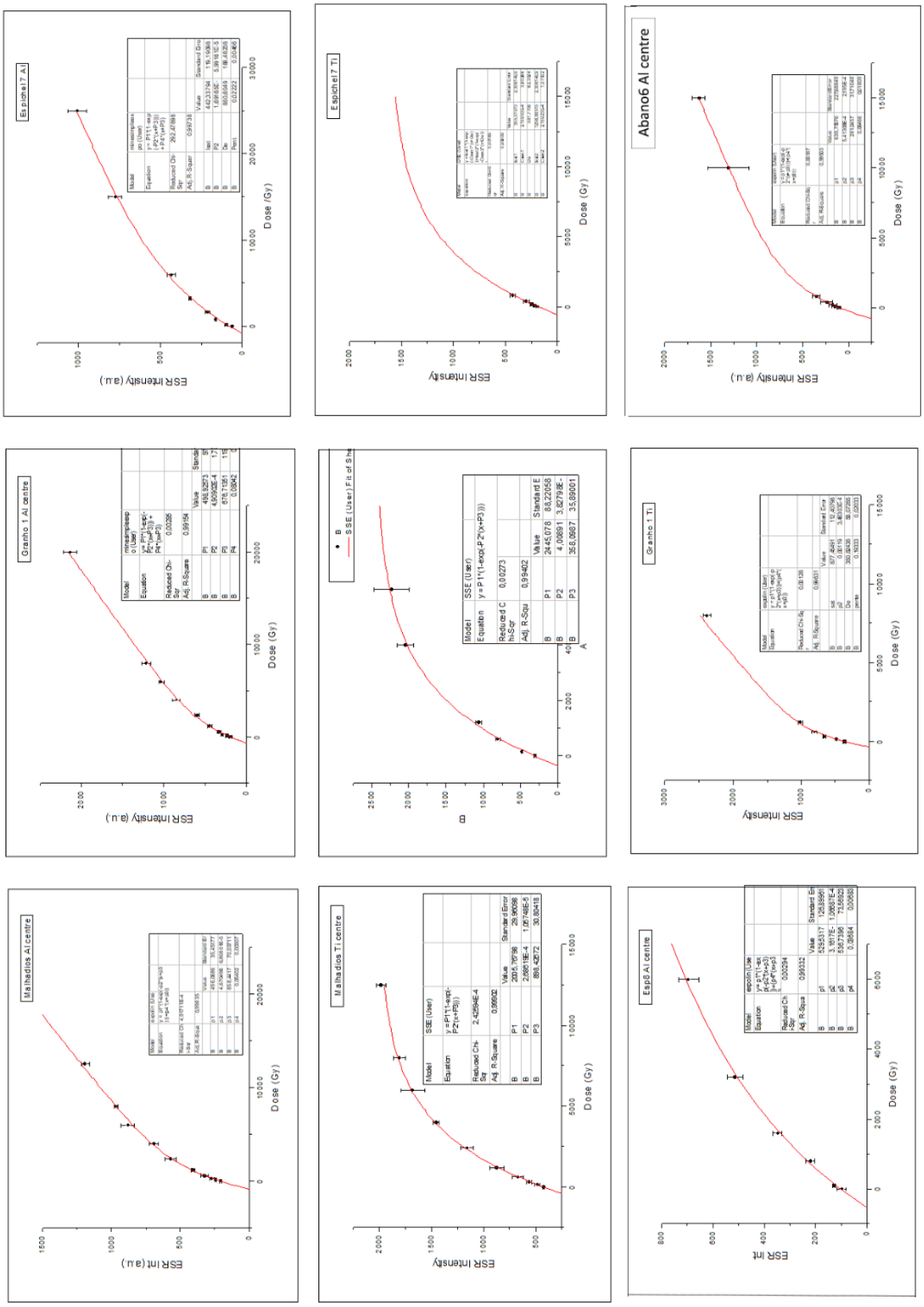

Figure VI. 17. Examples of the fitting curves with Exp+lin and SSE of fluvial quartz samples, showing the ESR dose-response curves. Legend: p1-saturation intensity;p2-csen; p3- De; p4 - pente (inclination).

Table VI. 9. Bleaching mean values of all samples.

Bleaching	Peso VG1	Malhadios-1	Granho-1	Espi-7	Espi-8	Abano-6
ESR1	38.188	63.910	64.643	43.389	58.187	51.369
ESR2	40.362	65.720	57.999	52.902	50.740	44.489
ESR3	42.160	73.560	58.614	-	-	45.153
Mean (%)	**40.24**	**67.73**	**60.42**	**48.15**	**54.46**	**47.00**

V.7. Discussion

Throughout the Pleistocene, during warm periods (corresponding to interglacials) Atlantic rivers had Mediterranean climate conditions, but in cold periods, the climate was Oceanic but preserving some continentally (Silva et al., 2017). In the Lower Tejo valley (reach IV) six terrace levels are documented, with relative heights (a.r.b.) at: +102-112 m (LT1), +83-92 m (LT2), +57-73 m (LT3), +28-37 m (LT4), +24-16 m (LT5) and +7-10 m (LT6) and the modern alluvial plain at +2-5m (Cunha et al., 2016), The set of OSL, post-IR-IRSL and ESR ages provided some ages for each terrace level: 903± 58 ka (LT1), 405-461 ka (LT3), 340-160 ka (LT4), 135-75 ka (LT5) and 62-32 ka (LT6).

The sample Peso Vg1 was collected at the base of the sedimentary sequence, immediately above the coarse gravels, in a coarse sand unit enriched with iron oxides concretions at the top. Peso Vg1 was previously dated by OSL using a post-IRIR 290 protocol (k-feldspar; KF), but only provided a minimum age (>304 ka) because the signal is in saturation (Cunha et al., 2017). Based on geomorphological interpretation and geochronology studies in this sector, this terrace at +78 m a.r.b., is equivalent to T1 of the upstream reaches III and I of the Lower Tejo. At reach IV, an ESR finite age of 903± 58 ka (Rosina et al., 2014) was already obtained for a T1 sand sample.

The ESR intensity values of nine measures revealed some heterogeneity in the grains of each aliquot, which may define more than one origin of the sediments. The different sources could explain the high beta dose contribution to the dose rate values. For annual dose, the values of U, Th and K were used, assuming that no gain or loss of uranium or thorium occurred since the time of deposition. The radioisotopes values present some disequilibrium between U, Ra and Rn (Table VI18), which is not unusual, given the sedimentary heterogeneity context (lenses of sands surrounded by coarser sediments) (Fig.VI.4). The Peso Vg1 fitted curve and the De values obtained in both centres (622 and 734 Gy) indicate that the sediment is old, but the annual dose present (2.9 Gy) only enables poor reconstruction the age calculation process. The high content in 40K explains the annual dose values, and the apparent saturation of the signal at doses >3200 Gy in both centres do not provide an accurate burial age (>300 ka).

Comparing the radiometric data of the previous study Rosina et al. (2014) (from another outcrop, but at the same reach), the Dose rate estimated was much lower 1574 μG/a than the dose obtained for Peso Vg1 sample (2923 μG/a). The underestimation is clearly because of an inadequate annual dose rate measurement.

At reach IV, the middle sand deposits of T3 were already dated by ESR, with a finite age result of ~410 ka (Rosina et al., 2014). Our new ESR age results of Malhadios1 and Granho1 are between 310 and 430 ka, with good agreement between both centres (Al and Ti-Li) in Malhadios-1. The De of Malhadios-1 (858 Gy in Al and 898 Gy in Ti-Li centres) is bigger than in Granho-1 (676 Gy and 365 Gy, respectively), which indicates to be the oldest. Based on a radionuclide activity research study (Madruga et al., 2014) carried out on the Tejo River sediments, the mean activity radionuclide concentration value for 40K is 400 Bq/kg. In Malhadios-1, the mean concentration data of the 40K is more than two times higher (~950 Bq/Kg). It may be related to the distribution of the radionuclide in the sediment beds. Therefore, the 40K content (3 times higher than in Granho-1) justifies the higher value of the annual dose in Malhadios-1. As 40K is concentrated within clay minerals, the silt/clay fraction of this sediment was in higher concentration than in the Granho-1 sample, affecting the real sediment age result.

In the Lower Tejo, each terrace has a larger thickness and seems to record large time-spans (Fig.VI.15) than in the terraces located in central Spain (Upper Tejo); so could correspond to more than one fluvial terrace of the Upper Tejo, explained by more uplift upstream. For the reach IV of the Lower Tejo, the uplit rate was estimated as ~0.07 m/ka.

The record of Pleistocene coastal sequences across the western Atlantic littoral is quite discontinuous, with some most complete sequence occurring in Raso Cape and Espichel Cape. The characterisation and absolute dating of the terrace staircases are crucial to understanding the past sea-level changes and the uplift rates. The terrace deposits are located in irregularly scattered remnants along the coast, sometimes in places difficult to reach, such as cliffs.

At Raso Cape, four terraces located below a culminant wave-cut platform have been identified by Cunha et al. (2015). In the present study, one sample collected from the Tm2 sedimentary sequence (34-37 m a.s.l.) at Abano beach was dated (Abano-6). The ESR ages from the two centres for the Tm2 sample are similar in Al (320±30 ka) and Ti-Li (340±50 ka) centres. The De is a little higher in Ti−Li than in Al centre, and the annual dose is not very high. However, there are values with an error of more than 50% and apparently, a saturation of the signal at doses >3200 Gy in both centres, showed by the very similar intensities at higher doses, which does not ensure an accurate burial age.

Espichel Cape rises higher than the Raso Cape sector and has a marine staircase composed of nine terraces while the Raso Cape sector has four terraces. Thus, the Abano deposit will have to be older than the obtained unprecise ESR age; otherwise, it would have an uplift equivalent to Espichel Cape, which is not recognised by the present geomorphology.

This terrace probably correlates to the MIS13 and indicates an uplift rate of 0.07m/ka (35 m/490 ka) or may even accommodate more than one MIS (13 and 11?), with an uplift range of 0.08-0.07m/ka. Indeed, this terrace has colluvium in the upper part, probably related to a colder period (MIS12) as in Espichel Cape, for the same interglacial.

In the western reach of the Espichel Cape, Tm1 is represented below the Espichel Cape platform (considered to be the base of the UBS13; ~3.7 Ma), at 108 m a.s.l. Based on geomorphological interpretation and previous ESR dating of the T1 of the Tejo river (903±58 ka) at 98 m a.s.l. (+89 m a.r.b.), the T1 is probably equivalent to Tm1 (with a probable age of ca. 1000? to 900 ka) and could comprise more than one MIS stage (MIS25-21?).

Tm2, represented by the W Espichel Cape platform at 83 m a.s.l. was yet not possible to date by ESR, but is probably equivalent to MIS 19, with the sea-level peak at 780 ka. The estimated uplift rate using the Tm2 as a reference is of ~0.1 m/ka (83 m/780 ka).

Tm3, at 72 m a.s.l., could be related with the MIS 17 which had the sea level peak at about 680 ka, allowing to estimate an uplift rate of ~0.1 m/ka (72 m/680 ka).

Tm4 could be correlated with MIS 15, with a high sea level similar to the present (Siddal et al., 2007), resulting in an uplift rate of ~0.1 m/ka (65 m/540 ka).

Espi-8 sample seems to have some contamination causing a remarkable contribution of 40K, responsible for high Da content (~ 3 times higher than Espi-7), which gave an underestimate age using the Ti−Li centre by the presence of manganese oxides cover in the quartz grains. According to Siddal et al. (2007), diagenetic effects are one of the main issues in older samples, that will be solved by ongoing technical developments. According to the ESR minimum age estimated for Espi-8, sampled at 56 m a.s.l., the Tm5 may have been formed during the MIS 13 to MIS 12 (Fig.VI.11, 16). The glaciation period correlated to MIS 12 (Elsterian glaciation) was considered as probably the most extensive in the North Sea Pleistocene glacial history (Gibbard and Cohen, 2008; Graham et al., 2011), and could be responsible for an enhanced of clastic flux deposition (breccia) in the upper part of the Tm5. The uplift rate for Tm5 is ~0.1 m/ka (53 m/480 ka).

The ESR age of Espi-7 (417±40 ka in Al centre) is in good agreement with the geomorphology (32 m a.s.l) and with the high sea-level of MIS11 (sea level at ±6 m of the present and probably stable through this long interglacial) and also with the beginning of the glacial period of MIS 10. The succession to the MIS 10 featured an abrupt drop on the temperature with major ice-rafted debris deposition events in Iberian and western Mediterranean margins (Regattieri et al., 2016). This interstadial could be responsible for the high thickness of breccia in the upper part of the Tm6. The estimated uplift rate for the Tm6 is ~0.08 m/ka (32 m/417 ka).

Without sediments, Tm7 was not possible to date. We assume that this terrace may represent the MIS9, and an uplift rate of ~0.06 m/ka (20 m/312 ka) could be estimated.

The Tm8 (+12 m a.s.l.) could be formed during the interglacial MIS 7 (240-190 ka, with sea-level estimates from -5 to-10 m, Antonioli, 2004) and with uplift of ~0.07 to 0.115 m/ka (17 or 22 m/240 ka, respectively). In fact, according to the literature, MIS 7 was marked by three warm phases but without big oscillations in ice volume (Rocoux et al., 2006) after climatic warming phases, giving a limit drop in the sea during this stage. This could explain the existence of only one platform for this interglacial period.

A rocky platform level is present at ~8 m a.s.l., with coastal notches found and deposits which probably correspond to the MIS 5.

In the submerged area, the level identified at -7 m, evidenced by a rocky level with local cliffs, notch and deposits, probably correlates with Holocene high sea levels.

The correlation between the complete marine terrace levels (Espichel Cape) and the fluvial staircase located in the reach IV of the Lower Tejo is presented on Fig.VI.18.

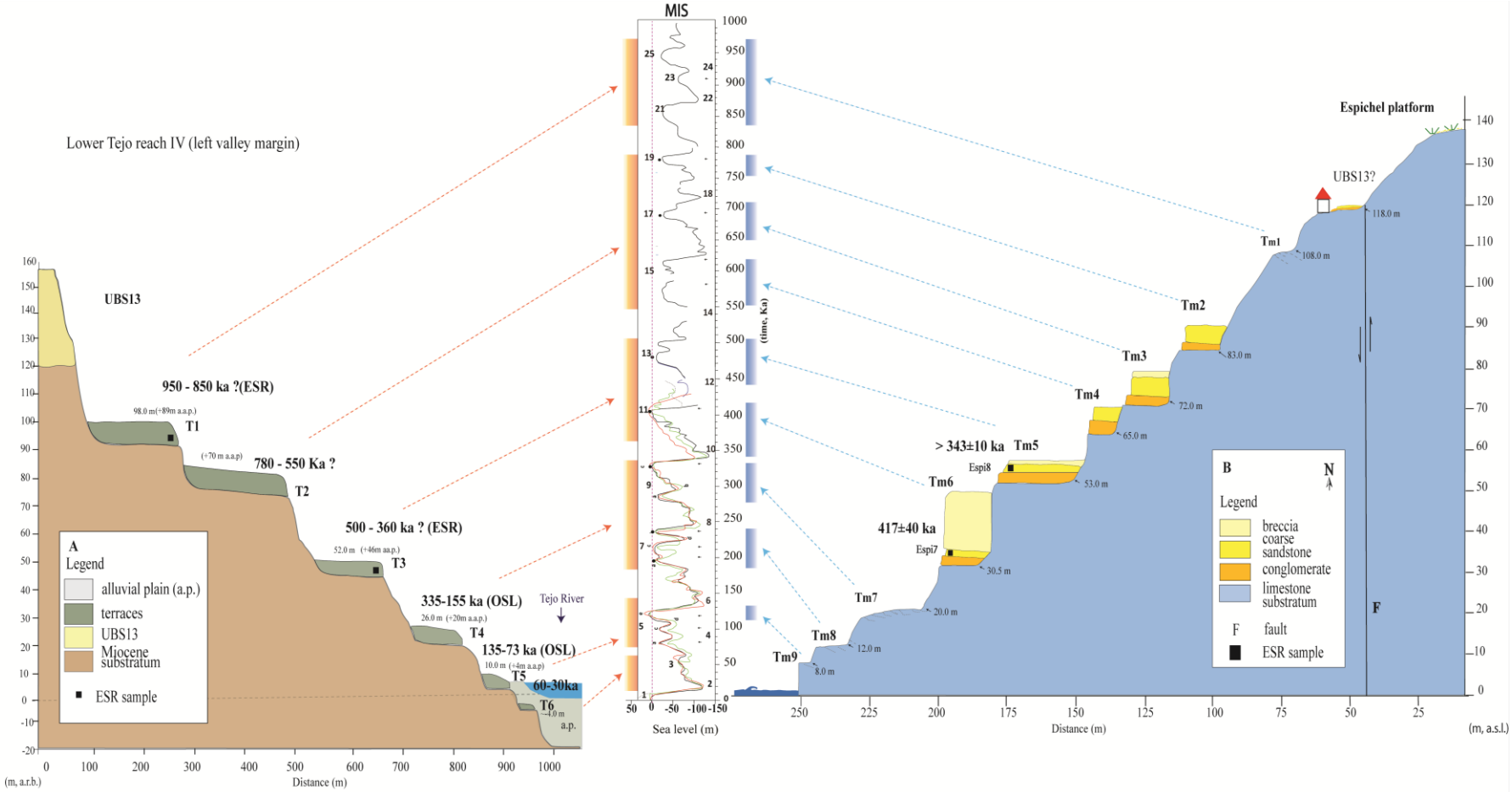

Figure VI. 18. Schematic terrace staircases of the Lower Tejo (reach IV) and Espichel Cape, with ESR and OSL dating results (previous ESR ages from Rosina et al., 2014; OSL ages from Martins et al., 2010 and Cunha et al., 2017). Sea-level estimates by Lisiecki and Raymo (2005) and Lambeck et al. (2014) The rectangles indicate the proposed aggradation intervals.

V.8. Conclusions

Despite some probable uncertainties due to the rather high annual dose rates in some fluvial and marine sediments, the ESR data obtained in the study area was crucial to propose a correlation between the studied staircases and with MISs.

Peso Vg1 fitted curve, and the D_e values obtained proved that the sediment is old, but the annual dose present only enables poor age calculation. Based on the geomorphological interpretation and previous ESR dating (903 ± 58 ka), this terrace remains at 98 m a.s.l. (+89 m a.r.b.), is probably equivalent to T1 (with a probable age of ~ 1000 to 900 ka). It was not possible to date by ESR a correlative marine terrace adjacent to the Tejo river mouth, but at the W Espichel Cape, it could correlate to the platform at 108 m a.s.l. (Tm1; MIS25-21?).

The Lower Tejo T2 terrace was yet not possible to date by ESR, but it could comprise several interglacials with probable age between 780-550 ka. This long duration fluvial terrace could correlate to a set of platforms represented in the W Espichel Cape at 83 m a.s.l. (Tm2; MIS19?– sea-level peak at 780 ka), 76 m a.s.l. (Tm3; MIS17? – sea-level peak at 690 ka), 65 m a.s.l. (Tm4; MIS15? – sea-level peak at 620-550 ka) and 53 m a.s.l. (Tm5; MIS13? – sea-level peak at 480 ka).

Granho1 and Malhadios1, sampled in the T3 fluvial terrace of the Lower Tejo (with a probable age of ca. 430 to 360? ka), provided ESR ages of ca. 430 and 310 ka which is compatible with the previous ESR age of ca. 410 ka (Rosina et al., 2014). The T3 fluvial terrace could correlate with two platforms represented in the W Espichel Cape at 34-30 m a.s.l. (Tm5; MIS13?) and at 31 m a.s.l. (Tm6; MIS11).

The Lower Tejo T4 terrace was previously yet dated by OSL, as ~ 335 to 155 ka, comprising the MIS9 to the earlier part of MIS6 intervals. It probably correlates with two platforms identified in the W Espichel Cape at 20 m a.s.l. (Tm7; MIS9) and 12 m a.s.l. (Tm8; MIS7).

The Lower Tejo T5 terrace was previously dated by OSL, as ~135 to 73 ka, comprising the last part of MIS6 and the MIS5 interglacials. This fluvial terrace can be correlated with the Espichel Cape marine platform level at 8 m a.s.l. (Tm9; MIS5).

Considering the results obtained, we can assume that along the Quaternary, the sea level during interglacial periods produced abrasion platforms with subsequent sediment filling at the same terrace levels, but now at different elevations along the western central Portugal coast. This results from the combination of eustatic changes and continuous but differential uplift that occurs at a regional level, confirmed by the same ages at different elevations a.s.l. even at a shorter distance, such as on Raso Cape. The study area has been subject to an overall uplift, however with different rates as the inner edge positions, with higher uplift rates in Espichel Cape than in Raso Cape.

The uplift of the study area during Pliocene and Quaternary is in accordance with the main active fault systems that are responsible for the regional seismicity: the NNE-SSW system (as the Lower Tejo valley fault zone), the WSW-ENE system (as the Arrábida thrust) and the NW-SE system (which affects the Espichel Cape and the Lower Tejo valley).

CHAPTER VII. DISCUSSION, MAIN CONCLUSIONS AND FUTURE WORK

This chapter comprises discussion and conclusions regarding the data presented in chapters III, IV, V and VI, but also with future research work. The first subsection is focused on identifying the uplifting trend during the Quaternary in the study area using the results obtained in the chronological study of each terrace staircase. A comparison between the studied marine staircases of Mondego Cape, Peniche, Abano beach (Raso Cape) and Espichel Cape is made. The second subsection is mainly focused on ESR dating method (applicability and limitations) and the crucial geomorphological study during this research work. It highlights the new data concerning marine and fluvial terraces of the LMB and LTB, comparing the uplift results.

VII.1. Comparison between the marine terrace staircases

The Western Iberian Margin is a region where active tectonics plays a significant role in the geomorphic expression and distribution of Quaternary marine terraces (e.g., Ressurreição et al., 2018; Carvalhido et al., 2014; Cunha et al., 2015). The fossil sea cliff (shoreline angle/strandline) of marine terraces of the Late Cenozoic is a good approximation of sea level during the peak of a highstand (Lajoie, 1986; Lisiecki and Raymo, 2005, 2007). Beyond that, the intensification of eustatic sea-level oscillations during the Middle-Pleistocene has increased the formation of coastal staircases, preserved in the fossil sea cliffs. In the present study, the marine platforms and terrace deposits were measured in the field with a GPS RTK (in Peniche and Espichel Cape), where the access was possible.

The comparison between the studied coastal areas highlights the differential uplift and the geomorphic landscape of the studied sectors. According to other studies in the Iberia Peninsula, there are deposits correlated to the Late Pleistocene in passive margins (Fig. VII.1) (e.g., Santos et al., 2008; Johnson et al., 2011) and the mean coastal apparent uplift rates (based on MIS 5 and 11 benchmarks) estimated for the passive margins of W Europe is ~ 0.06 ± 0.02 m/ka (Pedoja et al., 2014).

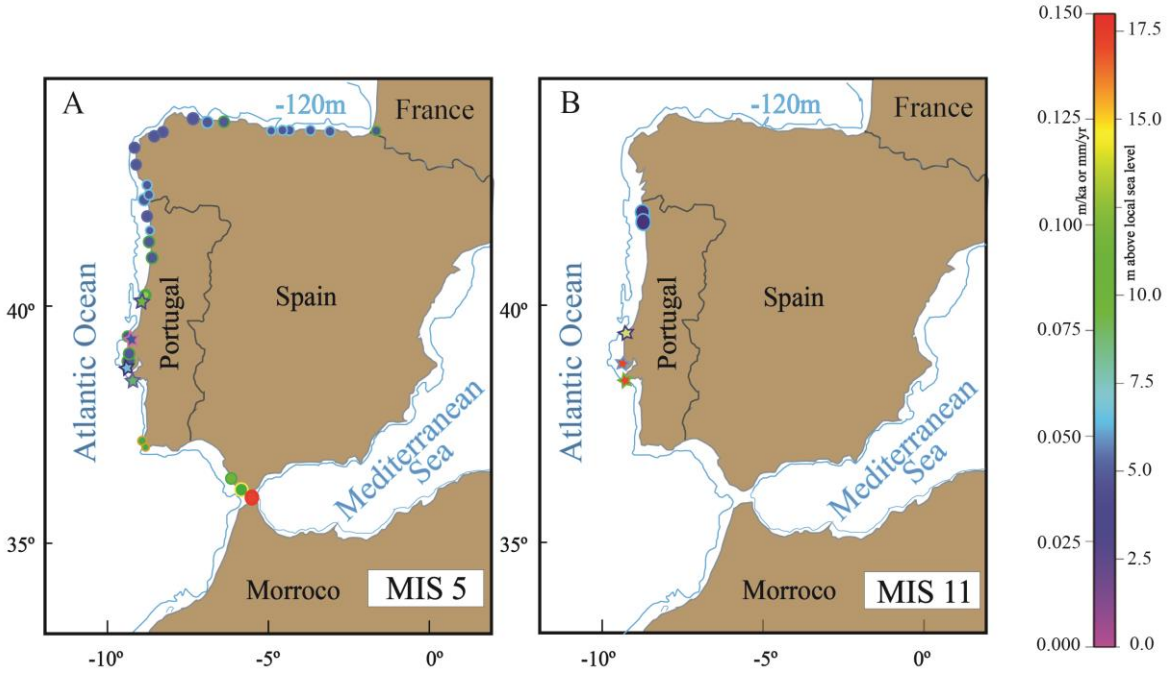

Figure VII. 1. Coastal uplift of the Iberian Peninsula. A) MIS 5; B) MIS 11. Stars are the data that resulted from this study. The circles are Iberia data available in the literature, (modified from Pedoja et al., 2018).

Despite many uncertainties regarding the sea-level highstands for each Middle Pleistocene interglacial periods, it was possible to estimate the regional differential uplift along the central coast of mainland Portugal, in the Mondego Cape (40^{0}11'N; 8^{0}54'W), Peniche (39^{0}21'N; 9^{0}24'W), Abano beach (38^{0}44'N; 9^{0}28'W) and Espichel Cape (38^{0}24'N; 9^{0}13'W), (Fig. VII.2).

For the uplift calculation, the eustatic corrections for the MIS 11 high-stand were according to Spratt and Lisiecki (2016) and, for the MIS 5 high-stand to Murray-Wallace and Woodroffe (2014) (mean predicted to be at +6 m for the both MIS). The uplift rate was determined by subtracting the relative sea-level during each stage from altitudinal position of the preserved shoreline angle and then dividing by the considered age (Bull, 1985; Burbank and Anderson, 2012).

Given the lack of data available and the higher uncertainties of age determinations for old shorelines, the mean sea level during the MIS 7, MIS 9 and MIS 13 to 25 was considered to be 0 m. The apparent uplift rate was determined by dividing the altitudinal position of the marine terrace shoreline angle in the present sea-level, by the considered age (Pedoja et al., 2018).

The geomorphologic maps, profiles and detailed stratigraphy work, the new DTM produced (higher resolution and higher scale) in all areas studied, and the new age data of the almost entire staircase in Peniche allowed a better interpretation of the correlations along the coast.

In Mondego Cape (reaching 256 m, a.s.l.) and Espichel Cape (140 m, a.s.l.) several terrace deposits were identified, dated and correlated to interglacials (Fig. VII.1), (e.g., Tm 2 and Tm 6 for Mondego and Espichel capes, respectively).

Since the Middle Pleistocene (MIS 19-17) to Late Pleistocene (MIS 5), the apparent uplift rates show a slight decrease, from ~0.17 m/ka to 0.02 m/ka in the coastal area.

The uplift results show a higher uplift for the Mondego Cape, as expected by the Quiaos Fault Structure, a fault scarp striking WE to WNW-ESE (Barbosa et al., 1988, Cabral, 1995), responsible for the higher relief of the Serra da Boa Viagem (Table VII.1, Fig. VII.2 A). Five marine terraces are preserved and culminate with the UBS13 Pliocene unit (~3.7 Ma). It was expected that more than five marine terraces were preserved in the paleo cliff. However, given the lithology present (resistant Jurassic marls and limestones), climate variability that probably affects the waves and winds regime and the vertical cliff exposition to the Atlantic sea, some sea levels highstands shorelines could be disappeared or destroyed, mostly in which the sea level oscillated more quickly, as for MIS 19,17, 9 (Spratt and Lisiecki, 2016).

In contrast, at the Peniche (elevation reaching 31 m, a.s.l.) and Abano (reaching 72 m, a.s.l.) staircases, each terrace deposit may represent more than one interglacial period, as already described in the literature for other regions of the world, most generally associated to areas with low uplift (e.g., Muhs et al., 2002; Zomenia, 2012; Pedoja et al., 2018) (Table VII.1). In fact, in Peniche all the terraces were dated by ESR, except Tm7 (the younger one). The age results evidence this fact, for the Tm1 (MIS25-19), Tm3 (MIS15-13) and Tm4 (MIS11-9) levels. This could result from one or more factors: 1) sea-level highstands with a shorter duration, 2) sea-level highstands with shorter periods and higher amplitudes than the antecedent; and 3) coasts with lower uplift, (< 0.2 m/ka, Pedoja et al., 2018) can easily promote the reoccupation of ancient marine platforms. Considering the resulting uplifts for the Mondego and Espichel Capes, we concluded that this is more expected in the coasts with uplift lower than 0.1m/ka.

In Abano beach, uplift rates are higher than in Peniche, as scheduled by the higher elevation of the terraces shorelines. However, in Abano beach, just four marine terraces are preserved below the culminant unit (Fig. VII.2 C). In the low uplift rate context, Tm3 was probably occupied by Mis11 and MIS9 highstands, as MIS 11 and MIS 9 sea-levels were ~+6 m (Sprattet and Lisiecki, 2016) and ±9 m of the present (Siddal et al., 2007), respectively. Tm4 is associated with MIS 7 as it cannot be with MIS 5 because its elevation position will be higher than in Espichel Cape, that is not possible. Probably, the lower marine outcrop correlated with MIS 5 was affected by current coastal erosion processes.

According to Pedoja et al., (2018), in Western Europe for the Late and the Middle Pleistocene, the mean apparent uplift rate is 0.05±0.01m/ka, and the mean apparent long-term uplift is 0.01 m/ka. In the Western Central Portuguese coast considering as geomorphic reference the UBS13 dated as 3.7 Ma, the mean apparent long uplift is ± 0.04 m/ka.

Table VII. 1. General information of the terrace staircase, sample code of ESR age results, terrace stratigraphic position, terrace elevation, ages used for the MIS reconstruction, apparent uplift rate calculation for each deposit from the Mondego Cape, Peniche, Abano and Espichel Cape. Paleo-sea level of each MIS interval according to the literature (Mis 5 is following Murray-Wallace and Woodroffe, 2014 and **Galve et al., 2019; high-stand estimates for MIS 9 and 11 according to Spratt and Lisiecki, 2016); ***OSL-age in Ramos et al., (2012), the age range for the respective MIS's is provided.

Sample Code	Stratigraphic position	Elevation (m, a.s.l.)	Assigned age (ka)	Apparent uplift rate (m/ka)	MIS	Probable eustatic p.s.l. (m)	Age Range
Fig.Foz (Mondego Cape)		210	3700	0.06		-	
	Tm1	153	900	0.17	21?	0	900? -782
	Tm2	**104**	**780**	0.13	**17**	0	697-682
Far-8 (592±49 ka)	**Tm3**	92.5	**600**	0.15	15?	0	620-486
	Tm4	17.5	217	0.12	7	0	255-197
Armazéns* **	**Tm5**	8	122	0.03;0.05	5	+6*; +2**	119-126
Peniche (Carvoeiro Cape)		31	~3700	0.01			
Pen-5	**Tm1**	**26.9**	**900**	0.03	25-19?	0	900-782
Pen-4	**Tm2**	**20.7**	**707±32**	0.03	17	0	697-682
Pen-3; 2;1	**Tm3**	**15**	**558±52**	0.025	**15**	0	620-486
				0.04	**13**	0	
Pen-8	**Tm4**	**12.9**	**390**	0.02- 0.01	11	+6*;0	408-315
			324		9?	0; +9*	
Pen-7	**Tm5**	6.4	324-217	0.02-0.03	9?-7	0	240-190
	Tm6	4	122	-0.02;0.02	5	+6*; +2**	119-126
Abano (Raso Cape)		72	~3700	0.02			
	Tm1	42	780?	0.05	19-17?	0	761-682
Abano-6 (> 340 ka)	**Tm2**	**34**	**600**	0.06	**15**	0	620-486
			502?	0.07	**13**		
	Tm3	22	**390**	0.04*;0.06	11	+6*;0;	408-315
			324	0.06; 0.07*	9	0; +9*	
	Tm4	9	217	0.04	**7**	0	255-119
		4	122	-0.02;0.02		+6*; +2**	
Espichel (Espichel Cape)		140	~3700	0.04			
	Tm1	108	900	0.12-0.14	**25-21?**	0	
	Tm2	83	780?	0.11	**19**	0	780
	Tm3	72	690?	0.1	**17**	0	697-682
	Tm4	65	600	0.1	**15**	0	620-580
Espi-8	**Tm5**	53	502	0.11	**13**	0	502-486
Espi-7	**Tm6**	**30.5**	**417±40**	0.06;0.08	**11**	+6*;0	408-399
	Tm7	20	330	0.08; 0.07*	**9?**	0; +9*	331-315
	Tm8	12	217	0.09	**7**	0	255-197
	Tm9	8	122	0.02;0.05	**5**	+6*; +2**	126-85

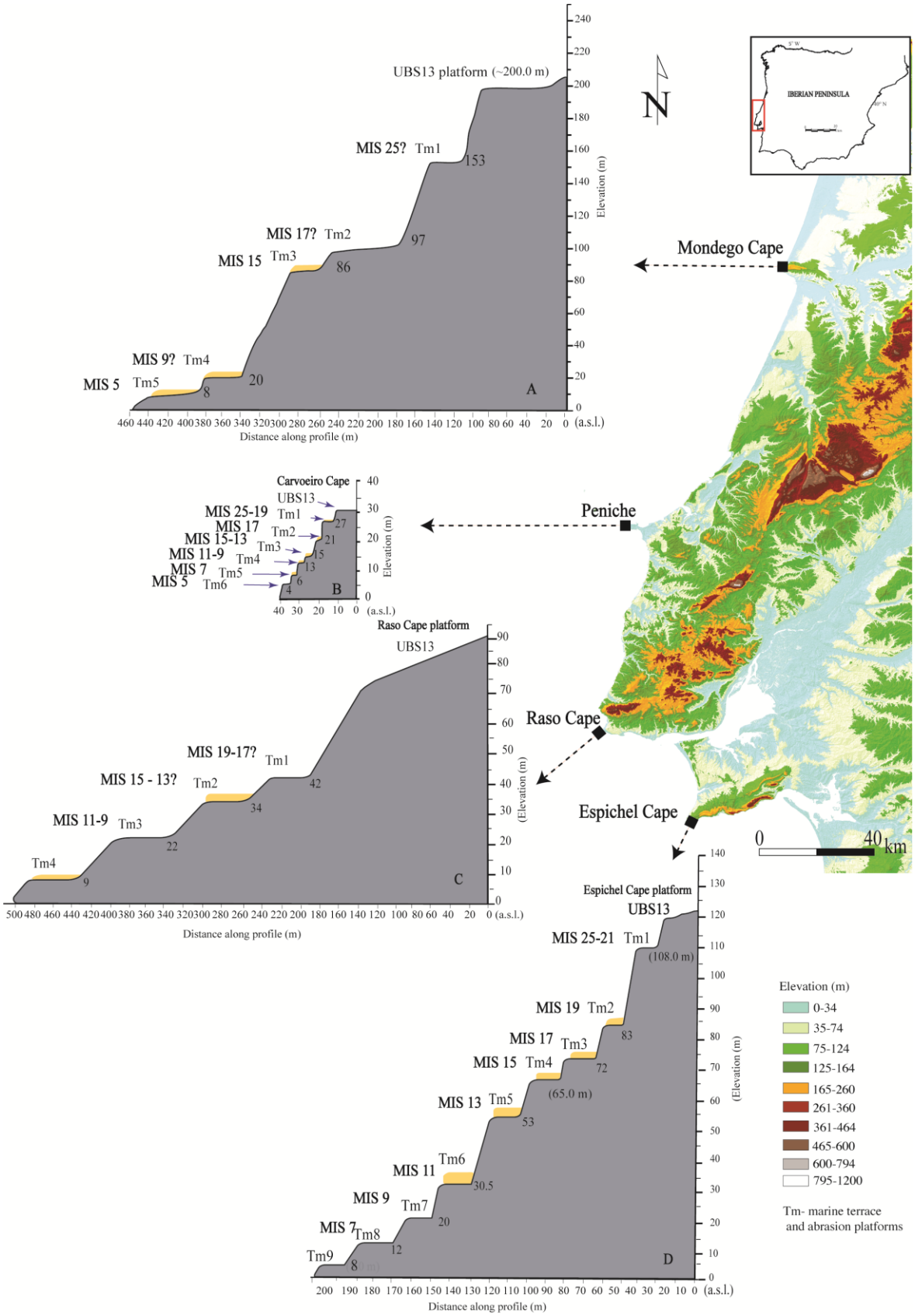

Figure VII. 2. Schematic profiles of the marine terraces between the Mondego Cape and Espichel Cape and location of each study sites in the Portuguese western central coast. The Mondego Cape profile (A) is with two

times (2x) reduction (elevation and distance) and Abano beach profile (C) with two times (2x) reduction in distance.

According to the Table VII. 2 and Fig. VII.2, that compares the different elevation on each marine terrace, and the ESR ages resulting from this study, the conclusions regarding the uplift ranges are:

- The marine terraces clearly differ in number and elevation position along the coast, with greater shorelines in higher uplift areas. Those are geomorphic markers of the Late-Cenozoic high-stands superimposed on an uplifting coast.
- Considering the apparent uplift range results, we can assume that the uplift has varied during the Middle Pleistocene, being higher in Espichel Cape, decreasing gradually until Peniche;
- In Mondego Cape, the highest uplift is correlated with the tectonic deformations affected by the Quiaios Fault and other structures associated with this fault.
- The differential uplift is relatively low in all the studied areas, ranging between 0.17 and 0.02 m/ka;
- Coasts with lower uplift as in Peniche and Raso Cape probably were reoccupied for more than one highstand sea-level;
- ESR ages obtained in this study are consistent with the terrace stratigraphic order and with the most relevant sea-level highstands during the Pleistocene;
- The long-term uplift rate, considering as geomorphic reference the UBS13 dated as 3.7 Ma, is spacially variable (differential uplift): in Mondego Cape is 0.07 m/ka; Espichel Cape is 0.04 m/ka, Abano beach is 0.02 m/ka, and Peniche is 0.01m/ka.
- The Middle Pleistocene mean uplift - rates (using the MIS 11) range from 0.06± 0.02 m/ka in Espichel Cape and Raso Cape and is 0.02 m/ka to Peniche and in Mondego Cape (using MIS 15) is 0.15 m/ka;
- Comparing the mean values for the sea level (n.m.m.) of MIS 5 against the uplift results, possibly the sea level (n.m.m.) more reliable would be closer to +2 m than +6 m a.s.l., for the Iberia.
- The terraces staircases confirm the ongoing regional uplift in the central-western Atlantic margin of the Iberia Peninsula, related to the generalized Cenozoic compression that accompanies the convergence between the Africa and Eurasia plates.

Finally, low crustal uplift conditions and differential uplift were determined, that are in agreement to a passive margin, probably in the transition to an active margin, resulting of an increase in intraplate compressive stress affecting the Western Iberian Margin (e.g., Martins et al., 2010; Cabral, 2012; Vilanova et al., 2014; Cunha et al., 2016; Cabral et al., 2018, 2019), but evidencing lower rates during the Late Pleistocene.

VII.2. Tectonic, eustatic and climatic control of the culminant sedimentary unit (UBS13) and fluvial terraces

The culminant allostratigraphical unit (UBS13) represents the final accumulation phase of the sedimentary basins before inversion occurred and the drainage systems began to cut large valleys in the south Cenozoic infill deposits and narrower valleys in the much harder pre-Cenozoic basement.

This sedimentary unit is thought to record the re-establishment of Atlantic drainage in the Lower Tejo and Mondego basins following a period of endorheism during the late Tortonian–Zanclean (~9.6 to 3.7 Ma). In an attempt to address the dearth of geochronological data on the timing of basin inversion, the unit UBS13 in the Mondego and Tejo Cenozoic basins was dated by using the ESR method. Reliable dates were obtained from the Al-centre. Some ESR data obtained using the Ti–Li centre have underestimated the real burial ages, particularly concerning the pre-existing biostratigraphical dating of the Vale Farpado site (3.7–3.6 Ma) for the basal UBS13 sediments (Cachão, 1990). ESR (Al-centre) ages of 3.0 to 2.3 Ma were obtained by for the mid-UBS13 deposits (in Barracão, near Pombal) and Azenheira (near Rio Maror) sites, whereas the uppermost part of the unit produced a probable age of ~1.8 Ma (N. Sra. da Victoria Beach). This age is older than the ages obtained for the same terrace level of the Lower Tejo (900 ka; Rosina et al., 2014), Ebro Basin (1.3 Ma; Duval et al., 2015) and Duero Basin (1.14 Ma; Moreno et al., 2012).

Large differences in values of the environment annual doses, from the top and base of the same outcrops, were found, probably partly explained by different sediment sources. The present study confirms that the Ti-Li centre ESR signal intensities of quartz grains is consistent and grew with the artificial doses for samples from the Middle Pleistocene (some beyond 8000 Gy), but this seems to result in underestimated ESR ages for successions from the Pliocene and Early Pleistocene (Tissoux et al., 2007). It also demonstrates that ESR ages are yielded with large error ranges for times older than 3-2.5 Ma if the De is < 3000 Gy, which has had a direct consequence on the age determination.

New field campaigns were carried out in the surrounding of Rio Maior during the year 2019 to better constrain the age of the UBS13 base. A new outcrop was founded, where new samples belonging to the same unit were collected. In the future, further ESR dating studies will be carried out.

The fluvial terraces of the Lower Mondego river were dated for the first time in Coimbra (Ingote, Conchada) and Tentúgal. ESR dating was also made in the lower reach of the river (Ervidinho), where there were already some OSL ages (Ramos et al., 2012). The integration of detailed geomorphological mapping the DEM's produced of each area, the reconstruction of the sedimentary environments, the profiles interpretation and the age determination, allowed the identification of terrace levels, the incision rates and the Lower Mondego River evolution during the Quaternary.

These terraces were compared with the terrace levels of the Lower Tejo, located at short distance and with a similar climatic, eustatic and tectonic control. In the reach IV of the Lower Tejo River, samples of the T1 and T3 (top and middle terrace) were also dated. Finally, the fluvial terraces of reach IV and the marine coastal terraces were correlated with the probable MISs.

Concerning the fluvial deposits, some D_e results obtained in some samples were not expected. The reason for a lower D_e mainly in the Ti-Li centre is explained by the heterogeneity of quartz grains in sedimentary material of different sources (metamorphic and sedimentary rocks) in the same sample or the presence of many clay fraction. For example, the Rio Maior, Ingote, Peso VG, Malhadios and Ervidinho samples were reproduced about four times, which corresponds to measurements of 12 times each set of 10 aliquots (1200 measures) and never on the same day to understand the Ti-Li behaviour in the samples. The total time estimated for spectrometer measurement was three hours/sample. The Ti-Li centre signal was always present in the samples, which allowed accurate result if the Al centre was well bleached. However, higher signal saturation was observed on older terraces, which did not allow an average age result for the two centres in some samples.

The study confirms that the Ti-Li centre ESR signal intensities of quartz grains is consistent and grew with the artificial doses for samples from the Middle Pleistocene, but this seems to be underestimated ESR ages for Pliocene and Early Pleistocene successions. It also demonstrates that ESR ages yield large error ranges for time older than 3-2.5 Ma if the D_e is < 3000 Gy. Another major issue is the need to measure the environmental dose in situ, especially on fluvial terrace sediments, as the annual dose is a crucial part of achieving age with accuracy.

This study shows that the ESR method using the Al signal, in optically bleached quartz, is available for dating deposits as old as the Late Pliocene - Early Pleistocene (e.g., Piacenzian - Gelasian) to Late Pleistocene.

The fluvial terraces studied on the LMR and on the LTR present differences in elevation and number of the several terrace staircases, that are the result of the same external controls: the ongoing differential uplift explained by the presence of active system faults (F1, F2, F3) and the climatic oscillations, responsible for the high amplitude of sea-level changes. In fact, each terrace can represent one or more aggradation phases during highstands sea levels, with different age intervals, and the incision phases are done during low-stand periods in shorter periods.

The LMR present different fluvial landforms on it last 50 km length studied, with several elevations in each bank side as a response of the strong structural control. It was shown by the vertical displacement rates results of the UBS13 and fluvial terraces, under different system faults present and by the longitudinal decreasing elevations from E to W, except for the western end of Serra da Boa Viagem. Only in the last reach of the river, the right valley margin is higher uplifted than the left margin as a response of the Quiaios - Maiorca fault activity during the Late Cenozoic period. Moreover, the differential uplift is relatively low, ranging between 0.01-0.05 m/ka using the ~2 Ma reference and 0.09-0.15 using the terraces as references.

On reach IV of the LTR a well-developed fluvial terraces staircase, especially on the left margin, and an extensive alluvial plain are present, but with lower elevations than in the upstream reaches (reach I to III). As in LMR, the activity of the faults is one of the main control of the landscape development in the Tejo valley, as the Ponsul fault (Reach I), the Gavião fault (reach II), Vila Nova da Barquinha fault (reach III), Lower Tejo valley system faults (reach IV) and the Vila Franca de Xira fault (reach V).

The incision rates for the LTR are similar to the LMR and present higher values for the end of the Late Pleistocene (<155 ka, 0.09-0.4 m/ka) than for the Early and Middle Pleistocene using the ~2 Ma reference, (0.04-0.28 m/ka) (Cunha et al., 2016).

This multidisciplinary investigation contributes to increasing the knowledge about the climatic forcing and the local tectonic constraints in the development and sedimentary evolution of the central west coast of Portugal during the Quaternary, including the more uplifted areas with long-lasting marine sequences (including rasas) and the interconnected foreland alluvial systems in the vestibular sectors of the Lower Mondego and Lower Tejo Rivers.

The possible future developments related to some limitations founded during these four years of investigation are:

- better constrain the age of the UBS13 (at the base);
- more dating is required at the base and the top of fluvial terrace levels to evaluate the aggradation interval of each terrace;
- more dating in the lowest marine terraces (MIS 5) to know the uplift /subsidence tendency to develop future coastal planning strategies;
- new ESR measurements, especially in the more uplifted marine terraces for an accurate age correlated with the most important sea-level highstands;
- according to sea elevation scenarios, GIS simulations of marine flooding are to be done with topographies conditioned by the current differential tectonic.

REFERENCES

ABAKUMOV, E., LODYGIN, E., TOMASHUNAS, V. (2015). 13C NMR and ESR characterization of humic substances isolated from soils of two Siberian arctic islands. International Journal of Ecology, 2015.

AITKEN, M. J. (1998). Introduction to optical dating: the dating of Quaternary sediments by the use of photon-stimulated luminescence. Clarendon Press. 263 p.

ALBERTI, A. P., DÍAZ, M. V., CHAO, R. B. (2004). Pleistocene glaciation in Spain.Quaternary glaciations–extent and chronology. Part I: Europe. Amsterdam, Elsevier. Developments in Quaternary Science 2, pp. 390–393.

ALMEIDA, A. C. (1997). Dunas de Quiaios, Gândara e Serra da Boa Viagem. Uma abordagem ecológica da paisagem. Lisboa, Fundação Calouste Gulbenkian, 320 p.

ALMEIDA, A. C., SOARES, A. F., CUNHA, L., MARQUES, J. F. (1991). Proémio ao estudo do Baixo Mondego. Biblos, Coimbra, LXVI, pp.17–47.

ALONSO, A. AND PAGÉS, J. L. (2007). Stratigraphy of Late Pleistocene coastal deposits in northern Spain. Journal of Iberian Geology, 33(2), pp. 207-220.

ANDERSON, R.F., FLEISHER, M.Q., LAO, Y., WINCKLER, G. (2008). Modern CaCO 3 preservation in equatorial Pacific sediments in the context of late-Pleistocene glacial cycles. Mar. Chem. 111, pp. 30–46. doi:10.1016/j.marchem.2007.11.011

ANDERSON, R.S., DENSMORE, A.L., ELLIS, M.A. (1999). The generation and degradation of marine terraces, Basin Research.

ANDRADE, F.C. (1937). Os vales submarinos portugueses e o diastrofismo das Berlengas e da Estremadura. Serviços Geológicos de Portugal.

ANDRADE, M.M. (1979). O tufo-brecha da Papôa: resto dum cone vulcânico de piroclastitos? Publicações do Mus. e Laboratório Miner. e Geológico da Fac. Ciências do Porto 4, pp. 214–222.

ANDRÉ, J. N., CUNHA, P.P., DINIS, J., DINIS, P., CORDEIRO, F. (2009). Características geomorfológicas e interpretação da evolução do campo dunar eólico na zona costeira entre Figueira da Foz e a Nazaré. PAPG, Vol. VI, APGEOM Braga, 39–44.

ANDREFSKY, W. (2001). Lithics: Macroscopic Approaches to Analysis. Cambridge University Press, 258 p.

ANTOINE P, LAUTRIDOU J.P., LAURENT M. (2000). Long-term fluvial archives in NW France: response of the Seine and Somme rivers to tectonic movements, climatic variations and sea level changes. Geomorphology 33, pp. 183–207.

ANTOINE, P. (1990). Chronostratigraphie et environnement du Paléolithique du Bassin de la Somme. Publ. du Centre d'Études et de Recherches Préhistoriques (CERP), Numéro spécial 2, pp. 231–187.

ANTOINE P. (1994). The Somme Valley terrace system (Northern France); a model of river response to Quaternary climatic variations since 800 000 BP. Terra-Nova 6, pp. 453–464.

ANTOINE, P., COUTARD, J. P., GIBBARD, P., HALLEGOUET, B., LAUTRIDOU, J. P., OZOUF, J. C. (2003). The Pleistocene rivers of the English Channel region. Journal of Quaternary Science: Published for the Quaternary Research Association, 18(3-4), pp. 227–243.

ANTOINE, P., MONCEL, M. H., LOCHT, J. L., LIMONDIN-LOZOUET, N., AUGUSTE, P., STOETZEL, E., DABKOWSKI, J.,VOINCHET, P, BAHAIN, J.J., FALGUERES, C. (2015). Dating the earliest human occupation of Western Europe: new evidence from the fluvial terrace system of the Somme basin (Northern France). Quaternary International, 370, pp. 77–99.

ANTÓN, L., RODÉS, A., DE VICENTE, G., PALLÀS, R., GARCIA-CASTELLANOS, D., STUART, F. M., BRAUCHER, R., BOURLÈS, D. (2012). Quantification of fluvial incision in the Duero Basin (NW Iberia) from longitudinal profile analysis and terrestrial cosmogenic nuclide concentrations. Geomorphology, 165, pp. 50–61.

ARAÚJO, M. A. (1991). Evolução geomorfológica da plataforma litoral da região do Porto. PhD thesis. Universidade do Porto

ARAÚJO, M. A. (2014). Depósitos do Pleistocénico Superior e do Holocénico na plataforma litoral da região do Porto: a morfologia das plataformas de erosão marinha e a tectónica recente. Estudos do Quaternário/Quaternary Studies, 5.

ASSENHEIM, H. M. (1966). The Interpretation of Electron Spin Resonance Spectra. In Introduction to Electron Spin Resonance , pp. 99-139. Springer, Boston, MA.

AZEVÊDO M.T. (1982a). As formações quaternárias continentais da Península de Setúbal e sua passagem às formações litorais. Cad Lab Xeol Laxe Geologia 3, pp.287–303.

AYDAS, C., ENGIN, B., & AYDIN, T. (2011). Radiation-induced signals of gypsum crystals analysed by ESR and TL techniques applied to dating. Nuclear Instruments and Methods in Physics Research Section B: Beam Interactions with Materials and Atoms, 269(4), pp. 417–424.

BAHAIN, J.J., YOKOYAMA, Y., FALGUÈRES, C., BIBRON, R. (1995). Datation par résonance de spin électronique (ESR) de carbonates marins quaternaires (Coraux et coquilles de mollusques). Electron spin resonance (ESR) dating of quaternary marine carbonates (corals and mollusc shells). Quaternaire 6(1), pp.13–19. doi: 10.3406/quate.1995.2033

BAHAIN, J.J, FALGUÈRES, C., VOINCHET, P.; DUVAL, M.; DOLO, J.M., DESPRIÉE, J., GARCIA, T. , TISSOUX, H. (2007). Electron Spin resonance (ESR) dating of some European Late Lower Pleistocene sites, Quaternaire, 18(2), pp. 175–186.

BAHAIN, J. J., DUVAL, M., VOINCHET, P., TISSOUX, H., FALGUÈRES, C., GRÜN, R., MORENO, D., SHAO, Q., TOMBRET, O., JAMET, G., FAIVRE, J. P., CLIQUET, D. (2020). ESR and ESR/U-series chronology of the Middle Pleistocene site of Tourville-la-Rivière (Normandy, France)-A multi-laboratory approach. Quaternary International, 556,pp. 58–70.

BAILIFF, I. K., SHOLOM, S., & MCKEEVER, S. W. S. (2016). Retrospective and emergency dosimetry in response to radiological incidents and nuclear mass-casualty events: A review. Radiation Measurements, 94, pp. 83–139.

BARBOSA, B. (1983). Argilas Especiais do Barracão – Pombal. Est. Not. Trab. Serv. Fomento Mineiro, 25 (3-4), pp. 193–212.

BARBOSA, B. (1995). Alostratigrafia e litostratigrafia das unidades continentais da Bacia Terciária do Baixo Tejo. Relações com o eustatismo e a tectónica. Ph.D., Univ. de Lisboa, 253 p.

BARBOSA, B. P., SOARES, A. F., ROCHA, R. B., MANUPPELLA, G., HENRIQUES, M. H. (1988). Carta Geológica de Portugal, Escala de 1/50 000, Folha 19-A, Cantanhede. Serviços Geológicos de Portugal. Lisboa. 46 p.

BARDAJÍ, T., GOY, J.L., ZAZO, C., HILLAIRE-MARCEL, C., DABRIO, C.J., CABERO, A., GHALEB, B., SILVA, P.G., LARIO, J. (2009). Sea level and climate changes during OIS 5e in the Western Mediterranean. Geomorphology 104, pp. 22–37. doi:10.1016/j.geomorph.2008.05.027

BARNOLAS, A., LARRASOAÑA, J.C., PUJALTE, V., SCHMITZ, B., SIERRO, F.J., MATA, M.P., VAN DEN BERG, B.C.J., PÉREZ-ASENSIO, J.N., SALAZAR, A., SALVANY, J.M., LEDESMA, S., GARCIA-CASTELLANOS, D., CIVIS, J., CUNHA, P.P. (2019). Chapter 2 – Alpine Foreland Basins, pp. 7-59. In: C. Quesada and J. T. Oliveira (eds). The Geology of Iberia: A Geodynamic Approach. Regional Geology Reviews, Springer International Publishing, Vol. 4 – Cenozoic Basins. doi: 10.1007/978-3-030-11190-8

BARTZ, M., RIXHON, G., DUVAL, M., KING, G. E., POSADA, C. Á., PARÉS, J. M., BRÜCKNER, H. (2018). Successful combination of electron spin resonance, luminescence and palaeomagnetic dating methods allows reconstruction of the Pleistocene evolution of the lower Moulouya river (NE Morocco). Quaternary science reviews, 185, 153–171. BATEMAN, H., 1910. Solution of a system of differential equations occurring in the theory of radioactive transformations. Proc Cambridge Phil Soc 15, pp. 423–427.

BENEDETTI, M.M., HAWS, J.A., FUNK, C.L., DANIELS, J.M., HESP, P.A., BICHO, N.F., MINCKLEY, T.A., ELLWOOD, B.B., FORMAN, S.L. (2009). Late Pleistocene raised beaches of coastal Estremadura, central Portugal. Quat. Sci. Rev. 28, pp. 3428–3447. doi:10.1016/j.quascirev.2009.09.029

BERGER, W. H. AND JANSEN, E. (1994). Mid-Pleistocene climate shift-the Nansen connection. GMS, 85, pp. 295–311.

BICHO, N.F. AND CARDOSO, L. (2010). Paleolithic occupations and lithic assemblages from Furninha cave , Peniche (Portugal) Ocupaciones paleolíticas e industrias líticas de la Gruta Furninha , Peniche (Portugal). Zepbyrus LXVI, pp. 17–38.

BINTANJA, R., VAN DE WAL, R.S.W.(2008). North American ice-sheet dynamics and the onset of 100,000-year glacial cycles. Nature 454, 869–872. doi:10.1038/nature07158

BISCHOFF, J.L., ROSENBAUER, R.J., TAVOSO, A., LUMLEY, H. (1988). A test of uranium-series dating of fossil tooth enamel: results from Tournal cave, France. Applied Geochemistry 3, pp. 135–141.

BORDES, F. (1961). Typologie du Paléolithique ancien et moyen. CNRS, Paris.

BOURDON, B., TURNER,S., HENDERSON, G.M., LUNDSTROM, C.C. (2003). Introduction to U-series geochemistry. Reviews in mineralogy and geochemistry, 52, pp. 1.

BRADLEY, W. C. AND GRIGGS, G. B. (1976). Form, genesis, and deformation of central California wave-cut platforms. Geological Society of America Bulletin, 87(3), pp. 433-449.

BRENNAN, B.J., LYONS, R.G., PHILLIPS, S.W. (1991). Attenuation of alpha particle track dose for spherical grains. Int. J. Radiat. Appl. Instrumentation. Part 18, pp. 249–253. doi:10.1016/1359-0189(91)90119-3

BRENNAN, B.J. (2003). Beta doses to spherical grains, in: Radiation Measurements. pp. 299–303. doi:10.1016/S1350-4487(03)00011-8

BREUIL, H., VAULTIER, M., ZBYSZEWSKI, G. (1942). Les plages anciennes portugaises entre le cap d'Espichel et la presqu'île de Peniche et leurs industries paléolithiques. Comptes-rendus des séances l année - Académie des inscriptions B.-lett. 86, pp. 102–109. doi:10.3406/crai.1942.77511

BREUIL, H., ZBYSZEWSKI, G. (1942). Contribution a l'étude des industries paléolithiques du Portugal et de leurs rapports avec la géologie du Quaternaire. Les principaux gisements des deux rives de láncien estuaire du Tage. Comun. dos Serviços Geológicos Port. 23, pp. 1–369.

BREUIL, H., ZBYSZEWSKI, G. (1945). Les principaux gisements des plages quatemaires du littoral d'Estremadura et des terrasses fluviales de la basse vallée du Tage. Comun. dos Serviços Geológicos Port. 26, 662 p.

BRÉZILLON, M. (1983). LA denomination des objets de Pierre taillée: matériaux pour un vocabulaire de préhistoriens de langue française. IV Supplément à Gallia Préhistorique. Bordeaux: CNRS.

BRIDGLAND, D. R. (1994). Quaternary of the Thames (Geological Conservation Review Series, no. 7). Chamman and Hall, London.

BRIDGLAND, D., MADDY, D., BATES, M. (2004). River terrace sequences: templates for Quaternary geochronology and marine–terrestrial correlation. Journal of Quaternary Science, 19(2), pp. 203–218.

BRIDGLAND, D. R., ANTOINE, P., LIMONDIN-LOZOUET, N., SANTISTEBAN, J. I., WESTAWAY, R., WHITE, M. J. (2006). The Palaeolithic occupation of Europe as revealed by evidence from the rivers: data from IGCP 449. Journal of Quaternary Science: Published for the Quaternary Research Association, 21(5), pp. 437–455.

BRIDGLAND, D. AND WESTAWAY, R.(2008). Climatically controlled river terrace staircases: a Worldwide Quayernary Phenomenon. Geomorphology, 98(3-4), pp. 285–315. doi: 10.1016/j.geomorph.2006.12.032

BRIDGLAND, D. R. AND WESTAWAY, R. (2014). Quaternary fluvial archives and landscape evolution: a global synthesis. Proceedings of the Geologists' Association, 125(5-6), pp. 600-629.

BRILHA, J., ANDRADE, C., AZERÊDO, A., BARRIGA, F.J.A.S., CACHÃO, M., COUTO, H., CUNHA, P.P., CRISPIM, J.A., DANTAS, P., DUARTE, L. V., FREITAS, M.C., GRANJA, H.M., HENRIQUES, M.H., HENRIQUES, P., LOPES, L., MADEIRA, J., MATOS, J.M.X., NORONHA, F., PAIS, J., PIÇARRA, J., RAMALHO, M.M., RELVAS, J.M.R.S., RIBEIRO, A., SANTOS, A., SANTOS, V.F., TERRINHA, P. (2005). Definition of the Portuguese frameworks with international relevance as an input for the European geological heritage characterisation. Episodes 28, 177–186. doi:10.18814/epiiugs/2005/v28i3/004

BRUGAL, J., ARGANT, J., CRISPIM, J.A., FIGUEIREDO, S.D., MARTÍN-SERRA, A., PALMQVIST, P. (2012). The complex carnivore-rich assembalges from Furninha (Peniche, Portugal): a multidisciplinary approach. J. Taphon. 10, pp. 417–438.

BRUNEAU, N., BONNETON, P., CASTELLE, B., PEDREROS, R. (2011). Modeling rip current circulations and vorticity in a high-energy mesotidal-macrotidal environment. J. Geophys. Res. Ocean. 116. doi:10.1029/2010JC006693

BULL, W.B. (1985). Correlation of flights of global marine terraces. In: M. Morisawa and J. Hack (Editors), Tectonic Geomorphology. Proc. 15th Annual Geomorphology Symp., State Univ. of New York at Binghamton, George Allen and Unwin, Hemelhempstead, pp. 129–152.

BULL, W. B., (1991). Geomorphic responses to Climate Change. Oxford University Press, Oxford, 326 pp.

BURBANK, D. W. AND ANDERSON, R. S. (2012). Tectonic Geomorphology, 454 pp.

CABRAL, J. M. L. C., RIBEIRO, A. (1988). Carta neotectónica de Portugal continental 1: 1 000 000. Serviçios Geológicos de Portugal.

CABRAL, J. (1995). Neotectónica em Portugal Continental. Memorias do Inst. Geológico e Min. 265.

CABRAL, J. (2012). Neotectonics of mainland Portugal: state of the art and future perspectives. J. Iber. Geol. 38. doi:10.5209/rev_jige.2012.v38.n1.39206

CABRAL, J., MONIZ, C., BATLLÓ, J., FIGUEIREDO, P., CARVALHO, J., MATIAS, L., TEVES-COSTA, P., DIAS, R., SIMÃO, N. (2013). The 1909 Benavente (Portugal) earthquake: search for the source. Natural Hazards, 69(2), pp. 1211–1227.

CABRAL, J., DIAS, R.P., CUNHA, P.P., CABRAL, M.C. (2019). Quaternary activity of the São Marcos - Quarteira fault (Algarve, southern Portugal): a case study for the characterisation of the active geodynamic setting of SW Iberia. Journal of Iberian Geology, Vol. 45, Issue 3, pp. 427–442; DOI: 10.1007/s41513-019-00102-2

CABRAL, J., RIBEIRO, P., RAMOS, A., CUNHA, P.P. (2018). Diapiric activity affecting Late Pliocene to Pleistocene sediments under a tectonic compressive regime: an example from the Western Iberian Margin (Sra da Vitória beach, central Portugal). J. Iber. Geol. 44, pp. 431–445. doi:10.1007/s41513-018-0073-3

CABRAL, J. AND RIBEIRO, A. (1989). Carta Neotectónica de Portugal Continental, Escala 1:1.000.000. Nota explicativa. Serv. Geol. Portugal, Lisboa, 10p.

CACHÃO, M. (1989). Contribuição para o estudo do Pliocénico Marinho Português (sector Pombal/Marinha Grande). Dissertação apresentada no âmbito das provas de Aptidão Pedagógica e Capacidade Científica , Fac. de Ciências, Universidade de Lisboa, 204 p.

CACHÃO, M. 1990. Posicionamento biostratigráfico da jazida pliocénica de Carnide (Pombal). Gaia, 2, pp. 11–16.

CACHÃO, M. 1995. Utilização de Nanofósseis calcários em Biostratigrafia, Paleoceanografia e Paleoecologia. Aplicações no Neogénico do Algarve (Portugal) e do Mediterrâneo Ocidental (ODP 653) e à problemática de Coccolithus pelagicus. Tese de doutoramento apresentada à Fac. de Ciências, Universidade de Lisboa, 356 p.

CALAIS, E., DE METS, C., AND NOCQUET, J. M. (2003). Evidence for a post-3.16 Ma change in Nubia-Eurasia-North America plate motions? Earth and Planetary Science Letters, 216(1-2), pp. 81–92.

CALVO J., DAAMS R., MORALES J., LOPEZ-MARTÍNEZ N., AGUSTI J., ANADON P., ARMENTEROS I., CABRERA L., CIVIS J., CORROCHANO A, DIAZ-MOLINA M, ELIZAGA E, HOYOS M, MARTIN-SUAREZ E, MARTÍNEZ J, MOISSENET E, MUÑOZ A, PÉREZ-GARCIA A, PÉREZ-GONZALEZ A, PORTERO J, ROBLES F, SANTISTEBAN C, TORRES T, VAN DER MEULEN AJ, VERA J, MEIN P. (1993). Up-to-date Spanish continental Neogene synthesis and paleoclimatic interpretation. Rev Soc Geol Espana 6 (3–4), pp. 29–40.

CAPUTO, R. (2007). Sea-level curves: Perplexities of an end-user in morphotectonic applications. Glob. Planet. Change 57, pp. 417–423. doi:10.1016/j.gloplacha.2007.03.003

CARAPITO, C. (1985). Quantificação dos minerais argilos. Alguns problemas da aplicação da difracção de raio-x. Trabalho de Provas de A.P.C.C. da Univ. Aveiro, 55p.

CARBONELL, E., MORA, R, 1986. El Sistema Lógico-Analític e la Teoria del "Transfer" en l'estudi des complexes lítics. Barcelona: Dossiers de la Societat Catalana d'Arqueologia.

CARDOSO, J.L. AND CARVALHO, A.F. (2011). A Gruta da Furninha (Peniche): Estudo dos Espólios das Necrópoles Neolíticas. Estud. Arqueol. Oeiras 18.

CARVALHIDO, R. P.; PEREIRA, D. I.; CUNHA, P. P.; BUYLAERT, J.-P.; MURRAY, A. S. (2014) - Characterisation and dating of coastal deposits of NW Portugal (Minho-Neiva area): A record of climate, eustasy and crustal uplift during the Quaternary. Quaternary International, vol. 328-329, pp. 94–106. doi: 10.1016/j.quaint.2014.01.025

CARVALHO, G. S., 1951. A geologia do Baixo Mondego nos arredores de Coimbra. Memórias e Notícias.Publ. Mus. Lab. Mineral. Geol. Univ. Coimbra, pp. 1–33.

CARVALHO, G. S. (1964). Areias da Gândara (Portugal). Uma formação eólica quaternária. Anais Fac. Ciências Porto, nº 81, pp. 1–32.

CARVALHO, G. S., GRANJA, H. M., LOUREIRO, E. AND HENRIQUES, R. (2006). Late Pleistocene and Holocene environmental changes in the coastal zone of northwestern Portugal. Journal of Quaternary Science: Published for the Quaternary Research Association, 21(8), pp.859–877.

CATTANEO, A., SEEL, R.J.. (2003). Transgressive deposits: a review of their variability.Earth Scien. Rev.,62, pp.187–228.

CHAPPELL, J. (2002). Sea level changes forced ice breakouts in the Last Glacial cycle: New results from coral terraces. Quat. Sci. Rev. 21, pp. 1229–1240. doi:10.1016/S0277-3791(01)00141-X

CHOFFAT, P. 1889. Observations sur le Pliocéne du Portugal. Mém. Soc. Belge Geol. Paleont. Hydrol. Bruxelas, 3, pp. 119–123.

CHOFFAT, P. 1903. L'Ifralias et le Sinémurien au Portugal. Commun. Comm. Serv. Geol. Portugal, Lisboa, 5, pp. 4 –114.

CLARK, P.U., ARCHER, D., POLLARD, D., BLUM, J.D., RIAL, J.A., BROVKIN, V., MIX, A.C., PISIAS, N.G., ROY, M. (2006). The middle Pleistocene transition: characteristics, mechanisms, and implications for long-term changes in atmospheric pCO2. Quat. Sci. Rev. 25, pp. 3150–3184. doi:10.1016/j.quascirev.2006.07.008

CLOETINGH, S., ZIEGLER, P.A., BEEKMAN, F., ANDRIESSEN, P.A.M., MATENCO, L.,BADA, G., GARCIA-CASTELLANOS, D., HARDEBOL, M, DÈZES, P., SOKOUTIS, D.(2005). Lithospheric memory, state and stress and rheology: Neotectonic controls on Europe´s intraplate continental topography. Quaternary Science Reviews, 24, pp. 241–304.

CORDIER, S., HARMAND, D., FRECHEN, M., BEINER, M. (2006). Fluvial system response to Middle and Upper Pleistocene climate change in the Meurthe and Moselle valleys (Eastern Paris Basin and Rhenish Massif). Quaternary Science Reviews, 25(13–14), pp. 1460–1474.

CORRAL-FERNANDEZ, I., 1998A, Depositos Cuaternarios en el área de Constância-Barquinha-Entroncamento y la Rib. del Bezelga. Arkeos, 4, pp. 59–144.

CORRAL-FERNANDEZ, I., 1998B, Secciones com material arqueológico en estrato en las proximidades de Atalaia. Arkeos, 4, pp. 227–250.

CUNHA, L., SOARES, A.F., 1997. Alguns problemas geomorfológicos no sector oriental do Baixo Mondego. O confronto de morfologias nas áreas de Coimbra e de Condeixa. Actas do Seminário O Baixo Mondego – Organização Geossistémica dos Recursos Naturais, pp. 41–49.

CUNHA, L., SOARES, A.F., TAVARES, A., MARQUES, J.F. (1999). O julgamento geomorfológico de Coimbra, O testemunho dos depósitos quaternários. Actas de I Colóquio de Geografia de Coimbra, Cadernos da Geografia, pp. 15–26.

CUNHA, L., SANTOS, J., RAMOS, A. (2020). The Mondego river and its valley. In: Landscapes and Landforms of Portugal. World Geomorphological Landscapes. Springer, Cham, pp. 175–184.

CUNHA, P.P. (1992a). Estratigrafia e Sedimentologia dos Depósitos do Cretácico Superior e Terciário de Portugal Central, a Leste de Coimbra/Stratigraphy and Sedimentology of the Upper Cretaceous and Tertiary of Central Portugal, East of Coimbra. Ph.D. Thesis, University of Coimbra, Coimbra, Portugal, 262p.

CUNHA, P. P. (1992b). Establishment of unconformity-bounded sequences in the Cenozoic record of the western Iberian margin and syntesis of the tectonic and sedimentary evolution in central Portugal during Neogene. Abstracts of the First Congress R.C.A.N.S. - “Atlantic General Events During Neogene”, Lisboa, pp. 33–35.

CUNHA, P.P. PROENÇA; BARBOSA, B. P.; PENA DOS REIS, R. (1993). Synthesis of the Piacenzian onshore record, between the Aveiro and Setúbal parallels (Western Portuguese margin), Ciências da Terra 12, pp. 35–43.

CUNHA, P.P. (1996). Unidades litostratigráficas do Terciário da Beira-Baixa (Portugal). Com Inst. Geo Mineiro 82, pp. 87–130.

CUNHA, P. P. AND MARTINS, A. A. (2000).Transição doenchimento terciário para o encaixe fluvial quaternário na área de Vila Velha de Rodão (Sector NE da Bacia do Baixo tejo). Ciencias da Terra, Lisboa 14, pp. 171–182.

CUNHA, P. P. AND MARTINS, A. A. (2004). Principais aspectos geomorfológicos de Portugal central, sua relação com o registo sedimentar e a importância do controlo tectónico. Faculdade Letras U.Porto, pp. 151–178.

CUNHA, P. P., AND DINIS, J. (2002). Sedimentary dynamics of the Mondego estuary.In: Pardal et al. Aquatic Ecology of the Mondego River, pp. 43-63.

CUNHA, P.P., MARTINS, A.A., DAVEAU, S., FRIEND, P.F. (2005). Tectonic control of the Tejo river fluvial incision during the late Cenozoic, in Ródão - Central Portugal (Atlantic Iberian border). Geomorphology 64, pp. 271–298. doi:10.1016/j.geomorph.2004.07.004

CUNHA, P.P. (2008). Papel desempeñado por la tectónica, el clima y el eustatismo en la génesis de los depósitos de Raña al pie de la Cordillera Central Portuguesa (Iberia occidental). Geo-temas pp. 1507–1510.

CUNHA, P.P. (2019). Cenozoic Basins of Western Iberia: Mondego, Lower Tejo and Alvalade Basin. In The Geology of Iberia. A Geodynamic Aproach. Springer Nature Switzerland AG, 4 pp. 1–25.

CUNHA, P.P. (2019). Cenozoic Basins of Western Iberia: Mondego, Lower Tejo and Alvalade basins. In: C. Quesada and J. T. Oliveira (eds). The Geology of Iberia: A Geodynamic Approach. Regional Geology Reviews, Springer International Publishing, Vol. 4 – Cenozoic Basins, Chapter 4, pp. 105–130. doi: 10.1007/978-3-030-11190-8;

CUNHA, P.P., MARTINS, A.A., HUOT, S., MURRAY, A., RAPOSO, L. (2008). Dating the Tejo river lower terraces in the Ródão area (Portugal) to assess the role of tectonics and uplift. Geomorphology 102, pp. 43–54. doi:10.1016/j.geomorph.2007.05.019

CUNHA, P.P., PAIS, L., LEGOINHA, P. (2009). Evolução geológica de Portugal continental durante o Cenozóico- sedimentação aluvial e marinha numa margem continental passive (Ibéria ocidental). 6º Simposio sobre el Margem Ibérico Atlántico MIA09, pp. 9–20.

CUNHA, P.P., BUYLAERT, J.P., MURRAY, A.S., ANDRADE, C., FREITAS, M.C., FATELA, F., MUNHÁ, J.M., MARTINS, A.A., SUGISAKI, S. (2010). Optical dating of clastic deposits generated by an extreme marine coastal flood: The 1755 tsunami deposits in the Algarve (Portugal). Quat. Geochronol. 5, pp. 329–335. doi:10.1016/j.quageo.2009.09.004

CUNHA, P. P., ALMEIDA, N. A., AUBRY, T., MARTINS, A. A., MURRAY, A. S., BUYLAERT, J. P., SOHBATI, R., RAPOSO, L., ROCHA, L. (2012). Records of human occupation from Pleistocene river terrace and aeolian sediments in the Arneiro depression (Lower Tejo River, central eastern Portugal). Geomorphology, 165, 78–90.

CUNHA, P. P., MARTINS, A. A., CABRAL, J., GOUVEIA, M. P., BUYLAERT, J.P., MURRAY, A. S. (2015). Staircases of wave-cut platforms in western central Portugal (Cape Mondego to Cape Espichel) – relevance as indicators of crustal uplift. In V. Díaz del Rio, P. Bárcenas, L.M. Fernandéz-Salas, N. López-González, D.Palomino, J.L. Rueda, O. Sanchéz-Guillamón, J.T. Vasquez (eds.), VIII Symposium on the Iberian Atlantic Margin (Proceedings), Malaga, 21-23 September (2015), Ediciones Sia Graf. Málaga, pp. 141-144. Nº Depósito Legal: MA 1272–2015

CUNHA, P. P., MARTINS, A. A., GOUVEIA, M. P. (2016) - As escadarias de terraços do Ródão à Chamusca (Baixo Tejo) – caracterização e interpretação de dados sedimentares, tectónicos, climáticos e do Paleolítico / The terrace staircases of the Lower Tagus River (Ródão to Chamusca) – characterisation and interpretation of the sedimentary, tectonic, climatic and Palaeolithic data. Estudos do Quaternário, vol. 14, pp. 1–24. doi: 10.30893/eq.v0i14.116

CUNHA, P.P., MARTINS, A.A., GOUVEIA, M.P., MARTINS, A.A. (2017). Geometria da unidade alostraigráfica SLD13 (zancleano Sup.- Gelasiano) no sector SW da bacia Cenozoica do baixo Tejo (Alpiarça- Península de Stetúbal). Reunião do Quaternário Ibérico pp. 103–106. ISBN: 978-989-96462-7-8

CUNHA, P. P., MARTINS, A. A., BUYLAERT, J. P., MURRAY, A. S., RAPOSO, L., MOZZI, P., STOKES, M. , (2017). New data on the chronology of the Vale do Forno sedimentary sequence (Lower Tejo River terrace staircase) and its relevance as a fluvial archive of the Middle Pleistocene in western Iberia. Quaternary Science Reviews, 166, pp. 204–226.

CUNHA, P.P., MARTINS, A.A., GOMES, A., STOKES, M., CABRAL, J., LOPES, F.C., PEREIRA, D., DE VICENTE, G., BUYLAERT, J.P., MURRAY, A.S., ANTÓN, L. (2019). Mechanisms and age estimates of continental-scale endorheic to exorheic drainage transition: Douro River, Western Iberia. Glob. Planet. Change, 181. doi:10.1016/j.gloplacha.2019.102985

CUNHA, P.P., MARTINS, A.A., GOUVEIA, M.P., GOMES, A.A., FIGUEIREDO, S., DUARTE, J., PEREIRA, T., COSTA, A.B. (2017). Registos geomorfológicos e sedimentares do Plio-Plistocénico de Peniche - Atouguia da Baleia, in: 8o Congresso Nacional de Geomorfologia (Proceedings), pp. 103–106. ISBN: 978-989-96462-7-8

CURNOE, D., GRÜN, R., TAYLOR, L., THACKERAY, F., (2001). Direct ESR dating of a Pliocene hominin from Swartkrans. Journal of Human Evolution 40 (5), pp.379–391.

DAVEAU, S. (1993). Terraços fluviais e litorais. In O Quaternário em Portugal. Balanço e perspectivas, pp. 17–28.

DAVEAU, S., AZEVEDO, T. M,. (1980). Aspectos e evoluçao do relevo da extremidade sudoeste da Arrabida (Portugal) in Volume de homenagem ao Professor Doutor Carlos Teixeira. Boletim da Sociedade geologica de Portugal Lisboa, 22, pp. 163–180.

DE GELDER, FERNÁNDEZ-BLANCO, D., MELNICK, D., DUCLAUX, G.,BELL, R.E., JARA-MUÑOZ, J., ARMIJO, R, LACASSIN, R. (2018). Fault flexure and lithospheric rheology set from climate cycles in the Corinth Rift, Geology.

DE GELDER, G., JARA-MUÑOZ, J., MELNICK, D., FERNÁNDEZ-BLANCO, D., ROUBY, H., PEDOJA, K., HUSSON, L., ARMIJO, R., LACASSIN, R. (2018). How do sea-level curves influence modeled marine terrace sequences? doi:10.31223/osf.io/bp4a

DELMAS, M., CALVET, M., GUNNELL, Y., VOINCHET, P., MANEL, C., BRAUCHER, R., TISSOUX, H.,BAHAIN, J.J.,PERRENOUD, C., SAOS, T. ASTER TEAM. (2018). Terrestrial 10Be and electron spin resonance dating of fluvial terraces quantifies quaternary tectonic uplift gradients in the eastern Pyrenees. Quaternary Science Reviews, 193, pp. 188–211.

DE VICENTE, G., CLOETINGH, S., MUÑOZ-MARTÍN, A., OLAIZ, A., STICH, D., VEGAS, R., GALINDO-ZALDÍVAR, J., FERNÁNDEZ-LOZANO, J.(2008). Inversion of moment tensor focal mechanisms for active stresses around the microcontinent Iberia: Tectonic implications. Tectonics 27. doi:10.1029/2006TC002093

DE VICENTE, G., VEGAS, R. (2009). Large-scale distributed deformation controlled topography along the western Africa–Eurasia limit: tectonic constraints. Tectonophysics, 474(1-2), pp. 124–143.

DE VICENTE G., CLOETINGH S., VAN WEES J.D., CUNHA P.P. (2011). Tectonic classification of Cenozoic Iberian foreland basins. Tectonophysics 502(1–2), pp.38–61. doi:10.1016/j.tecto.2011.02.007

DE VICENTE, G., CUNHA, P. P., MUÑOZ-MARTÍN, A., CLOETINGH, S. A. P. L., OLAIZ, A., VEGAS, R,. (2018). The Spanish-Portuguese Central System: An example of intense intraplate deformation and strain partitioning. Tectonics, 37(12), pp. 4444–4469.

DE VICENTE, G., CUNHA, P.P., MUÑOZ-MARTÍN, A., CLOETINGH, S.A.P.L., OLAIZ, A., VEGAS, R. (2018). The Spanish-Portuguese Central System: an example of intense intraplate deformation and strain partitioning. Tectonics, 37, pp. 1-26. doi: 10.1029/2018TC005204

DEL VAL, M., DUVAL, M., MEDIALDEA, A., BATEMAN, M.D., MORENO, D., ARRIOLABENGOA, M., ARANBURU, A., IRIARTE, E. (2019). First chronostratigraphic framework of fluvial terrace systems in the eastern Cantabrian margin (Bay of Biscay, Spain). Quat. Geochronol. 49, pp. 108–114. doi:10.1016/j.quageo.2018.07.001

DELGADO, J.F.N.. (1884). La Grotte de Furninha a Peniche, in: Congrès International d'Anthropologie et d'Archéologie Préhistoriques. Compte-rendu de La Neuvième Session à Lisbonne (1880). Académie Royale des Sciences, Lisbonne, pp. 207–279.

DEMOULIN, A., MATHER, A., WHITTAKER, A. (2017). Fluvial archives, a valuable record of vertical crustal deformation. Quaternary Science Reviews, 166, pp. 10–37.

DEMURO, M., ARNOLD, L. J., DUVAL, M., MÉNDEZ-QUINTAS, E., SANTONJA, M., PÉREZ-GONZÁLEZ, A. (2020). Refining the chronology of Acheulean deposits at Porto Maior in the River Miño basin (Galicia, Spain) using a comparative luminescence and ESR dating approach. Quaternary International. 556, pp. 96–112.

DESPRAT, S., GOÑI, M. F. S., TURON, J. L., DUPRAT, J., MALAIZÉ, B., PEYPOUQUET, J. P. (2006. Climatic variability of Marine Isotope Stage 7: direct land–sea–ice correlation from a multiproxy analysis of a north-western Iberian margin deep-sea core. Quaternary Science Reviews, 25, pp. 9–10, 1010-1026.

DIAS, J.A. AND BASTOS,M.R. (2017). De ínsula a península: o caso de Peniche (Portugal). In: Silvia Dias Pereira et al., O Homem e o Litoral: Transformações na paisagem ao longo do tempo, pp. 79–82, Rio de Janeiro. ISBN 978-85-5676-018-0

DINIS, P. A., OLIVEIRA, A. (2016). Provenance of Pliocene clay deposits from the Iberian Atlantic Margin and compositional changes during recycling. Sedimentary Geology, 336, pp.171–182, doi:10.1016/j.sedgeo.2015.12.011

DINIZ, F. (1984). Apports de la palynology à la connaissance du Pliocène portugais. Rio Maior : un basin de référence pour l´histoire de la flore, de la végétation et du climat de la façade atlantique de l´Europe meridionale. Dissertação de Doutoramento, Université des Sciences et Techniques de Languedoc, Montpellier, 230 p.

DINIZ, F. (2001). Aspects of the Plio-Quaternary Transition in Rio Maior: Pollen Records, Vegetation and Climate. /Actas V Reunião do Quaternário Ibérico – I Congresso do Quaternário de Países de Línguas Ibéricas, pp.109–112.

DINIZ, F. (2003). Os depósitos detrítico-diatomíticos de Abum (Rio Maior). Novos aspectos paleoflorísticos e implicações paleoclimáticas. Ciências da Terra, no especial V, p. 7.

DINIZ, F. AND MÖRNER, N.A. (1995). The Reuverian / Pretiglian transition in Rio Maior, Portugal. XIV International Congress INQUA, Schriften der Alfred-Wegner-Stiftung 2, pp. 95 – 100.

DINIZ, F., DA SILVA, C. M., CACHÃO, M. (2016). O Pliocénico de Pombal (Bacia do Mondego, Portugal Oeste): biostratigrafia, paleoecologia e paleobiogeografia. Estudos do Quaternário/Quaternary Studies, 14, pp. 41–59.

DOLFUS G.F., COTTER, J.C.B. (1909). Mollusques tertiaries du Portugal. Le Pliocène au nord du Tage (Plaisancian). 1re Partie. Pelecypoda. Mem.Com. Serv. Geol. Portugal. Lisboa, 40, pp.1–103.

DOWSETT, H.J., POORE, R.Z. 1991. Pliocene sea surface temperatures of the North Atlantic Ocean at 3.0 Ma. Quaternary Science Reviews 10, pp.189–204.

DOWSETT, H., BARRON, J., POORE, R. (1996). Middle Pliocene sea surface temperatures: A global reconstruction. Mar. Micropaleontol. 27, 13–25. doi:10.1016/0377-8398(95)00050-X

DOWSETT, H., FOLEY, K., STOLL, D., RIESSELMAN, C.R., ROBINSON, M.M., STROTHER, S. L., CHANDLER, M .A., SOHL,L.E., JONAS, J.A., BENTSEN, M., NISANCIOGLU, K.H., ZHANG,Z., OTTO-BLIESNER, B.L., ROSENBLOOM, N.A., BRAGG, F., LUNT, D.J., CHAN, W.L., AB-OUCHI, A., CONTOUX, C., RAMSTEIN, G., DOLAN, A., HAYWOOD,A., KAMAE, Y., UEDA, H., YAN, Q., ZANG, Z. (2013). Sea Surface Temperature of the mid-Piacenzian Ocean: A Data-Model Comparison. Sci Rep 3, 2013 doi:10.1038/srep0201

DUARTE, L.V. (2004). The geological heritage of the lower jurassic of central Portugal: selected sites, inventory and main scientific arguments. Rivista Italiana di Paleontologia e Stratigrafia, 110 (1), pp.381–388.

DUARTE, L.V. AND SOARES, A.F. (2002).Litostratigrafia das séries margo-calcárias do Jurássico inferior da Bacia Lusitânica (Portugal). Com.Inst.Geol. e Min. 89, pp.135–154.

DUARTE, D., VOLOCHAY, K., MAGALHÃES, R., AMARO, S., CABRAL, J. (2014). Caracterização dos terraços marinhos entre Cascais e Cabo da Roca,com recurso a elementos cartográficos e de detecção remota.Implicações Neotectónicas.Geonovas, 7, pp. 39-46.

DUTTINE, M., VILLENEUVE, G., BECHTEL, F., DEMAZEAU, G. (2002). Caractérisation par résonance paramagnétique électronique (RPE) de quartzs naturels issus de différentes sources. C.R. Geoscience 334, pp.949–955.

DUTTON, A., CARLSON, A.E., LONG, A.J., MILNE, G.A., CLARK, P.U., DECONTO, R., HORTON, B.P., RAHMSTORF, S., RAYMO, M.E. (2015). Sea-level rise due to polar ice-sheet mass loss during past warm periods. Science (80). doi:10.1126/science.aaa4019

DUVAL, M.(2008). Evaluation du potentiel de la méthode de datation per Résonance de Spin Electronique (ESR) appliquée aux gisements du Pléistocène inérieur: étude des gisements d'Orce (bassin de Guadix-Baza, Espagne) et contribution à la connaissance des premiers peupleme.

DUVAL, M. (2012). Dose response curve of the ESR signal of Aluminium center in quartz grains extracted from sediment. Anc. TL 30 (2), pp. 41–49.

DUVAL, M., GRÜN, R., FALGUERES, C., BAHAIN, J. J., DOLO, J. M. (2009). ESR dating of Lower Pleistocene fossil teeth: limits of the single saturating exponential (SSE) function for the equivalent dose determination. Radiation Measurements, 44(5-6), 477–482.

DUVAL, M.AND GUILARTE, V. (2012). Assessing the influence of the cavity temperature on the ESR signal of the Aluminum center in quartz grains extracted from sediment. Anc. TL 30 (2), pp. 51–56.

DUVAL, M., FALGUÈRES, C., BAHAIN, J., GRÜN, R., SHAO, Q., AUBERT, M., DOLO, J., AGUSTÍ, J., MARTÍNEZ-NAVARRO, B., PALMQVIST, P., AND TORO-MOYANO, I. (2012). On the limits of using combined U-series/ESR method to date fossil teeth from two Early Pleistocene archaeological sites of the Orce area (Guadix-Baza basin, Spain). Quaternary Research, 77, pp.482–491.

DUVAL, M. AND GUILARTE, V. (2015). ESR dosimetry of optically bleached quartz grains extracted from Plio-Quaternary sediment: evaluating some key aspects of the ESR signal associated to the Ti-center. Radiat. Meas. 78, pp. 28–41. doi:10.1016/j.radmeas.2014.10.002

DUVAL, M., SANCHO, C., CALLE, M., GUILARTE, V., AND PEÑA-MONNÉ, J. L. (2015). On the interest of using the multiple center approach in ESR dating of optically bleached quartz grains: Some examples from the Early Pleistocene terraces of the Alcanadre River (Ebro basin, Spain). Quaternary Geochronology, 29, pp.58–69.

DUVAL, M., BAHAIN, J. J., BARTZ, M., FALGUERES, C., GUILARTE, V., MORENO GARCÍA, D., ARNOLD, L. J. (2017). Defining minimum reporting requirements for ESR dating of optically bleached quartz grains. Ancient TL, 35 (1), pp. 11–19.

DUVAL, M., VOINCHET, P., ARNOLD, L.J., PARÉS, J.M., MINNELLA, W., GUILARTE, V., DEMURO, M., FALGUÈRES, C., BAHAIN, J.-J., DESPRIÉE, J. (2020). A multi-technique dating study of two Lower Palaeolithic sites from the Cher valley (Middle Loire Catchment, France): Lunery-la Terre-des-Sablons and Brinay-la Noira. Quat. Int., 556, pp.71-87.

EL KADIRI, K., DE GALDEANO, C.S., PEDRERA, A., CHALOUAN, A., GALINDO-ZALDÍVAR, J., JULIÀ, R., AKIL, M., HLILA, R., AHMAMOU, M. (2010). Eustatic and tectonic controls on Quaternary Ras Leona marine terraces (Strait of Gibraltar, northern Morocco). Quat. Res. 74, 277–288. doi:10.1016/j.yqres.2010.06.008

EULER, F. K., KAHAN, A. (1987). Radiation effects and anelastic loss in germanium-doped quartz. Phys. Rev. B 35, 4351–4359. doi:10.1103/PhysRevB.35.4351

FALGUÈRES, C. (1986). Datation de sites acheuléens et moustériens du Midi méditerranéen par la méthode de résonance de spin électronique. Thèse doctorale du Muséum National d'Histoire Naturelle de Paris.

FALGUÈRES C., YOKOYAMA Y., MIALLIER D. (1991). Stability of some centres in quartz. Nucl. Tracks Radiat. Meas., 18, 155–161.

FALGUÈRES, C., BAHAIN, J.J., SALEKI, H. (1997). U-series and ESR dating of teeth from Acheulian and Mousterian levels at La Micoque (Dordogne, France). Journal of Archaeological Science 24, pp.537–545.

FALGUÈRES, C., BAHAIN, J. J., YOKOYAMA, Y., ARSUAGA, J. L., BERMÚDEZ DE CASTRO, J. M., CARBONELL, E., BISCHOFF, J. L., DOLO, J. M. (1999). Earliest humans in Europe: the age of TD6 Gran Dolina, Atapuerca, Spain. Journal of Human Evolution 37, pp. 343–352.

FALGUÈRES, C., BAHAIN, J.J. (2002). La datation par résonance paramagnétique électronique (RPE). In: Miskovsky, J.C. (Ed.), Geologie de la Préhhistoire. Méthodes, techniques, applications, Seconde édition. Géoopré, pp. 1273–1296.

FALGUÈRES, C., BAHAIN, J.J., PEREZ-GONZALEZ, A., MERCIER, N., SANTONJA, M., DOLO, J.M., (2006). The lower Acheulian site of Ambrona, Soria (Spain): ages derived from a combined ESR/U-series model. Journal of Archaeological Science 33, pp.149–157.

FALGUÈRES, C., BAHAIN, J. J., DUVAL, M., SHAO, Q., HAN, F., LEBON, M., MERCIER, N., PÉREZ-GONZÁLEZ, A., DOLO, J. M., GARCIA, T. (2010). A 300-600 ka ESR/U-series chronology of Acheulian sites in Western Europe. Quaternary International pp. 223-224, issue 1, 293–298.

FALGUÈRES, C., SÉMAH, F., SALEKI, H., TU, H., FÉRAUD, G., SIMANJUNTAK, H., WIDIANTO, H. (2015). Geochronology of early human settlements in Java: What is stake? Quaternary International, pp. 1-7.

FATTIBENE, P., AND CALLENS, F. (2010). EPR dosimetry with tooth enamel: a review. Applied Radiation and Isotopes, 68(11), pp. 2033–2116.

FERNANDES, R. M. S., MIRANDA, J. M., MEIJNINGER, B. M. L., BOS, M. S., NOOMEN, R., BASTOS, L., AMBROSIUS, B.A.C., RIVA, R. E. M. (2007). Surface velocity field of the Ibero-Maghrebian segment of the Eurasia-Nubia plate boundary. Geophysical Journal International, 169(1), pp. 315–324.

FERNÁNDEZ-SALAS, L.M., DURÁN, R., CANALS, M., RIBÓ, M., MENDES, I., ROSA, F., GALPARSORO, I., LOBO, F.J., BÁRCENAS, P., GARCÍA-GIL, S., FERRÍN, A., CARRARA, G., ROQUE, C. (2015). Shelves of the Iberian Peninsula and the Balearic islands (I): Morphology and sediment types. Bol. Geol. y Min. 126, pp. 327–376.

FERREIRA, D. B. (1981). Carte Géomorphologique du Portugal. Memórias do Centro de Est. Geogr., 6.

FIGUEIREDO, P. (2014). Neotectonics of the Southwest Portugal Mainland: Implications on the regional seismic hazard. Doctoral dissertation. Univ. Lisboa, (Portugal), 261 p.

FIGUEIREDO, P. M., CABRAL, J., ROCKWELL, T. K. (2013). Recognition of Pleistocene marine terraces in the southwest of Portugal (Iberian Peninsula): evidences of regional Quaternary Uplift. Annals of Geophysics,56(6), S0672. doi: 10.4401/ag-6276.

FIGUEIREDO, P. M., ROCKWELL, T. K., CABRAL, J., LIRA, C. P. (2019). Morphotectonics in a low tectonic rate area: Analysis of the southern Portuguese Atlantic coastal region. Geomorphology, 326, pp. 132–151.

FIGUEIREDO, S.M.D. (2010). A Avifauna Plistocénica de Portugal: especificidades evolutivas, anatómicas e o seu contexto paleontológico, geológico e arqueológico. PhD Thesis. Univer. Salamanca. doi: 10.14201/gredos.76422

FIGUEIREDO, S., ROSA, M.A. (2014). Indicadores Paleoecológicos Resultantes do Estudo da Avifauna do Plistocénico Médio e Superior Português: evolução paleoclimática e comparação com os ambientes atuais, in: Arqueofauna e Paisagem. pp. 37–41.

FIGUEIREDO, S.D., CUNHA, P.P., SOUSA, F., PEREIRA, T., ROSA, A. (2017). Pleistocene Birds of Gruta da Furninha (Peniche-Portugal): A Paleontological and Paleoenvironmental Aproach. J. Environ. Sci. Eng. A 6, pp. 502–509. doi:10.17265/2162-5298/2017.10.003

FLEMING, N.C., HARFF, J., MOURA, D., BURGESS, A., BAILEY, G.N. (2017). Submerged landscapes of the European Continental shelf: Quaternary paleoenvironments. Wiley Blackwell 552 p.

FOLK, R. L. AND WARD, W. C. (1957). Brazos River bar [Texas]; a study in the significance of grain size parameters. Journal of Sedimentary Research, 27(1), pp. 3–26.

FONSECA, A. F., ZÊZERE, J. L., NEVES, M. (2015). Contribuição para o conhecimento da geomorfologia da Cadeia da Arrábida (Portugal): cartografia geomorfológica e geomorfometria. Revista Brasileira de Geomorfologia, 16(1).

FONSECA, A. F., ZÊZERE, J. L., NEVES, M. (2020). The Arrábida Chain: The Alpine Orogeny in the Vicinity of the Atlantic Ocean. In Landscapes and Landforms of Portugal, pp. 273–278. Springer, Cham.

FRANÇA, J.C., ZBYSZEWSKI, G., MOITINHO DE ALMEIDA, F., 1960. Carta Geológica de Portugal, à escala 1:50 000. Notícia explicativa da Folha 26-C (Peniche). Serviços Geológicos de Portugal, 33.

GALVE, J.P., PÉREZ-PEÑA, J.V., AZAÑÓN, J.M., PEREIRA, D.M.I., CUNHA, P.P., PEREIRA, P., ORTUÑO, M., VIAPLANA-MUZAS, M., GRACIA PRIETO, F.J., REMONDO, J., JABALOY, A., BARDAJÍ, T., SILVA, P.G., LARIO, J., ZAZO, C., GOY, J.L., DABRIO, C.J., CABERO, A. (2019). Chapter 5 - Active Landscapes of Iberia, pp. 77-124, In: C. Quesada and J. T. Oliveira (eds). The Geology of Iberia: A Geodynamic Approach. Springer Nature Switzerland AG, Regional Geology Reviews, Vol. 5 – Active Processes: Seismicity, Active Faulting and Relief (eBook ISBN 978-3-030-10931-8; doi: 10.1007/978-3-030-10931-8–5

GIBBARD, P., COHEN, K. M.(2008). Global chronostratigraphical correlation table for the last 2.7 million years. Episodes, 31(2), 243p.

GONZÁLEZ-ACEBRÓN, L., MAS, R., ARRIBAS, J., GUTIÉRREZ-MAS, J.M., PÉREZ-GARRIDO, C. (2016). Very coarse-grained beaches as a response to generalized sea level drops in a complex active tectonic setting: Pleistocene marine terraces at the Cadiz coast, SW Spain. Mar. Geol. 382, pp. 92–110. doi:10.1016/j.margeo.2016.09.007

GOUVEIA, M.P., CUNHA, P.P., FALGUÈRES, C., VOINCHET, P., MARTINS, A.A., BAHAIN, J.J., PEREIRA, A. (2020). Electron spin resonance dating of the culminant allostratigraphic unit of the Mondego and Lower Tejo Cenozoic basins (W Iberia), which predates fluvial incision into the basin-fill sediments. Glob Plan.Chan. 184, 103081. doi:10.1016/j.gloplacha.2019.103081

GOY ZAZO, C., SILVA, P.G., LARIO, J., BARDAJÍ, T., SOMOZA, L., J.L., 1995. Evaluación geomorfológica del comportamiento neotectónico del Estrecho de Gibraltar (Zona Norte) durante el Cuaternario. IV Coloq. Int. sobre el enlace fijo del Estrecho Gibraltar. Sevilla pp. 51–69.

GRAHAM , A.G.C., STOKER, M. S., LONERGAN, L., BRADWELL, T., STEWART, M.A. (2011). Chapter 21-The Pleistocene Glaciations of the North Sea basin. Developments in Quaternary Sciences, 15, 261–278. doi:10.1016/B978-0-444-53447-7.00021-0

GRÜN, R. (1989). Electron spin resonance (ESR) dating. Quaternary International 1, pp.65-109.

GRÜN, R. (1994). A cautionary note: use of water content' and 'depth for cosmic ray dose rate' in AGE and DATA programs. Anc. TL 12, pp.50–51.

GRÜN, R., KATZENBERGER-APEL, O. (1994). An alpha irradiator for ESR dating. Ancient TL 2, pp. 35–38.

GRÜN, R., AND MCDERMOTT, F. (1994). Open system modelling for U-series and ESR dating of teeth. Quaternary Geochronology 13, pp.121–125.

GRÜN, R. (1997). Electron Spin Resonance Dating. Dans "Chronometric Dating in Archaeology." (T. a. Aitken, Ed.), pp. 217–260. Plenum Press, New York.

GRÜN, R., MAROTO, J., EGGINS, S., STRINGER, C., ROBERTSON, S., TAYLOR, L, MORTIMER, G., MCCULLOCH, M. (2006). ESR and U-series analyses of enamel and dentine fragments of the Banyoles mandible. Journal of Human Evolution, 50(3), pp. 347–358.

GUÉRIN, G., MERCIER, N., ADAMIEC, G. (2011). Dose-rate conversion factors: update. Ancient TL 29, pp. 5–8.

GUÉRIN, G., MERCIER, N., NATHAN, R., ADAMIEC, G., LEFRAIS, Y. (2012). On the use of the infinite matrix assumption and associated concepts: A critical review, in: Radiation Measurements. pp. 778–785. doi:10.1016/j.radmeas.2012.04.004

GUTIÉRREZ, F., MORENO, D., LÓPEZ, G. I., JIMÉNEZ, F., DEL VAL, M., ALONSO, M. J., MARTINEZ-PILADO, V., GUZMÁN, O., MARTINEZ, D., CARBONEL, D. (2020). Revisiting the slip rate of Quaternary faults in the Iberian Chain, NE Spain. Geomorphic and seismic-hazard implications. Geomorphology, 107233.

HANSON, K. L., WESLING, J. R., LETTIS, W. R., KELSON, K. I., MEZGER, L. (1994). Correlation, ages, and uplift rates of Quaternary marine terraces: South-central coastal California. Special Papers-Geological Society of America, pp.45–45.

HARLÉ, E., 1910. Les mammifères et oiseaux quaternaires connus jusqu'ici en Portugal. : Mémoire suivi d'une liste générale de ceux de la péninsule ibérique. Comun. dos Serviços Geológicos Port. 8, pp. 22–85.

HARVEY, A. M., MATHER, A.E., STOKES, M. (2005). Alluvial Fans: Geomorphology, Sedimentology, Dynamics. Geological Society, London, Special Publications, 251, pp.1–7.

HAWS, J.A., BENEDETTI, M.M., FUNK, C.L., DANIELS, J.M., HESP, P. A., BICHO, N.F., MINCKLEY, T. A., ELLWOOD, B.B., FORMAN, S.L. (2009). Late Pleistocene raised beaches of coastal Estremadura, central Portugal. Quat. Sci. Rev. 28, pp.3428–3447. doi:10.1016/j.quascirev.2009.09.029

HAWS, J. A., FUNK, C. L., BENEDETTI, M. M., BICHO, N. F., DANIELS, J. M., MINCKLEY, T. A., DENNISTON, R.F., JERAJ, M., GIBAJA, J.F., HOCKETT, B.S., FORMAN, S. L. (2011). Paleolithic landscapes and seascapes of the west coast of Portugal. In Trekking the Shore, Springer, New York, NY, pp.203–246.

HAYWOOD, A.M., DOWSETT, H.J., ROBINSON, M.M., STOLL, D.K., DOLAN, A.M., LUNT, D.J., OTTO-BLIESNER, B., CHANDLER, M.A. (2011). Geoscientific Model Development Pliocene Model Intercomparison Project (PlioMIP): experimental design and boundary conditions (Experiment 2). Geosci. Model Dev 4, pp. 571–577. doi:10.5194/gmd-4-571-2011

HAYWOOD, A.M., RIDGWELL, A., LUNT, D.J., HILL, D.J., POUND, M.J., DOWSETT, H.J., DOLAN, A.M., FRANCIS, J.E., WILLIAMS, M. (2011). Are there pre-Quaternary geological analogues for a future greenhouse warming? Philosophical Transactions of the Royal Society A: Mathematical, Physical and Engineering Sciences 369, pp. 933–956.

HAYWOOD, A. M., DOWSETT, H. J., DOLAN, A. M., ROWLEY, D., ABE-OUCHI, A., OTTO-BLIESNER, B., CHANDLER, M. A., HUNTER, S. J., LUNT, D. J., POUND, M., SALZMANN, U. (2016).The Pliocene Model Intercomparison Project (PlioMIP) Phase 2: scientific objectives and experimental design, Clim. Past, 12, pp. 663–675, doi:10.5194/cp-12-663-2016,.

HE, Z., ZHANG, X., BAO, S., QIAO, Y., SHENG, Y., HE, X, YANG, X., ZHAO, J., LIU, X., LU, C. (2015). Multiple climatic cycles imprinted on regional uplift-controlled fluvial terraces in the lower Yalong River and Anning River, SE Tibetan Plateau. Geomorphology, 250, pp. 95–112.

HENNIG, G. J., AND GRÜN, R. (1983). ESR dating in Quaternary geology. Quaternary Science Reviews, 2(2-3), pp. 157–238.

HENRIQUES, M.V. AND NETO, C. (2002). Caracterização geo-ecológica dos sistemas de cordões dunares da Estremadura Nazaré, S. Martinho do Porto e Peniche-Baleal). Finisterra XXXVII, 74, pp. 5–31.

HILLAIRE-MARCEL, C., CARRO, O., CASANOVA, J. (1986). 14C and ThU dating of Pleistocene and Holocene stromatolites from East African paleolakes. Quaternary Research, 25(3), pp. 312–329.

HILLAIRE-MARCEL, C., GARIÉPY, C., GHALEB, B., GOY, J.L., ZAZO, C., BARCELO, J.C. (1996). U-series measurements in Tyrrhenian deposits from mallorca - Further evidence for two last-interglacial high sea levels in the Balearic Islands. Quat. Sci. Rev. 15, pp. 53–62. doi:10.1016/0277-3791(95)00079-8

IKEDA, S., AND IKEYA, M. (1992). Electron spin resonance (ESR) signals in natural and synthetic gypsum: An application of ESR to the age estimation of gypsum precipitates from the San Andreas Fault. Japanese journal of applied physics, 31(2A), L136.

IKEYA, M. (1975). Dating a stalactite by electron paramagnetic resonance. Nature 255, pp. 48–50.

IKEYA, M. (1978). Electron spin resonance as a method of dating. Archaeometry 20, pp. 147–158.

IKEYA, M. (1993). New applications of Electron Spin Resonance Dating, Dosimetry and Microscopy Eds Worl Scientific, 500 p.

JAHN, A. (1956). Geomorphology and Quaternary history of Lublin plateau (Vol. 7). Państwowe Wydawn. Naukowe.

JANSEN, E., OVERPECK, J., BRIFFA, K.R., DUPLESSY, J.C., JOOS, F., MASSON-DELMOTTE, V., OLAGO, D., OTTO-BLIESNER, B., PELTIER, W.R., RAHMSTORF, S., RAMESH, R., RAYNAUD, D., RIND, D., SOLOMINA, O., VILLALBA, R., D. ZHANG. (2007). Paleoclimate. In Climate change 2007: the physical science basis. Contribution of Working Group I to the Fourth Assessment Report of the Intergovernmental Panel on Climate Change. Solomon, S., Qin, D., Manning, M., Chen, Z., Marquis, M., Averyt, K.B., Tignor, M., Miller, H.L., Eds. Cambridge University Press, pp. 433-497.

JIA, Z., PEI, S., BENITO-CALVO, A., MA, D., SANCHEZ-ROMERO, L., WEI, Q. (2019). Site formation processes at Donggutuo: a major Early Pleistocene site in the Nihewan Basin, North China. Journal of Quaternary Science, 34(8), pp. 621–632.

JIMÉNEZ-MORENO, G., FAUQUETTE, S., SUC , J.P. (2010). Miocene to Pliocene vegetation reconstruction and climate estimates in the Iberian Peninsula from pollen data. Review of Palaeobotany and Palynology, Volume 162, 3, pp. 403–415.

JOHNSTON, A. C. (1996). Seismic moment assessment of earthquakes in stable continental regions—III. New Madrid 1811–1812, Charleston 1886 and Lisbon 1755. Geophysical Journal International,126, pp. 314–344. doi:10.1111/j.1365-246X.1996. tb070 28.x.

JONAS, M. (1997). Concepts and methods of ESR dating. Radiation Measurements, 27(5-6), pp. 943–973.

JULL, A. T. (2013). Electron spin resonance dating. In Encyclopedia of Quaternary Science: Second Edition (pp. 667-677). Elsevier Inc.

KENNETH G. MILLER1, M.E. RAYMO2, J.V. BROWNING1, Y. ROSENTHAL1 AND J.D. WRIGHT, (2019). Peak sea level during the warm Pliocene: Errors, limitations, and constraints. Pages Magazine 27 (1), doi:10.22498/pages.27.1.4

KITABA, I., HARADA, M., HYODO, M., KATOH, S., SATO, H., MATSUSHITA, M. (2011). MIS 21 and the Mid-Pleistocene climate transition: Climate and sea-level variation from a sediment core in Osaka Bay, Japan. Palaeog., Palaeoc., Palaeoec., 299 (1-2), pp. 227–239. doi:10.1016/j.palaeo.2010.11.004

KUKLA, G. J. (1975). Loess stratigraphy of Central Europe.K.W. Butzer, G.L. Isaac (Eds.), After the Australopithecines: Stratigraphy, Ecology and Culture Change in the Middle Pleistocene, Mouton, The Hague, pp. 99–188.

KUKLA, G. J. (1977). Pleistocene land-sea correlations. I. Europe. Earth Science Reviews, 13, pp. 307–374.

KULLBERG, J. C., KULLBERG, M. C. (2017). The tectono-stratigraphic evolution of an Atlantic-type basin: an example from the Arrábida sector of the Lusitanian Basin. Ciências da Terra / Earth Sciences Journal, (19), 1, pp. 55-74.

LABEYRIE, L.D., DUPLESSY, J.C., BLANC, P.L. (1987). Variations in mode of formation and temperature of oceanic deep waters over the past 125,000 years. Nature 327, pp. 477–482. doi:10.1038/327477a0

LAJOIE, E., (1986). Coastal Tectonics, active tectonics, Studies in Geophysics—Active Tectonics. National Academy Press, Washington, DC.

LAJOIE, K. R., PONTI, D. J., POWELL II, C. L., MATHIESON, S. A., SARNA-WOJCICKI, A. M. (1992). Emergent marine strandlines and associated sediments, coastal California; a record of Quaternary sea-level fluctuations, vertical tectonic movements, climatic changes, and coastal processes, pp. 81–104.

LAMBECK, K., CHAPPELL, J., (2001). Sea level change through the last glacial cycle. Science (80-.). doi:10.1126/science.1059549

LAMBECK, K., ROUBY, H., PURCELL, A., SUN, Y., & SAMBRIDGE, M. (2014). Sea level and global ice volumes from the Last Glacial Maximum to the Holocene. Proceedings of the National Academy of Sciences, 111(43), pp. 15296–15303.

LAMBECK, K.,CHAPPELL, J. (2001). Sea level change through the last glacial cycle. Science, 292 (5517), pp.679–686. doi:10.1126/science.105954

LAPLACE, G. (1966). Recherch sur L'Origine et L'èvolution des Complexes Leptolithiques. çcole Franéaise de Rome. Mélanges D'Archéologie et D'Histoire, Suppléments 4, Paris. 641 p.

LAURENT, M (1993). "Datation par résonance de spin électronique (ESR) de quartz de formations quaternaires: comparaison avec la paléomagnétisme." Thèse doctorale du Muséum National d'Histoire Naturelle de Paris.

LAURENT, M., FALGUÈRES, C., BAHAIN, J. J., ROUSSEAU, L. AND LANOË, B. V. V., (1998). ESR dating of quartz extracted from Quaternary and Neogene sediments: method, potential and actual limits. Quaternary Science Reviews, 17(11), pp.1057–1062.

LEWIN, J., GIBBARD, P. L. (2010). Quaternary river terraces in England: forms, sediments and processes. Geomorphology, 120(3-4), pp.293–301.

LI, J., (1991). The environmental effects of the uplift of the Qinghai-Xizang Plateau. Quaternary Scien. Rev., 10 (6), pp. 479–483. doi: 10.1016/0277-3791(91)90041-R

LISIECKI, L.E., RAYMO, M.E. (2006). A Pliocene-Pleistocene stack of 57 globally distributed benthic δ 18O records. Paleoceanography 20, pp.1–17. doi:10.1029/(2004)PA001071

LISIECKI, L.E., RAYMO, M.E. (2007). Plio-Pleistocene climate evolution: trends and transitions in glacial cycle dynamics. Quat. Sci. Rev. 26, pp.56–69. doi:10.1016/j.quascirev.2006.09.005

LIN, M., YIN, G., DING, Y., CUI, Y., CHEN, K., WU, C., XU, L. (2006). Reliability study on ESR dating of the aluminium center in quartz. Radiation Measurements 41, pp. 1045–1049.

LIU, C., GRÜN, R. (2011). Fluvio-mechanical resetting of the Al and Ti centres in quartz. Radiation Meas., 46(10), pp.1038–1042. Doi: 10.1016/j.radmeas.2011.06.076

LIU, C. R., YIN, G. M., HAN, F. (2015). Effects of grain size on quartz ESR dating of Ti–Li center in fluvial and lacustrine sediments. Quaternary Geochronology, 30, 513–518.

LÓPEZ, R. T., HEYDT, G. G. (2014). The Guadiana River: the role of tectonics on drainage configuration.

LÓPEZ-RECIO, M., SILVA, P. G., ROQUERO, E., CUNHA, P. P., TAPIAS, F., ALCARAZ-CASTAÑO, M., BAENA, J., CUARTERO, F., MORIN, J., TORRES, T, ORTIZ, J. E., MURRAY, A.S., BUYLART, J.P. (2015). Geocronología de los yacimientos achelenses de Pinedo y Cien Fanegas (Valle del Tajo) e implicaciones en la evolución fluvial en el entorno de Toledo (España). Estudios Geológicos, 71(1), pp.1-19. doi: 10.3989/egeol.41816.340

LOUTRE, M.F., BERGER, A. (2003). Marine Isotope Stage 11 as an analogue for the present interglacial, Global Planet. Change, 36, pp. 209–217.

LUDWIG, K.R.(2008). Isoplot 3.70, a geochronological toolkit for Microsoft Excel. Berkeley Geochronology Center Special Publi. 4.

MADDY, D., 1997. Uplift-driven valley incision and river terrace formation in southern England. Journal of Quaternary Science: Published for the Quaternary Research Association, 12(6), pp. 539–545.

MADDY, D., BRIDGLAND, D. R., GREEN, C. P. (2000). Crustal uplift in southern England: evidence from the river terrace records. Geomorphology, 33(3-4), pp.167–181.

MADRUGA, M. J., SILVA, L., GOMES, A. R., LIBÂNIO, A., REIS, M. (2014). The influence of particle size on radionuclide activity concentrations in Tejo River sediments. Journal of environmental radioactivity,132, pp. 65-72.

MAESTRO, A., LOPEZ-MARTÍNEZ, J., LLAVE, E., BOHOYO, F., ACOSTA, J., HERNÁNDEZ-MOLINA, F.J., MUNOZ, A., JANÉ, G. (2013). Geomorphology of the Iberian Continental Margin, Geomorphology, 196, pp. 13–35. doi: 10.1016/j.geomorph.2012.08.022

MARTÍN, J.M., BRAGA, J.C., AGUIRRE,J., PUGA-BERNABÉU, A. (2009). History and evolution of the North Betic Strait (Prebetic Zone, Betic Cordillera): a narrow, early Tortorian tidal –dominated, Atlantic –Mediterranean marine passage. Sediment. Geol. 216, pp. 80-90.

MARTÍNEZ-SOLARES, J. M. & LÓPEZ-ARROYO, A. ((2004)). The great historical 1755 earthquake. Effects and damage in Spain. Journal of Seismology, 8(2), pp. 275–294, doi: 10.1023/B:J OSE.0000021365.94606.03.

MARTINS, A.F. (1949). O esforço do homem na Bacia do Mondego. Tese de Licenciatura, Coimbra.

MARTINS, A.A. (1999).Caracterização morfotectónica e morfossedimentar da Bacia do Baixo Tejo (Pliocénico e Quaternário). Doctoral Thesis, Universidade Évora, Évora, 500 p. (em português) ("Morphotectonic and morphosedimentary characterization of the Lower Tagus Basin (Pliocene and Quaternary)

MARTINS, A. A., CUNHA, P. P., MATOS, J., GUIOMAR, N. (2009a). Quantificação da incisão do rio Tejo no sector entre Gavião e Chamusca, usando os terraços fluviais como referências geomorfológicas. Publ. Ass.Port.Geomorf., VI, pp. 83–86.

MARTINS, A. A., CUNHA, P. P., HUOT, S., MURRAY, A. S., BUYLAERT, J. P. (2009b). Geomorphological correlation of the tectonically displaced Tejo River terraces (Gavião–Chamusca area, central Portugal) supported by luminescence dating. Quaternary International, 199(1-2), pp. 75–91.

MARTINS, A.A. CUNHA, P.P., BUYLAERT, J. P., HUOT, S, MURRAY, A.S., DINIS, P., STOKES, M. (2010a). K-Feldspar IRSL dating of a Pleistocene river terrace staircase sequence of the Lower Tejo River (Portugal, western Iberia). Quaternary Geochronology, Volume 5, Issues 2-3, pp. 176–180. doi: 10.1016/j.quageo.2009.06.004

MARTINS, A.A., CABRAL, J., CUNHA, P.P., STOKES, M., BORGES, J., CALDEIRA, B., CARDOSO MARTINS, A. (2017). Tectonic and lithological controls on fluvial landscape development in central- eastern Portugal: insights from long profile tributary stream analyses. Geomorphology, 276, pp. 144–163.

MARTINS, A., CUNHA, P., PAIVA, A. (2017). Cartografia geomorfológica do vale inferior do rio Tejo (Alvega a Vila Franca de Xira, Portugal central).

MATHER, A.E., SILVA, P.G., GOY, J.L., HARVEY, A.M., ZAZO, C., (1995). Tectonics versus climate: an example from late Quaternary aggradational and dissectinal sequences of the Mula basin, southeast Spain. J. Lewin, M.G. Macklin, J.C. Woodward (Eds.), Mediterranean Quaternary river environments, Balkema, Rotterdam, pp. 77–87.

MATHER, A.E., STOKES, M., WHITFIELD, E. (2017). River terraces and alluvial fans: The case for an integrated Quaternary fluvial archive. Quaternary Science Reviews 166, pp. 74–90.

MAUZ, B., HIJMA, M.P., AMOROSI, A., PORAT, N.,GALILI, E., BLOMENDAL, J. (2013). aeolian beach ridges and their significance for climate and sealevel: concept and nsight from the Levant coast (Esat Mediterranean). Esarth Scien. Rev., 121, pp. 31–54.

MCMANUS, J., OPPO, D., CULLEN, J.L., HEALEY, S. (2003). Marine isotope stage 11 (MIS11): analog for Holocene and future climate? In: Droxler, A.W., Poore,R.Z., Burckle, L.H. (Eds.), Earth's Climate and Orbital Eccentricity: TheMarine Isotope Stage 11 Question. American Geophysical Union Mono-graph Series, Washington, DC, pp. 69–85

MCMORRIS, D.W. (1971). Impurity color centers in quartz and trapped electron dating: electron spin resonance, thermoluminescence studies. J. Geophys. Res. 76, pp.7875–7887.

MÉNDEZ-QUINTAS, E., SANTONJA, M., PÉREZ-GONZÁLEZ, A., DUVAL, M., DEMURO, M., ARNOLD, L. J. (2018). First evidence of an extensive Acheulean large cutting tool accumulation in Europe from Porto Maior (Galicia, Spain). Scientific reports, 8 (1), 3082.

MÉNDEZ-QUINTAS, E., SANTONJA, M., ARNOLD, L. J., CUNHA-RIBEIRO, J. P., DA SILVA, P. X., DEMURO, M., DUVAL, M.,GOMES, A., MEIRELES, J., MONTEIRO RODRIGUES, S.,& PÉREZ-GONZÁLEZ, A. (2020). The Acheulean Technocomplex of the Iberian Atlantic Margin as an Example of Technology Continuity Through the Middle Pleistocene. Journal of Paleolithic Archaeology, pp. 1–26.

MERCIER N., FALGUÈRES C. (2007). Field gamma dose-rate measurement with a NaI(Tl) detector: re-evaluation of the "threshold" technique. Ancient TL 25(1), pp. 1– 4.

MIALL, A.D. (1985). Architectural-element analysis: a new method of facies analysis applied to fluvial deposits. Earth-Science Reviews, 22(4), pp. 261–308.

MIALL, A.D. (1996). The Geology of Fluvial Deposits: Sedimentary Facies, Basin Analysis, and Petroleum Geology. Springer, Berlin.

MILANCOVICH, M., 1930. Mathematische Klimalehre und Astromnomische Theorie der Klimaschwankungen. Handbuch der Klimatologie, Band I, Teil A. GebruÌˆder Borntraeger, Berlin.

MILLER, K. G., KOMINZ, M. A., BROWNING, J. V., WRIGHT, J. D., MOUNTAIN, G. S., KATZ, M. E., SUGARMAN, P.J., BENJAMIN, S.C., CHRISTIE-BICK, N., PEKAN, S.F. (2005). The Phanerozoic record of global sea-level change. Science, 310(1), pp. 293–1298.

MILLER, K. G., MOUNTAIN, G. S., WRIGHT, J. D., BROWNING, J. V. (2011). A 180-million-year record of sea level and ice volume variations from continental margin and deep-sea isotopic records. Oceanography, 24(2), pp. 40–53. doi: 10.5670/oceanog.2011.26

MONGE SOARES A. M., MONIZ C., CABRAL J. (2006. A duna consolidada de Oitavos (a Oeste de Cascais – região de Lisboa) – a sua datação pelo método do radiocarbono. Com. Geológicas, 93, pp. 105–118.

MONIZ, C. M. D. F. B. (2010). Contributo para o conhecimento da falha de Pinhal Novo-Alcochete, no âmbito da neotectónica do vale inferior do Tejo (Doctoral dissertation).

MORENO, D., FALGUÈRES, C., PÉREZ-GONZÁLEZ, A., DUVAL, M., VOINCHET, P., BENITO-CALVO, A., ORTEGA, A.I., BAHAIN, J.J., SALA, R., CARBONEL, E., DE CASTRO, J. M. B., ARSUAGA, J.L. (2012). ESR chronology of alluvial deposits in the Arlanzón valley (Atapuerca, Spain): contemporaneity with Atapuerca Gran Dolina site. Quaternary Geochronology, 10, pp. 418–423.

MORENO, D., RICHARD, M., BAHAIN, J. J., DUVAL, M., FALGUÈRES, C., TISSOUX, H., VOINCHET, P. (2017). ESR dating of sedimentary quartz grains: some basic guidelines to ensure optimal sampling conditions. Quaternaire. Revue de l'Association française pour l'étude du Quaternaire, 28(2), pp. 161-166.

MORENO, D., DUVAL, M., RUBIO-JARA, S., PANERA, J., BAHAIN, J. J., SHAO, Q.,GONZALEZ, P., FALGUÈRES, C. (2019). ESR dating of Middle Pleistocene archaeo-paleontological sites from the Manzanares and Jarama river valleys (Madrid basin, Spain). Quaternary International, 520, pp. 23–38.

MÖRNER, N. A. (1987). Pre-Quaternary long-term changes in sea level. In Sea Surface Studies, Springer, Dordrecht pp. 233–241.

MOURA, D., GOMES, A., HORTA, J. (2017). The Iberian Atlantic margin. Submerged landscapes of the European continental shelf. Quaternary paleoenvironments. Wiley-Blackwell, Oxford, pp. 281–300.

MOZZI, P., AZEVEDO, M.T., NUNES, E., RAPOSO, L. (2000). Middle Terrace Deposits of the Tagus River in Alpiarça, Portugal, in relation to Early Human Occupation, Quaternary Research, 54: 359–371. (em inglês) ("Depósitos dos terraços médios do Rio Tejo em Alpiarça, Portugal, em relação à ocupação humana antiga") doi:10.1006/qres.2000.2154

MUHS, D. R., ROCKWELL, T. K., AND KENNEDY, G. L. (1992). Late Quaternary uplift rates of marine terraces on the Pacific coast of North America, southern Oregon to Baja California Sur. Quaternary International, 15, 121-133.MUHS, D.R. (2002). Evidence for the timing and duration of the last interglacial period from high-precision uranium-series ages of corals on tectonically stable coastlines. Quat. Res. 58, pp. 36–40. doi:10.1006/qres.2002.2339

MUHS, D.R., SIMMONS, K.R., KENNEDY, G.L., AND ROCKWELL, T.K. (2002). The last interglacial period on the Pacific Coast of North America. Geological Society of America Bulletin 114, pp. 569–592.

MUHS, D. R, PANDOLFI, J. M., SIMMONS, K. R. AND SCHUMANN, R. R. (2012) - Sea-level history of past interglacial periods: New evidence from uranium-series dating of corals from Curaçao, Leeward Antilles islands. Quaternary Research. doi: 10.1016/j.yqres.2012.05.008

MUHS, D.R., GROVES, L.T. (2019). Little Islands Recording Global Events: Late Quaternary Sea Level History and Paleozoogeography of Santa Barbara and Anacapa Islands, Channel Islands National Park, California. West. North Am. Nat. 78, 540. doi:10.3398/064.078.0403

MÜLLER, D.W.,(1993). Pliocene Transgression in the Western Mediterranean Sea: Strontium Isotopes from Cuevas Del Almanzora (Se Spain). AGU100, https://doi.org/10.1029/92PA02795

MURRAY-WALLACE, C. V. (2002). Pleistocene coastal stratigraphy, sea-level highstands and neotectonism of the southern Australian passive continental margin - A review. J. Quat. Sci. 17, pp. 469–489. doi:10.1002/jqs.717

MURRAY-WALLACE, C.V., WOODROFFE, C. (2014). Quaternary Sea-Level Changes: A Global Perspective. Cambridge University Press, Cambridge.

NOCQUET, J. M. AND CALAIS, E. (2004). Geodetic measurements of crustal deformation in the Western Mediterranean and Europe. Pure and applied geophysics, 161(3), pp. 661–681.

NORMAND, R., SIMPSON, G., HERMAN, F., HAQUE BISWAS, R., BAHROUDI, A., SCHNEIDER, B. (2019). Dating and morpho-stratigraphy of uplifted marine terraces in the Makran subduction zone (Iran). Earth Surf. Dyn. 7, pp. 321–344. doi:10.5194/esurf-7-321-2019.

O'CONNOR, S., BARHAM, A., SPRIGGS, M., VETH, P., APLIN, K., & ST PIERRE, E. (2010). Cave archaeology and sampling issues in the tropics: a case study from Lene Hara Cave, a 42,000-year-old occupation site in East Timor, Island Southeast Asia. *Australian Archaeology*, *71*(1), pp. 29–40.

ODRIOZOLA, C. P., BURBIDGE, C. I., DIAS, M. I., HURTADO, V. (2014). Dating of Las Mesas Copper Age walled enclosure (La Fuente, Spain). Trabajos de prehistoria, 71, pp. 343-352.

OLSZAK, J. (2017). Climatically controlled terrace staircases in uplifting mountainous areas. Glob. Planet. Change 156, pp. 13–23. doi:10.1016/j.gloplacha.2017.07.013

PAIS J. (1981). Contribuição para o conhecimento da vegetação miocénica da parte ocidental da bacia do Tejo. Ph.D., Univ. Nova Lisboa, 328 p.

PAIS J. (1992). Contributions to the Eocene paleontology and stratigraphy of Beira Alta, Portugal. III - Eocene plant remains from Naia and Sobreda (Beira Alta, Portugal). Ciências da Terra 11, pp. 91–108.

PAIS, J., CUNHA, P.P., PEREIRA, D., LEGOINHA, P., DIAS, R., MOURA, D., BRUM DA SILVEIRA, A., KULLBERG, J. C., GONZÁLEZ-DELGADO, J.A. (2012). The Paleogene and Neogene of Western Iberia (Portugal). A Cenozoic record in the European Atlantic domain. SpringerBriefs in Earth Sciences, Springer, Series ID: 8897, 1st Edition, 1 vol., 158 p.

PANITZ, S., SALZMANN, U., RISEBROBAKKEN, B., DE SCHEPPER, S., POUND, M. (2016). Climate variability and long-term expansion of peatlands in Arctic Norway during the late Pliocene (ODP Site 642, Norwegian Sea). Climate of the Past, 12, pp.1043–1060.

PEDOJA, K., HUSSON, L., JOHNSON, M.E., MELNICK, D., WITT, C., POCHAT, S., NEXER, M., DELCAILLAU, B., PINEGINA, T., POPRAWSKI, Y., AUTHEMAYOU, C., ELLIOT, M., REGARD, V., GARESTIER, F. (2014). Coastal staircase sequences reflecting sea-level oscillations and tectonic uplift during the Quaternary and Neogene. Earth-Science Rev. doi:10.1016/j.earscirev.2014.01.007

PEDOJA, K., JARA-MUÑOZ, J., DE GELDER, G., ROBERTSON, J., MESCHIS, M., FERNANDEZ-BLANCO, D., NEXER, M., POPRAWSKI, Y., DUGUÉ, O., DELCAILLAU, B., BESSIN, P., BENABDELOUAHED, M., AUTHEMAYOU, C., HUSSON, L., REGARD, V., MENIER, D., PINEL, B. (2018). Neogene-Quaternary slow coastal uplift of Western Europe through the perspective of sequences of strandlines from the Cotentin Peninsula (Normandy, France). Geomorphology 303, pp. 338–356. doi:10.1016/j.geomorph.2017.11.021

PEEL, M.C., FINLAYSON, B.L., MCMAHON, T.A.(2007).Updated world map of the Koppen-Geiger climate classification. Hidrol. Earth Syst. Sci., pp.1633–1644.

PELEGRIN, J. (1990). Prehistoric lithic technology: some aspects of research. Archeological Review from Cambridge, 9(1), pp. 116–125.

PEREIRA, A. R. (1991). A margem continental portuguesa. Breve síntese do conhecimento actual. Finisterra, 26 (51).

PEREIRA, A. R., NEVES, M., TRINDADE, J.,BORGES, B., ANGELUCCI, D., SOARES,A. (2020). Dunas carbonatadas e depósitos correlativos na Estremadura (Portugal). Variações do nível do mar e neotectónica.

PEREIRA, A. R., REGNAULD, H. (1994). Litorais quaternários (emersos e submersos) na extremidade sudoeste da Arrábida (Portugal). Contribuições para a Geomorfologia e Dinâmicas Litorais em Portugal, pp. 55–53.

PÉREZ-GONZÁLEZ, A., RUBIO-JARA, S. PANERA, J. & URIBELARREA, D. (2008). Geocronología de la sucesión arqueoestratigráfica de Los Estragales en la Terraza Compleja de Butarque (Valle del río Manzanares, Madrid). Geogaceta, 45, pp. 39–42.

PIRAZZOLI, P.A. (2005)A. A review of possible eustatic, isostatic and tectonic contributions in eight late-Holocene relative sea-level histories from the Mediterranean area, in: Quaternary Science Reviews. pp. 1989–2001. doi:10.1016/j.quascirev.(2004).06.026

PIRAZZOLI, P.A. (2005b). Marine erosion features and bioconstructions as indicators of tectonic movements, with special attention to the eastern Mediterranean area. Zeitschrift fur Geomorphol. Suppl. 137, pp. 71–77.

PRESCOTT, J. R., AND HUTTON, J. T. (1988). Cosmic ray and gamma ray dosimetry for TL and ESR. Nuclear Tracks Radiation Measurements 14, pp. 223–227.

PRESCOTT, J.R., HUTTON, J.T. (1994). Cosmic ray contributions to dose rates for luminescence and ESR dating: large depths and long-term time variations. Radiat. Meas. 23, pp. 497 - 500 .

PREUSSER, F., CHITHAMBO, M., L., GÖTTE, T., MARTINI, M., RAMSEYER, K., SENDEZERA, E. J., SUSINO, G. J., WINTLE, A. G. (2009). Quartz as a natural luminescence dosimeter. Earth-Science Reviews 97, pp.184–214.

PRUDÊNCIO M., MARQUES R., REBELO L., COOK G., CARDOSO G., NAYSMITH P., FREEMAN S., FRANCO D., BRITO P., DIAS M. (2007). Radiocarbon and blue Optically Stimulated Luminescence chronologies of the Oitavos consolidated dune (western Portugal). Radiocabon, 49 (2), pp.1145–1151.

QIU, D., LIU, Q., YUN, J., JIN, Z., ZHU, D., LI, T., SUN, D. (2018). Electron spin resonance (ESR) dating of pre-Quaternary faults in the Sichuan basin, SW China. Journal of Asian Earth Sciences, 163, 142–151.

RAMOS, A. M. (2008). O Pliocénico e o Plistocénico da Plataforma Litoral entre os Paralelos do Cabo Mondego e da Nazaré. PhD dissertation, University of Coimbra. 317 p.

RAMOS, A., CUNHA, P. P. (2004). Facies associations and palaeo-geography of the Zanclean–Piacenzian marine incursion in the Mondego Cape-Nazaré area (onshore of central Portugal). 23rd IAS Meeting of Sedimentology, Abstracts book, pp. 227.

RAMOS, A.M., CUNHA, P.P., CUNHA, L.S., GOMES, A., LOPES, F.C., BUYLAERT, J.P., MURRAY, A.S. (2012). The River Mondego terraces at the Figueira da Foz coastal area (western central Portugal): Geomorphological and sedimentological scharacterisation of a terrace staircase affected by differential uplift and glacio-eustasy. Geomorphology pp. 165–166, 107–123. doi:10.1016/j.geomorph.2012.03.037

RAPOSO, L. (1995). Ambientes, territorios y subsistencia en el Paleolítico Medio de Portugal. Complutum 6, 57.

RAYMO, M.E., MITROVICA, J.X., O'LEARY, M. J., DECONTO, R. M., HEARTY, P.J. (2011). Departures from eustasy in Pliocene sea-level records. Nature Geoscience (4), pp. 328-332.

RESSURREIÇÃO, R.J.V. (2018). Evolução tectono-estratigráfica cenozóica do litoral alentejano (sector Melides-Odemira) e enquadramento no regime geodinâmico actual. Tese de Doutoramento em Geologia, Univ. Lisboa, 327 p.

RESSURREIÇÃO, R., CABRAL, J., DIAS, R.P., CUNHA, P.P. (2018). Tectonic vertical displacements in the Sines-Vila Nova de Milfontes coastal sector (Alentejo, SW Portugal). IX Simposium on the Iberian Atlantic Margin - MIA2018 (Book of Proceedings), Coimbra, 4-7 September 2018. ISBN: 978-989-98914-3-2, pp. 255–256.

RIBEIRO, A., PEREIRA, E., DIAS, R. (1990). Structure of Centro-Iberian allochthon in northern Portugal, in: Dallmeyer, R.D., Martínez García, E., E. (Eds.), Pre-Mesozoic Geology of Iberia. Springer-Verlag, Berlin, pp. 220–236.

RIBEIRO, F., MATEUS, A., AZERÊDO, A. C. (2019). Fault-controlled magnetite-rich breccias in Jurassic limestones: Evidence for concealed epigenetic ore systems in the Lusitanian Basin (Portugal)? Ore Geology Reviews, 114, pp. 103–125.

RIBEIRO, P. (1998). Estudo de deformações tectónicas plio-quaternárias no bordo meridional da estrutura diapírica de S. Pedro de Moel (Vale de Paredes - Marinha Grande). MSc dissertation, University of Lisbon.

RIBEIRO, P. CABRAL, J. (1998). Study of Plio-Quaternary tectonic deformations on the Southern side of S. Pedro de Moel diapiric structure (Vale de Paredes-Marinha Grande). Actas do V Congresso Nacional de Geologia (Resumos alargados). Comunicações do Instituto Geológico e Mineiro, 84(I), D-73–D-76.

RIBEIRO, O. AND PATRÍCIO, A. (1943). Nótula sobre os terraços do Mondego nos arredores de Coimbra. Quarto Cong. Ass. Port. Progresso Ciências, 5, pp. 188–194.

RIBEIRO, A., PEREIRA, E., DIAS, R., (1990). Structure of Centro-Iberian allochthon in northern Portugal, in, Dallmeyer, R.D., Martínez García, E., E. (Eds.), Pre-Mesozoic Geology of Iberia. Springer-Verlag, Berlin, pp. 220–236.

RIBEIRO, A., CABRAL, J., BAPTISTA, R., AND MATIAS, L. (1996). Stress pattern in Portugal mainland and the adjacent Atlantic region, West Iberia. Tectonics, 15(3), pp. 641–659.

RILO, A.R., DUARTE, L.V., TAVARES, A. (2010). As falésias calcárias da península de Peniche (costa ocidental portuguesa): inventariação e caracterização do património geológico. Cuadernos del Museo Geominero 12, pp. 173–189. ISBN 978-84-7840-836-8

RINNEBERG, H., AND WEIL, J. A. (1972). EPR Studies of Ti3+–H+ Centers in X-Irradiated α-Quartz. The Journal of Chemical Physics, 56(5), pp. 2019–2028.

RINK, W. J., SCHWARCZ, H. P., LEE, H. K., REES-JONES, J., RABINOVICH, R., HOVERS, E. (2001). Electron spin resonance (ESR) and thermal ionization mass spectrometric (TIMS) 230Th/234U dating of teeth in Middle Paleolithic layers at Amud Cave, Israel. Geoarchaeology: An International Journal, 16(6), pp. 701–717.

RINK, W.J., BARTOLL, J., SCHWARCZ, H.P., SHANE, P., BAR-YOSEF, O. (2007). Testing the reliability of ESR dating of optically exposed buried quartz sediments. Radiat. Meas. 42, pp. 1618–1626. doi:10.1016/j.radmeas.2007.09.005

RINK, W.J., WANG, W., BEKKEN, D., JONES, H.L. (2008). Geochronology of Ailuropoda–Stegodon 272 fauna and Gigantopithecus in Guangxi Province, southern China. Quaternary Research 69, pp. 377- 387.

ROBERTS, G.G., WHITE, N.J., SHAW, B. (2013). An uplift history of Crete, Greece, from inverse modeling of longitudinal river profiles. Geomorphology 198, pp. 177–188. doi:10.1016/j.geomorph.2013.05.026

ROCHA, A.T., FERREIRA, J.M. 1953. Estudo dos Foraminíferos fósseis do Pliocénico da região de Pombal. Revista da Faculdade de Ciências de Lisboa, 2ª Série – C, Vol. III, Fasc. 1º, 129-156.

ROCHA, R. B., MANUPPELLA, G., MOUTERDE, R., RUGET-PERROT, C. , ZBYSZEWSKI, G. (1981). Noticia explicativa da folha 19-C (Figueira da Foz) da Carta Geológica de Portugal na escala de 1:50000. Serviços Geológicos de Portugal, Lisboa.

ROCOUX, K. H. P. C., TZEDAKIS, L. DE ABREU, SHACKLETON, N. J. (2006. Climate and vege- tation changes 180,000 to 345,000 years ago recorded in a deep-sea core off Portugal, Earth Planet. Sci. Lett., 249(3–4), 307–325, doi: 10.1016/j.epsl.2006.07.005.

RODRIGUES, T., VOELKER, A. H. L., GRIMALT, J. O., ABRANTES, F., NAUGHTON, F. (2011). Iberian Margin sea surface temperature during MIS 15 to 9 (580–300 ka): Glacial suborbital variability versus interglacial stability. Paleoceanography and Paleoclimatology, 26(1).

RODRIGUES, T., ALONSO-GARCÍA, M., HODELL, D. A., RUFINO, M., NAUGHTON, F., GRIMALT, J. O., VOELKER, A.H.L., ABRANTES, F. (2017). A 1-Ma record of sea surface temperature and extreme cooling events in the North Atlantic: A perspective from the Iberian Margin. Quaternary Science Reviews, 172, pp.118-130.

ROHLING, E. J., FOSTER, G. L., GRANT, K. M., MARINO, G., ROBERTS, A. P., TAMISIEA, M. E., & WILLIAMS, F. (2014). Sea-level and deep-sea-temperature variability over the past 5.3 million years. Nature, 508(7497), 477p.

ROMÃO, J.M. (2009). Património Geológico no litoral de Peniche: geomonumentos a valorizar e divulgar. Geonovas 22, pp. 21–33.

ROSINA, P. (2002). Stratigraphie et Géomorphologie des terrasses fluviatiles de la Moyenne Vallée du Tage (Haut Ribatejo - Portugal), Arkeos, 13, pp. 11–52.

ROSINA, P., VOINCHET, P., BAHAIN, J. J., CRISTOVÃO, J., FALGUÈRES, C. (2014). Dating the onset of Lower Tagus River terrace formation using electron spin resonance. Journal of Quaternary Science, 29(2), pp. 153–162.

SAILLARD, M., HALL, S.R., AUDIN, L., FARBER, D.L., HÉRAIL, G., MARTINOD, J., REGARD, V., FINKEL, R.C., BONDOUX, F. (2009). Non-steady long-term uplift rates and Pleistocene marine terrace development along the Andean margin of Chile (31°S) inferred from 10Be dating. Earth Planet. Sci. Lett. 277, pp. 50–63. doi:10.1016/j.epsl.2008.09.039

SALZMANN, U., DOLAN, A.M., HAYWOOD, A.M., CHAN, W.-L., VOSS, J., HILL, D.J., ABE-OUCHI, A., OTTO-BLIESNER, B., BRAGG, M.A. CHANDLER, C. CONTOUX, H.J. DOWSETT, A. JOST, Y. KAMAE, G. LOHMANN, D.J. LUNT, S.J. PICKERING, M.J. POUND, F., RAMSTEIN, G., ROSENBLOOM, N.A., SOHL, L., STEPANEK, C., UEDA, H., ZHANG., Z. (2013). Challenges in reconstructing terrestrial warming of the Pliocene revealed by data-model discord. Nature Clim. Change, 3, pp.969-974. doi:10.1038/nclimate2008

ZHANG., Z. (2013). Challenges in reconstructing terrestrial warming of the Pliocene revealed by data-model discord. Nature Clim. Change, 3, pp.969–974. doi:10.1038/nclimate2008

SANCHO, C., CALLE, M., PEÑA-MONNÉ, J. L., DUVAL, M., OLIVA-URCIA, B., PUEYO, E. L., BENITO, G. MORENO, A. (2016). Dating the Earliest Pleistocene alluvial terrace of the Alcanadre River (Ebro Basin, NE Spain): Insights into the landscape evolution and involved processes. Quaternary International, 407, pp. 86–95.

SANTISTEBAN, J. I., & SCHULTE, L. (2007). Fluvial networks of the Iberian Peninsula: a chronological framework. Quaternary Science Reviews, 26(22-24), 2738–2757.

SANTONJA, M., PÉREZ-GONZÁLEZ, A., PANERA, J., RUBIO-JARA, S., MÉNDEZ-QUINTAS, E. (2016). The coexistence of Acheulean and Ancient Middle Palaeolithic techno-complexes in the Middle Pleistocene of the Iberian Peninsula. Quaternary International, 411, pp. 367–377.

SANTOS, J. A. B. D. (2009). Geomorfologia fluvial e evolução quaternária da bacia do Mondego, PhD Thesis, Univ. Coimbra, 307 pp.

SAUCIER, R.T. (1996). Geomorphology and Quaternary geoogic history of the Lower Mississippi Valley. US Army Corps of Engineers, Vicksburg, 364pp.

SCHWARCZ, H. P. (1985). ESR studies of tooth enamel. Nucl. Tracks 10, pp. 865–867.

SCHWARCZ, H. P., GRÜN, R, TOBIAS, P. V. (1994). ESR dating studies of the australopithecine site of Sterkfontein, South Africa. *Journal of Human Evolution*, *26*(3), pp.175–181.

SHACKLETON, N. J. (1987). Oxygen isotopes, ice volume and sea level. Quaternary Science Reviews, 6(3-4), pp. 183–190.

SHACKLETON, N.J., BERGER, A., PELTIER, W.R., (1990). An alternative astronomical calibration of the lower Pleistocene timescale based on ODP Site 677. Trans. R. Soc. Edinb. Earth Sci. 81, pp. 251–261. doi:10.1017/S0263593300020782

SHACKLETON, N. J., (1995). New data on the evolution of Pliocene climatic variability. Paleoclimate and evolution with emphasis on human origins.

SHARMA, M. C. AND CHAND, P. R. I. T. A. M. (2016). Studies on quaternary glaciations in India during 2010-2016. In Proc Indian Natn Sci Acad , Vol. 82, pp. 869–880.

SCHELLMANN, G., AND RADTKE, U. (2004). A revised morpho-and chronostratigraphy of the Late and Middle Pleistcene coral reef terraces on Southern Barbados (West Indies). Earth-Science Reviews, 64(3-4), pp.157–187.

SHEPARD, F. P., AND MOORE, D. G. (1954). Sedimentary environments differentiated by coarse-fraction studies. AAPG Bulletin, 38(8), pp.1792-1802.

SIDDALL, M., ROHLING, E.J., ALMOGI-LABIN, A., HEMLEBEN, C., MEISCHNER, D., SCHMELZER, I., SMEED, D.A. (2003). Sea-level fluctuations during the last glacial cycle. Nature 423, pp. 853–858. doi:10.1038/nature01690

SIDDALL, M., SMEED, D.A., HEMLEBEN, C., ROHLING, E.J., SCHMELZER, I., PELTIER, W.R. (2004). Understanding the Red Sea response to sea level. Earth Planet. Sci. Lett. 225, pp. 421–434. doi:10.1016/j.epsl.(2004).06.008

SIDDALL, M., CHAPPELL, J., POTTER, E. K. (2007). 7. Eustatic sea level during past interglacials. In Developments in Quaternary Sciences, Vol. 7, 75–92.

SILVA, C.M. (2001). Gastrópodes Pliocénicos Marinhos de Portugal. Sistemática, Paleoecologia, Paleobiologia, Paleobiogeografia. Dissertação de Doutoramento, Univ. Lisboa, 747 p.

SILVA, C.M., LANDAU, B., Domènech, R., Martinell, R. (2010). Pliocene Atlantic molluscan assemblages from the Mondego Basin (Portugal): age and palaeoceanographic implications. Palaeogeography, Palaeoclimatology, Palaeoecology 285, pp.248–254

SILVA, P.G., ROQUERO, E., LÓPEZ-RECIO, M., HUERTA, P., MARTINEZ-GRAÑA, A.M. (2017). Chronology of fluvial terrace sequences for large Atlantic rivers n Iberian Peninsula (Upper Tagus and Duero drainage basins, Central Spain). Quat. Sci. Rev., 166, pp. 188–203.

SMEDLEY, R. K., BUYLAERT, J. P., & UJVARI, G. (2019). Comparing the accuracy and precision of luminescence ages for partially-bleached sediments using single grains of K-feldspar and quartz. Quaternary Geochronology, 53, 101007.

SOARES, A. F. (1999). As unidades pliocénicas e quaternárias no espaço do Baixo Mondego (uma prespectiva de ordem). Esudos do Quaternário, pp. 7–17.

SOARES, A.F., MARQUES, J.F, ROCHA R. (1985). Contribuição para o conhecimento geológico de Coimbra. Memórias e Notícias, vol. 100, pp. 41–71.

SOARES, A.F., CUNHA, L., MARQUES, J.F. (1989). Depósito quaternários do Baixo Mondego. Tentativa de coordenação morfogenética, El Quat. España y Portugal, 2.
doi:10.1016/j.quageo.2019.101007

SOARES, A.F., CUNHA, L., ALMEIDA, A.C., MARQUES, J.F. (1992). Depósito quaternários do Baixo Mondego. Estado actual do conhecimentos e coordenação morfogenética. Actas VI col. Iberico de Geografia.

SOARES, A. F., CUNHA, L., MARQUES, J. F. (1997). Les tufs calcaires dans la région du Baixo Mondego (Portugal): Les tufs de Condeixa. Présentation générale. Etudes de géographie physique, (26), pp. 55–58.

SOARES, A. F., GOMES, C. R. (1997). A geologia do Baixo Mondego–organização do Mesozóico. Seminário "O Baixo Mondego–Organização Geossistémica e Recursos Naturais, pp. 6–20.

SOARES, A., F., MARQUES, J. F., ROCHA, R.E., SEQUEIRA, A.J.D., SOUSA, M.B., PEREIRA, E. (2005). Carta Geológica de Portugal, Folha 19-d (Coimbra-Lousã). Inst. Nac. Eng. Tecn. Inov. (INETI). Lisboa.

SOARES, A. F., MARQUES, J. F. AND SEQUEIRA, A. J. D. (2007). Notícia explicativa da Folha 19-D (Coimbra-Lousã). Inst. Nac. Eng. Tecn. Inov., (I.N.E.T.I.), Lisboa, 71 pp.

SOARES, A. F., CALLAPEZ, P., MARQUES, J. F. (2007). The Farol Deposit (Depósito do Farol) –a Pleistocene beach deposit from Cape Mondego (Figueira da Foz, West Central Portugal).Ciencias da Terra, 16, pp. 163–173.

SOARES, P. M.; CARDOSO, R. M.; SEMEDO, A.; CHINITA M. J.; RANJHA, R. (2014) - Climatology of the Iberia coastal low-level wind jet: weather research forecasting model high-resolution results. Tellus Series A-Dynamic Meterology and Oceonagraphy. ISSN 0280-6495. Vol. 66, Art. nr. 22377. doi: 10.3402/tellusa.v66.22377

SOARES, A. F. (2017). Realidade e Mito (O Baixo Mondego). Academia das Ciências, 40p.

SPRATT, R. M. AND LISIECKI, L. E. (2016). A Late Pleistocene sea level stack. *Climate of the Past*, *12*(4), pp.1079–1092.

STARKEL, L. (2003). Climatically controlled terraces in uplifting mountain areas. Quaternary Science Reviews, 22(20), pp. 2189–2198.

SONNEVILLE-BORDES, D., PERROT, J. (1954). Lexique typologique du Paléolithique supérieur. Bull. la Société Préhistorique Française.

STEARNS, C.E., THURBER, D.L. (1965). Th230/U234 dates of late Pleistocene marine fossils from the Mediterranean and Moroccan littorals. Prog. Oceanogr. 4, pp. 293–305. doi:10.1016/0079-6611(65)90056-X

STICH, D., SERPELLONI, E., DE LIS MANCILLA, F., MORALES, J. (2006). Kinematics of the Iberia-Maghreb plate contact from seismic moment tensors and GPS observations. Tectonophysics 426, pp. 295–317. doi:10.1016/j.tecto.2006.08.004

STOKES, M. AND GARCIA, A. F. (2009). Late Quaternary landscape development along the Rancho Marino coastal range front (south-central Pacific Coast Ranges, California, USA). Journal of Quaternary Science: Published for the Quaternary Research Association, 24(7), pp. 728–746.

STOKES, M., CUNHA, P.P., MARTINS, A.A. (2012). Techniques for analysing river terrace sequences. Geomorphology, pp. 165–166, 1-6, doi:10.1016/j.geomorph.2012.03.022

SUGANUMA, Y., HANEDA, Y., KAMEO, K., KUBOTA, Y., HAYASHI, H., ITAKI, T., OKUDA, M., HEAD, M.J., SUGAYA, M., NAKAZATO, H., IGARASHI, A., SHIKOKU, K., HONGO, M., WATANABE, M., SATOGUCHI, Y., TAKESHITA, Y., NISHIDA, N., IZUMI, K., KAWAMURA, K., KAWAMATA, M., OKUNO, J., YOSHIDA, T., OGITSU, I., YABUSAKI, H., OKADA, M. (2018). Paleoclimatic and paleoceanographic records through Marine Isotope Stage 19 at the Chiba composite section, central Japan: A key reference for the Early–Middle Pleistocene Subseries boundary. Quat. Sci. Rev. 191, pp. 406–430. doi:10.1016/j.quascirev.2018.04.022

TARLING, D. H. (2012). Palaeomagnetism: principles and applications in geology, geophysics and archaeology. Springer Science & Business Media.

TAVARES, A. M. D. O. S. (2000). Condicionantes físicas ao planeamento: análise da susceptibilidade no espaço do Concelho de Coimbra, PhD Thesis, 316 p.

TEIXEIRA, C. (1979). Plio-Plistocénico de Portugal. Comun. Serv. Geol. Port. , Lisboa, 65, pp. 35–46.

TEIXEIRA, C. AND ZBYSZEWSKI, G. (1951). Note sur le Pliocéne de la région à l'Ouest de Pombal. Comunicações dos Serviços Geológicos de Portugal, Lisboa, 32 (1), pp. 295–302.

TEIXEIRA, C. AND ZBYSZEWSKI, G. (1954). Contribuition à l'étude du littoral pliocène au Portugal. C.R. 19éme Ses. Cong. Géol. Intern., Alger, 1952, 13, pp. 275–284.

TEIXEIRA, C. (1979). Plio-Plistocénico de Portugal.(Plio-pléistocène au Portugal). Comunicaçoes dos Serviços geologicos de Portugal Lisboa, (65), pp. 35–46.

THOMPSON, W.G. SPIEGELMAN, M.W., GOLDSTEIN, S.L., SPEED, R.C. (2003). An open-system model for U-series age determinations of fossil corals. Earth Planet. Sci. Lett. 210 (1–2), pp. 365–381.

TISSOUX, H., FALGUÈRES, C., VOINCHET, P., TOYODA, S., BAHAIN, J.J., DESPRIÉE, J. (2007). Potential use of Ti-center in ESR dating of fluvial sediment. Quat. Geochronol. 2, pp. 367–372. doi: 10.1016/j.quageo.2006.04.006

TISSOUX, H., VOINCHET, P., LACQUEMENT, F., PROGNON, F., MORENO, D., FALGUÈRES, C., BAHAIN, J.J. TOYODA, S. (2012). Investigation on non-optically bleachable components of ESR aluminium signal in quartz. Radiation measurements, 47(9), pp. 894–899.

TIXIER, J., INIZAN, M.-L., ROCHE, H. (1980). Préhistoire de la pierre taillée: Terminologie et technologie. CNRS.

TOYODA, S., IKEYA, M. (1991).Thermal stabilities of paramagnetic defects and impurity centers in quartz: basis for ESR dating of thermal history. Geochemical Journal 25: pp. 437–445.

TOYODA, S., AND YOSHIDA, N. (1999). Determination of nitrogen isotopomers of nitrous oxide on a modified isotope ratio mass spectrometer. Analytical Chemistry, 71(20), pp. 4711–4718.

TOYODA, S., VOINCHET, P., FALGUÈRES, C., DOLO, J.M., LAURENT, M. (2000). Bleaching of ESR signals by the sunlight: a laboratory experiment for establishing the ESR dating of sediments, in: Applied Radiation and Isotopes. pp. 1357–1362. doi:10.1016/S0969-8043(00)00095-6

TOYODA, S., C FALGUÈRES, C. (2003). The method to represent the ESR signal intensity of the aluminium hole center in quartz for the purpose of dating. Adv. ESR Appl. 20, pp. 7–10.

TOYODA, S. (2015). Paramagnetic lattice defects in quartz for applications to ESR dating. Quaternary Geochronology, 30, pp. 498–505.

TREVISAN, L. (1949). Gènese de terrasses fluviatiles en relation avec les cycles climatiques. Compt. Rendu Congr. Intern. Geogr. Lisbonne, 2, pp. 511–528.

TSAKALOS, E., ATHANASSAS, C., TSIPAS, P., TRIANTAPHYLLOU, M., GERAGA, M., PAPATHEODOROU, FILIPAKI, E., CRISTODOULAKIS, J. G., KAZANTZAKI, M. (2018). Luminescence geochronology and paleoenvironmental implications of coastal deposits of southeast Cyprus. Archaeological and Anthropological Sciences, 10(1), pp. 41–60.

TYRÀCEK, J. (1995). Stratigraphy of the Ohre River terraces in the Most Basin. Sborník geologických věd, Antropozoikum, 22, pp. 141–157.

VANDERNBERGHE, J. (1995b). Timescales, climate and river development. Quaternary Science Reviews, 14, pp. 631–638.

VIEIRA M. (2009). Palinologia do Pliocénico da Orla Ocidental Norte e Centro de Portugal : Contributo para a compreensão da cronostratigrafia e da evolução paleoambiental. Ph.D. thesis, Universidade do Minho, Braga, Portugal, 389 p.

VIEIRA, M.,POUND, M.J., PEREIRA, D.I. (2018). The late Pliocene palaeoenvironments and palaeoclimates of the Western Iberian Atlantic Margin from the Rio Maior flora, 495, pp.245–58

VITORINO, J., OLIVEIRA, A., JOUANNEAU, J. M., DRAGO, T. (2002). Winter dynamics on the northern Portuguese shelf. Part 2: bottom boundary layers and sediment dispersal. Progress in Oceanography, 52(2-4), pp.155–170.

VIVEEN, W., BRAUCHER, R., BOURLÈS, D., SCHOORL, J. M., VELDKAMP, A., VAN BALEN, R. T., WALLINGA, J., FERNANDEZ-MOSQUERA, D., VIDAL, ROMANI, J.R., SANJURJO-SANCHEZ, J. (2012). A 0.65 Ma chronology and incision rate assessment of the NW Iberian Miño River terraces based on 10Be and luminescence dating. Global and Planetary Change, 94, pp. 82–100.

VILANOVA, S.P., NEMSER, E.S., BESANA-OSTMAN, G.M., BEZZEGHOUD, M., BORGES, J.F., BRUM DA SILVEIRA, A., CABRAL, J., CARVALHO, J., CUNHA, P.P., DIAS, R.P., MADEIRA, J., LOPES, F.C., OLIVEIRA, C.S., PEREA, H., GARCÍA-MAYORDOMO, J., WONG, I., ARVIDSSON, R., FONSECA, J.F.D.B. (2014). Incorporating descriptive metadata into seismic source zone models for seismic-hazard assessment: a case study of the Azores-west Iberian region. Bulletin of the Seismological Society of America, vol. 104, nº 3, pp. 1212–1229. doi: 10.1785/0120130210

VIS, G.J., KASSE, C., KROON, D., JUNG, S., ZUUR, H., PRICK, A. (2010). Late Holocene sedimentary changes in floodplain and shelf environments of the Tagus River (Portugal). Proc. Geol. Assoc.

VITORINO, J., OLIVEIRA, A., JOUANNEAU, J.M., DRAGO, T. (2002). Winter dynamics on the northern Portuguese shelf. Part 2: Bottom boundary layers and sediment dispersal. Prog. Oceanogr. doi:10.1016/S0079-6611(02)00004-6

VIVEEN, W., SCHOORL, J. M., VELDKAMP, A., VAN BALEN, R. T., DESPRAT, S., VIDAL-ROMANI, J. R. (2013). Reconstructing the interacting effects of base level, climate, and tectonic uplift in the lower Miño River terrace record: a gradient modelling evaluation. Geomorphology, 186, pp. 96–118.

VOINCHET, P.(2002). Datation par résonance paramagnétique électronique (RPE) de quartz blanchis extraits de sédiments fluviatiles pléistocènes: contribuition méthodologique et application aux systèmes de la Creuse, du Loir et de l'Yonne. Phd Thesis in Museum National d'Histoire Naturelle, Paris.

VOINCHET, P., FALGUÈRES, C., LAURENT, M., TOYODA, S., BAHAIN, J.J., DOLO, J.M. (2003). Artificial optical bleaching of the aluminium center in quartz implications to ESR dating of sediments. Quat. Sci. Rev. 22, pp. 1335–1338.

VOINCHET, P., BAHAIN, J.J., FALGUÈRES, C., LAURENT, M., DOLO, J.M., DESPRIÉE, J., GAGEONNET, R., CHAUSSE, C. (2004). ESR dating of quartz extracted from Quaternary sediments application to fluvial terraces system of northern France. Quaternaire 15, pp. 135–141. doi:10.3406/quate.(2004).1761

VOINCHET, P., DESPRIÉE, J., GAGEONNET, R., BAHAIN, J.J., TISSOUX, H., FALGUÈRES, C., DÉPONT, J., DOLO, J.M., COURCIMAULT, G. (2007). Datation par ESR de quartz fluviatiles dans le bassin de la Loire moyenne en Région Centre: Mise en évidence de l'importance de la tectonique quaternaire et de son influence sur la géometrie des systèmes de terrasses. Quaternaire 18, pp. 335–347. doi:10.4000/quaternaire.1216

VOINCHET, P., FALGUÈRES, C., TISSOUX, H., BAHAIN, J.J., DESPRI EE, J., PIROUELLE, F. (2007). ESR dating of fluvial quartz: estimate of the minimal distance transport required for getting a maximum optical bleaching. Quat. Geochronol. 2, pp. 363 – 366.

VOINCHET, P., DESPRIÉE, J., TISSOUX, H., FALGUÈRES, C., BAHAIN, J.J., GAGEONNET, R., DÉPONT, J., DOLO, J.M. (2010). ESR chronology of alluvial deposits and first human settlements of the Middle Loire Basin (Region Centre, France). Quaternary Geochronology, 5, pp.381–384.

VOINCHET, P., YIN, G., FALGUÈRES, C., LIU, C., HAN, F., SUN, X., BAHAIN, J. (2013). ESR dose response of Al center measured in quartz samples from the Yellow River (China): Implications for the dating of Upper Pleistocene sediment. Geochronometria, 40(4), pp. 341–347.

VOINCHET, P., MORENO, D., BAHAIN, J. J., TISSOUX, H., TOMBRET, O., FALGUÈRES, C., MONCEL, M.H., SCHREVE, D., CANDY, I., ANTOINE, P., ASHTON, N., BEAMISH, M., CLIQUET, D., DESPRIÉE,J., LEWIS, S., LIMONDIN-LOZOUET, N., LOCHT, J.L., PARFITT, S., POPE, M. (2015). New chronological data (ESR and ESR/U-series) for the earliest Acheulian sites of north-western Europe. Journal of Quaternary Science, 30 (7), pp. 610–622.

VOINCHET, P., PEREIRA, A., NOMADE, S., FALGUÈRES, C., BIDDITTU, I., PIPERNO, M., MONCEL, M.H., BAHAIN, J. J. (2020). ESR dating applied to optically bleached quartz-a comparison with 40Ar/39Ar chronologies on Italian Middle Pleistocene sequences. Quaternary International., 556, pp. 113–123. https://doi.org/10.1016/j.quaint.2020.03.012

WAELBROECK, C., LABEYRIE, L., MICHEL, E., DUPLESSY, J.C., MCMANUS, J.F., LAMBECK, K., BALBON, E., LABRACHERIE, M. (2002). Sea-level and deep water temperature changes derived from benthic foraminifera isotopic records. Quat. Sci. Rev. 21, pp. 295–305. doi:10.1016/S0277-3791(01)00101-9

WEIL, J. A. (1984). A review of electron spin spectroscopy and its application to the study of paramagnetic defects in crystalline quartz. Phys. Chem. Minerals 10, pp. 149–165.

WEIL, J. A. (1994). EPR of iron centres in silicon dioxide. Applied Magnetic Resonance, 6(1-2), pp. 1–16.

WESTAWAY, R. (1993). Quaternary uplift of southern Italy. J. Geophys. Res. 98. doi:10.1029/93jb01566

WESTAWAY, R. (2002). Long-term river terrace sequences: Evidence for global increases in surface uplift rates in the Late Pliocene and early Middle Pleistocene caused by flow in the lower continental crust induced by surface processes. Netherlands Journal of Geosciences, 81(3-4), pp. 305–328.

WESTAWAY, R., GUILLOU, H., SEYREK, A., DEMIR, T., BRIDGLAND, D., SCAILLET, S., BECK, A. (2009). Late Cenozoic surface uplift, basaltic volcanism, and incision by the River Tigris around Diyarbakır, SE Turkey. International Journal of Earth Sciences, 98(3), 601–625.

YOKOYAMA, Y., QUAEGEBEUR, J. P., BIBRON, R., LEGER, C., NGUYEN, H. V., POUPEAU, G. (1981). Electron spin resonance (ESR) dating of fossil bones of the Caune of l'Arago at Tautavel. Dans "Absolute dating and isotope analysis in prehistory methods and limits proceeding." (D. L. e. Labeyrie, Ed.), pp. 457–492. CNRS.

YOKOYAMA, Y., NGUYEN, H. V., QUAEGEBEUR, J. P., POUPEAU, G. (1982). Some problems encountered in the evaluation of annual dose-rate in the electron spin resonance dating of fossil bonés. PACT 6.

YOKOYAMA, Y., FALGUERES, C., QUAEGEBEUR, J.P. (1985). ESR dating of sediment baked by lava flows companson of paleodoses for A1 and Ti centers, in: ESR Dating and Dosimetry. IONICS, Tokyo, pp. 197–204.

ZAVOISKY, E. (1945). Spin-magnetic resonance in paramagnetics. J. Phys. 9, 245 p.

ZAZO, C., GOY, J.L., DABRIO, C.J., BARDAJÍ, T., HILLAIRE-MARCEL, C., GHALEB, B., GONZÁLEZ-DELGADO, J.Á., SOLER, V. (2003). Pleistocene raised marine terraces of the Spanish Mediterranean and Atlantic Coasts: Records of coastal uplift, sea-level highstands and climate changes, in: Marine Geology. Elsevier B.V., pp. 103–133. doi:10.1016/S0025-3227(02)00701-6

ZAZO, C., GOY, J.L., DABRIO, C.J., BARDAJI, T., SOMOZA, L., SILVA, P.G. (1993). The last interglacial in the Mediterranean as a model for the present interglacial. Glob. Planet. Change 7, pp. 109–117. doi:10.1016/0921-8181(93)90043-N

ZAZO, C., GOY, J.L., DABRIO, C.J., LARIO, J., GONZÁLEZ-DELGADO, J.A., BARDAJÍ, T., HILLAIRE-MARCEL, C., CABERO, A., GHALEB, B., BORJA, F., SILVA, P.G., ROQUERO, E., SOLER, V. (2013). Retracing the Quaternary history of sea-level changes in the Spanish Mediterranean-Atlantic coasts: Geomorphological and sedimentological approach. Geomorphology 196, pp. 36–49. doi:10.1016/j.geomorph.2012.10.020

ZBYSZEWSKI, G. (1943). La classification du Paleolithique ancien et la chronologie du Ouaternaire de Portugal en 1942. Boletim da Sociedade Geologica de Portugal, 2 (2-3), 111.

ZBYSZEWSKI, G. (1943b). Eléments pour server à l´étude du Pliocène marin au Sud du Tage: la faune des couches supereures dÁlfeite. Comunicações dos Serviços Geológicos de Portugal, Lisboa, 24, pp. 125–156.

ZBYSZEWSKI, G. (1946). Etude geologique de la reg,on d'Alpiarça. C.S.G. de Portugal, XXVII, pp.145–268.

ZBYSZEWSKI, G. (1949). Contribution à la conaissance du Pliocène Portugais. Comunicações dos Serviços Geológicos de Portugal 30, pp. 59–78.

ZBYSZEWSKI, G. (1958). Le quaternaire du Portugal. Bol. da Soc. Geológica Port. XIII, pp. 3–227.

ZBYSZEWSKI, G. (1967). Estudo geológico da bacia dos lignitos de Rio Maior. Estudos Notas e Trabalhos do Serviço Fomento Mineiro 17, pp. 5–105.

ZBYSZEWSKI, G. (1970). Indústrias paleolíticas da região de Peniche. O Arqueólogo Português, 3(4), pp. 19–40.

ZELLER, E. J., LEVY, P. W., MATTERN, P. L. (1967). Geologic dating by Electron Spin Resonance. Proceedings of the Symposium on radioactive dating and low level counting, pp. 531–539.

ZILHÃO, J. (1997). O Paleolítico Superior da Estremadura portuguesa. 2 vols., Colibri, Lisboa.

ZITELLINI, N., GRACIA, E., MATIAS, L., TERRINHA, P., ABREU, M.A., DEALTERIIS, G., HENRIET, J.P., DANOBEITIA, J.J., MASSON, D.G., MULDER, T., RAMELLA, R., SOMOZA, L., DIEZ, S. (2009). The quest for the Africa–Eurasia plate boundary west of the strait of Gibraltar. Earth Planet. Sci. Lett. 280 (1–4), pp. 13–50.

ZOMENIA, Z. (2012). Quaternary Marine Terraces on Cyprus: Constraints on Uplift and Pedogenesis, and the Geoarchaeology of Palaipafos. Oregon State University, 274p.